Alma Mater Studiorum – Università di Bologna

DOTTORATO DI RICERCA IN

Chimica Industriale

Ciclo XXIV

Settore Concorsuale di afferenza: **03/C2**

Settore Scientifico Disciplinare: **CHIM/04**

New reactants and improved catalysts for maleic anhydride synthesis

Presentata da:

Aurora Caldarelli

Coordinatore Dottorato:

Prof. Fabrizio Cavani

Relatore:

Prof. Fabrizio Cavani

Esame finale anno 2012

Abstract

Several topics have been investigated and discussed in this thesis, with the aims of both improving the catalytic behaviour of vanadyl pyrophosphate catalyst (VPP) in n-butane oxidation into maleic anhydride (MA), and studying the development of a new process for the synthesis of MA, starting from 1-butanol, a bio-based building block.

The role of the amount of Nb, used as a dopant for VPP, and how its presence may affect the generation of the active and selective δ-$VOPO_4$ compound at the VPP surface under reaction conditions, was investigated, by means of both ex-situ and in-situ characterisation techniques. We found that Nb indeed may favour, under specific conditions, the generation of the desired δ-$VOPO_4$ compound; however, its effect of enhancement of catalytic behaviour was not simply proportional to its concentration, since other factors influenced its effect, for example, the preparation method used for the synthesis of the VPP precursor. In order to better understand how Nb may affect the generation of the active phase, we prepared V/Nb mixed phosphates; the formation of a solid solution was possible only under specific conditions, with a limited reciprocal dissolution of the two elements. We concluded that even though the incorporation of small amounts of Nb^{5+} in the $VOPO_4$ (and also of V^{5+} in $NbOPO_4$) cannot be excluded, a phenomenon which might favour the generation of the desired δ-$VOPO_4$ compound, however the main role of Nb^{5+} was related to a modification of the redox properties of V^{4+} in the VPP, and specifically of the redox potential associated to the couple V^{4+}/V^{5+}. This led to a catalyst that during reaction was more oxidized than the corresponding undoped VPP, which under specific reaction conditions allowed obtain a better selectivity to MA. On the other hand, an excessive oxidation of the VPP (which occurred in catalysts having the greater amount of Nb) turned out to affect negatively the selectivity to MA, because of the excessive formation of carbon oxides. Another important output of the research is that the VPP probably acts as a sort of “template” for the in-situ generation of the δ-$VOPO_4$.

Moreover, we set up a new procedure for the synthesis of $VOHPO_4.0.5H_2O$ (VPP precursor) - in collaboration with the University of Pisa (prof. Anna Maria Raspolli Galletti and co-workers) and Polynt S.p.A. - using microwave heating (by CEM Discover S-class system) of the synthesis slurry: the method showed several advantages as compared to the conventional preparation and allowed obtain VPP catalysts with interesting precursor morphologies and showing very good catalytic performance.

A preliminary study regarding the oxidehydration of 1-butanol into MA was carried out testing various catalysts: still the best catalyst resulted to be the VPP; however the MA selectivity was by far lower than that obtained from n-butane. The results permitted to understand the role of some parameters which influence the reactivity of the alcohol.

Finally, an in-situ/operando Raman study of the Nb-doped and undoped catalysts, was carried out during my stage abroad (at CSIC laboratory in Madrid - Dr. M.A. Bañares): this study

allowed obtaining the experimental proof that the redox cycle involves the VPP and the δ-$VOPO_4$ compounds, that the reoxidation step of V^{4+} in VPP is the rate-determining one, and that the presence of Nb may accelerate the rate of this latter step. On the other hand, this study revealed that the surface heterogeneity of these V/P/O samples may represent a hurdle for the clear identification of the active and selective compounds.

SUMMARY

1

INTRODUCTION

1.1 MALEIC ANHYDRIDE: PRODUCTION AND USES

Maleic Anhydride (MA) is the anhydride of cis-butenedioic acid (maleic acid); this molecule has a four carbon cyclic structure, containing also one oxygen atom, as shown in Figure 1.1. The molecule is also known with other names: 2,5-Furandione, Dihydro-2,5-dioxofuran, cis-Butanedioic anhydride. b

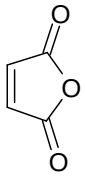

Fig.1.1_ Maleic anhydride structure.

At room temperature, MA is a white crystalline solid with pungent odour. The most important physical-chemical characteristics are summarized in Table 1.1.

Molecular Weight (g/mol)	98.01
Melting Point (°C)	52.85
Boiling Point (°C)	202
Combustion heat (kJ/mol)	1391.2
Explosion limits (%vol.)	Lower: 1.4 Upper: 7.1
Solubility in xylene (g/l at 30°C)	163.2
Solubility in water (g/l at 30°C)	572
Solubility in benzene (g/l at 35°C)	439.4

Table.1.1_ Physical-chemical features of MA [1-2].

1.1.1 Maleic anhydride uses

Global production and consumption of maleic anhydride in 2010 were both approximately 1.7 million tons. Maleic anhydride consumption is estimated to have increased by 5.7% in 2010 and the percentage pro year is expected to grow (5.6%/year from 2010 to 2015, 3.5%/year from 2015 to 2020), although the demand for MA decreased over the past few years, due to a drastic slowdown in the construction, automobile and marine industries [1].

The molecule possess interesting functional groups: the unsaturated double bond and two carbonyl groups; which render MA a quite reactive molecule and, especially, a good monomer for polyaddition and polycondensation reactions. In Table 1.2 main reactions involving MA are summarized [1].

Reaction	*Reagents involved (examples)*	*Final product*
Polymerization	Glycols, epoxides, and vinyl monomer or styrene	Unsaturated polyester resins
	Stirene, vinyl compounds, nitrogen containing monomers, alkenes, MA	Copolymers
Hydration	H_2O	Maleic acid, fumaric acid
Cycloaddition	1,3-butadiene; isoprene	Tetrahydrophtalic anhydride; methyl-esahydrophthalic anhydride
Reduction	H_2	Succinic anhydride, γ-butyrolactone, tetrahydrofuran, 1,4-butanediol

Table.1.2_ Main reactions involving MA, reagents employed and final products [1d].

More than 50% of MA global production is used to manufacture unsaturated polyester resins (UPR), which are used in a lot of applications such as boat hulls, bathroom fixtures, car parts, furniture, tanks and pipes. MA is also used to produce copolymers (such as MA-styrene, MA-acrylic acid), paints, lubricants, pesticides, and other organic compounds. The second-largest market for MA derivatives is represented by 1,4-butandiol (BDO). Tetrahydrophthalic anhydride, derived by Diels-Alder reaction of MA with butadiene, can be hydrogenated to esahydrophthalic anhydride. Methyl-esahydrophthalic anhydride is used (with esahydrophthalic anhydride) as vulcanizer agent and in the production of epoxy resins. Finally, regarding fine chemistry, MA is hydrolyzed to maleic acid and fumaric acid, which are used as additives to adjust the acid flavour; further, MA is used for the production of aspartic acid, an intermediate of aspartame production.

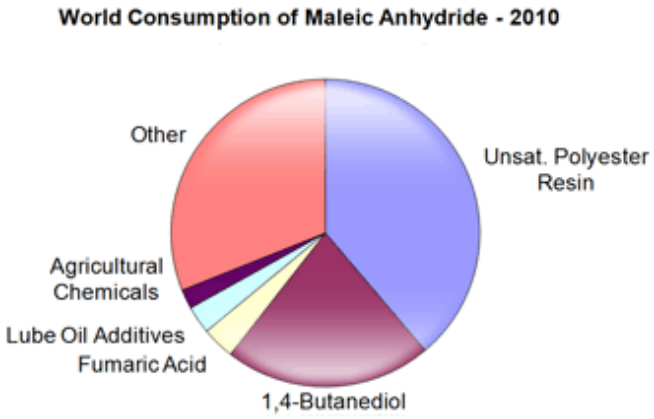

Fig.1.2_ World consumption of maleic anhydride (2010) [1b].

1.1.2 Maleic anhydride production

MA can be produced either by selective oxidation of n-butane or by selective oxidation of benzene. The reactor technology involves both fixed-bed and fluidized bed configurations, moreover it has been also developed a circulating fluidized bed, as discussed below.

For the selective oxidation of benzene, that is the older process developed for MA production, the reactor technology is a fixed bed configuration: the reaction occurs in the gas phase, at 400-450°C, in a multi tubular plug flow reactor. Catalyst (essentially a V/Mo mixed oxide) is deposed on an inert and high-conductive support (i.e. steatite) to permit a better heat removal, coming from the selective reaction but also from undesired reactions (total combustion of benzene and products).

At these conditions, benzene conversion is almost total (about 96%) and MA selectivity can reach 73%. Due to environmental regulations (limit emission in the atmosphere of 5μg/m^3) [4], the small quantity of unreacted benzene must be treated: adsorbed and recycled, or burned.

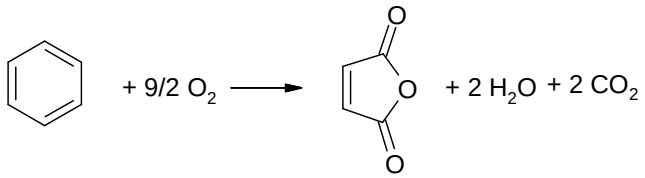

Fig.1.3_ Selective oxidation of benzene to MA.

The quantity of heat generated for this reaction is about -447 kcal/mol of benzene (fig.1.3)..

In the case of Polynt's process, the so-called High-Load-Technology is used, which allows operation up to 210 g/h/tube (2% mol. concentration) of benzene. The reaction gases are cooled down by means of gas coolers and crude MA is partially recovered by condensation and partially as maleic acid solution, in a water scrubber. Off gases leaving the scrubber, are sent to a catalytic incinerator. Pure MA is obtained in a distillation column operated batch wise [5].

Around 1970, emerged the possibility of using n-butane, instead of benzene, as reagent for MA production. The catalyst is a bulky mixed vanadium phosphorus oxide. The quantity of heat generated for this reaction is -300 kcal/mol of butane, lower than the oxidation of benzene, to MA (fig.1.4). The employed technologies regards both fixed or fluidized bed configurations, correspondently n-butane conversion varies from 53 to 65% and MA selectivity doesn't exceed 86% (see below).

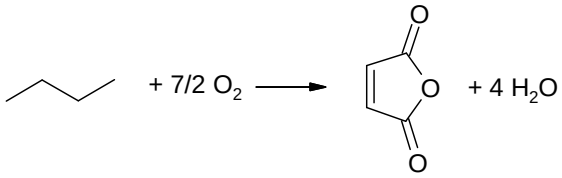

Fig.1.4_ Selective oxidation of n-butane to MA.

The use of *n*-butane instead of benzene involves many advantages:

1. lower cost of the reactant: n-butane is present in natural gas and also produced by steam cracking of oil;
2. better safety and lower environmental impact: benzene is a proven carcinogenic compound;
3. better atom economy ("E factor", ratio of waste mass per unit of product): for benzene oxidation two of the six C atoms are transformed to CO_2;
4. lower costs of MA separation and purification: starting from benzene some heavy compounds (such as benzoquinone and phthalic anhydride) form as by-products.

Nowadays, approximately 80% of MA is produced from *n*-butane, the remaining 20% is produced starting from benzene [3]: only a few smaller plants in Asia, Europe and in the U.S. continue to use benzene, due to rising and volatile benzene prices [1c].

The selective oxidation of n-butane to maleic anhydride is the most successful industrial example, of the use of an alkane, as the reactant, for the synthesis of a bulk chemical compound. This achievement was possible thanks to the discovery of an appropriate catalyst, the vanadyl pyrophosphate ($(VO)_2P_2O_7$), which boosted the development of reactor and process technologies. However, the n-butane to MA process still suffers of some disadvantages, which commonly regard alkane oxidation processes:

1. high amount of CO and CO_2, formed by parallel and consecutive combustion reactions of unreacted n-butane and products. The formation of these by-products, is favoured at the reaction temperature, consequently, n-butane conversion is maintained lower than 80%;
2. reaction highly exothermic: the run-away of the reaction must be avoided by rendering more efficient the heat removal;
3. process safety: flammable mixtures may be generated, consequently the gas composition must be controlled, maintaining the n-butane percentage lower than its correspondent flammability limit (except in the reactor) [3].

MA is produced from *n*-butane by different technologies: (1) fixed-bed (Scientific Design, Huntsman, BASF, Pantochim) or (2) fluidized-bed (Polynt, BP, Mitsubishi); the transported-bed (Circulating Fluidized Bed Reactor, CFBR) technology developed by DuPont, has been recently abandoned.

Table 1.3 summarizes the possible process technologies, which are distinguished by type of reactor, recover method of crude MA, gas phase composition, catalyst (synthesis, activation step, presence of promoters and regeneration).

Process	Type of reactor	Recover method	Gas phase composition
ALMA	Fluidized bed	Anhydrous	3.6-5% of n-butane in air
Mitsubishi	Fluidized bed	Aqueous	3.6-5% of n-butane in air
Sohio-UCB	Fluidized bed	Aqueous	3.6-5% of n-butane in air
Monsanto	Fixed bed	Anhydrous	1.8% of n-butane in air
Denka-Scientific Design	Fixed bed	Aqueous	1.8% of n-butane in air
DuPont	Transported bed (CFBR)	Aqueous	<4% of n-butane in air

Table 1.3_ Industrial technologies for MA production from n-butane [6, 7].

1) Fixed bed technology.

The reaction is carried out in a multi tubular reactor; the catalyst is loaded in pellets. The concentration of *n*-butane in feed has to be less than 1.85% mol (lower explosion limit). The outlet gas mixture is recovered in two different ways:

(i) absorption in water: MA hydrolyzes to the maleic acid, which is dehydrated at temperature below 130°C, to minimize the isomerization to fumaric acid; thus crude MA is purified by distillation under vacuum;

(ii) absorption in an organic solvent (i.e. o-xylene): in such way about 98% of the MA produced is recovered, avoiding fumaric acid formation.

Regardingn the Denka-Scientific Design process, 1.7% n-butane in air is fed to the fixed bed reactor, working at 390-400°C. The *n*-butane conversion is about 83%, with MA yield of 54%. The crude MA is recovered by adsorption in water; the formed maleic acid is distilled by means of azeotropic distillation in o-xylene, to obtain pure MA.

2) Fluidized bed technology.

The reactor technology permits:

1. absence of temperature hot-spots and of heat-removal problems, because of an uniform thermal profile, guaranteed by efficient dissipation of the reaction heat.
2. high productivity, due to the possibility of operating at high inlet concentration of n-butane (inside the explosion limits).

However there are also some drawbacks:

1. feed back-mixing, responsible for a decrease of MA selectivity;
2. high mechanical stress and abrasion phenomena regarding the catalyst,

To limit the abrasion of bulk catalyst particles, different techniques can be employed:

- impregnation of the active components on an inert support characterized by good fluidization properties and high attrition resistance;
- addition of additives to the precursor, to improve the mechanical resistance;
- encapsulation of the active phase in a silica structure.

One of the most advanced fluidized bed technology is the ALMA (Alusuisse Italia-Lummus Crest) process. The bulk VPO catalyst is spray-dried with a low amount of additives, to improve the mechanical resistance. The n-butane concentration in the feed is about 4% mol; conversion is typically 80-85%, with a molar yield to MA over 50%. [9].

Considering the ALMA process: n-butane and air are fed to a fluidized bed catalytic reactor to produce MA. Cooling coils are merged in the bed to generate high-pressure steam. In the recovery section, an organic solvent is used to remove the MA from the reaction effluent gas; a conventional absorption/stripping scheme is used. Crude MA is refined by continuous distillation to separate light compounds and heavy impurities. Tail gas is sent to an incinerator, which converts residual hydrocarbon (and CO) and the developed energy is recovered for producing extra steam [5].

3) Transported bed process.

The transported fluidized bed was developed by Monsanto and Du-Pont; it was working from 1996 to 2004, for tetrahydrofuran (THF) production. In 2005, the plant was shut down. Figure 1.8 shows the flow sheet of the Du-Pont process, which can be schematically divided into two parts: in the riser reactor only n-butane is fed (eventually diluted with an inert gas), here the catalyst converts by lattice oxygen the hydrocarbon to MA, being itself consequently reduced; the outlet stream contains both the reduced catalyst and the mixture of n-butane, CO_x and MA. The second part regards catalyst re-oxidation process: the catalyst is recovered by a cyclone and transported to the regenerator reactor, where solely air is fed to restore the oxidation state of the catalyst.

MA is recovered using water; after the hydrolysis, aqueous MA and maleic acid are reduced to tetrahydrofuran in a hydrogenation reactor. The peculiarity of this process is that it works in complete absence of oxygen in the feed; the oxygen used for the reaction is the lattice oxygen of the catalyst, the vanadyl pyrophosphate. The absence of oxygen in the feed avoids the formation of flammable mixtures and permit to work with high concentration of n-butane. The n-butane conversion is about 50%, with MA yield of about 37%. This technology has been operating with a new generation of catalyst, highly resistant to the attrition in the riser reactor.

The catalyst was coated by silica, which gives a very high mechanical resistance and does not cause any selectivity decreasing.

The fluidized bed consumes more of the n-butane feedstock, because of the lower selectivity to MA due to back-mixing phenomena, that favours the consecutive combustion of MA. Nevertheless, given the more efficient technology for heat recovery (that also allows production of high-pressure steam), the energy consumption is lower. In overall, the fluidized bed technology still consumes less energy than the fixed bed; moreover, working inside the flammable area (up to 5% mol. of n-butane) is possible. Although a slightly lower selectivity to MA, the technology permits improved productivity and lowers the cost of post-reactor treatment, because of the more concentrated streams [10].

1.2 CATALYTIC SYSTEM

1.2.1 Synthesis of vanadyl pyrophosphate

The catalyst used in industry for the selective oxidation of n-butane to maleic anhydride, is bulk vanadium-phosphorus mixed oxide, with a particular crystalline structure, the vanadyl pyrophosphate $(VO)_2P_2O_7$ [9, 11-13]. In the literature different preparation methods are reported, however it's possible to distinguish some common steps:

1. synthesis of catalyst precursor: $VOHPO_4 \cdot 0.5H_2O$ (VHP);
2. thermal decomposition of catalyst precursor;
3. catalyst forming;
4. catalyst activation.

Synthesis of the precursor: $VOHPO_4.0.5H_2O$

The precursor is obtained by the reduction of a V^{5+} compound (normally V_2O_5) to V^{4+} species, followed by addition of H_3PO_4). Regarding the catalyst precursor synthesis, we can distinguish at least three kind of preparation [1c]: the VPA, VPO and VPD routes. The VPA route is the precursor's synthesis made by using an aqueous reductant (as HCl or hydrazine) and it has been well explored in the past; whereas the VPO route is the synthesis with organic reductant (a single alcohol –generally isobutanol- or mixture of alcohols) and this is the most common preparation. The VPD route is the precursor's synthesis consisting in a two-step preparation: in the first one, the dihydrate vanadyl phosphate ($VOPO_4 \cdot 2H_2O$) formed, subsequently the organic reductant is added, to yield the precursor phase (VHP).

The VPA method is affected by two disadvantages: low surface area can be achieved (<10 m^2/g) and often, an impurity phase, $VO(H_2PO_4)_2$, also formed. For the VPO method, it's possible to obtain higher values of surface area and also a defective structure, which is interesting for improving catalyst performances: these aspects are a consequence of alcohols molecules, retained inside the VHP layers. The precursors samples obtained by VPO method are less crystalline and preferentially expose (001) planes, correspondent to (100) planes of

vanadyl pyrophosphate, which possess higher density of active sites [6, 15]. The VPD method is recently attracting attention: this method permits a good control of the precursor morphology and reports similar characteristics typically observed with catalysts prepared by VPO method.
However, the most common preparation of vanadyl orthophosphate hydrogen hemihydrate is carried out by VPO method, especially for industrial preparations, because active and selective catalysts are obtainable.
Nevertheless also preparations, carried out with different V and P sources, were reported in the literature [1c]: i) the use of V_2O_4, H_3PO_4 or $H_4P_2O_7$ in an autoclave at 145°C (hydrothermal synthesis); ii) the employ of NH_4VO_3, with oxalic acid and H_3PO_4, or iii) a mixture of VCl_3 and V_2O_5, or even iv) vanadium metal to reduce V_2O_5; finally, also v) V_4O_9 was utilized as a vanadium source.
The VPA and VPO routes differ by the kind of V_2O_5 reducing agent: in VPA method, the solid is solubilized by HCl or hydrazine, forming $VOCl_3$, which is subsequently reduced to V_2O_4 by the aqueous reductant; for VPO method, V_2O_5 is solubilized forming vanadium alcoholates, which are reduced by the organic solvent to V_2O_4. Thus, H_3PO_4 is added and reacts with V_2O_4, forming $VOHPO_4 \cdot 0.5H_2O$, at the liquid-solid interface.
For VPA preparation, the strong acid conditions don't permit precursor precipitation, thus the final compound is obtained by solvent evaporation, together with an amorphous phase, or after a crystallization process, adding water or by seeding (using hydrothermal conditions) [11, 16,17]. Finally, the VHP solid is obtained after filtration, washing and drying.

Thermal treatment of the precusor

Hemihydrate vanadyl acid orthophosphate is thermally treated to get the final catalyst, $(VO)_2P_2O_7$. Normally the thermal treatment is carried out using a two-step procedure:

1) drying of the precursor at low temperature (<300°C), to permit realising of organic molecules or chlorine ions, trapped inside the precursor's layers, but avoiding dehydration;
2) dehydration of the precursor; this step can be carried out using different methods:
    (i) dehydration inside the reactor, starting at low temperature (280°C), feeding lean reactant mixture at low residence time and subsequently, increasing all these parameters until reaching common reaction conditions; this procedure is carried out in about one day;
    (ii) dehydration under oxygen-free atmosphere at high temperature (>400°C) and then feeding the reaction mixture [19,20];
    (iii) calcination at high temperature (>400°C) and then feeding the reaction mixture [21, 22];
    (iv) hydrothermal treatment (first, the precursor is treated at 280°C under air and water, subsequently under nitrogen at 390°C).

Regarding the second step of the thermal treatment, the dehydration occurs realising two water molecules each VHP molecule [16]:

$$\mathbf{2\ VOHPO_4 \cdot 0{,}5H_2O \rightarrow 2\ VOHPO_4 + H_2O}$$

$$\mathbf{2\ VOHPO_4 \rightarrow (VO)_2P_2O_7 + H_2O}$$

The first dehydration leads to an amorphous or microcrystalline compound, having still typical functional groups of hemihydrate vanadyl acid orthophosphate. The second dehydration step involves the condensation of orthophosphate groups to pyrophosphate groups.

In the literature, different hypotheses have been proposed for the mechanism of transformation of the precursor into vanadyl pyrophosphate, however all agree considering that vanadyl pyrophosphate compound, finally obtained, retains the morphology of the precursor. This was demonstrated by XRD data [83], which showed a relation between the precursor and the catalyst: the structural (001) -basal planes- and (220) planes of the former are transformed, respectively, in the correspondent (200) –parallel to the basal planes- and (024) planes of the latter, maintaining further the same relative broadening. Bordes [23] proposed a topotactic transformation of $VOHPO_4 \cdot 0.5H_2O$ to $(VO)_2P_2O_7$, and supported the hypothesis by TEM and SEM analysis of the two compounds. This transformation consists in a structural conversion, in which V-O and P-O bonds remain unaltered, while weak V-H_2O, e P-H_2O are broken: a couple of HPO_4 unit condense into pyrophosphate groups.

The physical and chemical characteristics of the final catalyst are affected by several different parameters:

- temperature, time and atmosphere of treatment;
- precursor morphology;
- P/V ratio;
- presence of additives;
- presence of structural defects;

Due to all these parameters, a variety of crystalline V/P/O phases may be present in fresh catalyst composition or may even be prepared as pure compounds; moreover these parameters influence catalyst composition during reaction, as well. For this reason there's still a debate regarding the real active phase, being pure vanadyl pyrophosphate or a combinations of V/P/O phases.

One of the most important catalyst characteristics, at the end of the thermal treatment, is the V oxidation state. Even though vanadium is present as V^{4+} in stoichiometric vanadyl pyrophosphate, the V/P/O obtained by thermal treatment of the crystalline precursor $VOHPO_4 \cdot 0.5H_2O$, could contain crystalline and amorphous vanadium phosphates other than $(VO)_2P_2O_7$ [24, 25]. These additional or spurious phases may contain V^{5+} or even V^{3+}, and the relative amount of each compound is a function of (i) the procedure employed for the preparation of the precursor, and (ii) the thermal treatment adopted for the transformation of

the precursor. Furthermore, the VPP itself may host V ions other than V^{4+} as defects, without undergoing substantial structural changes [26-28]. Outer surface layers of V^{5+} phosphates may develop in the reaction environment, and play active roles in the catalytic cycle.

Activation under reaction mixture

Activation (or equilibration) of the catalyst is obtained leaving the catalyst under reaction mixture at 400°C for several hours: generally 100 hours are necessary to get stable performances. During this period changes occur both in the catalytic performances, either in the catalyst chemical-physical features: the (001) plane, which is considered to be the most selective for MA formation, increases and correspondently, the MA selectivity. The "fresh" catalyst is referred as "equilibrated", after this period. A "reduced" catalyst containing only V^{4+}, needs a longer equilibration period (200-300h), while in the case of an "oxidized" sample containing also V^{5+} at least 500 hours are necessary to complete the transformation and obtain the vanadyl pyrophosphate.

In an equilibrated catalyst the average oxidation state of vanadium is 4.00-4.04, the specific surface area is about 16-25 m^2/g and the P/V ratio is higher than 1.0 [6]. During the activation step, the catalytic activity decreases, while the yield to MA increases, due to the increase of selectivity. The fresh catalyst is normally more active than the equilibrated one, because the V^{4+} easily oxidizes to V^{5+} [29].

1.2.2 The P/V ratio

The optimal catalytic performance of vanadyl pyrophosphate is obtained when the catalyst contains a slight excess of phosphorus (instead of the stoichiometric P/V 1.1 ratio in the compound), which limits the oxidation of V^{4+} in $(VO)_2P_2O_7$. Generally, on the catalyst surface, the P/V ratio is higher than in the bulk. A low P/V ratio leads to a catalyst active but not selective [6]; the different performances can be attributed to the oxidation state of V. In fact, it has been demonstrated that in catalysts having a lack of phosphorus (P/V=0.95) the oxidation takes place easier than in samples with a P/V ratio higher than 1.0.

1.2.3 The role of the different V species

The oxidation state of V in VPP under working conditions, and the role of V species having different oxidation states, have been debated for several years. The importance of having a defined amount of V^{5+} in order to obtain better selectivity has been pointed out by Volta and co-workers, with the optimal V^{5+}/V^{4+} ratio being equal to 0.25 [30-34]. Evidences of the V^{5+} role have been reported by other authors as well [24, 35-36]. Isolated V^{5+} sites, in strong interaction with the VPP, provide the optimal surface concentration of sites which permit the alkane activation and O-insertion; however, the formation of bulk $VOPO_4$ is detrimental for selectivity. Bordes [23] reported that apparently two opposite conditions are necessary to transform n-butane into MA: the activation of n-butane by oxygen associated with V^{4+} species and the incorporation of oxygen associated to V^{5+} species, consequently, to get MA.

It's worth to note that the selectivity to MA is given by V^{5+} species which are isolated, as during oxidation treatments, the development of micro-domains of V^{5+} leads rather to a decrease, of MA selectivity [32-33].

Regarding the role of V^{3+}, there's more debate however it is clear that the generation of V^{3+}/P/O compounds is negative for selectivity and the generation of a discrete number of these species in the lattice of the VPP, further the associated anionic vacancies, have been proposed to play a positive role on catalytic activity [37-38]. V^{3+} defects are generated during the thermal treatment of the precursor, and their concentration is function of the amount of organics retained in the precursor, and of the nature of the heat treatment carried out, for the transformation of the precursor into the active catalyst [40].

The V^{4+}/V^{5+} ratio in VPP under working conditions is function of reaction conditions, that is the gas-phase composition. Mallada et al. [41] investigated the effect of reducing (hydrocarbon-rich) and oxidizing (hydrocarbon-lean) conditions on the oxidation level of the catalyst. In the former case, V^{3+}/P/O surface phases developed, which are detrimental for the selectivity to MA. At the same time, substantial amounts of C deposits are accumulated on the catalyst, in the fraction of catalytic bed, which was operating under low oxygen partial pressure. The same conclusions were reached by Volta et al. [42]: the reduction of V^{5+} and the formation of C deposits are responsible for the decrease of the selectivity to MA. However, the deactivation is not so rapid when the catalyst is pre-oxidized at mild temperature. One way to overcome these limitations is to add promoters, which helps to maintain a higher V oxidation degree, probably through the formation of specific compounds, or through a mediation of V re-oxidation in the redox mechanism. Also the catalyst morphology was found to be an important parameter under hydrocarbon-rich conditions, more than under leaner conditions [43]. The rose-petals-like morphology gives the most active and selective catalyst, thanks to the higher V reducibility and re-oxidability as compared to VPP having a different morphology.

1.2.4 The role of amorphous material

In a recent review, Hutchings et al. [1c] reported an interesting discussion about the role of amorphous compound over VPP catalyst surface. The literature analysis regards different contributions: for example comparing different prepared VPP catalysts (employing VPA, VPO and VPD synthetic routes) it was found that all catalyst showed similar specific activities, regardless their effective morphological differences. This results leads to reconsider what is supposed to be the real active phase, the bulk or an amorphous overlayer on VPP surface. Indeed, other authors reported evidences of the presence of an amorphous layer (2 nm thick) covering (100) planes of fresh VPP catalyst, disappearing after equilibration. Oppositely H. Bluhm.et al. [120] using HRTEM images, reported evidences of a non-crystalline layer (ca. 1 nm thick) developed on surface of VPP not yet equilibrated, which was constituted by V_xO_y units, the growth of which is hindered by phosphates units. Furthermore, it is also known that an amorphous compound is formed during activation in reactive mixture, of the precursor (<400°C) and this results also in MA formation. Finally, the presence of an amorphous layer

could be favoured by the presence of a dopant (e.g. with Co). All these findings clearly show the difficulty to establish the real active phase, developed during reaction conditions, over VPP surface.

1.2.5 Recent developments to improve the catalytic system

Best catalytic performances reported in literature range from 53 to 65% molar yield to MA [6, 11, 56-59], with a conversion of *n*-butane not higher than 85-86%. The best performance for a fixed-bed reactor does not exceed 65% per-pass yield, while that in a fluidised-bed is typically lower due to back-mixing phenomena.

It is known that the maximum yield to MA is limited by: i) parallel reactions of n-butane combustion and of oxidative degradation to acetic and acrylic acids, as well as ii) consecutive reactions of combustion, relevant when the alkane conversion reaches 70-80%. This has been attributed to the development of local catalyst overheating, cosidering the high reaction exothermicity, and to the poor heat-transfer properties of the catalytic material.

To overcome these problems, different possibilities can be carried out:

1. use of highly heat-conductive supports for VPO, in order to better distribute the reaction heat and develop more homogeneous particle temperatures;
2. addition of specific dopants to modify the redox and acid-base properties of the active phase or the development of new procedures for the preparation of the catalyst that allow a modification of the chemical-physical or morphological features of the precursor;
3. development of new catalytic systems.

1) Supported systems

In the case of vanadyl pyrophosphate, the support should have other features:

1. good mechanical properties, to improve attrition resistance of the catalyst;
2. not very high specific surface area, to avoid high residence time of reactants inside catalyst pores;
3. chemical inertia not only to *n*-butane and oxygen, but also to the active phase, to avoid changes in its morphology.

Following are summarized the main characteristics of supported VPO catalysts [44].

VPO supported on TiO_2

The precipitated VPO phase was amorphous and well-dispersed over the surface of the support; the surface of P/V 1.1 supported catalysts resulted enriched in phosphorus (P/V=1.2-3) similar to the bulk VPO catalyst (typically, P/V=1.1-1.7). The supported VPO showed activity and selectivity in *n*-butane oxidation at temperatures 100°C lower than commercial VPO catalysts. Overbeek at al. [45,46] shows that the activity of titania-supported VPO catalysts is related to several characteristics:

- high surface area,
- strong interaction of the VPO component with the titania support,
- different reducibility of VPO on TiO_2,
- different average oxidation state of vanadium ions on the surface.

Ruitenbeek et al. [47] observed no changes in average vanadium oxidation state during equilibration, since they concluded that the lattice VPO oxygen species was not involved in *n*-butane oxidation and the reaction does not follow the Mars van Krevelen mechanism.

VPO supported on SiO_2

The VPO component in the silica-supported catalysts was well dispersed, but interacted weakly with the support surface as compared to the titania-supported system. In contrast to this latter system, the silica-supported VPO catalysts were less active, but more selective to MA. The lower catalytic activity of the silica-supported system was attributed to the non-reducible nature of silica support. However, the higher surface P/V ratios found in the silica-supported catalysts as compared to the titania-supported systems, may also be responsible for lower activity in *n*-butane oxidation and higher selectivity to maleic anhydride at high conversion in these catalysts [46].

VPO supported on Al_2O_3

The high affinity between Al and P limited the dispersion of VPO phase on the support and consequently catalysts obtained showed poor catalytic performances [48].

VPO supported on $AlPO_4$

The most used type of $AlPO_4$ was trydimite; in this case the main VPO phase is present as vanadyl pyrophosphate. The supportation of VPO on $AlPO_4$ improves both catalytic performances and activation time of the catalyst. Very high conversion (90%) and MA selectivity (42%) are reached and the activation time is lower (20h instead of the classical 100h, necessary for the bulk VPO) [49-51].

Highly-heat-conducting supports

Ledoux et al. studied the use of heat-conducting supports (β-SiC, thermal conductivity 14-270 W m^{-1} K^{-1}, Si_3N_4, 6 W m^{-1} K^{-1}, and BN, 31 W m^{-1} K^{-1}) for the VPP [52,53]. These materials possesses relatively high surface area (e.g., for β-SiC, >20 m^2/g, prepared via the "shape memory synthesis"), consequently this renders them useful supports for catalysts for exothermal oxidation reactions [54]. In fact, the heat transfer at catalyst surface is more controlled and this permits a significant gain in MA yield. Moreover, the chemical inertness of the support did not modify the reactivity properties of the precursor and of VPP, which instead is what happens with conventional supports [55]. In the case of the β-SiC-supported VPO (30 wt.% of active phase), the selectivity to MA at high *n*-butane conversion was higher than that obtained with the unsupported catalyst; furthermore, when hydrocarbon rich conditions were used (e.g., O_2/n-butane feed ratio 3.2, with 11 mol.% n-butane), it was obtained a conversion of 72% with a MA yield of 54%, at 485°C. This represents the best result ever reported in n-butane oxidation under hydrocarbon-rich conditions.

2.1) Addition of specific dopants

In the literature a lot of papers have been devoted to the study of the dopant effect of VPP [60-63], and still there is interest about this topic, in fact a more profound knowledge of the chemical physical properties of the VPP has made possible a better comprehension of the role of some known dopants (Co, Fe, Bi [64-72] and Nb [73-77]). Table 1.4 summarizes some important VPP dopants, recently studied, together with their effect and the reason of it.

Dopant, optimal amount	Promotional effect	Reasons for promotion
Co, Co/V 0.77%	C: 15 → 25% S: 0 → 11% under hydrocarbon-rich conditions	Control of the optimal V^{5+}/V^{4+} surface ratio; stabilization of an amorphous Co/V/P/O compound
Co, Co/V 13%	C: 55 → 79% S: 43 → 35% at 653K	Optimal surface Lewis acidity
Ce+Fe	C: 44 → 60% S: 63 → 66% in absence of O_2	Improvement of redox properties
Fe, Fe/V 0.08	Increase of catalytic activity	Fe replaces V^{4+} in $(VO)_2P_2O_7$ Re-oxidation rate is increased
Ga, Ga/V 0.10	C: 22 → 73% S: 55 → 51%	Increase of surface area + increase of intrinsic activity (electronic effect)
Nb, 0.25 wt%	C: 20 → 17% S: 35 → 53%	Increase of surface acidity promotes desorption of MA
Nb, Nb/V 0.01	C: 58 → 75% S: 70 →70%	Nb concentrates at the surface, where defects are generated. Nb acts a n-type dope; development of a more oxidized surface

Table 1.4_ Dopants for VPP catalyst: C= conversion and S = selectivity, for un-doped catalyst (left values, 2°column) and for doped catalyst in standard reaction conditions (right value, 2°column) [78].

2.2) Modifications of VPP chemical-physical properties

Methods to modify the preparation procedure, to get catalysts with improved performances, include:

a) Preparation of the precursor in the presence of glycols (1,2-etandiol, 1,3-propandiol, 1,4-butandiol). This method affects the morphology of the precursor [15,79] because the molecules can be trapped in the interlayer spacing of the precursor [80,71]. Increasing amounts of retained organic compounds disturb the stacking of crystallographic planes along the c direction: only [hk0] reflections remain sharp for the higher C contents, while a different aspect ratio is finally obtained and consequently, also a different crystal morphology (confirmed by SEM micrographs). In this regard, the thermal treatment influences the final VPP morphology [82]. Moreover, the organics retained in defined amounts in the precursor, may lead to a controlled defectivity in the final VPP [15], with a limited number of V^{3+} species. This method lead to catalysts with higher activity [79].

b) Tribomechanical (ball-milling) activation of the precursor or of the VPP [83-85]. Ball milling of the precursor is carried out with the aim of increasing the surface area by reducing particle size; this results in higher catalyst activity [86]. However, as the process involves the generation of high energy, lattice imperfections are introduced and these defects are transferred to the VPP, and finally affect catalytic performance [87]. This leads to an improvement of the activity and selectivity.

c) Intercalation of layered $VOPO_4 \cdot 2H_2O$ with various compounds (e.g., alcohols and amines), followed by exfoliation in polar solvents to delaminated sheets; finally, impregnation of silica with the previous solution [88-90]. The same procedure can be adopted to reduce the $VOPO_4 \cdot 2H_2O$ into $VOHPO_4 \cdot 0.5H_2O$ [91,92], to obtain a high-surface-area precursor, and finally a VPP more active and selective in comparison with the standard preparation (60% conversion, 78% selectivity at 390°C) [90]. Dispersion of VPP inside or over high-surface-area silica was also tried by other researchers, without obtaining active catalysts [93-95].

d) Preparation of an amorphous, microspheroidal VPO catalyst using supercritical CO_2 as an antisolvent [96,97]. The amorphous compound demonstrated higher activity compared to standard preparation but a maximum MA yield of only 7%.

e) Preparation of mesostructured VPO phases and of VPO/surfactant composites [98-103]. Guliants et al. described the preparation of microporous mesostructured VPO, with surfactants as structure-directing agents, and optimised the thermal treatment and template removal. They obtained systems with high surface area but, although a good MA selectivity was reached at low temperature, when increasing the n-butane conversion, being these systems unstable under reaction conditions, it resulted finally in a decrease of MA selectivity.

3) New catalysts for *n*-butane oxidation

Recently it has been reported that the pyridine salt of Nb-exchanged molydo(vanado)phosphoric acid is the precursor of a catalyst, mostly consisting of amorphous molybdenum oxide, which is active and selective in the oxidation of propane to acrylic acid and of n-butane to maleic anhydride [104-106]. The authors found that key-properties to achieve good catalytic performance are (i) the development of reduced Mo^{5+} and Nb^{4+} species, that are stable when hydrocarbon-rich reaction conditions are used, and (ii) the contemporaneous presence of P, Nb and pyridine in the polyoxometalate (pyridine reduces Mo^{6+} during the thermal treatment). Catalysts are active under both n-butane-rich (15% of conversion with 90% of MA selectivity, at 380°C, as best results) and n-butane-lean conditions (62% of conversion with 46% of MA selectivity, at 340°C, as best results).

1.3 REACTION SCHEME AND MECHANISM

1.3.1 Reaction scheme

The study of the reaction mechanism is quite difficult, due to the absence of by-products, which can give information about reaction intermediates and also, due to the fact that generally, the latter do not desorb from catalyst surface. The most proposed reaction scheme is represented in Figure 1.5, as inferred from some experimental evidences, n-butane is transformed into MA through sequential steps of oxidative dehydrogenation, oxidation and oxygen insertion [6,11,107]:

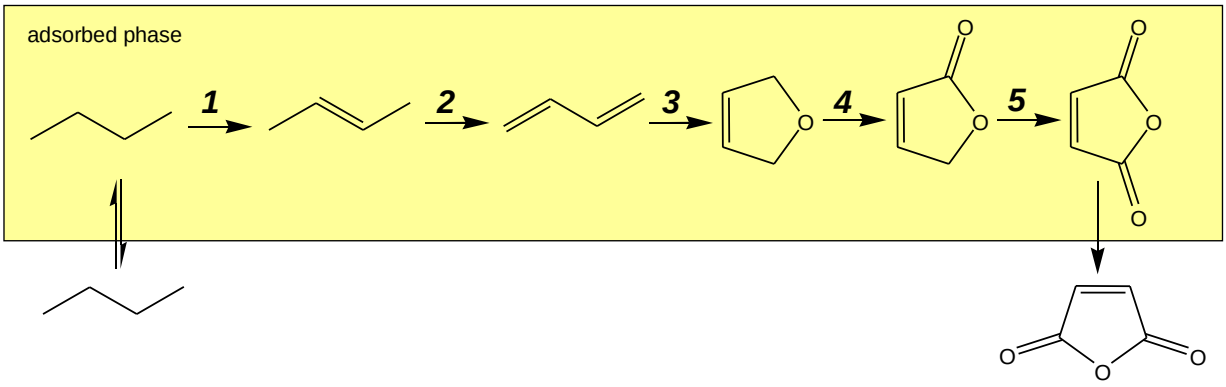

1) *n*-butane + 1/2 O_2 → butenes + H_2O
(oxidative dehydrogenation)

2) butenes + 1/2 O_2 → butadienes + H_2O
(allylic H extraction)

3) butadienes + 1/2 O_2 → 2,5-dihydrofurane
(1,4-oxygen insertion)

4-5) 2,5-dihydrofurane +2 O_2 → AM + 2 H_2O
(o-allylic insertion lactone mediated)

6a) 2,5-dihydrofurane + 1/2 O_2 → furan + H_2O
(allylic extraction)

6b) furan + 3/2 O_2 → AM + H_2O
(electrophilic oxygen insertion)

Fig.1.5_ Reaction scheme.

The proposed mechanism was confirmed by isolation of some intermediates at unusual reaction conditions (such as under high butane/oxygen ratio or at low residence time) [108-110]. Moreover n-butene, butadiene and furan were identified by Kubias et al. [35] under vacuum conditions.

It is also known, that olefinic intermediates are the first products in all C_3-C_5 alkane oxidation reactions to the corresponding oxidized compounds [109]. The rate determining step is the

oxidative deydrogenation of n-butane to butenes. To obtain high MA selectivity, the rate of the oxidative dehydrogenation reaction has to be higher than the one of oxygen insertion, that is favouring the butadiene formation instead of other reactive molecules, such as crotonaldehyde, methylvinylketone, precursors of CO_X.
New recent information are obtained by *in-situ* IR measurements; studying the molecules adsorbed on the catalytic surface during the reaction [111]. Different molecules were fed (1-butene, 1,3-butadiene, furan, maleic anhydride) and the adsorbed species on VPO were studied: at low T (<100°C) n-butane is activated by VPO and forms unsaturated compounds (butenes and 1,3-butadiene).

However, recent computational calculations revealed that 1-butene does not interact with VPO and could not be a reaction intermediate [112-115].

1.3.2 Reaction mechanism

The selective oxidation of butane follows the Mars Van Krevelen mechanism, as the catalytic cycle can be divided in two steps. In the first step, the "reduction" one, lattice oxygen atoms of the catalyst are involved in the oxidation of n-butane and V^{4+} ions of vanadyl pyrophosphate are reduced to V^{3+}. In the subsequent step, the "oxidation" one, molecular oxygen permits the re-oxidation of V^{3+} ions to V^{4+} and forms O^{2-} ions, which are incorporated in the structural vacancies generated during the reduction step. In particular 7 O^{2-} ions are employed: four are used to co-produce water while the remaining three are inserted in the n-butane molecule, considering a total transfer of 14 electrons, to form AM.
The catalytic cycle is here represented:

$$\textit{reduction}: \quad \text{R-CH} + 2\text{KO} \rightarrow \text{R-C-O} + \text{H}_2\text{O} + 2\text{K}$$

$$\textit{oxidation}: \quad 2\text{K} + \text{O}_2(\text{gas}) \rightarrow 2\text{KO}$$

where R-CH e R-C-O are respectively, the reactant and the products, while KO e K are the oxidised and reduced form of the catalysts.
Recently, Hodnett and coworkers [112-115] have demonstrated, studying the electronical properties of VPO using the DFT method, that the superficial V is only a chemisorption site, while the nucleophil oxygen atoms of terminal P-O are selective in the oxy-functionalization of n-butane.

1.3.3 Nature of active sites

The catalyst has to own active sites for the activation of the paraffin and for subsequent redox reactions, to get MA, but also a proper acidity to quickly desorb the product, avoiding over-oxidation reactions [18].
VPO catalyst shows all the necessary multifunction properties and correspondent active sites, necessary to transform n-butane into MA [116,117], which are resumed in Table 1.5.

Nature of active sites on $(VO)_2P_2O_7$ surface
Lewis acidic sites
Bröensted acidic sites
Redox couple with one electron: V^{5+}/V^{4+}, V^{4+}/V^{3+}
Redox couple with two electrons: V^{5+}/V^{3+}
Bridged oxygen in the groups V-O-V e V-O-P
Terminal oxygen in the groups $(V=O)^{3+}$, $(V=O)^{2+}$
Adsorbed molecular oxygen: species η^1-peroxo and η^2-superperoxo

Table 1.5_ Active sites in vanadyl pyrophosphate.

Acid Lewis sites: the Lewis acid sites are attributed to the presence of V ions coordinatively unsatured in the VPP (100) planes and are identified by FT-IR absorption of basic probe molecules. The most part of acid sites are Lewis acid sites (quite twice respect to the Bröensted ones) which permit the H-abstraction from n-butane [6].

Bröensted acid sites: they were identified by FT-IR spectroscopy and correspond to P-OH groups in the terminal position. These sites belong to P-O bonds broken in terminal position in the phosphorus tetrahedra.
The main functions of these surface P-OH groups are [6, 118]:

- facilitate the H removal, favouring the H shift toward the H_2O formation and desorption sites;
- facilitate maleic anhydride desorption avoiding total oxidation;
- activate the C-H bonds.

V^{5+}: the amount of V^{5+} at the surface, may vary from 20 to 100%, depending on different parameter (preparation, thermal treatment, dopants, reaction atmosphere). This specie is active in the oxygen insertion of activated paraffins and leads to oxidized compounds, in particular to MA but also to CO_x. Thus, a defined amount of V^{5+} is necessary to improve activity, but an excess of oxidized V is detrimental for selectivity. Volta e al. have demonstrated that the best performances are obtained when the V^{5+}/V^{4+} ratio is about 0,25 [29,31-34].

V^{4+}: this specie is responsible for butane activation. The specie $(V=O)^{2+}$, in correspondence of the cleavage of layer (100), is involved in the H-extraction from n-butane and in the allylic oxidation [6]. Ebner and Thompson [20] suggested that V^{4+} species are involved in the oxygen insertion reaction on butadiene with the formation of the 5-elements ring compounds.

V^{3+}: their role is difficult to be clarified; the formation of V^{3+}/P/O compounds is detrimental for the VPO selectivity, small amount of V^{3+} (and its associated anionic vacancies) could be positive for the catalytic activity [26-28, 39].

V-O-P: are involved in the oxidative dehydrogenation of activated n-butane (and adsorbed butadienes) to butadiene, moreover they play a role in the oxygen insertion reaction on the 5-elements ring compounds.

Adsorbed molecular oxygen: the adsorbed molecular oxygen is a non-selective specie, because it forms nucleophilic species, which lead to over-oxidation reactions. Molecular oxygen is absorbed in two different ways: it could form the η^1-superoxo species and the η^2-peroxo species; these species can interact with the V=O group, thus activating n-butane [119].

1.4 REFERENCES

[1] Ulmann's Chemical Encyclopedia, Vol A16, 54 (2011); b) www.chemical.ihs.com/WP/Public/Reports/ma ; c) N. F. Dummer, J. K. Bartley, G. J. Hutchings, Adv. Catal. 54 (2011) 189; d) www.southalabama.edu/chemistry/barletta/felthouse.pdf .

[2] MSDS of Maleic Anhydride.

[3] Tecnon Orbichem, London SW11 3TN, UK.

[4] For Italy: Decreto Ministeriale n°60, 2nd April 2002.

[5] www.polynt.com .

[6] F. Cavani, F. Trifirò, Chem. Tech., 24 (1994) 18.

[7] G. Centi, F. Cavani, F. Trifirò, Selective Oxidation by Heterogeneous Catalysis, Kluwer Academic, 2001.

[8] Meyers, Handbook of chemicals production processes, McGraw-Hill

[9] P. Arpentier, F. Cavani, F. Trifirò, The Tecnology of Catalytic Oxidation, Technip, 2001.

[10] BRIDGES to Sustainability, "A Pilot Study of Energy performance Levels for the U.S. Chemical Industry", report ot the U.S. Department of Energy, June 2001. Available at http://www.bridgestos.org/Publications.htm

[11] G. Centi, F. Trifirò, J. R. Ebner and V. Franchetti, Chem. Rev., 88 (1988) 55.

[12] F. Cavani, F. Trifirò, Appl. Catal. A, 88 (1992) 115.

[13] R. M. Contractor, A. W. Sleight, Catal. Today, 3 (1988) 175.

[14] C. C. Torardi and J. C. Calabrese, Inorg. Chem., 23 (1984) 1308.

[15] S. Albonetti, F. Cavani, S. Ligi, F. Pierelli, F. Trifirò, F. Ghelfi, G. Mazzoni, Stud. Surf. Sci. Catal. 143, 963 (2002).

[16] F. Cavani, A. Colombo, F. Giuntoli, F. Trifirò, P.Vazquez, P. Venturoli, "Advanced Catalysis and Nanostructured Materials", W.R. Moser (Ed.), Academic Press, (1996), page 43.

[17] M. Meisel, G. U. Wolf, A. Bruckner, Proceed. DGMK Conference on "Selective Oxidations in Petrolchemistry", M. Boerus and J. Wertkamp (Eds.), Tagungsbericht, 1992, page 27.

[18] F. Cavani, F. Trifirò, 3rd World Congress on Oxidation Catalysis, R. K. Grasselli, S. T. Oyama, A. M. Gaffney and J. E. Lyons (Edt.), (1997) 19.

[19] J. W. Johnson, D. C. Johnston, A. J. Jacobson, J. F. Brody, J. Am. Chem. Soc., 106 (1984) 8123.

[20] M. R. Thompson, J. R. Ebner in P. Ruyiz, B. Delmon (Eds.) "New Developments in Selective Oxidation by Heterogeneous Catalysis", Elsevier, Amsterdam, 1992, page 353.

[21] L. M. Cornaglia, C. Caspani, E. A. Lombardo, Appl. Catal., 15 (1991) 74.

[22] R. M. Contractor, J. R. Ebner, M. J. Mummey in "New Developments in Selective Oxidations", G. Centi and F. Trifirò (Eds.), Elsevier Science, Amsterdam, 1990, page 553.

[23] E. Bordes, Catal. Today, 16 (1993) 27.

[24] S. Albonetti, F. Cavani, F. Trifirò, P. Venturoli, G. Calestani, M. Lopez Granados, J.L.G. Fierro, J. Catal., 160 (1996) 52.

[25] S. Albonetti, F. Budi, F. Cavani, S. Ligi, G. Mazzoni, F. Pierelli, F. Trifirò, Stud. Surf. Sci. Catal., 136 (2001) 141.

[26] P.L. Gai, K. Kourtakis, Science, 267 (1995) 661.

[27] F. Cavani, S. Ligi, T. Monti, F. Pierelli, F. Trifirò, S. Albonetti, G. Mazzoni, Catal. Today 61 (2000) 203.

[28] P.T. Nguyen, A.W. Sleight, N. Roberts, W.W. Warren, J. Solid State Chem. 122 (1996) 259.

[29] F. Cavani and F. Trifirò, In Preparation of Catalysis VI, G. Poncelet et al. edt (1995).

[30] G.J. Hutchings, A. Desmartin-Chomel, R. Olier, J.C. Volta, Nature, 368 (1994) 41.

[31] M. Abon, K. Béré, A. Tuel, P. Delichere, J. Catal., 156 (1995) 28.

[32] K. Ait-Lachgar, M. Abon, J.C. Volta, J. Catal., 171 (1997) 383.

[33] K. Ait-Lachgar, A. Tuel, M. Brun, J.M. Herrmann, J.M. Krafft, J.R. Martin, J.C. Volta, J. Catal., 177 (1998) 224.

[34] G.J. Hutchings, C.J. Kiely, M.T. Sananes-Schulz, A. Burrows, J.C. Volta, Catal. Today, 40 (1998) 273.

[35] U. Rodemerck, B. Kubias, H.W. Zanthoff, M. Baerns, Appl. Catal., 153 (1997) 203.

[36] U. Rodemerck, B. Kubias, H.W. Zanthoff, G.U. Wolf, M. Baerns, Appl. Catal., 153 (1997) 217.

[37] G.W. Coulston, S.R. Bare, H. Kung, K. Birkeland, G.K. Bethke, R. Harlow, N. Herron, P.L. Lee, Science, 275 (1997) 191.

[38] P.L. Gai, K. Kourtakis, D.R. Coulson, G.C. Sonnichsen, J. Phys. Chem. B, 101 (1997) 9916.

[39] P.L. Gai, Topics Catal., 8 (1999) 97.

[40] F. Cavani, F. Trifirò, in "Basic Principles in Applied Catalysis", M. Baerns (Ed.), Springer-Verlag, Berlin, (2004) 21.

[41] Mallada, S. Sajip, C.J. Kiely, M. Menendez, J. Santamaria, J. Catal., 196 (2000) 1.

[42] S. Mota, M. Abon, J.C. Volta, J.A. Dalmon, J. Catal., 193 (2000) 308.

[43] Y. Kamiya, E. Nishikawa, T. Okuhara, T. Hattori, Appl. Catal. A, 206 (2001) 103.

[44] V.V. Guliants, Catal. Today, 51 (1999) 255.

[45] R.A. Overbeek, P.A. Warringa, M.J.D. Crombag, L.M. Visser, A.J. van Dillen, J.W. Geus, Appl. Catal. A 135 (1996) 209.

[46] R.A. Overbeek, A.R.C.J. Pekelharing, A.J. van Dillen, J.W. Geus, Appl. Catal. A 135 (1996) 231.

[47] M. Ruitenbeek, R.A. Overbeek, A.J. van Dillen, D.C.Koningsberger, J.W. Geus, Recl. Trav. Chim. Pays-Bas 115 (1996) 519.

[48] M. Nakamura, K. Kawai, Y. Fujiwara, J. Catal. 34 (1974) 345.

[49] S. Holmes, L. Sartoni, A. Burrows , V. Martin , G.J. Hutchings , C. Kiely , J.C. Volta, Stud. Surf. Sci. Catal.,130 (2000) 1709.

[50] P.S. Kuo, B.L. Yang, J. Catal., 117 (1989) 301.

[51] L. Sartoni, J.K. Bartley, R.P.K. Wells, A. Delimitis, A. Burrows, C. Kiely , J.C. Volta, G.J. Hutchings , J. of Mater. Chem., 15(40) (2005) 4295.

[52] C. Bouchy, M.J. Ledoux, C. Crouzet, H. Baudouin, K. Kourtakis and J.J. Lerou, WO 62,925 (2000).

[53] M.J. Ledoux, C. Crouzet, C. Pham-Huu, V. Turines, K. Kourtakis, P. Mills and J.J. Lerou, J. Catal. 203 (2001) 495.

[54] M.J. Ledoux, S. Hantzer, C. Pham-Huu, J. Guille and M.P. Desanaux, J. Catal. 114 (1998) 176.

[55] R.A. Overbeek, P.A. Warringa, M.J.D. Crombag, L.M. Visser, A.J. van Dillen and J.W. Geus, Appl. Catal. A 135 (1996) 209.

[56] F. Cavani and F. Trifirò, Stud. Surf. Sci. Catal. 91 (1995) 1.

[57] J. Weiguny, S. Storck, M. Duda and C. Dobner, US Patent 222,436 (2005), assigned to BASF AG.

[58] I. Sawaki, Eur. Patent 1,359,138 (2003), assigned to Mitsubishi Chem Co.

[59] H. Hibst, R. Noe, M. Exner Kai and M. Duda, Eur Patent 1,417,194 (2004), assigned to BASF AG.

[60] G.J. Hutchings, Appl. Catal. 72 (1991) 1.
[61] F. Cavani and F. Trifirò, Catalysis 11 (1994) 246.
[62] B.K. Hodnett, Catal. Rev. Sci. Eng. 27 (1985) 373.
[63] G.J. Hutchings and R. Higgins, J. Catal. 162 (1996) 153.
[64] M. Abon, J.M. Herrmann and J.C. Volta, Catal. Today 71 (2001) 121.
[65] S. Mota, J.C. Volta, G. Vorbeck and J.A. Dalmon, J. Catal. 193 (2000) 319.
[66] S. Sajip, J.K. Bartley, A. Burrows, M.T. Sananes-Schulz, A. Tuel, J.C. Volta, C.J. Kiely and G.J. Hutchings, New J. Chem. 25 (2001) 125.
[67] S. Sajip, J.K. Bartley, A. Burrows, C. Rhodes, J.C. Volta, C.J. Kiely and G.J. Hutchings, Phys. Chem. Chem. Phys. 3 (2001) 2143.
[68] L. Cornaglia, S. Irusta, E.A. Lombardo, M.C. Durupty and J.C. Volta, Catal. Today 78 (2003) 291.
[69] L.M. Cornaglia, C.R. Carrara, J.O. Petunchi and E.A. Lombardo, Catal. Today 57 (2000) 313.
[70] L. Cornaglia, C. Carrara, J. Petunchi and E. Lombardo, Stud. Surf. Sci. Catal. 130 (2000) 1727.
[71] C. Carrara, S. Irusta, E. Lombardo and L. Cornaglia, Appl. Catal. A 217 (2001) 275.
[72] Y.H. Taufiq-Yap, K.P. Tan, K.C. Waugh, M.Z. Hussein, I. Ramli and M.B. Abdul Rahman, Catal. Lett. 89 (2003) 87.
[73] R. Higgins and G.J. Hutchings, US Patent 4,418,003 (1983), assigned to ICI.
[74] I. Matsuura, T. Ishimura, S. Hayakawa and N. Kimura, Catal. Today 28 (1996) 133.
[75] V.V. Guliants, J.B. Benziger, S. Sundaresan and I.E. Wachs, Stud. Surf. Sci. Catal. 130 (2000) 1721.
[76] A.M. Duarte de Farias, W. De A. Gonzalez, P.G. Pris de Oliveira, J.G. Eon, J.M. Herrmann, M. Aouine, S. Loridant and J.C. Volta, J. Catal. 208 (2002) 238.
[77] P.G. Pries de Oliveira, J.G. Eon, M. Chavant, A.S. Riché, V. Martin, S. Caldarelli and J.C. Volta, Catal. Today 57 (2000) 177.
[78] F. Cavani, C. Cortelli, S. Ligi, F. Pierelli, F. Trifirò, DGMK Tagungsbericht, 2004-3 (2004) 87.
[79] S. Ligi, F. Cavani, S. Albonetti and G. Mazzoni, US Patent 6,734,135 (2004), assigned to Lonza SpA.
[80] C.J. Kiely, A. Burrows, S. Saijp, G.J. Hutchings, M.T. Sananes, A. Tuel and J.C. Volta, J. Catal. 162 (1996) 31.
[81] G.J. Hutchings, M.T. Sananes, S. Sajip, C.J. Kiely, A. Burrows, I.J. Ellison and J.C. Volta, Catal. Today 33 (1997) 161.
[82] N. Duvauchelle, E. Kesteman, F. Oudet and E. Bordes, J. Solid State Chem. 137 (1998) 311.
[83] a) H.S. Horowitz, C.M. Blackstone, A.W. Sleight and G. Teuref, Appl. Catal. 38 (1988) 193; b) T.Okamura and M.Misono, Catal. Today 16 (1993) 61.

[84] V.A. Zazhigalov, J. Haber, J. Stoch, A.I. Kharlamov, L.V. Bogutskya, I.V. Bacherikova and A. Kowal, Stud. Surf. Sci. Catal. 110 (1997) 337.
[85] G.J. Hutchings and R. Higgins, Appl. Catal. A 154 (1997) 103.
[86] W. Ji, L. Xu, X. Wang, Z. Hu, Q. Yan and Y. Chen, Catal. Today 74 (2002) 101.
[87] M. Fait, B. Kubias, H.J. Eberle, M. Estenfelder, U. Steinike and M. Schneider, Catal. Lett. 68 (2000) 13.
[88] N. Hiyoshi, N. Yamamoto, N. Terao, T. Nakato and T. Okuhara, Stud. Surf. Sci. Catal. 130 (2000) 1715.
[89] N. Yamamoto, N. Hiyoshi and T. Okuhara, Chem. Mater. 14 (2002) 3882.
[90] N. Hiyoshi, N. Yamamoto, N. Ryumon, Y. Kamiya and T. Okuhara, J. Catal. 221 (2004) 225.
[91] G.J. Hutchings, M.T. Sananes, S. Sajip, C.J. Kiely, A. Burrows, I.J. Ellison and J.C. Volta, Catal. Today 33 (1997) 161.
[92] G.J. Hutchings, R. Olier, M.T. Sananes and J.C. Volta, Stud. Surf. Sci. Catal. 82 (1994) 213.
[93] K.E. Birkeland, S.M. Babitz, G.K. Bethke, H. Kung, G.W. Coulson and S.R. Bare, J. Phys. Chem. B 101 (1997) 6895.
[94] N. Herron, D.L.Thorn, R.L. Harlow and G.W. Coulston, J. Amer. Chem. Soc. 119 (1997) 7149.
[95] Z.Q. Zhou, H.Y. Xu, W.J. Ji and Y. Chen, Catal. Lett. 96 (2004) 221.
[96] G.J. Hutchings, J.K. Bartley, J.M. Webster, J.A. Lopez-Sanchez, D. Gilbert, C.J. Kiely, A.F. Carley, S.M. Howdle, S. Sajip, S. Caldarelli, C. Rhodes, J.C. Volta and M. Polyakoff, J. Catal. 197 (2001) 232.
[97] G.J. Hutchings, J.A. Lopez-Sanchez, J.K. Bartley, J.M. Webster, A. Burrows, C.J. Kiely, A.F. Carley, C. Rhodes, M. Hävecker, A. Knop-Gericke, R.W. Mayer, R. Schlögl, J.C. Volta and M. Polyakoff, J. Catal. 208 (2002) 197.
[98] N. Mizuno, H. Hatayama, S. Uccida and A. Taguchi, Chem. Mater. 13 (2001) 179.
[99] M.A. Carreon and V.V. Guliants, Chem. Commun. (2001) 1438.
[100] M.A. Carreon and V.V. Guliants, Microp. Mesop. Mat. 55 (2002) 297.
[101] M.A. Carreon and V.V. Guliants, Catal. Today 78 (2003) 303.
[102] M.A. Carreon, V.V. Guliants, M.O. Guerrero-Perez and M.A. Bañares, Microp. Mesop. Mat. 71 (2004) 57.
[103] M.A. Carreon, V.V. Guliants, F. Pierelli and F. Cavani, Catal. Lett. 92 (2004) 11.
[104] J.H. Holles, C.J. Dillon, J.A. Labinger and M.E. Davis, J. Catal. 218 (2003) 42.
[105] C.J. Dillon, J.H. Holles, R.J. Davis, J.A. Labinger and M.E. Davis, J. Catal. 218 (2003) 54.
[106] C.J. Dillon, J.H. Holles, M.E. Davis and J.A. Labinger, Catal. Today 81 (2003) 189.
[107] F. Trifirò, Catal. Today, 16 (1993) 91.
[108] G. Centi, G. Fornasari and F. Trifirò, J. Catal. , 89 (1984) 44.

[109] S. Albonetti, F. Cavani and F. Trifirò, Catal. Rev.-Sci. Eng., (1996) 413.

[110] G. Centi and F. Trifirò, Catal. Today, 3 (1988) 151.

[111] Z.Y. Xue, G.L. Schrader, J. Catal, 184 (1999) 87.

[112] D.J. Thompson, I.M. Ciobîca, B.K. Hodnett, R.A. van Santen, M.O. Fanning, Surface Science, 547 (2003) 438.

[113] D.J. Thompson, M.O. Fanning, B.K. Hodnett, J. Molec. Catal A, 198 (2003) 125.

[114] D.J. Thompson, M.O. Fanning, B.K. Hodnett, J. Molec. Catal A, 206 (2003) 435.

[115] D.J. Thompson, I.M. Ciobîca, B.K. Hodnett, R.A. van Santen, M.O. Fanning, Catal. Today 91 (2004) 177.

[116] F. Cavani, F. Trifirò, Appl. Catal. 157 (1997) 195.

[117] G. Busca, E. Finocchio, G. Ramis, G. Ricchiaroli, Catal. Today 32 (1996) 1330.

[118] V. A. Zazhigalov, J. Haber, J. Stoch, V. M. Belousov, Appl. Catal. 96 (1993) 135.

[119] P. A. Agaskar, L. De Caul, R. K. Grasselli, Catal. Lett. 23 (1994) 339.

[120] H. Bluhm, M.Haevecker, E. Kleimenov, A. Knop-Gericke, A. Liskowski, R. Schoegl and D.S. Su, Topis Catal. 23 (2003) 99.

2

EXPERIMENTAL

2.1 CATALYST PREPARATION

2.1.1 Synthesis of vanadyl pyrophosphate, $(VO)_2P_2O_7$ (conventional method)

The VPP catalyst were prepared by the organic-route: $VOHPO_4 \cdot 0.5H_2O$ (VHP), precursor of vanadyl pyrophosphate, was synthesized suspending the desired amounts of V_2O_5 (99% Sigma Aldrich) and H_3PO_4 (98% Sigma Aldrich) in isobutanol (99% Sigma Aldrich). Figure 2.1 shows the equipment (a three-necks flask) used for the VPP precursor synthesis.

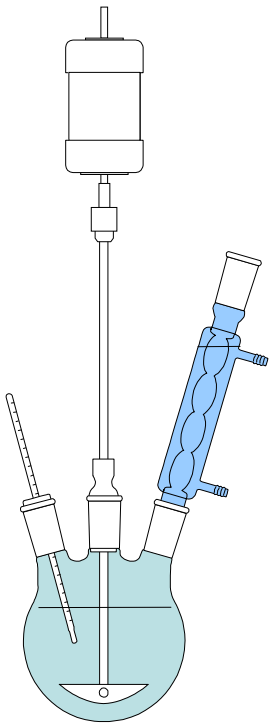

Fig.2.1_ Apparatus for VPP precursor synthesis.

In the case of Nb-doped catalyst, the Nb source (ammonium niobate(V) oxalate hydrate, Sigma-Aldrich) was added to the synthesis mixture after V_2O_5 and H_3PO_4 addition.

The precipitation of hemihydrate acid vanadyl orthophosphate occurred through the reduction of vanadium (V) oxide to vanadyl ions (VO^{2+}) by isobutanol; in presence of

H_3PO_4 the precursor precipitated:

$$V_2O_5 + C_4H_9OH + 2\ H^+ \rightarrow 2\ VO^{2+} + C_4H_8O + 2\ H_2O$$
$$VO^{2+} + H_3PO_4 + 0.5\ H_2O \rightarrow VOHPO_4{\cdot}0.5H_2O + 2H^+$$

By-products of isobutanol oxidation were isobutyric aldheyde and other oxidation products (such as: acetaldehyde, acetic acid, formic acid, etc.); moreover water was co-produced.
The mixture was heated at reflux temperature (120°C) for 6 hours. The colour varied from the typical dark orange of V_2O_5, to an intense light blue, characteristics of $VOHPO_4{\cdot}0.5H_2O$, except when Nb was used in which case the final product was light green.
After filtration, the obtained precipitate was thermally treated according to the following procedure:

(a) drying at 120°C for 12 h, in static air, to obtain the so called Precursor;

(b) pre-calcination step in flowing air (130 ml/min), with temperature gradient (1°C/min) from room temperature up to 300°C; then isothermal step at 300°C in air for 6 h;

$$2\ (VO)HPO_4 0.5H_2O \rightarrow 2\ (VO)HPO_4 + H_2O$$

(c) thermal treatment in flowing N_2 (17 ml/min), with temperature gradient (1°C/min) from room temperature up to 550°C, and final isothermal step at the latter T for 6h.

$$2\ (VO)HPO_4 \rightarrow (VO)_2P_2O_7 + H_2O$$

2.1.2 Synthesis of $VOPO_4{\cdot}2H_2O$, hydrated $NbOPO_4$ and mixed V/Nb hydrated phosphates

The synthesis of $VOPO_4{\cdot}2H_2O$ was prepared suspending the desired amounts of V_2O_5 (99% Sigma Aldrich) and H_3PO_4 (85% Sigma Aldrich) in water; the synthesis of hydrated $NbOPO_4$ was prepared suspending the desired amounts of hydrated Nb_2O_5 (AD1653-HY-340 by CBMM, H_2O %wt. = 18%) and H_3PO_4 (85% Sigma Aldrich) in water; finally the mixed phosphates were prepared using V_2O_5 (99% Sigma Aldrich), hydrated Nb_2O_5 (HY-340 by CBMM, H_2O %wt. = 18%) and H_3PO_4 (85% Sigma Aldrich)) in water (Chapter 3).
The equipment used for phosphates synthesis is the same used for VPP precursor synthesis (Fig.2.1). The synthesis can be considered properly a precipitation and not a dissolution.
The mixture is heated at reflux temperature (100°C) for 17 hours, under vigorous stirring: the colour changes from dark orange (V_2O_5) to bright yellow ($VOPO_4{\cdot}2H_2O$) or to yellow-green (mixed phosphate). In the case of pure hydrated $NbOPO_4$ synthesis, the mixture colour remained white, as the initial solid. After the mixture filtering and washing, the solid obtained is dried for few hours at 100°C. In particular, in the case of $VOPO_4{\cdot}2H_2O$ one sample was obtained as above described (sample 1 VPD), while a second one was obtained from filtration of mother-liquor left one day at ambient conditions, then leaving at

room temperature the filtered yellow solid for one day (sample 2 VPD). The thermal treatment (when performed) was done in static air, with temperature gradient (1°C/min) from room temperature up to 450°C; then in isothermal step at 450°C for 6 h**.**

2.1.3 Synthesis of vanadyl pyrophosphate, $(VO)_2P_2O_7$, (microwave method)

The organic synthesis of $VOHPO_4 \cdot 0.5H_2O$ (VHP), vanadyl pyrophosphate precursor, by microwave method, was performed by a CEM Discover S-class system, at Pisa University (Dep. of Chemistry and Industrial Chemistry). The reagents employed were V_2O_5 (99%), H_3PO_4 (99%) and ammonium niobate(V) oxalate hydrate (Sigma-Aldrich). The apparatus is described in detail at Chapter 5.

Fig.2.2_ CEM Discover instrument for MW-assisted synthesis of V/P/O samples.

2.2 CATALYST CHARACTERIZATION

Raman spectroscopy analysis

Raman studies were performed using a Renishaw 1000 instrument, equipped with a Leica DMLM microscope, laser source Argon ion (514 nm) with power 25 mW.

Ex-situ analysis

Generally for all samples different spectra (meaning a change of surface's position) were recorded. The parameters of spectrum acquisition are, generally, 5 accumulations, 10 seconds, using 25% of laser power to prevent sample's damage. It's used objective 50x.

In-situ analysis

"*In-situ"* analysis were performed using a commercial Raman cell (Linkam Instruments TS1500). The quantity of sample used for the analysis is about 5-10 mg. The gas flow, fed from the beginning of the experiment, is about 10 ml/min; to get an humid flow, air (or N_2) was fed through a bubbler containing water, the temperature of which was changed (partial pressure of steam from 0.03 to 0.10 bar). Spectra are recorded at room temperature (rt), while increasing temperature (heating rate generally of 100°C/min, except 10°C/min for NP4 and NP2 samples) up to the desired one and during the isotherm period.

The laser power used is 25% which permits a good spectrum acquisition without damaging the sample; the acquisition parameters are 10 accumulations, 10 s each one; the objective used is 20x.

UV-Vis DRS analysis

UV-Vis spectra were recorded in diffuse reflectance using a Perkin-Elmer UV/VIS/NIR Lambda 19 instrument, equipped with an integrating sphere, between 190 and 1200 nm, with a scansion rate of 480 nm/min. After recording, spectra were transformed in F(R) by the Kubelka-Munch law:

$$F(R) = \frac{(1-R)^2}{2R}$$

FT-IR analysis

The IR-spectra were recorded using a FT-IR Perkin-Elmer spectrometer, with the KBr method, with a resolution of 4 cm^{-1}, using 14 scansions, between 4000 and 450 cm^{-1}.

X-Ray powder diffraction analysis

The XRD measurements were carried out using a Philips PW 1710 apparatus, with Cu Kα (λ = 1.5406 Å) as radiation source in the range of 5°<2θ<80°, with steps of 0.1 grade and acquiring the signal for 2 seconds for each step (phosphates samples) or in the range of 10°<2θ<50°, with steps of 0.05 grade and acquiring the signal for 3 seconds (VPP samples). Reflects attribution was done by the Bragg law, using the d value: $2d\,sen\theta = n\lambda$.

Thermogravimetric analysis (TGA)

The thermogravimetric analysis is performed with Rehometric Scientific sta 1500+ instrument, in air flow (30 ml/min), from room temperature up to 550°C, with a heating rate of 15°C/min.

Specific surface area analysis (BET single point)

The specific surface area was determined by N_2 adsorption at 77K (the boiling T of nitrogen), with a Sorpty 1750 Instrument (Carlo Erba). The sample was heated at 150°C under vacuum, to eliminate water and other molecules eventually adsorbed on the surface. After this pre-treatment, sample was maintained at 77K in a liquid nitrogen bath, while the instrument slowly sent gaseous N_2, which was adsorbed on the surface. By BET equation it was possible to calculate the volume of monostrate and finally the sample surface area.

2.3 CATALYTIC TESTS

2.3.1 Laboratory scale plant

Catalytic tests were carried out in a continuous-flow, fixed bed, quartz reactor. The system permits to change different reaction parameters: feed composition, contact time and temperature. The laboratory plant is schematized in Figure 2.3, for catalytic tests with n-butane and air, and in Figure 2.4, for catalytic tests with 1-butanol in He or in air . The apparatus could be divided in three main different parts:

1) “feed”
2) “reaction”
3) “downstream”

1) Feed:

Gases (n-butane, He, air) were fed to the reactor, in separated streams or simultaneously, by three mass-flow meters ((2) in fig.2.3; (3) in fig.2.4). The 1-butanol was fed by a syringe pump ((2) in fig.2.4), properly calibrated for the desired quantity of liquid flow. The 1-butanol, when used, was vaporized in the reactor inlet line, which was heated at 120°C. The helium flow could be fed to the reactor and simultaneously *n*-butane and air, mixed together in a three-ways valve, could be fed to the gascromatograph or to a bubble flow meter, which was used to check the real entrance flow (5). In case of feeding the reactive mixture, after the three-ways valve, the switch of a four-ways commutation valve permitted to feed, to the reactor, the reactive mixture, instead of He flow. In particular, when sampling the outlet mixture by a on-line heated valve, it was possible to feed helium to the reactor, switching again the four ways valve.

2) Reaction:

The fixed bed reactor was constituted by a quartz tube, operating at ambient pressure. At the top of the reactor (room temperature), a porous septum allowed to sample the fed gas using a syringe. In the interior of the reactor a second quartz tube, much thinner, allowed to place a thermocouple, which permitted the measure of the real temperature of the catalytic bed. With the aim of minimize dispersions and equalize temperature on the axial direction, the reactor was wrapped in a copper block surrounded by a resistance (reactor oven), the temperature of which was varied and controlled thank to a inner thermocouple. At the reactor exit a heater string, maintained at 200°C, avoided any crystallization of the products on the inner walls leading the gaseous mixture to reach the gascromatograph.

3) <u>Downstream</u>:

At the reactor exit, a gas split was placed: a part of the flow was sent to the gascromatograph, when opened the on/off valve, permitting the direct analysis of the reaction products and unconverted butane, by the FID detector; the resting part flowed to the vent, passing through a crystallizer then to a glass bubbler filled with acetone, which permitted the condensation of organic products not yet collected in the crystallizer. From the crystallizer septum, it was possible to sample by a syringe incondensable gases. The measure of the outlet flow was carried out using a bubble flow meter, prior to the vent.

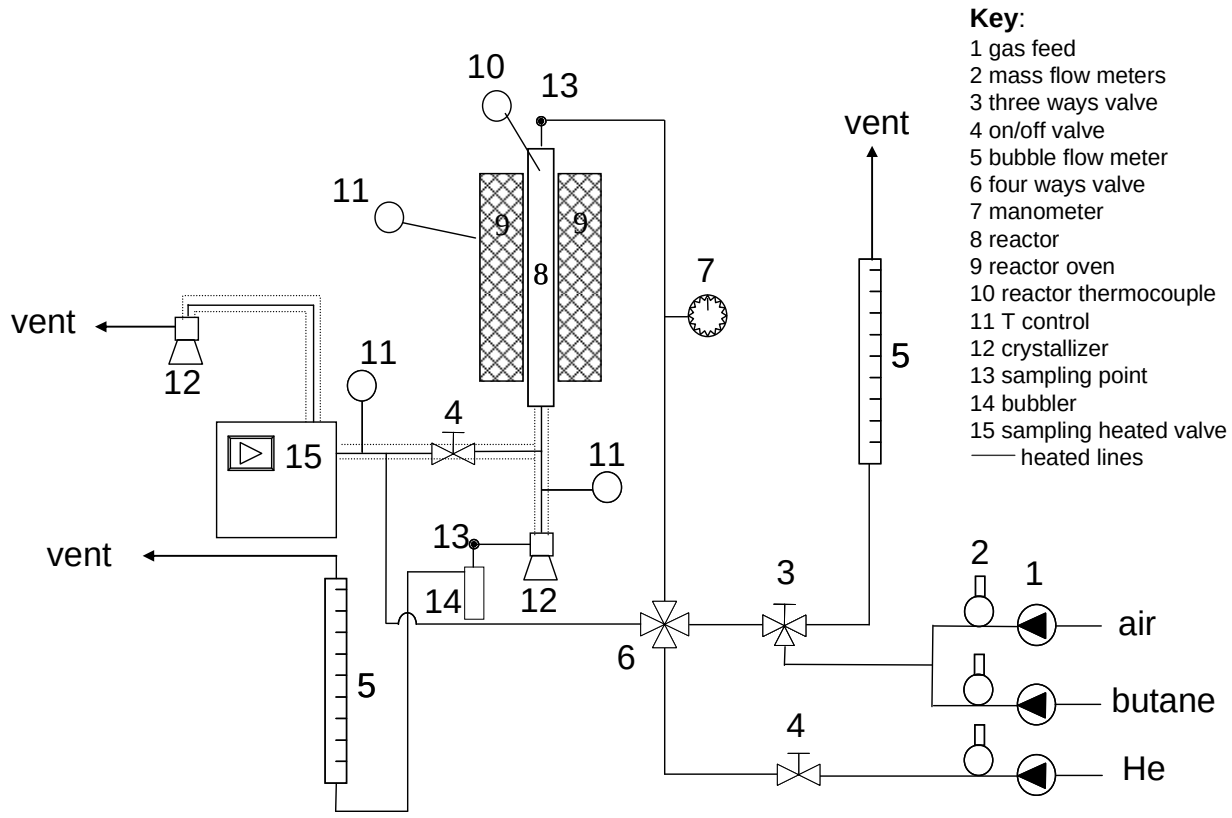

Fig.2.3_ Scheme of laboratory scale plant, feeding n-butane for catalytic tests.

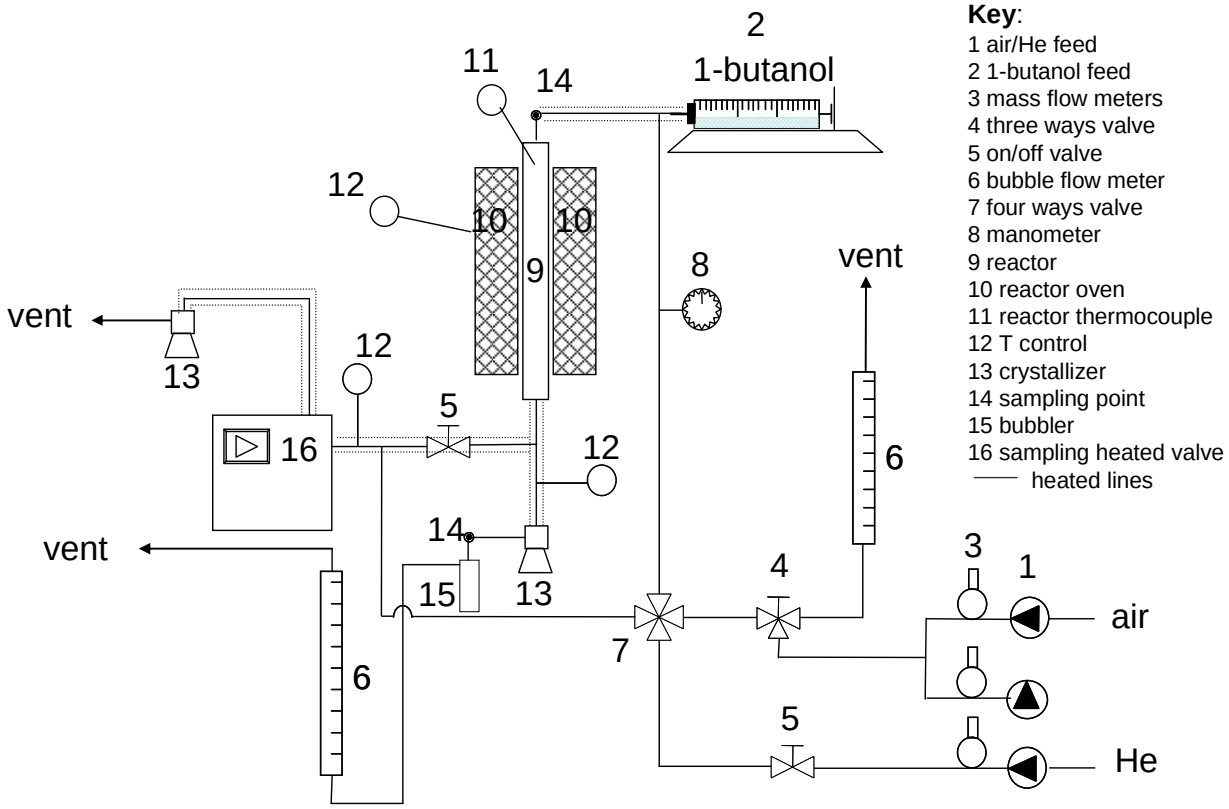

Fig.2.4_ Scheme of laboratory scale plant, feeding 1-butanol for catalytic tests.

2.3.2 Products Analysis

Reactants and products were analyzed by gascromatography, employing a Varian GC Varian equipped with the following columns and detectors:

1) semicapillar CPSil-5CB column (30m length; i.d. 0.53mm; stationary phase of 100% dimethylpolysiloxane with a thickness of 3.00 μm). By this column are separated maleic anhydride, by-products (acetic acid, acrylic acid and other light compounds e.g. butenes) and *n*-butane (in and out). The correspondent detector is a FID.

2) packed Carbosieve SII column (2m length, stationary phase of active carbons having dimensions of 80-100 mesh). In this column CO, CO_2, H_2O, O_2 and N_2 are separated and detected by a TCD.

The carrier gas used for the column is He. The temperature program of the oven (method analysis) was the following: 7 minutes at 40°C, then heating up to 220°C (heating rate of 30°C/min), finally isothermal step at 220°C for 10 minutes.

For analyses of products, relative to semicapillary column and FID detector, it was an on-line heated (200°C) sampling valve (ca. 600 μl volume) which allowed the direct determination of the amount of maleic anhydride in the outlet gas stream and also permitted the analysis of a constant volume of mixture gas.

The incondensable products (CO, CO_2, O_2, N_2) were sampled with a gas syringe (500 μl volume) through the porous septum positioned in the crystallizer or at the top of the

reactor; then the sampled gaseous mixture was injected in the packed column, linked to the TCD.

2.3.3 Catalytic performances: conversion, yield and selectivity

By gascromathographic analyses the percentage values of conversion, yield and selectivity were determined, using the following equations:

$$Conversion = \frac{n^{\circ}\ mols\ of\ converted\ reactant}{n^{\circ} mols\ of\ fed\ reactant} \times 100$$

$$Yield = \frac{n^{\circ}\ mols\ of\ product/stoichiometric\ coeff.}{n^{\circ}\ mols\ of\ fed\ reactant/stoichiometric\ coeff.} \times 100$$

$$Selectivity = \frac{Yield}{Conversion} \times 100$$

$$C\ balance = \frac{\sum Yields}{Conversion} \approx 100$$

3

DOPING VANADYL PYROPHOSPHATE WITH Nb : THE EFFECT ON SURFACE COMPOSITION AND REACTIVITY

3.1 INTRODUCTION

In catalysis, a method used to improve activity and selectivity to the desired product is the addition of an opportune element, named dopant or promoter, to the catalyst precursor. The presence of this element may affect catalyst physical or chemical characteristics or even both; moreover, as well-known, its effect may change catalytic performance, depending on its quantity, the method used to add it to the synthesis mixture, its relationship with other dopants, etc.

Nb is a known dopant of $(VO)_2P_2O_7$ (VPP) catalyst, claimed in the literature and in patents [1], however a clear explanation of its effect has not been reported yet.

In this work, Nb-doped VPP catalysts have been synthesized in the aim of understanding the role of this promoter, in particular its relationship with the δ-$VOPO_4$ phase, considered to be the active and selective phase which develops at the VPP surface during reaction.

Before discussing our results, some general aspects dealing with the use of dopants will be discussed here below.

Many different elements (metal cations) used as dopants for VPP, are reported in the patent literature, whereas in the open literature most studies try to explain the role of the dopant by considering its effect on the structure of different V/P/O phases, on the catalytic activity and selectivity, on surface acidity and on the V^{4+}/V^{5+} ratio, moreover all these aspects being in close relationship one to each other.

Hutchings [2] first elaborated an extensive review about patents dealing with VPP dopants, and recently the same author considered again this theme in a review [3].

Hutchings gives general considerations about promoting the VPP catalyst, which must be considered with care when comparing the effect of a specific dopant to that given by another one.

First, it must be highlighted that two routes are possible for adding the dopant: a) together with the other reagents during the preparation of catalyst precursor (coprecipitation), or b) by impregnation

of the already prepared precursor. Secondly, we have to consider that there are two classes of dopants (D): 1) type 1_promoters, added in high quantity (with atomic ratio P/V>1 and excess P/D ratio about 1, that is a V/D ratio equal to 5-20) by means of the first addition route, which will show a structural effect; 2) type 2_ promoters, added in low quantity (with P/V>1 and V/D>20), the effect of which is related to the formation of a solid solution of D either in VPP or in $VOPO_4$ phases. Furthermore, the authors warned against misinterpretation of the results (catalytic performances, morphology etc.) when comparing doped catalysts, and the latter with that of an un-doped one: in fact, the method of preparation affects the precursor characteristics, and as a consequence also those of the final catalyst. For example the positive effect of a promoter may be masked due to the presence of impurities phases (e.g. $VO(H_2PO_4)_2$ easily obtained with aqueous preparations) which are detrimental for the catalyst performances; moreover, especially when using high amount of a dopant, it is important to choose the opportune solvent for its solubilisation and also the correct addition method, because these factors could cause an inaccurate dopant dispersion. In the latter case, undesired phases could form and these in turn could negatively affect catalytic performance.

Finally, it's important to check the specific surface area, because the increased catalytic activity could be due to an increase of this parameter (impregnation method usually provides higher catalyst surface areas for doped VPP catalysts as compared to the co-precipitation method) rather than to the presence of the dopant itself. In fact, the true promotional effect should be independent from catalyst surface area.

To sum up his analysis of the patent literature, Hutchings [2] finally comments that the role of metal cations in the VPP compound may be: a) to stabilize an average "medium" oxidation vanadium state which favours the first step of the reaction mechanism, that is the paraffin activation; b) to control oxygen diffusion and products adsorption, and to minimize unselective oxidation reactions.

In the present work, considering the quantity of Nb used by us, the dopant belongs to type 2 of Hutchings' classification: the element may form a solid solution, yielding a compound of general composition $((VO)_{1-x}M_x)_2P_2O_7$, if dissolved inside the VPP structure.

Considering the open literature about Nb doping of VPP, the addition of this element may lead to: a) an increase of the activity, due to the generation of strong acid Lewis sites, and of MA selectivity as well, because it prevents overoxidation of the products [4-5]; b) a decrease of catalyst activation time (equilibration time), a period which finally permits to get stable catalytic performances [5]; and c) a control of the superficial V^{5+}/V^{4+} ratio [5].

Nb belongs to the fifth group as vanadium, and possesses three different valence states (3+, 4+, and 5+), with corresponding Nb oxides which are stable in air, but within different temperature ranges.

V and Nb form mixed compounds, for example $VNbO_4$ (where V is mainly present as V^{3+} and Nb is Nb^{5+}) and $VNbO_5$ (with V^{5+} and Nb^{5+}); but these elements may also form mixed oxides with molar ratios other than 1/1. As a consequence of this, Nb is potentially a good dopant because the possibility of influencing the reactivity characteristics of V, is related to the formation of either a solid solution or a mixed oxide between the guest element, and the hosting structure (in our case, the VPP or the $VOPO_4$).

For example, it is reported that for the redox reaction occurring at solid state:

$$2\ VO_2 + 2\ NbO_2 \rightarrow V_2O_3 + Nb_2O_5$$

the reaction free energy is -125 kJ/mol [6-7], which also suggests that the nature of the Nb-containing starting compound may affect the valence state of V.

On the other hand, Nb may be incorporated in the VPP lattice, forming a solid solution like $[(VO)_{2-x}(Nb)_x(P_2O_7)_{1-x}(PO_4)_{2x}]$: in the literature a few works deal with this aspect.

Duarte de Faria et al. [8] prepared VPP doped with Nb (V/Nb=100, starting from Nb^{5+} ethoxide) and compared characterization and catalytic performances with those of the corresponding undoped catalyst: Nb changed the morphology of the precursor, and as a consequence of this, the thermal treatment behaviour was different from that of the undoped precursor (the second water molecule release occurred at lower temperature). The XRD analysis of the activated doped catalyst revealed the presence of some $VOPO_4$ phase besides VPP, but the authors did not find any evidence for the formation of either $NbOPO_4$ or any other mixed V/Nb phosphate; XPS and ^{31}P NMR analysis showed that the Nb-doped catalyst was more oxidized, possessed a lower P/V ratio and also showed a Nb surface enrichment (V/Nb=31 instead of the bulk value V/Nb=100). Finally, TEM analysis of the doped catalyst demonstrated an high density of defects, and EDX analysis showed a good dispersion of Nb. The authors found that Nb affects positively the n-butane conversion, which was higher during the activation period (400°C, 1,7% n-butane in air) for the doped VPP, while the MA selectivity remained similar. Because of these findings, the authors hypothesized that the replacement of V^{4+} with Nb^{5+} (which lowered the electrical conductivity of the catalyst) generated oxidizing species, which were responsible for n-butane activation, which in turn led to the observed increase of activity.

Guliants et al. [9] reported the synthesis of VPP by means of the organic route, doped with different promoters; in particular the Nb doped catalyst (V/Nb~200, added by impregnation of an alcoholic solution of the correspondent alkoxide) gave the best catalytic performances, both in terms of activity and selectivity; however, the authors did not find any relevant change of morphology. The authors addressed the good results to an higher surface acidity, which favoured the alkane activation and the desorption of MA, avoiding complete oxidation reactions.

However, it is also possible that, depending principally on its quantity, Nb forms either a mixed compound with V and P, e.g., $((VO)_{1-x}(NbO)_xPO_4)$, or mixed phosphates (e.g. $NbOPO_4$): Mastuura et al. [10] synthesized Nb-doped VPP by reducing the doped oxidized precursor $(V_{1-x}Nb_xOPO_4 \cdot 2H_2O$ with x=0-0.3, that is V/Nb=2.33-19). In this case the Nb content (source $Nb_2O_5 \cdot 3.3H_2O$) was quite high, in fact with x=0.3 it was not possible to obtain a solid solution; however when the solid solution formed (as confirmed by XRD analysis), the structure of the calcined mixed compound ($V_{1-x}Nb_xOPO_4$) changed from α_I-$VOPO_4$ to α_{II}-$VOPO_4$. Regarding the catalyst, the number of strong acid sites increased with Nb content and also the activity showed a concomitant increase, while no positive effect was observed in regard to MA selectivity. The authors interpreted the effect of Nb on activity by hypothesizing the formation of a solid solution like $(V^{4+}_{1-x}Nb^{5+}_xO)_2(P_2O_7)_{1-x}(PO_4)_{2x}$; the presence of Nb in the higher oxidation state was due to its

scarce reducibility (Nb^{5+} was not reduced by benzyl alcohol, the reagent used to form $VOHPO_4 \cdot 0.5H_2O$ from the oxidized V precursor), and its incorporation in the mixed compound caused a fraction of the pyrophosphate groups $[P_2O_7]^{4-}$ to convert into more acidic orthophosphate units $[PO_4]^{3-}$; the latter, together with coordinatively-unsaturated Nb^{5+} ions, increased the catalyst acidity, a property which is needed for the first step of the mechanism in selective n-butane oxidation.

In regard to the role of a $NbOPO_4$ phase, which is possibly formed either at the surface of VPP, because of the excess of phosphorus typically used in the synthesis of VPP (P/V molar ratio 1.1-1.2), Pries de Oliveira et al. [5] prepared catalysts as a mixture of VPP and $NbOPO_4$: Nb source (CBMM) was added in the synthesis mixture together with V_2O_5 (V/Nb=20-10). The characterization analysis of doped precursors showed that the presence of the $NbOPO_4$ compound changed the precursor morphology. In particular, a EDX-STEM study revealed four different compounds: some V was present on, or even inside, the $NbOPO_4$, whereas some Nb was present inside the $VOHPO_4 \cdot 0.5H_2O$. The presence of Nb (in catalysts with low VPP/$NbOPO_4$ ratio) permitted to shorten the equilibration time of the catalyst and also to increase MA selectivity, with respect to the undoped VPP. The authors concluded that Nb acted as a dopant for VPP because Nb was not present as an isolated compound; they proposed that Nb influenced the V^{4+}/V^{5+} ratio according to the equilibrium: $V^{4+} + Nb^{5+} \Leftrightarrow V^{5+} + Nb^{4+}$, both in the precursor and in the final catalyst.

In another work [11], VPP catalyst was doped with Nb, with the aim of increasing the catalytic performance; an effect of stabilization of V^{5+} even under strongly reducing reaction conditions was hypothesized. This possibility was put forward considering that: 1) Nb and V may form mixed phosphates, with general formula $(VO)_{1-x}(NbO)_xPO_4$ [12]; 2) for the redox couple Nb^{4+}/Nb^{5+} in corresponding oxides the value of the standard potential (-0.29 V) is lower than that of the V^{4+}/V^{5+} redox couple (0.67 V), so it may be expected that a mixed V/Nb phosphate is less reducible than pure vanadium phosphate.

Tetragonal $NbOPO_4$ is isostructural with α_I-$VOPO_4$ and this similarity should favour the formation of a mixed compound; in particular, Hutchings [2] hypothesized that $NbOPO_4$ could work as a P supplier (the P/V ratio being always >1), and in this way might restore the loss of P from VPP catalyst, during reaction. Pierelli et al. [11] reported that when Nb was present in high amount (V/Nb=17), it was still possible to form a solid solution and the catalytic performances were improved when the reaction was carried out under n-butane rich conditions (10% n-butane in air), because of the presence of a more oxidized VPP surface: Nb affected both the activity and the selectivity.

In the present thesis, mixed Nb/V phosphates and niobium hydrated phosphate were discussed in chapter 4, in the aim of finding out whether Nb^{5+} could induce the transformation of the $VOPO_4 \cdot 2H_2O$ into δ-$VOPO_4$, the phase responsible of the optimal catalytic behavior of the VPP catalyst. Indeed, the formation of this phase was never observed, and also it was not possible to ascertain the formation of the solid solution between Nb and $VOPO_4$, although the latter could not

be definitely excluded; on the other hand, a solid solution was obtained when V was used as a dopant for $NbOPO_4$.
All these aspects render quite difficult the understanding of the role of Nb in VPP catalysts and highlight that, probably, there is not a single explanation.

3.2 RESULTS AND DISCUSSION

3.2.1 Synthesis of the Nb-doped vanadyl pyrophosphate

A series of Nb-doped VPP catalysts, synthesized by means of the organic-route (Chapter 2), is reported here: samples were prepared by using a specific source of Nb (ammonium niobate(V) oxalate hydrate, Sigma-Aldrich) (Table 3.1) and pure isobutanol as the reductant and solvent. Furthermore, we also prepared a sample using a different synthesis method (Table 3.2): specifically, we used a mixture of alcohols (80% v/v of isobutanol, 20% v/v of 1,4-butanediol) as reducing agents and $NbCl_5$ as the Nb source. This preparation was carried out in the aim of studying the role of the method used for catalyst preparation: the second preparation should bring to a better catalyst, because the use of a mixture glycol/isobutanol, instead of isobutanol only, is known to lead to a better catalytic performance [22]. In all cases, the Nb source was added in the slurry, before the precursor formation.
Tables 3.1 compiles the samples prepared, included the catalyst used as the reference, that did not contain Nb (B2), while Table 3.2 reports the main characteristics of the sampleprepared using the different synthetic method.
In all cases, the same thermal treatment was used (Chapter 2); moreover, samples have been characterized both before and after the treatment; then, the calcined samples were equilibrated at 440°C in the reaction mixture (1,7% of n-butane in air; W/F=1.33·g s·ml^{-1}) for 100-120 h.

	B2	**O150**	**O80**	**O46**	**O17**
P/V	1,1	1,1	1,1	1,1	1,1
V/Nb	∞	150	80	46	17
Nb/(Nb+V) %	0	0,7	1,2	2,1	5,6
Solvent	isobutanol	isobutanol	isobutanol	isobutanol	isobutanol

Tab.3.1_ Nb-doped VPP catalysts, synthesized in pure isobutanol: theoretical molar P/V ratio, V/Nb ratio, Nb/(Nb+V)% ratio and solvent used for the synthesis.

	O80Cl
P/V	1,1
V/Nb	80
Nb/(Nb+V) %	1,2
Solvent	80% v/v isobutanol; 20% v/v 1,4-butanediol

Tab.3.2_ Nb-doped VPP catalysts, synthesized in a mixture of alcohols: theoretical molar P/V ratio, V/Nb ratio, and Nb/(Nb+V)% ratio, and solvent used for the synthesis.

Before investigating the role of Nb dopant, present in small quantity in VPP catalyst, it is useful to discuss about its effect, when present in higher quantity (V/Nb=17), during reactivity at high n-butane concentration. A correlation between catalytic performance (10% n-butane in air, under "hydrocarbon-rich" conditions) and Nb concentration was found by Pierelli [11], with catalysts prepared by means of the same method as that used for O80Cl sample.

Figure 3.1 compares n-butane conversion and MA selectivity for the undoped and the Nb-doped catalyst (V/Nb=17). The reaction conditions used were: 10% of n-butane and 17% O_2 (W/F=1,3 $g \cdot s \cdot ml^{-1}$).

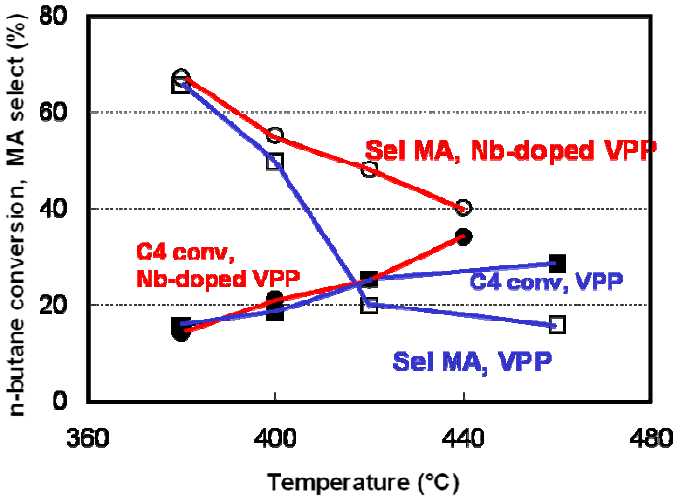

Fig. 3.1_Conversion of n-butane (filled symbols) and maleic anhydride (MA) selectivity (empty symbols) for undoped catalyst (squares) and doped catalysts (th. molar ratio V/Nb=17) (circles). Conditions: 10% n-butane, 17% O_2.

The two catalysts did not differ so much in regard to n-butane conversion in function of temperature, but differed considerably in terms of selectivity to MA. In fact, with the undoped catalyst the selectivity to MA fell down rapidly when the temperature was raised, which was due to both a relevant production of carbon oxides, and to the formation of phthalic anhydride, a by-product generated by cycloaddition of MA itself with butadiene; conversely, the decline of selectivity was much less important with the Nb-doped VPP. It is worth highlighting two important aspects, observed during reaction at n-butane-rich conditions [18]: (a) the contribution of homogeneous reactions is very important, with preferred formation of carbon oxides because of radicalic-type combustion; (b) the multi-step mechanism of n-butane oxidation into MA includes

the formation of butadiene as the key reaction intermediate; however, the latter may either be oxidized into dihydrofuran and then MA, when a suitable concentration of oxidizing sites is available in the neighborhoods of the adsorbed olefin, or desorbs into the gas phase, or even react with the already formed MA to generate phthalic anhydride. This implies that the surface availability of oxidizing sites is the key point to address the selectivity of the reaction, especially under conditions at which the gas-phase is strongly reducing (which implies an average oxidation state for V which is lower than the optimal one). Therefore, it is evident that the lower selectivity to phthalic anhydride experimentally observed with the Nb-doped catalyst, and the corresponding higher selectivity to MA, is due to the fact that the presence of Nb allows the maintenance of the proper oxidation state for V.

In conclusion, this experiment demonstrated that an high quantity of Nb was effective for improving catalytic performances, under "hydrocarbon-rich" conditions.

In the present work, we investigated the catalytic performances related to VPP catalysts doped with low amount of Nb, under "hydrocarbon-lean" conditions, which are much more oxidizing that those used for the experiment shown in figure 3.1. It may be expected that a positive effect of Nb on the oxidation state of V which develops at the catalyst surface under steady-state conditions may be achieved using relatively lower amount of Nb as comared to the experiment carried under "hydrocarbon-rich" conditions.

Raman in-situ tests (chap.3.2.5) were further carried out with different Nb-doped catalysts, in order to understand the relationship between Nb and the active and selective phase, which develops at the VPP surface under reaction conditions. As it will be shown below, Nb improved catalytic performances because it favoured the formation and the stability of limited amounts of δ-$VOPO_4$.

3.2.2 Characterization of Nb-doped catalysts

Precursors characterizations

The catalysts precursors were characterized by means of XRD analysis (fig.3.2): the main compound was crystalline $VO(HPO_4)\cdot 0{,}5H_2O$ (JCPDS 00-037-269), as expected; moreover it was observed, as a background signal, the presence of an amorphous compound, more evident in samples containing a Nb content. In the case of O17 (V/Nb=17) and O46 (V/Nb=46) precursors, there were also traces of $VO(HPO_4)\cdot H_2O$ (peaks at 2θ=13,5°-28,5°, JCPDS 00-046-0126), never observed before in samples prepared with the standard organic procedure; its presence was probably due to the high water content in the synthesis mixture, resulting from the Nb source used; in fact, when the content of Nb was decreased, and so it was also for the water content, the $VO(HPO_4)\cdot H_2O$ phase formed in a minor amount (O46 compared to O17). Furthermore, for these samples and for sample O80 (V/Nb=80) as well, traces of $Nb_{1.91}O_{12}P_{2.82}$ (peak at 2θ=20,7° - JCPDS 00-051-1738) and of $(VO)_3(PO_4)_2\cdot 6H_2O$ (2θ=12,9°- 45,6°, JCPDS 00-052-0209), a V^{4+} compound, were found. The presence of $Nb_{1.91}O_{12}P_{2.82}$ could mean that Nb was not well dispersed in the precursor, while the occurrence of $(VO)_3(PO_4)_2\cdot 6H_2O$ may be related to the presence of water in high amount

between the layers of $VO(HPO_4)\cdot 0{,}5H_2O$. It is interesting to note that the formation of the Nb/P/O compound subtracts P to the formation of the main desired phase, $VO(HPO_4)\cdot 0{,}5H_2O$.

In regard to the reflections of the hemihydrate vanadyl hydrogen phosphate, there was no specific effect of the dopant on crystallites morphology, since the intensities of the two strongest peaks (at 2θ=15,5° and 30,4°, related to (001) and to (220) planes, respectively), were maintained for all samples: the "aspect-ratio" (FWHM(001)/FWHM(220)) was similar for all samples; however, all the reflections in patters of O80, O150 and O80Cl, were less intense than the corresponding ones in the other samples.

In the case of sample O80Cl (the precursor obtained by means of a different method of preparation, using glycol and $NbCl_5$), the pattern registered was that of pure $VO(HPO_4)\cdot 0{,}5H_2O$; no relevant difference with the pattern of sample O80 was observed.

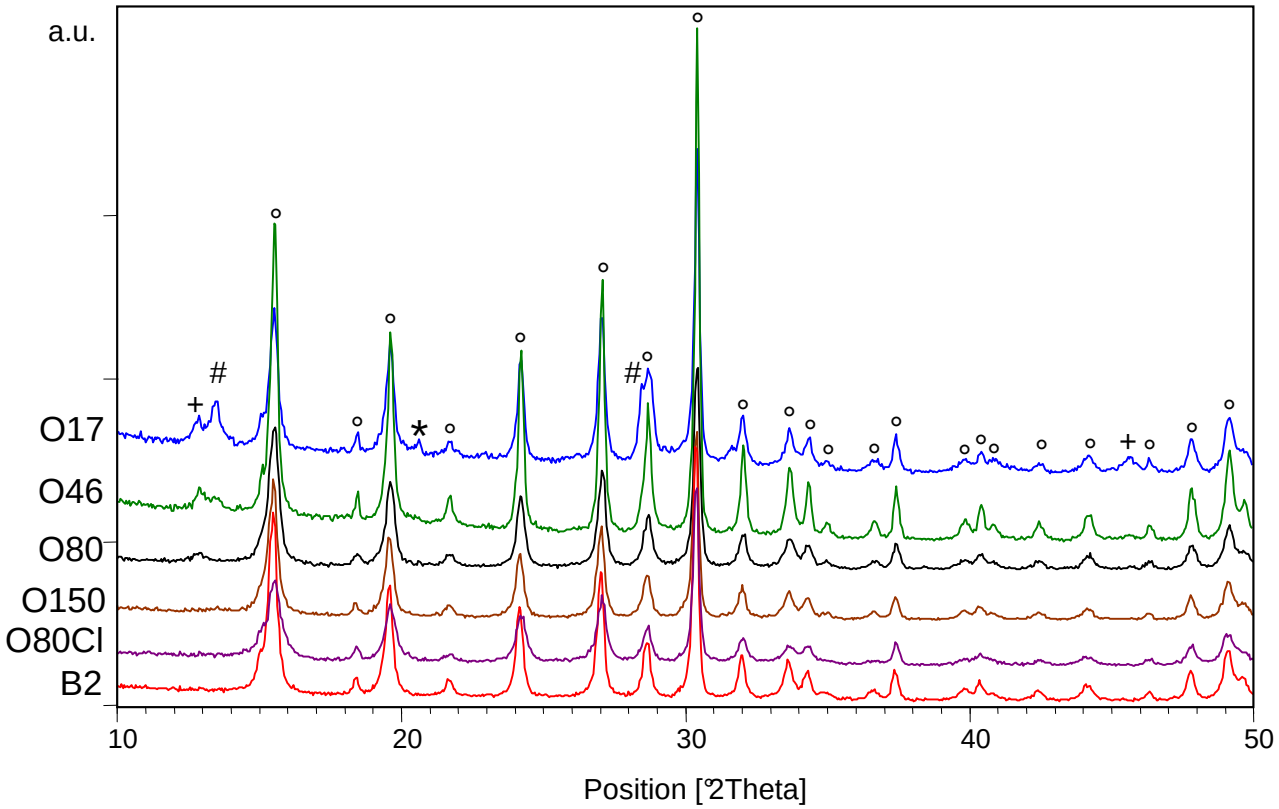

Fig. 3.2_ XRD patterns of sample precursors: B2 (Nb=0), O150 (V/Nb=150), O80 (V/Nb=80), O80Cl (V/Nb=80, glycol and $NbCl_5$), O46 (V/Nb=46) and O17 (V/Nb=17). Symbols: °= $VO(HPO_4)\cdot 0{,}5H_2O$; # = $VO(HPO_4)\cdot H_2O$; + = $(VO)_3(PO_4)_2\cdot 6H_2O$; * = $Nb_{1.91}O_{12}P_{2.82}$.

The ex-situ Raman analyses of doped precursors (fig.3.3) showed the presence of $VO(HPO_4)\cdot 0{,}5H_2O$ (VHP) as the main compound, in accordance with the XRD analyses, and similarly to the un-doped precursor (B2): the only band visible was the strongest one at 986 cm^{-1}, because spectra were strongly affected by fluorescence, due to the high organic content in samples.

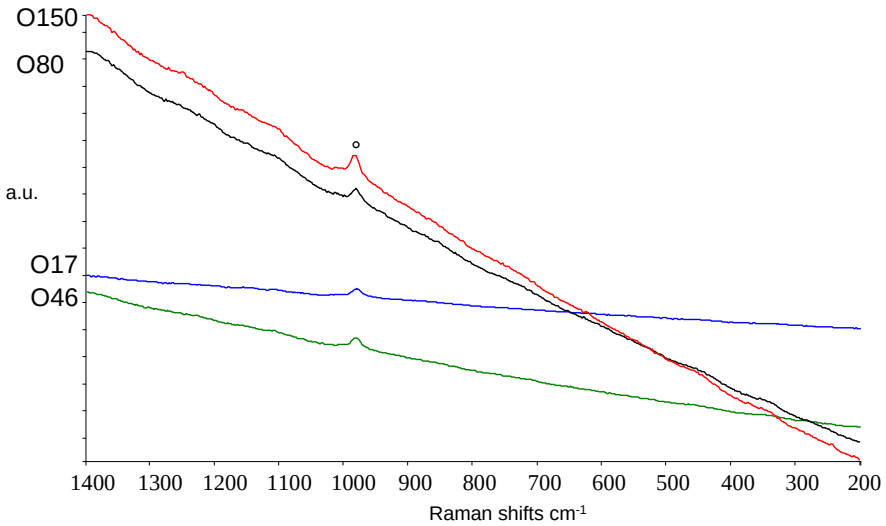

Fig. 3.3_ Raman spectra of doped precursors: O150, O80, O46 and O17. Symbols: ° = $VO(HPO_4)\cdot 0{,}5H_2O$.

Worth of note, although most of the Raman spectra recorded at different spots of the precursors surface showed the characteristic band of the vanadyl hydrogen phosphate hemihydrate, there were however few positions in spectra of precursors O80, O46 and O17 which showed another type of spectrum: bands at 1140, 1013, 880, 687, 558, 531, 360 cm^{-1} were registered, as shown in Fig. 3.4. It is possible that the unusual bands observed for precursors O80, O46 and O17 were related to the Nb source which was not dissolved during the synthesis, or to some other type of Nb-containing compound. For example, the broad band centred at 870 cm^{-1} is comprised in the range of Raman vibrations of distorted octahedral [NbO_6] units in niobium oxides [14]; moreover, the strongest band of $VO(HPO_4)\cdot H_2O$, which falls at 888 cm^{-1}, might be covered by the broad band at 870 cm^{-1}, even though the other intense bands typical for this compound were not observed, as also other bands attributable to any V/P/O compound were not observed as well.

In the case of sample O80Cl, the Raman spectra were similar to those shown in figure 3.3; however, also spectra relative to V_2O_5 were collected, although in a very minor amount.

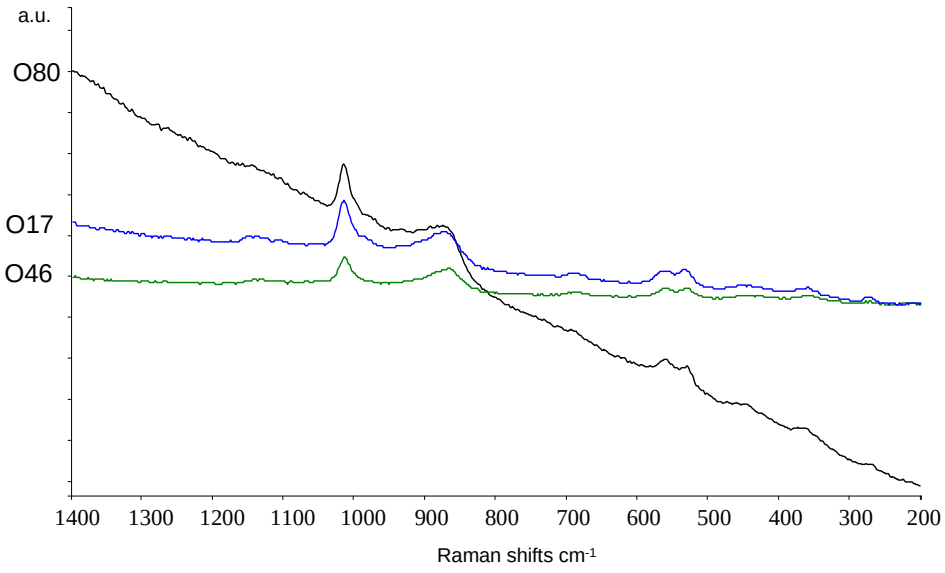

Fig. 3.4_Raman spectra of particular surface positions of doped precursors (O80, O46 and O17).

Interestingly, the UV-vis spectra (fig.3.5) of the precursors showed some differences: first, all the doped samples showed a relatively high quantity of oxidized species (V^{5+}) in comparison with the un-doped sample; when the Nb content was increased, the intensity of bands relative to V^{5+} species (at about 320 and 420 nm) [19-20] grew in comparison with that of the band relative to a CT transition of V^{4+} (at 270 nm) [21]. This was particularly evident for sample O17; in overall, sample B2 appeared to be less oxidized as compared to the other precursors. Sample O80Cl reported a spectrum similar to that of O150: this means that the preparation employed for the former catalyst (using a mixture of isobutanol and 1,4-butanediol) permitted a lower degree of oxidation for the final compound than with O80, despite the same quantity of Nb used.

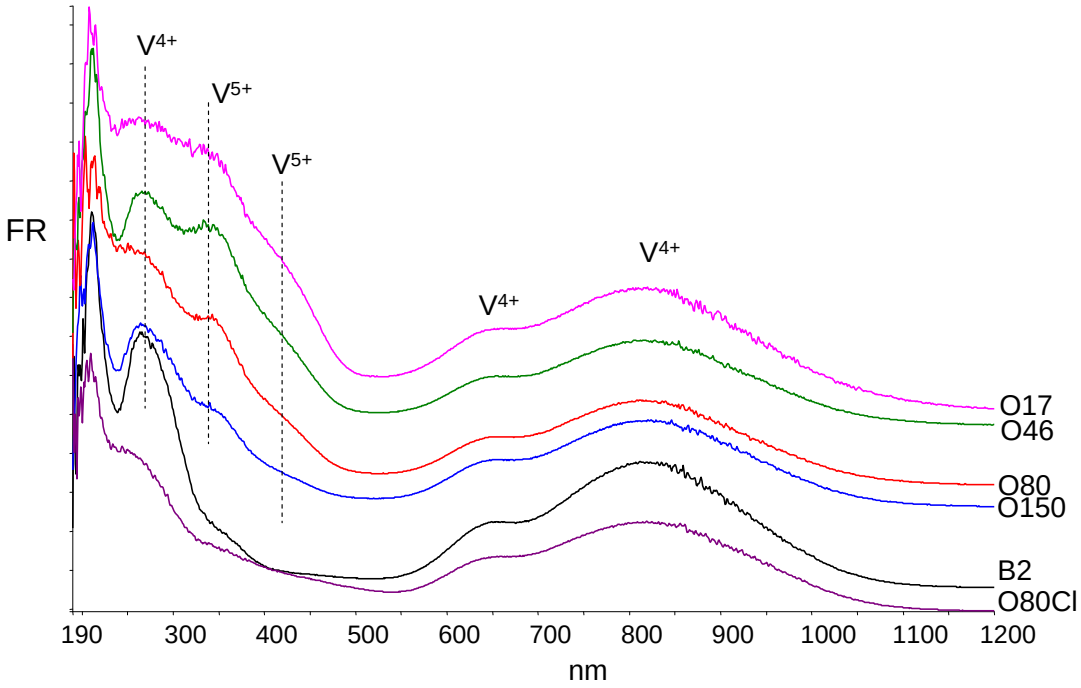

Fig. 3.5_UV-vis DR spectra of doped dried precursors (O150, O80, O46, O17) compared with the spectrum of the un-doped precursor (B2).

Fresh catalysts characterizations

Figure 3.6 shows the XRD patterns for calcined samples; the diffraction patterns were quite noisy, indicating a poorly crystallized $(VO)_2P_2O_7$, which however the main phase (JCPDS 00-034-1381); moreover, for all samples with the exception of O150 and O80Cl, also the characteristic peak at $2\theta=12°$, relative to $VOPO_4 \cdot 2H_2O$ (JCPDS 00-036-1472) was present.

The broad reflection between $2\theta=21°$-$22°$ is attributable to a $VOPO_4$ phase, but a more precise attribution to any specific crystalline phase is difficult, because strong reflections of several $VOPO_4$ phases fall within this range of diffraction angles: δ-$VOPO_4$ (at $2\theta=22,1°$, JCPDS 00-047-0951), γ-$VOPO_4$ (at $2\theta=21,4°$ (JCPDS 00-047-0950), ω-$VOPO_4$ (at $2\theta=21,2°$, JCPDS 00-037-0809) and α_I-$VOPO_4$ (at $2\theta=21,7°$, JCPDS 00-027-0947). In particular, in O150 the intensity of this peak was high compared to that of the neighbouring reflection of VPP (at $2\theta=22,9°$); this could suggest a relative higher amount of the oxidized phase ω-$VOPO_4$ in this sample.

In the case of B2, a reflection attributable to β-$VOPO_4$ was also present (peak at 2θ=26,2° - JCPDS 00-071-0859), which moreover was the most intense one of this phase.

It seems that the higher was the Nb content, the more preferred was the $VOPO_4$ formation; no proof was obtained for the formation of either Nb/P/O or V/Nb/P/O phases, although the presence of some amorphous compound was evident, especially at high Nb content.

The diffraction pattern of calcined O17, in agreement with Raman ex-situ characterization (fig.3.12), is conducive of the presence of an highly amorphous VPP compound: the stronger reflections attributable to the VPP were still visible, however with very low intensity compared to the other samples.

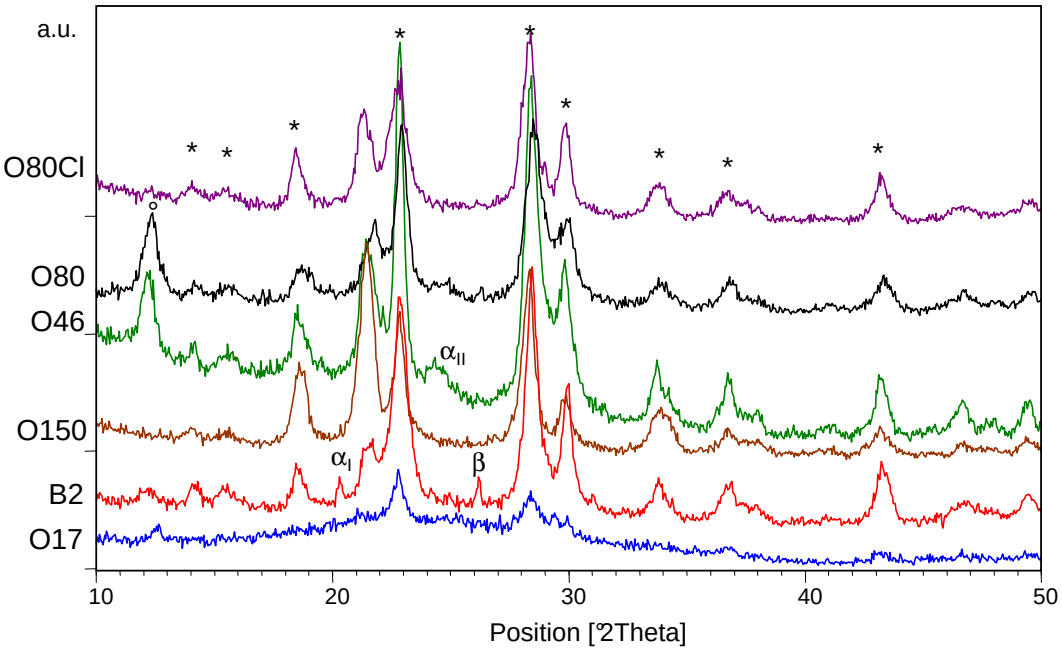

Fig. 3.6_XRD patterns of calcined samples: B2 (Nb=0), O150 (V/Nb=150), O80 (V/Nb=80), O80Cl (V/Nb=80, preparation with glycol/isobutanol mixture and $NbCl_5$), O46 (V/Nb=46) and O17 (V/Nb=17). Symbols: * = $(VO)_2P_2O_7$; ° = $VOPO_4{\cdot}2H_2O$; β = β–$VOPO_4$; α_I = α_I $VOPO_4$; α_{II} = α_{II} $VOPO_4$.

Raman spectra of calcined samples (B2, O150, O80, O80Cl, O46 and O17) are reported in figures 3.7-3.12.

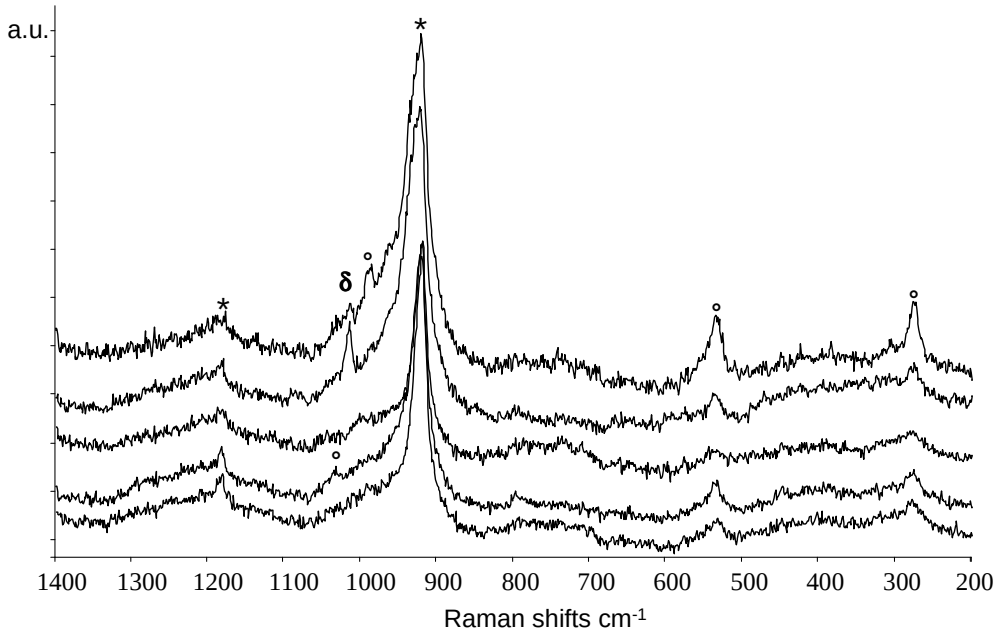

Fig. 3.7_ Raman spectra at different surface positions for sample B2 calcined. Symbols: * = $(VO)_2P_2O_7$; δ = δ $VOPO_4$; ° = $VOPO_4 \cdot 2H_2O$; δ = δ $VOPO_4$.

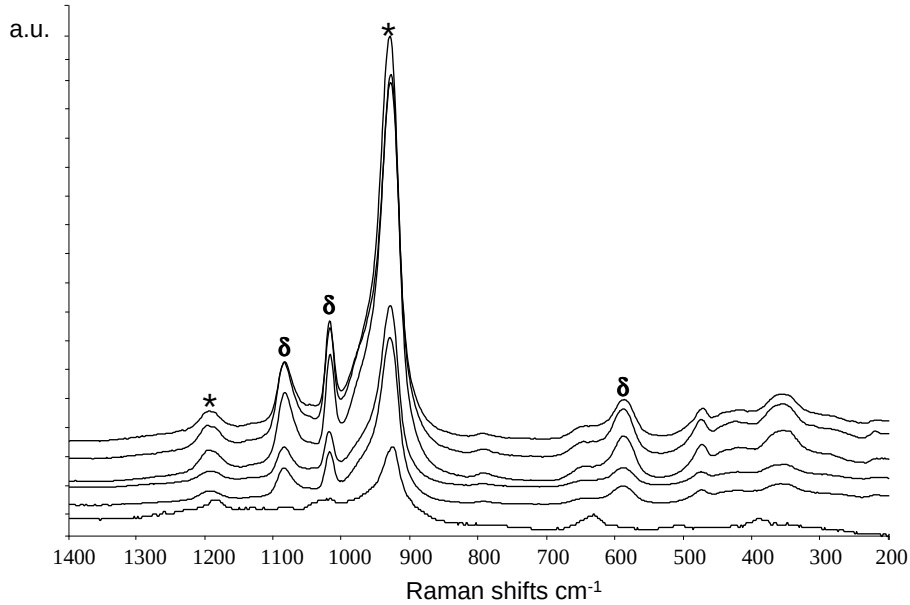

Fig. 3.8_ Raman spectra at different surface positions for sample O150 calcined. Symbols: * = $(VO)_2P_2O_7$; δ = δ $VOPO_4$.

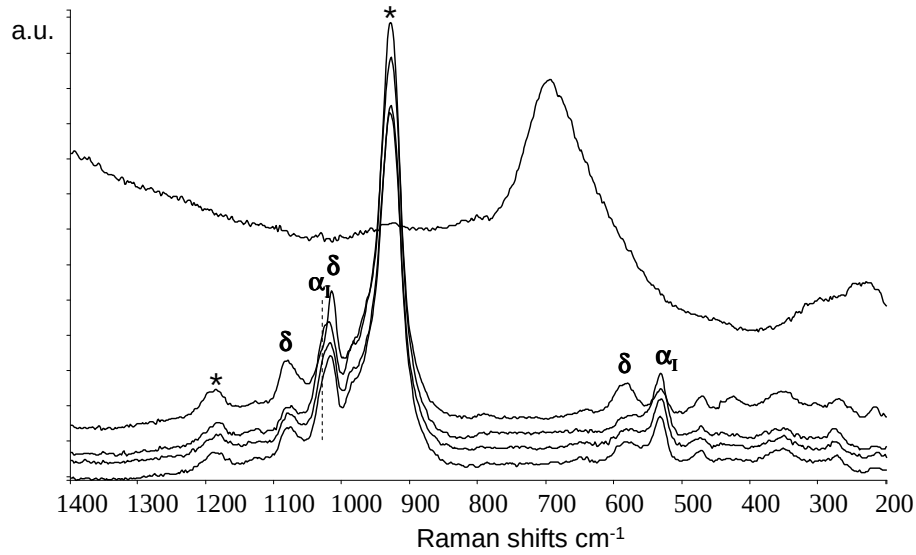

Fig. 3.9_ Raman spectra at different surface positions for sample O80 calcined. Symbols: * = $(VO)_2P_2O_7$; δ = δ $VOPO_4$; α_I = α_I $VOPO_4$.

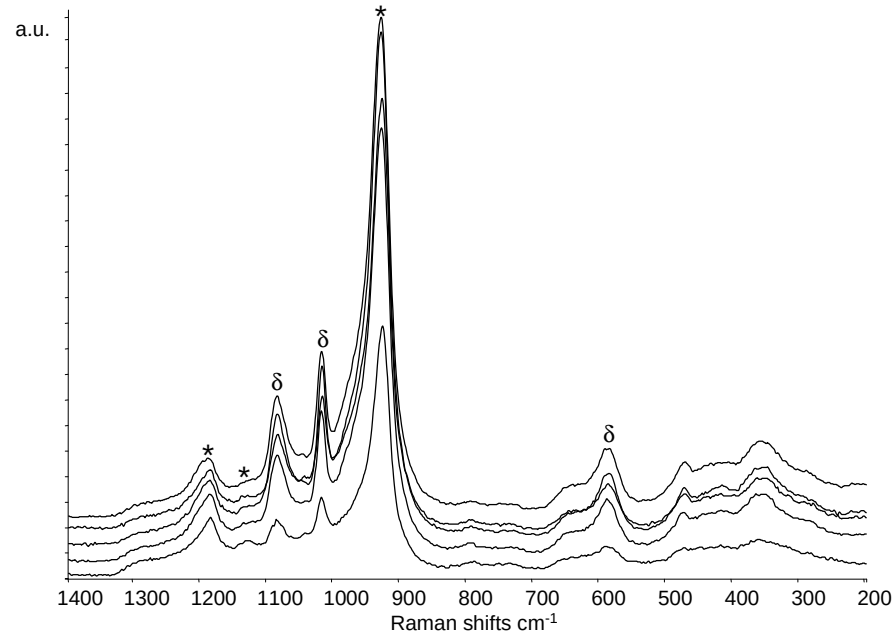

Fig. 3.10_ Raman spectra at different surface positions for sample O80Cl (glycol, $NbCl_5$) calcined. Symbols: * = $(VO)_2P_2O_7$; δ = δ $VOPO_4$; α_I = α_I $VOPO_4$.

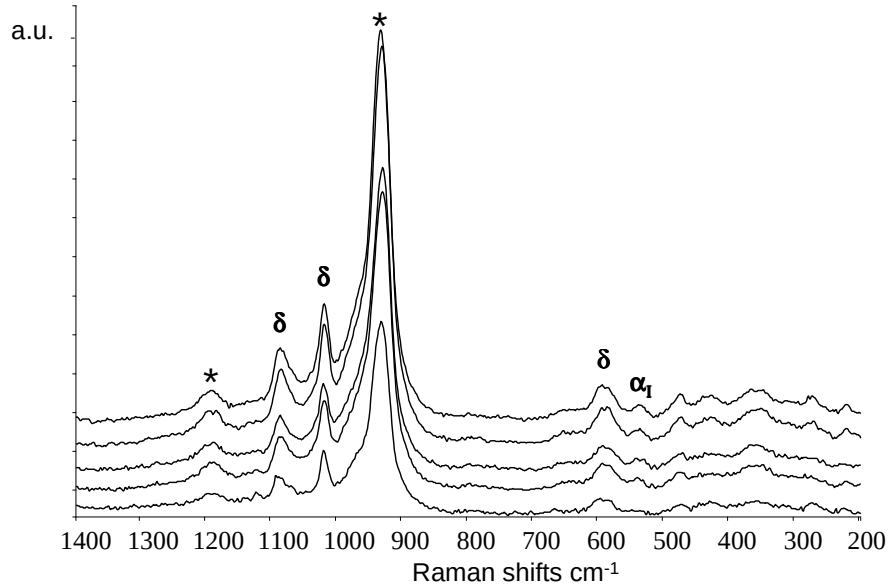

Fig. 3.11_ Raman spectra at different surface positions for sample O46 calcined. Symbols: * = $(VO)_2P_2O_7$; α_I = α_I $VOPO_4$; δ = δ $VOPO_4$.

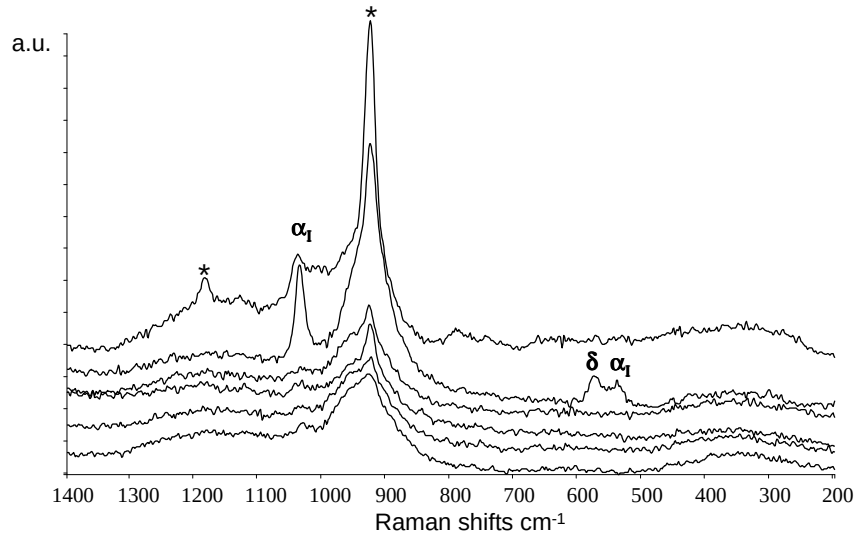

Fig. 3.12_ Raman spectra at different surface positions for sample O17 calcined. Symbols: * = $(VO)_2P_2O_7$; δ = δ $VOPO_4$; α_I = α_I $VOPO_4$.

In the case of sample O17, the different spectra recorded showed bands attributable to VPP, which however appeared to be strongly amorphous, since the characteristic bands at 1180, 1135 and 920 cm^{-1} were quite broad and of low intensity. However, in some spots it was possible to find spectra characteristic of the presence of more crystalline VPP and of oxidized phases (α_I-$VOPO_4$ and δ-$VOPO_4$). Spectra of catalysts O46, O80, O80Cl and O150 were quite similar, showing the presence of both VPP as the main phase and of minor quantities of α_I-$VOPO_4$ and δ-$VOPO_4$.

It is worth noting that, in a particular position of O80, we found bands attributable to amorphous $NbPO_4$. This indicates that with the preparation method used for the precursor synthesis it was not possible to disperse efficiently the Nb compound, a phenomenon which could affect catalytic performances.

The presence of $VOPO_4$ phases was not unexpected: their formation occurred during the first step of the thermal treatment, carried out in air, due to the development of hot-spots inside the catalytic bed.

In overall, the characterization indicates that Nb favoured the formation of δ-$VOPO_4$. The presence of δ-$VOPO_4$ may positively affect the catalytic performance, because this phase is considered the active and selective one; however, we have to remind that indeed the selective phase in the VPP-based catalyst is made of "patches" of δ-$VOPO_4$ dispersed over the VPP surface, which are generated during the reaction, not of bulk δ-$VOPO_4$ (all bulk $VOPO_4$ compounds have a negative effect on catalytic behaviour, as widely demonstrated in the literature). Therefore, stable bulk domains of δ-$VOPO_4$ are not involved in the selective reaction path, and may be detrimental for the catalytic behaviour, favouring total oxidation of the product and of reaction intermediates.

The UV-vis spectra (fig.3.13) showed quite a high oxidation degree for all calcined Nb-doped samples, with the exception of O17: with this sample, the spectrum showed V^{5+} bands (at 320 and 420 nm) of low intensity, but also a band attributable to V^{3+} species (520 nm). For all samples, bands relative to V^{4+} species, in the VPP structure, were also visible (at 300 and 850 nm). The finding of the V^{3+} band in O17 led us to consider the processes occurring during the thermal treatment of the precursor; the formation of this species is supposed to be a consequence of the redox reaction between strongly retained organic molecules and V atoms in the precursor. The V^{4+} species in the precursor are reduced by the organic compounds during the anaerobic step of the thermal treatment, carried out at 550°C in flowing nitrogen. In other words, the presence of V^{3+} might be due to the presence of a relatively high quantity of organic compounds retained in the O17 precursor. Nb-uncoordinated species or Nb/P/O species might favour the adsorption of organic molecules, probably generating Nb-alcoxides [11].

An alternative explanation is that because of the presence of a great amount of Nb in the catalyst, during the thermal treatment a fraction of the Nb^{5+} is incorporated in the VPP structure; the excess of positive charge may be compensated either by introduction of excess O^{2-} (for example, by generation of orthophosphate groups in place of pyrophosphate), or by the reduction of a corresponding amount of V^{4+} into V^{3+}. However, the formation of V^{3+} is undesired because it may lower MA selectivity.

Finally, it must be pointed that the eventual presence of Nb/P/O species cannot be excluded, as also suggested by the comparison with the spectrum of the pure hydrated niobium phosphate (delivered by CBMM), which showed a unique band centred at about 270 nm.

It's worth to note that sample O80 and O80Cl reported similar UV-vis spectrum; however O80Cl possessed a contribution at high energy (visible also for all other doped samples, excluding O80), in the 200-to-300 nm region.

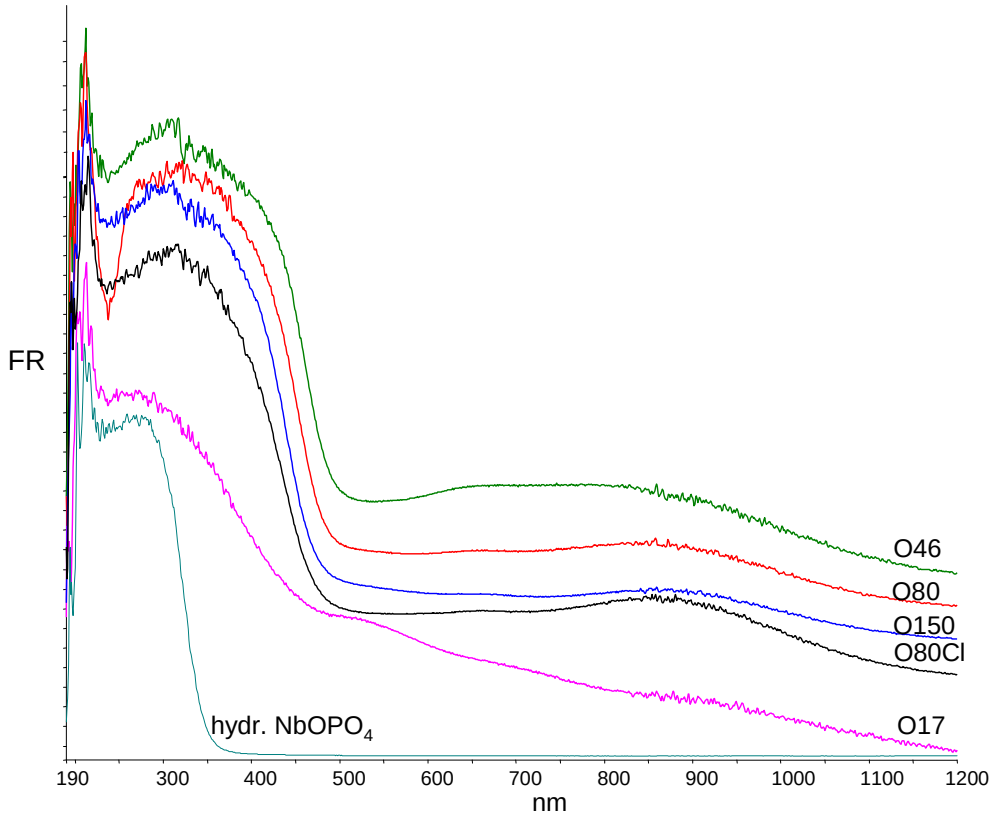

Fig. 3.13_UV-vis DR spectra of doped calcined samples (O150, O80, O46, O17) and doped sample O80Cl (prepared with glycol and $NbCl_5$) compared with spectrum of hydrated $NbOPO_4$ (CBMM).

3.2.3 Reactivity of Nb-doped catalysts under "hydrocarbon-lean" conditions

The catalytic tests of Nb-doped VPP catalysts were carried out in the aim of investigating the role of Nb. Furthermore, we also compare two methods of synthesis of Nb-doped catalyst, because the sample having a V/Nb atomic ratio equal to 80 was prepared according to two different procedures. Figure 3.14 compares the n-butane conversion and figures 3.15 and 3.16 the MA and $CO+CO_2$ (CO_x) selectivities, as a function of temperature for equilibrated catalysts B2, O150, O80, O46 and O80Cl.

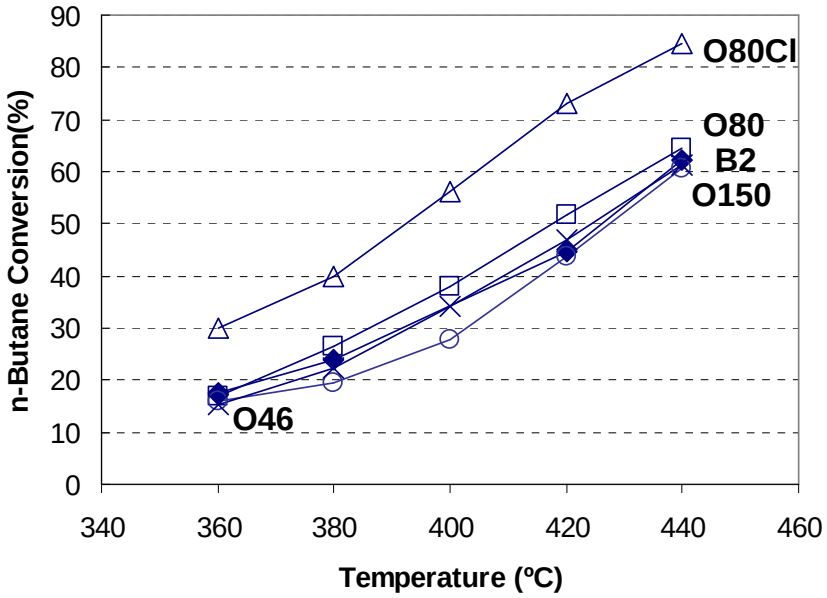

Fig. 3.14_ Conversion of n-butane for doped catalysts O150 (○), O80 (□), O80Cl (△), O46 (X) and for the un-doped B2 (♦). Conditions: 1,7% n-butane, 17% O_2; W/F=1.33 g·s·ml^{-1}.

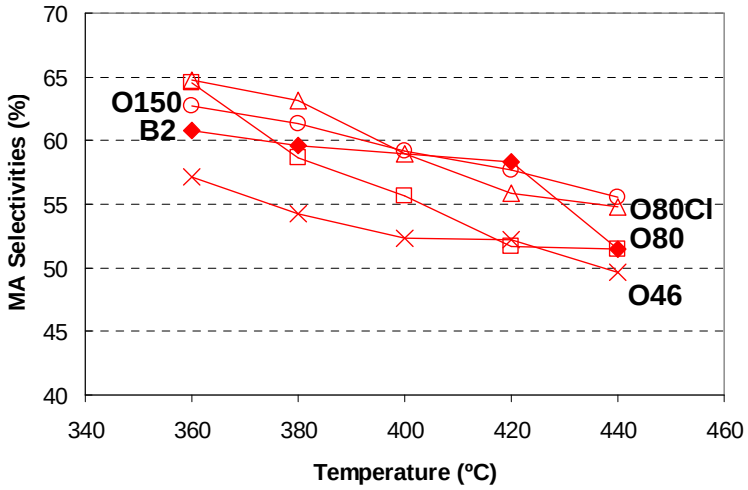

Fig. 3.15_ MA selectivity for doped catalysts O150 (○), O80 (□), O80Cl (△), O46 (X) and for the un-doped B2 (♦). Conditions: 1,7% n-butane, 17% O_2; W/F=1.33 g·s·ml^{-1}.

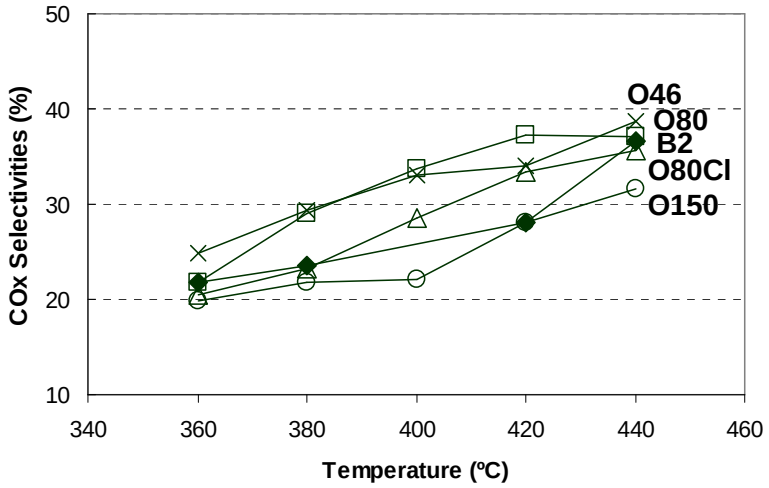

Fig. 3.16_ CO_x selectivities for doped catalysts O150 (○), O80 (□), O80Cl (△), O46 (X) and for the un-doped B2 (♦). Conditions: 1,7% n-butane, 17% O_2; W/F=1.33 g·s·ml^{-1}.

For all catalysts the n-butane conversion increased with temperature, as expected; the main products were carbon oxides (CO_x) and maleic anhydride (MA), however also acetic and acrylic acids were detected, especially at low temperature, as by-products.

The selectivity of MA slowly decreased with increasing temperature, because undesired combustion reactions occurred, leading to CO_x.

The presence of Nb led to more active catalysts only when the dopant was present in relative high quantity (V/Nb=80). Conversely, with the highest (V/Nb=46) and the lowest (V/Nb=150) Nb amount, a different behaviour was observed: at low temperature, sample O150 showed lower n-butane conversion compared to the reference catalyst (B2), while at higher temperature (420°C-440°C) both catalysts demonstrated similar values of n-butane conversion. In all cases however, the higher conversion values were obtained with catalysts having V/Nb=80. In particular, sample O80Cl reported the highest n-butane conversion, but this was probably due to the presence of the glycol in the synthesis procedure, rather than to Nb. In fact, it was reported in the literature that the preparation of the precursor using mixtures of isobutanol and glycols finally led to more active VPP catalysts [22]. In the case of sample O80Cl, an higher surface area was probably a consequence of molecules of glycol intercalated between the layers of the precursor lamellar structure, or adsorbed on the precursor surface [22].

In regard to MA selectivity, the effect of Nb was more complex. The main peculiarity of the undoped B2 catalyst was that at high temperature (440°C) the selectivity to MA showed a remarkable decrease with respect to experiments carried out at lower temperature. In general, the Nb-doped catalysts O80, O80Cl and O150 showed a better selectivity to MA at low temperature (360°C and 380°C), but then the selectivity declined more rapidly than for the B2 when the temperature was raised in the interval 380-420°C. On the other hand, no Nb-doped catalyst showed the fall of selectivity at 440°C, that was instead the main negative feature of the B2 catalyst. Because of these differences, the only catalyst showing better selectivity to MA than the B2 sample at both low and high temperature was O150 (the sample containing the lower amount of Nb); in

fact, O80 gave better selectivity than B2 only at 360°C, whereas the O46 sample gave worse selectivity than B2 at both low and high temperature. Sample O80Cl showed a behaviour similar to that of O150 (better selectivity than B2 at both low -360 and 380°C- and high temperature -440°C). Because of the better activity of O80Cl, finally this sample gave a considerably better yield to MA than that obtained with all the other samples. We can tentatively attribute a better selecdtivity at low temperature to an enhanced in-situ generation of the δ-$VOPO_4$, because of the presence of Nb.

.

In previous works [13,17], it was reported that the VPP catalyst showing the best catalytic behaviour is that one which generates a limited amount of δ-$VOPO_4$ over the VPP surface, in the form of microcrystalline or amorphous domains; on the other hand, the generation of bulk crystalline $VOPO_4$ compounds is detrimental for catalytic behaviour, because the selectivity to MA is lowered down considerably, whereas the intrinsic activity may be either higher or lower than that of the optimal catalyst, in function of the type of $VOPO_4$ compound formed. This agrees with most literature findings from other authors [3], highlighting the role of V^{5+} phosphate in the development of the species responsible for n-butane activation. From our data, it can be inferred that at low temperature the presence of increasing Nb amounts might play the role of favouring the generation of limited quantities of the active V^{5+} compound over the VPP surface. However, when the reaction temperature is raised (> 400°C), that is under conditions at which the gas-phase is more oxidant because of the increased n-butane conversion, while oxygen concentration still being present in large excess, Nb plays a negative role on selectivity, possibly because of the generation of excessive amounts of crystalline $VOPO_4$ compounds. Only the Nb content is very low (i.e., in sample O150), the selectivity to MA is better at loth low and high temperature; in other words, with V/Nb ratio equal to 80 (sample O80), the amount of Nb is optimal if the catalyst is used at low temperature, but it's too much if the catalyst is used at high temperature. Worth of note, from an industrial standpoint the most important results are those achieved under conditions at which the conversion of n-butane is 70-80%, that implies using temperatures higher than 400-420°C.

This means that a proper quantity of Nb favours the formation of the desired active and selective phase, but when an excessive quantity of it is used, this leads to a decrease of MA selectivity. This is not unexpected, since it is known that an appropriate quantity of V^{5+}, in redox equilibrium with V^{4+} during steady-state conditions, is necessary to transform n-butane into MA, and that however at high V^{5+} concentration, which might be generated because of the high Nb^{5+} amount, total combustion is kinetically more favoured, which leads to a low MA selectivity. Under conditions of high n-butane conversion, at which the gas-phase is more oxidant because of the high average oxygen-to-hydrocarbon ratio along the reactor, a Nb content higher than that corresponding to a V/Nb 150 leads to the generation of an excessively oxidized catalyst. This may favour the combustion of the formed MA.

Figure 3.17 reports a better overview of the results, plotting the selectivity to MA in function of n-butane conversion. The better results obtained with O150 at both low and high temperature, and the outstanding performance of O80Cl are here confirmed. The better yield to MA obtained with O80Cl

sample was mainly due to its higher activity, which derived mainly from its higher surface area. This is evident from Table 3.3, which compiles the SSA values for spent catalysts.

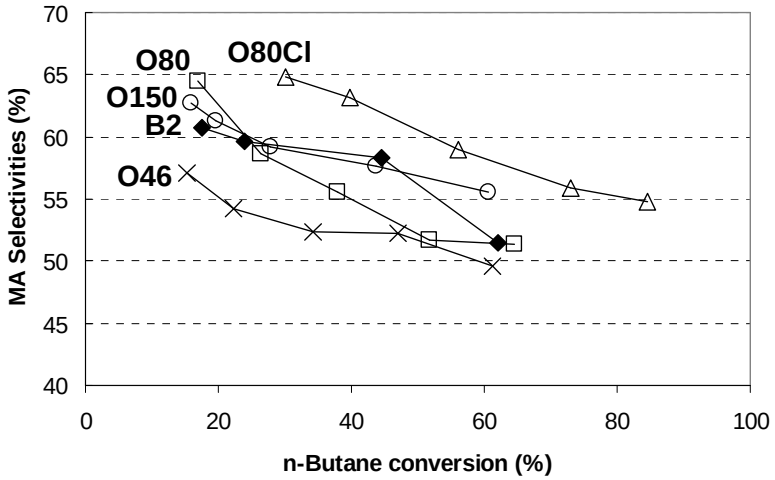

Fig. 3.17_ MA selectivity for doped catalysts O150 (○), O80 (□), O80Cl (△),O46 (X) and the un-doped B2 (♦) as a function of n-butane conversion. Conditions: 1,7% n-butane, 17% O_2; W/F=1.33 g·s·ml^{-1}.

	Surface area (m^2/g)
B2	14
O150	11
O80	10
O80Cl	19
O46	14

Table. 3.3_ Single point BET surface area for downloaded catalysts O150, O80, O80Cl, O46 and for the un-doped B2.

Finally, Figure 3.18 reports a summary of catalytic behaviour, plotting the conversion at 360°C and the selectivity at 360°C and at 440°C for all catalysts. Once again, it is possible to Figure out the incremental effect on catalytic behaviour achieved by the addition of small quantities of Nb (which however was a function of temperature), and the outstanding behaviour of the O80Cl sample.

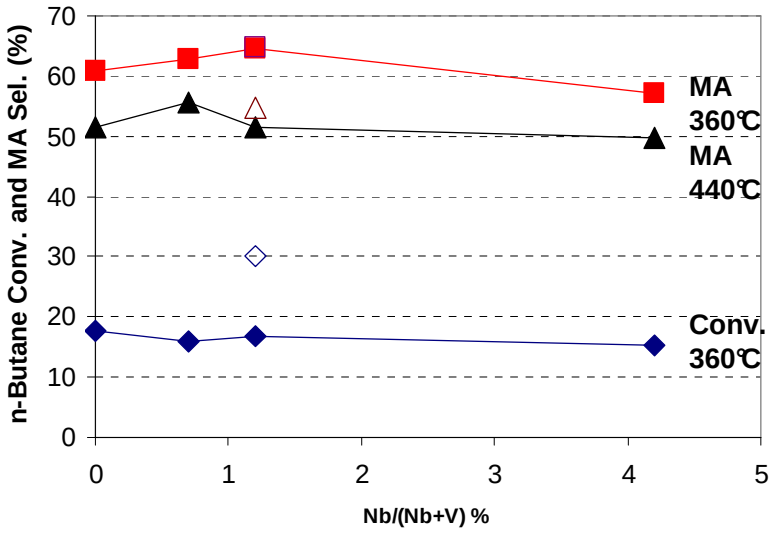

Fig. 3.18_ Conversion of n-butane (♦, ◊), maleic anhydride selectivity (■,□) at 360°C and maleic anhydride selectivity (▲,△) at 440°C for samples prepared with 100% isobutanol and Nb-salt and for sample O80Cl prepared with isobutanol/1,4-butanediol mixture and $NbCl_5$ (empty symbols), as a function of Nb/(Nb+V)% molar ratio. Conditions: 1,7% n-butane, 17% O_2, W/F=1.33 $g \cdot s \cdot ml^{-1}$.

We can not exclude that an additional problem derived from the use of higher Nb quantities may derive from an inaccurate dispersion of the dopant component, and to the formation of segregated phases. This came out to be a problem in the case of O46 (see the characterization of the calcined catalysts), but the same could occur also with sample O80.

An inappropriate dispersion of Nb could have caused the segregation of Nb/P/O, which finally may negatively contribute to the catalytic behaviour. Characterisation of spent catalyst will alow to better study this aspect, in the aim of understanding whether the negative role of Nb experimentally observed at higher Nb loadings was due either to an excessive oxidation of the VPP (boosted by the Nb itself), or to a direct contribution to reactivity deriving from unselective Nb-containing compounds.

In conclusion, the data obtained clearly indicate that the role of Nb and its effect on catalytic behaviour is strictly a function of both the Nb amount and the reaction conditions used; in other woprds, the optimal V/Nb ratio may vary depending on temperature and inlet feed composition.

For example, at oxidizing conditions, that is at low n-butane concentration (at which the hydrocarbon is the limiting reagent) and high working temperature, it is not possible to observe a positive effect of Nb, because the catalyst is already strongly oxidized; indeed, when a high amount of dopant is used (V/Nb=46 in O46), a worse catalyst performance is observed, probably as a consequence of an excessive formation of bulk $VOPO_4$, which finally is detrimental for the catalytic performance, and eventually also because of a direct negative contribution from segregated Nb-containing compounds (e.g., either a Nb/P/O compound, or even Nb oxide itself). As evident from the characterization of O46, an high concentration of Nb strongly affects, or even irreversibly change, the bulk catalyst structure.

On the other hand, catalysts with higher Nb concentration might show improved catalytic performances under “hydrocarbon-rich” conditions, that is at high n-butane concentration (more reducing conditions), as previously shown in fig. 3.1.

3.2.4 Characterization of Nb-doped used catalysts

The characterization of used catalysts may be helpful to interpret catalytic performances, since the latter are consequence function of catalyst surface composition, which effectively developed under reaction conditions reaction.

The ex-situ Raman spectra of used catalysts (B2, O150, O80, O80Cl, and O46,) are shown in figures 3.19-3.23.

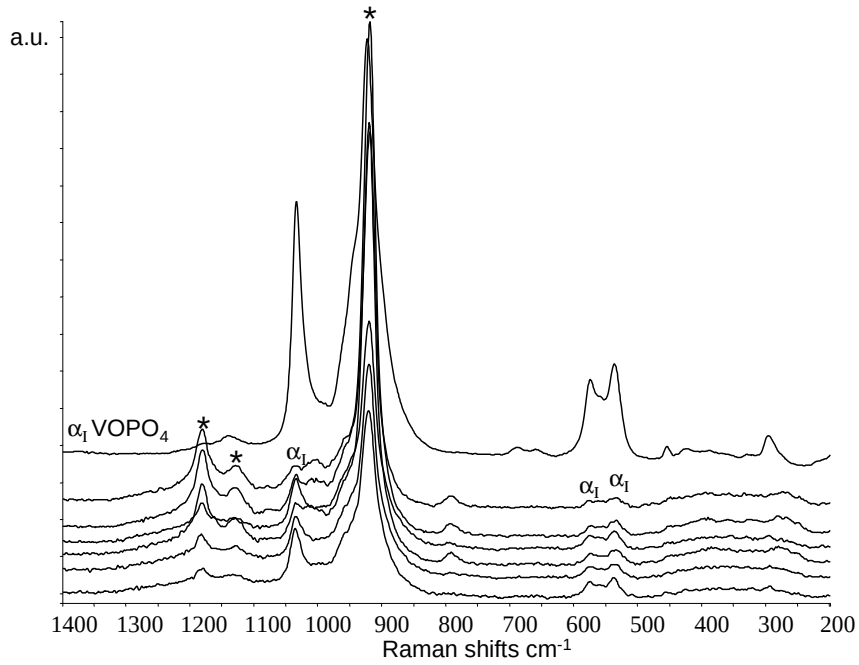

Fig. 3.19_ Raman spectra of used B2 (Nb=0) catalyst. Symbols: * = $(VO)_2P_2O_7$; α_I = α_I $VOPO_4$.

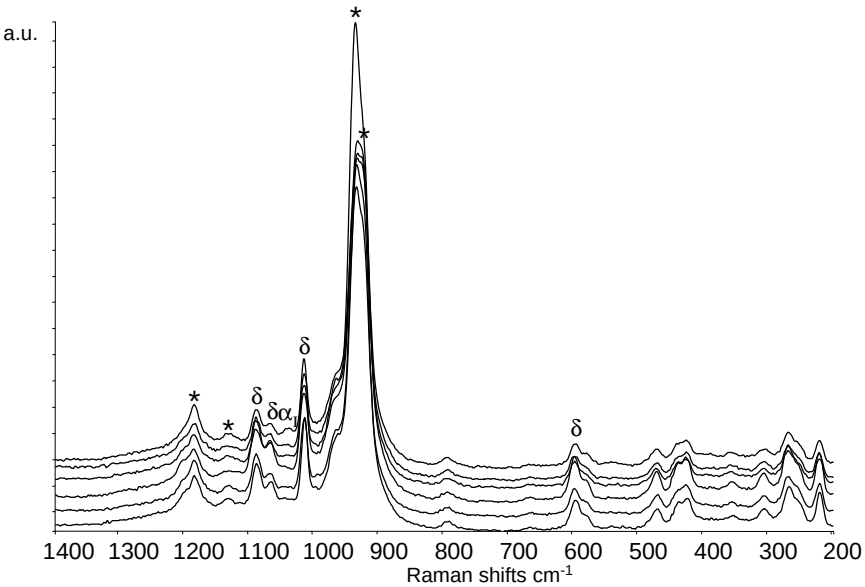

Fig. 3.20_ Raman spectra of used O150 (V/Nb=150) catalyst. Symbols: * = $(VO)_2P_2O_7$; δ = δ $VOPO_4$; α_I = α_I $VOPO_4$.

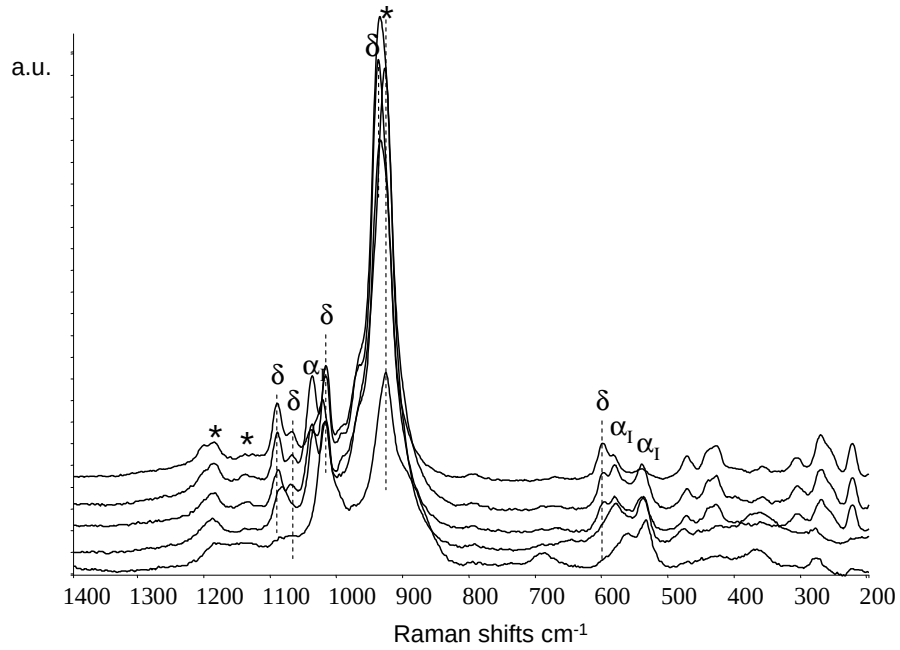

Fig. 3.21_ Raman spectra of used O80 (V/Nb=80) catalyst. Symbols: * = $(VO)_2P_2O_7$; δ = δ $VOPO_4$; α_I = α_I $VOPO_4$.

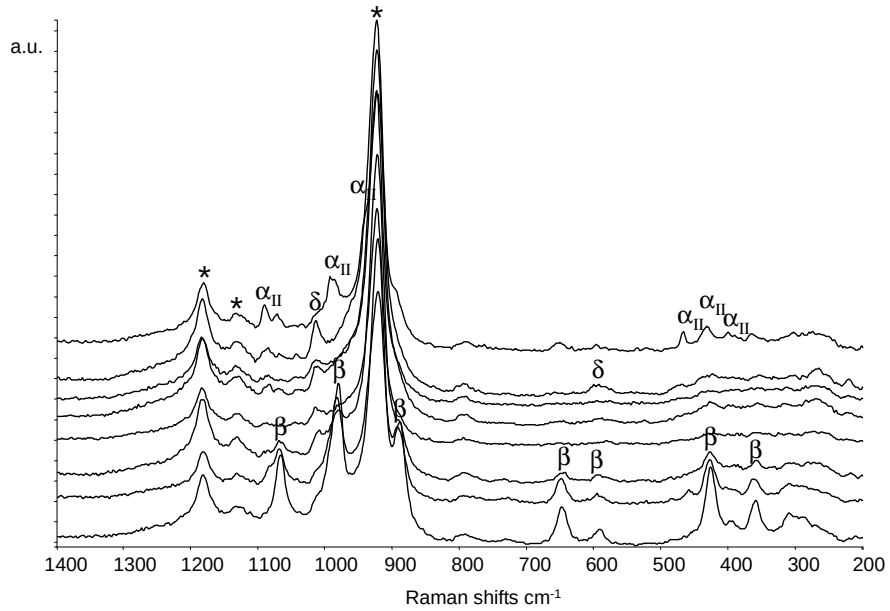

Fig. 3.22_ Raman spectra of used O80Cl (V/Nb=80, glycol, $NbCl_5$) catalyst. Symbols: * = $(VO)_2P_2O_7$; δ = δ $VOPO_4$; α_I = α_I $VOPO_4$; α_{II} = α_{II} $VOPO_4$.

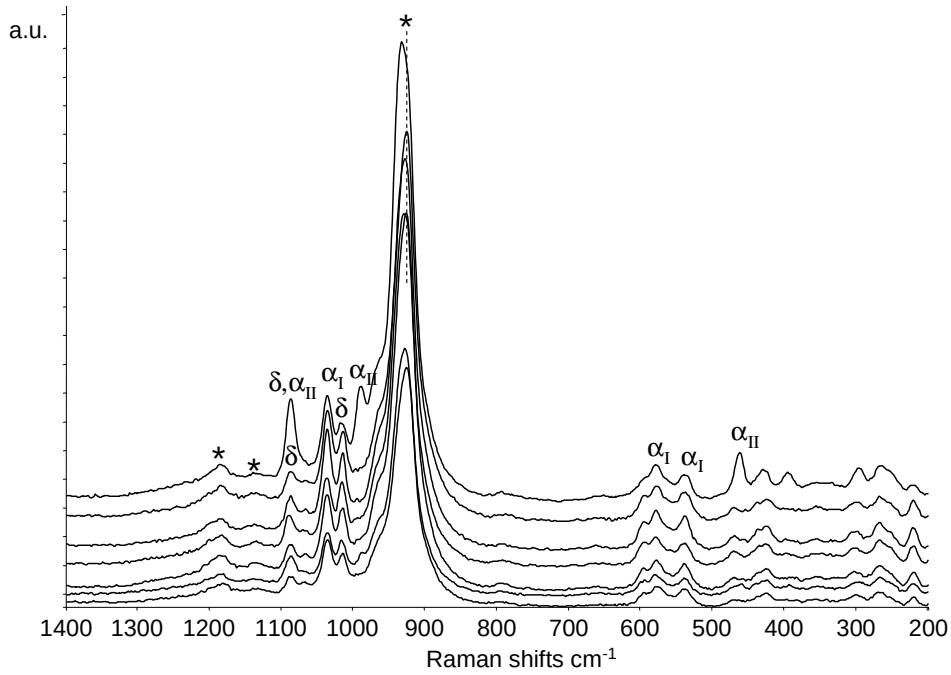

Fig..3.23_ Raman spectra of used O46 (V/Nb=46) catalyst. Symbols: * = $(VO)_2P_2O_7$; δ = δ $VOPO_4$; α_I = α_I $VOPO_4$; α_{II} = α_{II} $VOPO_4$.

In the case of Nb-doped samples (especially in O150 and O80), the presence of δ-$VOPO_4$ after catalytic tests (which instead was not observed in the spectrum of spent B2 catalyst) demonstrates that this compound was very stable, which probably was a consequence of Nb doping. The compound is supposed to be the active and selective phase, generated over the VPP surface during n-butane selective oxidation; however if this phase is present in big amount, the result is a poisoning effect of the catalyst, with a final lower MA selectivity.

The XRD (fig.3.24) and UV-vis (fig.3.25) analyses are consistent with Raman characterization.
The diffraction patterns of the samples are compared in figure 3.24. It is evident that sample O150 and reference one (B2) were quite similar, consisting of VPP as the predominant compound, and showing also additional reflections attributable to some oxidized phases (in accordance with previous characterizations). In regard to this, we have to note an interesting difference: O150 showed the presence of δ-$VOPO_4$ (reflections at 2θ=19,6°-22°-24,2°), in contrast B2 showed the α_I/β-$VOPO_4$ phases (reflections at 2θ=20,5° and 2θ=26,5° respectively). The used O80 catalyst showed a less crystalline VPP; in particular, the strong reflection at 2θ=29,9° was partially hidden by other strong reflections, attributable to different $VOPO_4$ phases. Moreover, it also showed a weak reflection at 2θ=21,2°, that could be attributed to ω-$VOPO_4$. Finally, other reflections were present at lower diffraction angles (2θ), more precisely at 2θ=12,7° and 2θ=13,1° (as well as reflections at 2θ=25,7° and 2θ=26,7°), which are relative to hydrated $(VO_3)(PO_4)_2$; the presence of this compound was unusual; evidently, it was not transformed into VPP during the thermal treatment. Interestingly, sample O80Cl, which differed from O80 in the preparation method used (glycols and $NbCl_5$) reported a diffraction pattern characterized solely by VPP reflections, whereas $VOPO_4$ phases were totally absent.

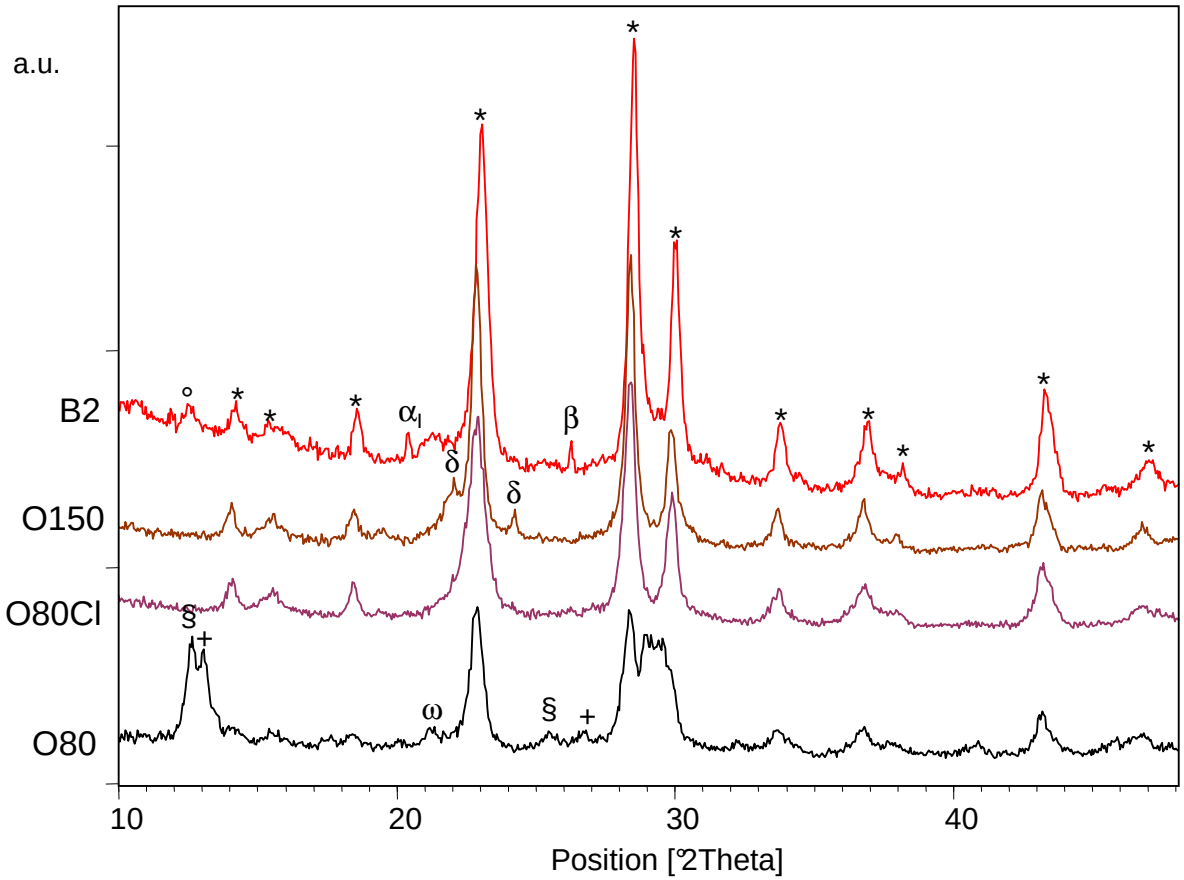

Fig. 3.24_ XRD analysis of O80 (V/Nb=80), O150 (V/Nb=150), B2 (Nb=0) and O80Cl (V/Nb=80, glycol preparation with $NbCl_5$) used catalysts. Symbols: * = $(VO)_2P_2O_7$; α_I = α_I $VOPO_4$; + = $(VO)_3(PO_4)_2 \cdot 6H_2O$ (JCPDS 00-049-1256); § = $(VO)_3(PO_4)_2 \cdot 7H_2O$ (JCPDS 00-049-1257); ° = $VOPO_4 \cdot 2H_2O$; β = β $VOPO_4$; ω = ω $VOPO_4$; δ = δ $VOPO_4$.

The UV-vis DR spectra (fig.3.25) showed the presence of less oxidized surfaces as compared to spectra in figure 3.13 (for calcined catalysts). In particular, the used O80 catalyst was more oxidized than the other used samples, as evident from a broad band centred at 350 nm and a relative shoulder at 410 nm, which is attributable to V^{5+} species. In contrast, these bands seemed almost absent with the un-doped B2 catalyst. Finally, the doped catalysts did not show the band at about 510 nm, attributed to a V^{3+} species [15], which was instead present in the spectrum of used B2. Moreover, O80Cl resulted to be more reduced than B2. It is worth noting that all samples, except O80Cl, possessed a contribution at lower wavelength, regardless the presence of Nb; a unambiguous attribution of this band was not possible.

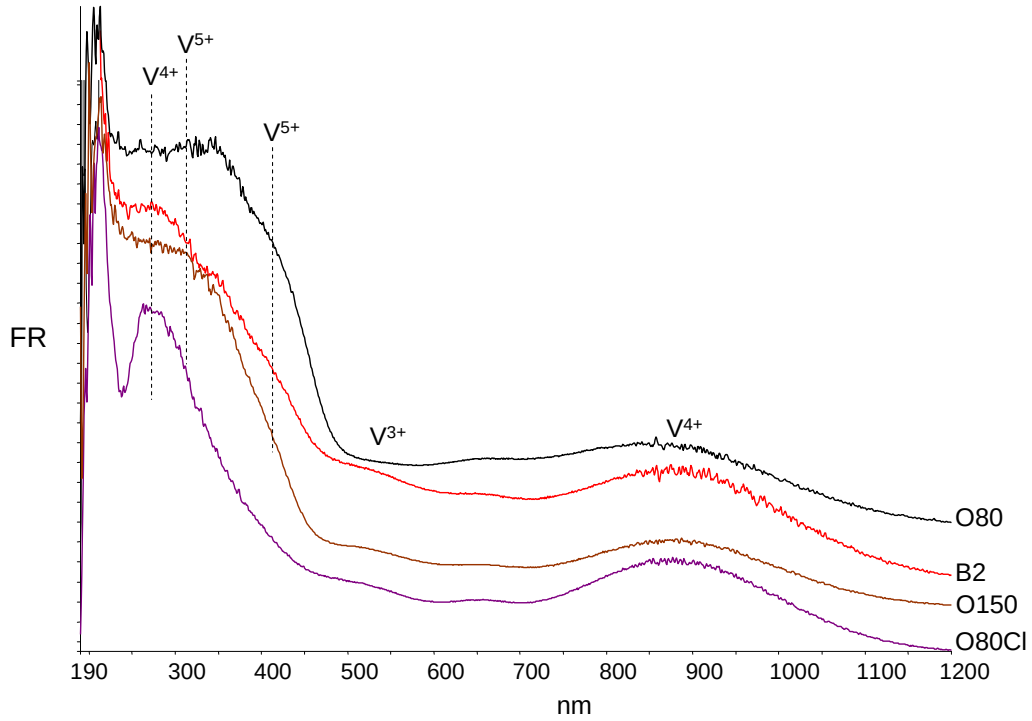

Fig..3.25_UV-vis spectra of O80 (V/Nb=80), O150 (V/Nb=150), B2 (Nb=0) and O80Cl (V/Nb=80, glycol preparation with $NbCl_5$) used catalysts.

3.2.5 In-situ Raman analysis of Nb-doped VPP catalysts

Raman in-situ characterisation was carried out with Nb-doped VPP catalysts, in order to correlate surface changes, especially the eventual development of δ-$VOPO_4$ phase and its range of stability, with catalytic performances.

We carried out these experiments with two used catalysts, downloaded after lifetime experiments in a pilot unit: an undoped VPP and a Nb-doped VPP containing a low Nb amount (for a V/Nb ratio higher than 100). The method of preparation used for these samples can not be disclosed. These catalysts were compared with our O46 and O80 samples, in order to check whether differences between samples in regard to the in-situ development of oxidized compounds could be observed, in function of the Nb content.

It is worth noting that these in-situ treatments lead to meaningful and reliable results only when the catalyst is homogeneous; this means that while choosing different surface spots, the resulting Raman spectrum is the same. This aspect is not obvious, especially when we consider catalysts having a not proper dispersion of the dopant, which could cause the development of an heterogeneous surface composition. However, catalysts used for this study were all equilibrated, which implies that they should have reached a stable composition; furthermore, their superficial composition (even considering the limits of Raman spectroscopy) was confirmed to be homogeneous. For this reason, we could compare the spectra of the various doped catalysts prepared.

The in-situ Raman study was carried out by loading a very small amount of each equilibrated catalyst inside the Raman cell.

First tests were carried out at low temperature (380°C) in flowing dry air: Raman spectra were collected during all the experiment, since the very beginning at room temperature, while heating up to the isotherm temperature and, finally, during this period. The spectra obtained with O46 are shown in figure 3.26; in fact, this was the only sample which showed relevant changes at 380°C in air. The in-situ formation of δ-$VOPO_4$ is evident, a phenomenon which occurred since the beginning of the isothermal step(bands at 1083, 1013 and 590 cm^{-1}).

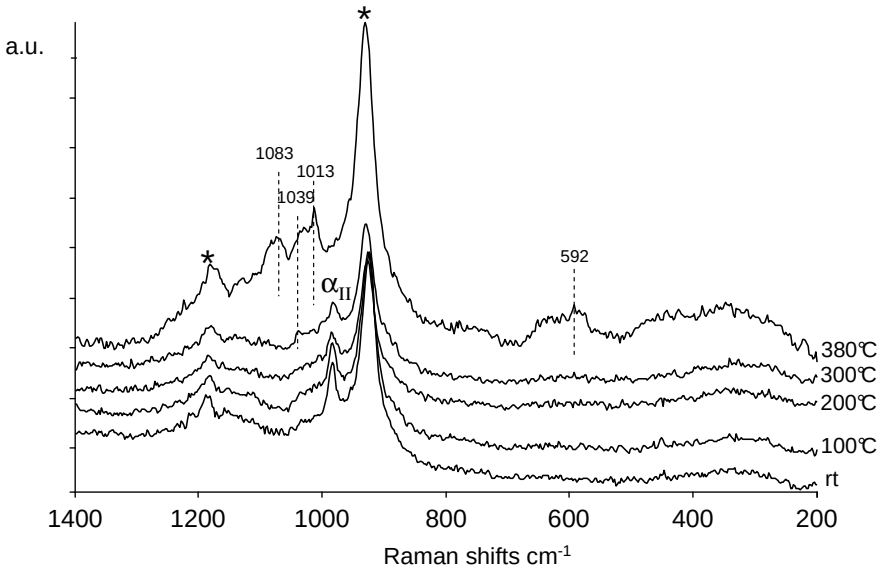

Fig. 3.26_Raman in-situ test with catalyst O46 (air, 380°C): spectra shown from room temperature (bottom) up to the isothermal temperature (top). Symbols: * = VPP; $\alpha_{II} = \alpha_{II}$ -$VOPO_4$.

δ-$VOPO_4$ formed together with α_I-$VOPO_4$ (band at 1039 cm^{-1}), but the latter disappeared very quickly; in fact, after only half an hour, the shoulder close to the main band at 1013 cm^{-1} was no longer visible, and only the strong bands attributable to δ-$VOPO_4$ were left (fig.3.27).

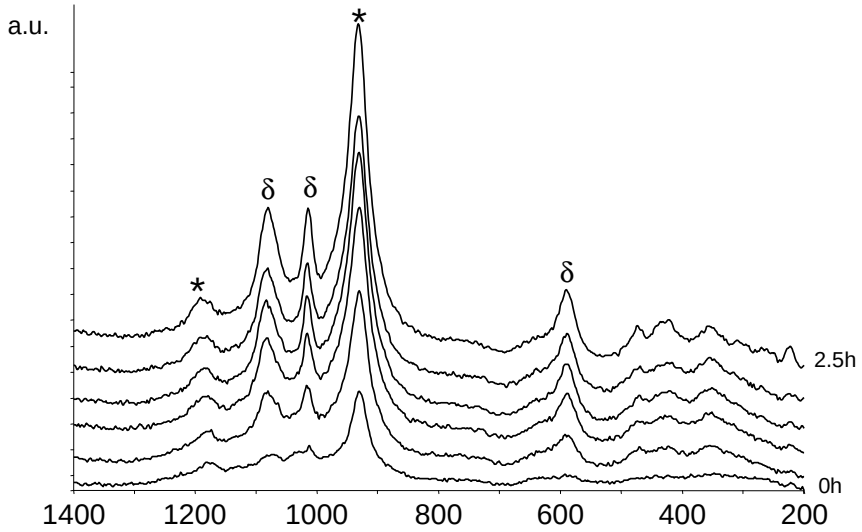

Fig. 3.27_Raman in-situ test with catalyst O46 (air, 380°C): spectra shown during the isothermal step, collected every 30 minutes, from 0h (bottom) to 2,5h (top). Symbols: * = VPP; δ = δ-$VOPO_4$.

The intensity of bands attributed to δ-$VOPO_4$ increased during the isothermal period (380°C), and were not affected neither after the addition of water vapour (~10%) in the inlet flow, nor when

temperature was increased up to 440°C (fig.3.28). This behaviour highlighted the strong stability of bulk δ-$VOPO_4$.

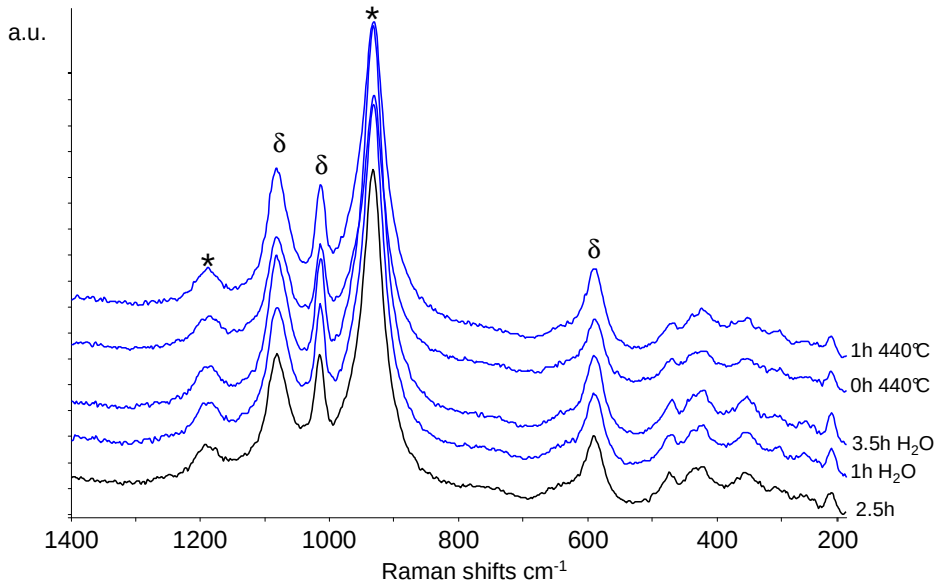

Fig. 3.28_Raman in-situ test with O46 (dry air and humid air, 380°C): spectra shown after 2,5h at 380°C in dry air (bottom), then at 380°C in humid air (middle), finally at 440°C in humid air (top). Symbols: * = VPP; δ = δ-$VOPO_4$.

The sample was then cooled down to room temperature, in humid air: the spectra collected didn't show any changes with respect to spectra previously registered (fig.3.29).

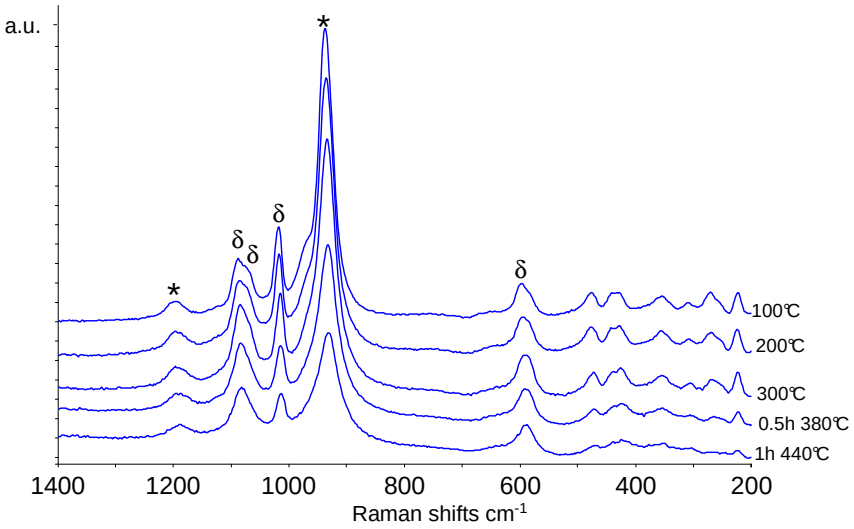

Fig. 3.29_Raman in-situ test with o46 (humid air, 380°C): spectra shown during the cooling step from 440°C (bottom) down to 100°C (top), in humid air. Symbols: * = VPP; δ = δ-$VOPO_4$.

The spectrum collected at room temperature, after the in-situ treatment (fig.3.30), showed bands attributable to δ-$VOPO_4$ (at 1202, 1089, 1071, 1016, 598, 474 cm^{-1}), while amongst the characteristic bands of VPP only weak bands were visible (at 1188, 272, 257 cm^{-1}) and the strongest one (923 cm^{-1}) resulted to be shifted at higher wavenumbers (937 cm^{-1}). However, it must be noted that, due to its asymmetric shape, this last band could result from an overlapping effect, between the two strongest bands of VPP and δ-$VOPO_4$, at 920 and 936 cm^{-1} respectively [16].

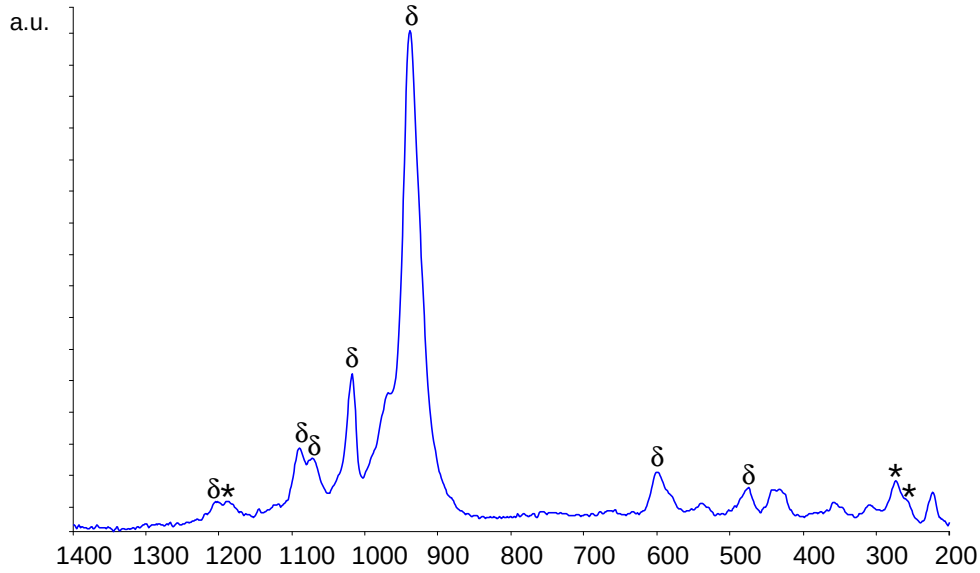

Fig. 3.30_Raman in-situ test with O46 (humid air, 380°C): spectra shown at the end of the thermal treatment. Symbols: * = VPP; δ = δ-$VOPO_4$.

Another experiment was carried out using sample O46 (fig.3.31). The catalyst was heated up to 380°C, in flowing air, to generate the δ-$VOPO_4$: this phenomenon occurred after 20 minutes at the isothermal temperature (bands at 1074, 1012, 585 cm^{-1}), and after one hour, bands of the oxidized phase were well formed (fig.3.32).

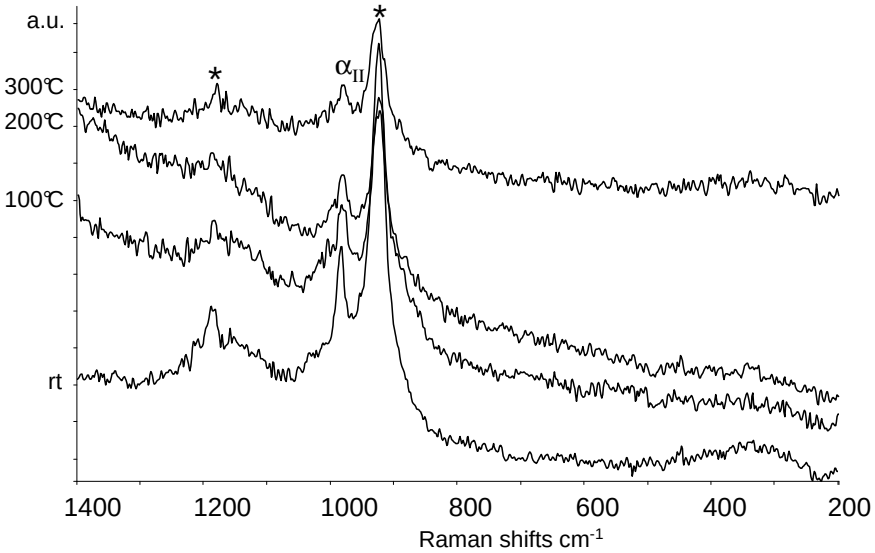

Fig. 3.31_Raman in-situ test with O46 (air, 380°C): spectra shown from room temperature (bottom) to 300°C (top). Symbols: * = VPP; α_{II} = α_{II} -$VOPO_4$.

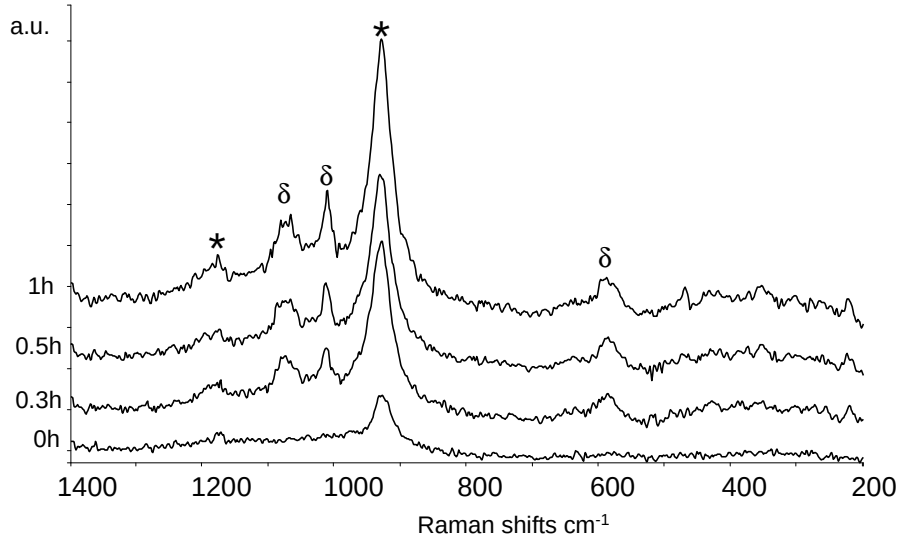

Fig. 3.32_Raman in-situ test with O46 (air, 380°C): spectra shown from 0 h (bottom) to 1 h (top), during the isothermal step. Symbols: * = VPP; δ = δ-$VOPO_4$.

At this moment, the flow was switched from air to nitrogen, and the sample was cooled in this inert flow down to room temperature (fig. 3.33): this change was done with the aim of investigating the self-reducibility behaviour of δ-$VOPO_4$. In other words, the reversibility of the δ-$VOPO_4$ formation is an expected event, because this phase is not generally observed during the ex-situ characterization of used catalysts, especially when they are cooled down from high to room temperature in an inert flow, after catalytic tests.

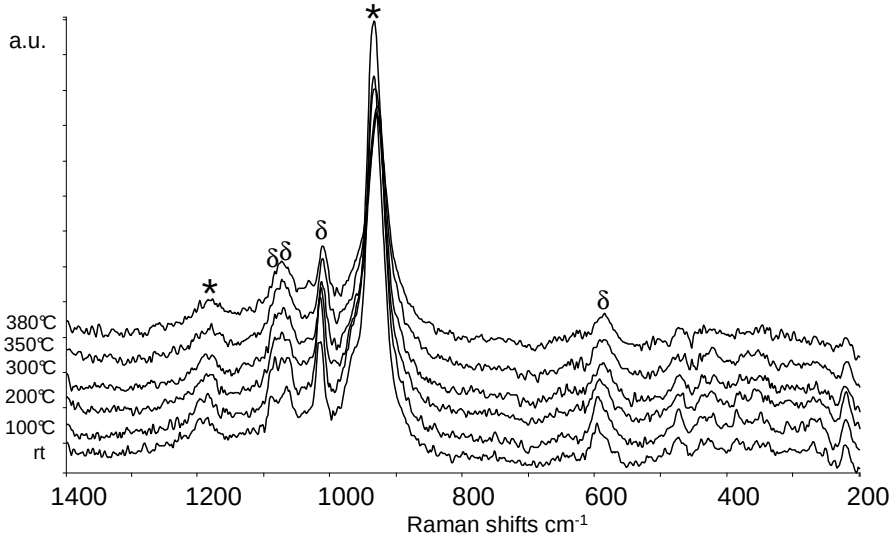

Fig. 3.33_Raman in-situ test with catalyst O46 (N_2, 380°C): spectra shown from 380°C (top) to room temperature (bottom). Symbols: * = VPP; δ = δ-$VOPO_4$.

The spectrum, after cooling down to room temperature (fig.3.33), still showed the strong bands of δ-$VOPO_4$ (1089, 1064, 596 cm^{-1}); the band at 1074 cm^{-1} was splitted into two components. We can conclude that the redox reversibility, reported in the literature for the δ-$VOPO_4$ formed in small domains over the surface of the VPP does not occur in the case of bulk δ-$VOPO_4$.

These experiments indicate that at high Nb loading: a) the formation of δ-$VOPO_4$ occurred very easily, considering the mild conditions used; and b) the compound formed was very stable.

The investigation was then focused on a fully equilibrated VPP catalyst, having low Nb content (V/Nb > 100). The sample behaviour during in-situ treatments was compared with tests on an undoped equilibrated sample .

The first in-situ treatment was carried out in flowing dry air, at 380°C. For both catalysts, a weak surface change occurred during this initial experiment (380°C, air): α_I-$VOPO_4$ (band at ca 1030 cm^{-1}) was the only phase formed since the very beginning of the isothermal period, but the intensity of this band was very low (fig.3.34).

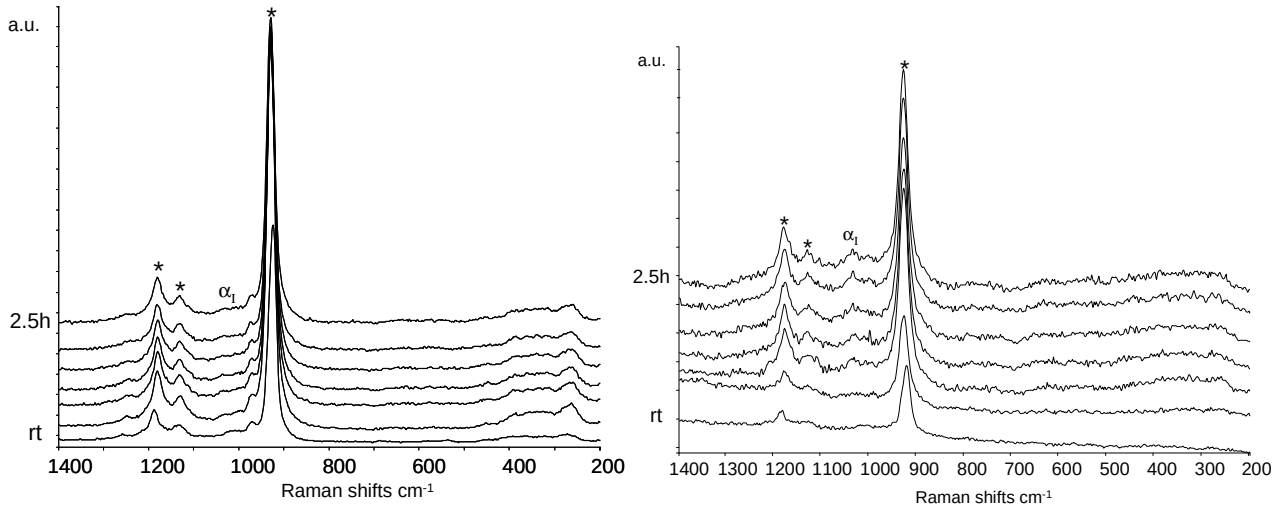

Fig. 3.34_Raman in-situ test (air, 380°C) with the undoped VPP equilibrated catalyst (left) and with the Nb-doped equilibrated catalyst (right): spectra shown at room temperature (bottom), and then during isothermal period at 380°C (every 30 min, from bottom to top). Symbols: * = VPP; $\alpha_I = \alpha_I$ -$VOPO_4$.

No other transformations were observed, and the characteristic spectrum of VPP was always shown during the test. This experiment demonstrated that stronger conditions are needed to observe any difference between the samples, attributable to the Nb presence.

In another experiment, the temperature was increased up to 440°C, in flowing air. For the un-doped catalyst, the spectrum registered at room temperature showed bands attributable to VPP and to $VO(PO_3)_2$ (1255, 1204, 965 cm^{-1}), the latter is a phase sometimes observed in used catalysts, and its presence is related to an excess of P. During heating up to 440°C, the α_I-$VOPO_4$ band (at ca 1030 cm^{-1}) appeared; moreover, after some hours weak bands attributable to δ-$VOPO_4$ (band centred at 1070 cm^{-1} and shoulder at 1017 cm^{-1} to α_I) began to be visible (fig. 3.35).

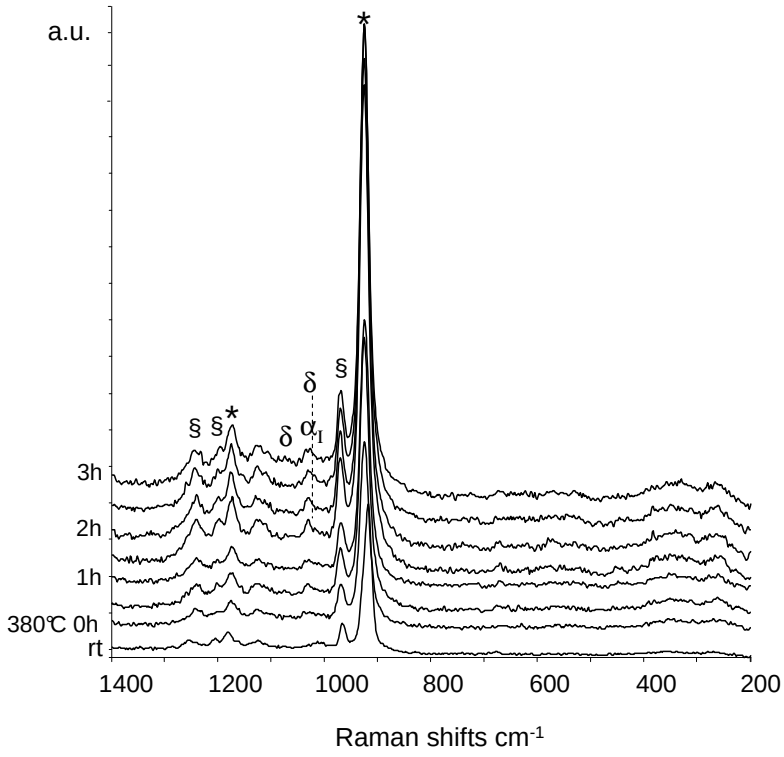

Fig. 3.35_Raman in-situ test (air, 440°C) with the undoped equilibrated VPP catalyst: spectra showed at room temperature (bottom), then during the isothermal period at 440°C (every 30 min, from bottom to top). Symbols: * = VPP; $\delta = \delta$-$VOPO_4$; $\alpha_I = \alpha_I$-$VOPO_4$; § = §-$VO(PO_3)_2$.

Regarding the doped catalyst, the behaviour observed was quite similar to that shown by the undoped sample (fig.3.36): broad and very weak bands attributable to δ-$VOPO_4$ (1080, 1017, 594 cm^{-1}) appeared after some hours at 440°C, in flowing air. However, due to the broadness of the band centred at ca 1020 cm^{-1}, it was not possible to exclude the presence of α_I-$VOPO_4$, which is usually observed at 1030 cm^{-1}.

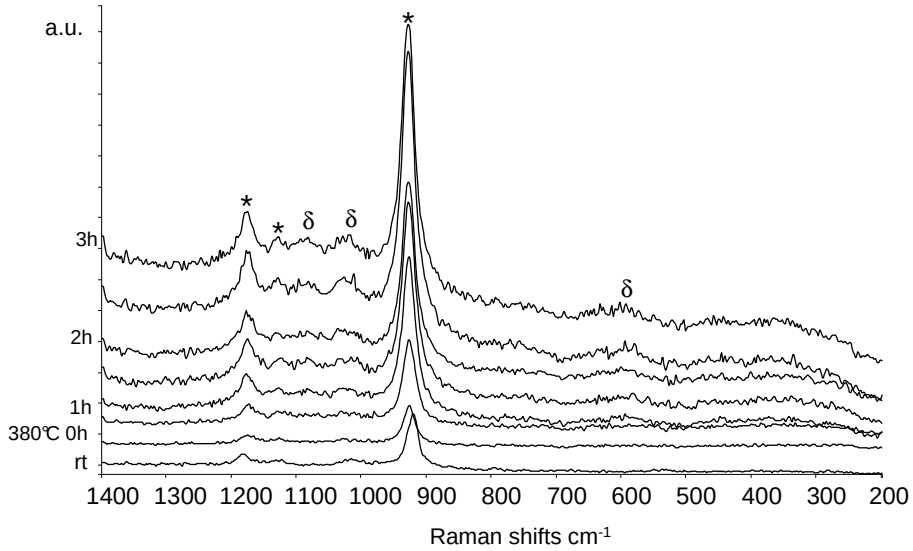

Fig. 3.36_Raman in-situ test (air, 440°C) with the equilibrated undoped catalyst: spectra shown at room temperature (bottom), and then during the isothermal period at 440°C (every 30 min, from bottom to top). Symbols: * = VPP; $\delta = \delta$-$VOPO_4$.

In conclusion, the two catalysts showed a similar behaviour, that was very much different from what observed at lower temperature with O46.

The presence of water vapour in the inlet stream should accelerate the surface changes [13]; therefore, we carried out an experiment by adding water vapour (~10%), in flowing air at 440°C.
Spectra registered during the in-situ treatment in humid air flow (440°C), for the undoped catalyst, are reported in figure 3.37. In this case, first the sample was left in dry air at 440°C for some hours: also in this case, the formation of the oxidized phase did not occur, but a broad and weak band at ca 1030 cm^{-1} appeared. After addition of water to the inlet flow, broad bands attributable to δ-$VOPO_4$ formed (at 1085, 1013 cm^{-1}); however also α_I-$VOPO_4$ (1030 cm^{-1}) was observed. We then withdrew water from the feed (fig.3.38): the spectra showed no relevant changes, and bands relative to δ-$VOPO_4$ remained unaltered.

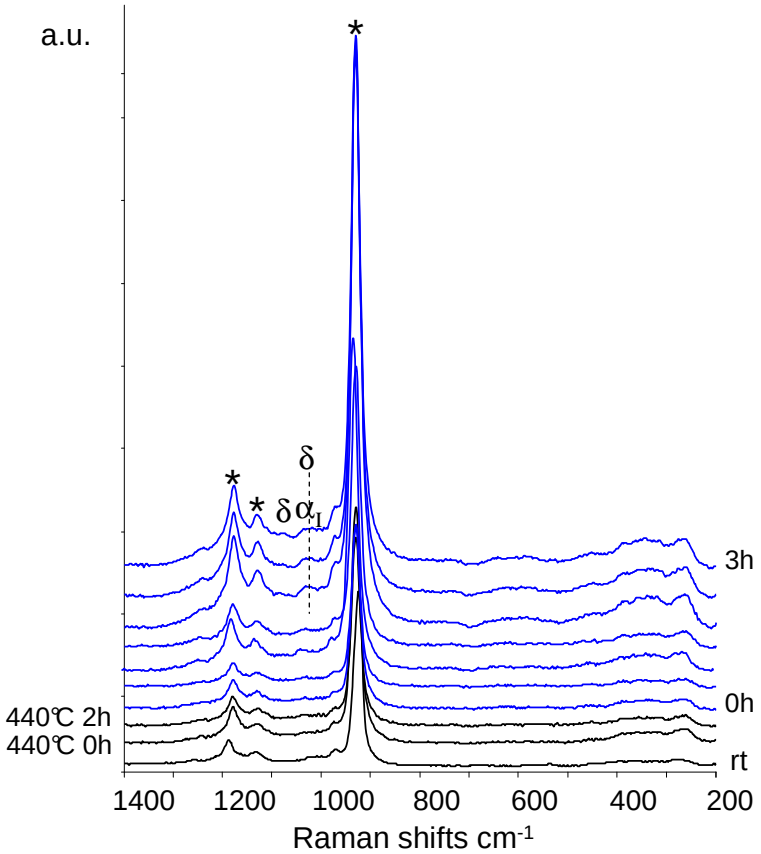

Fig. 3.37_Raman in-situ test (air, 440°C) with the equilibrated undoped VPP catalyst: spectra shown at room temperature (bottom), then during the isotherm period at 440°C (every 30 min, from bottom to top). Symbols: * = VPP; δ = δ-$VOPO_4$.

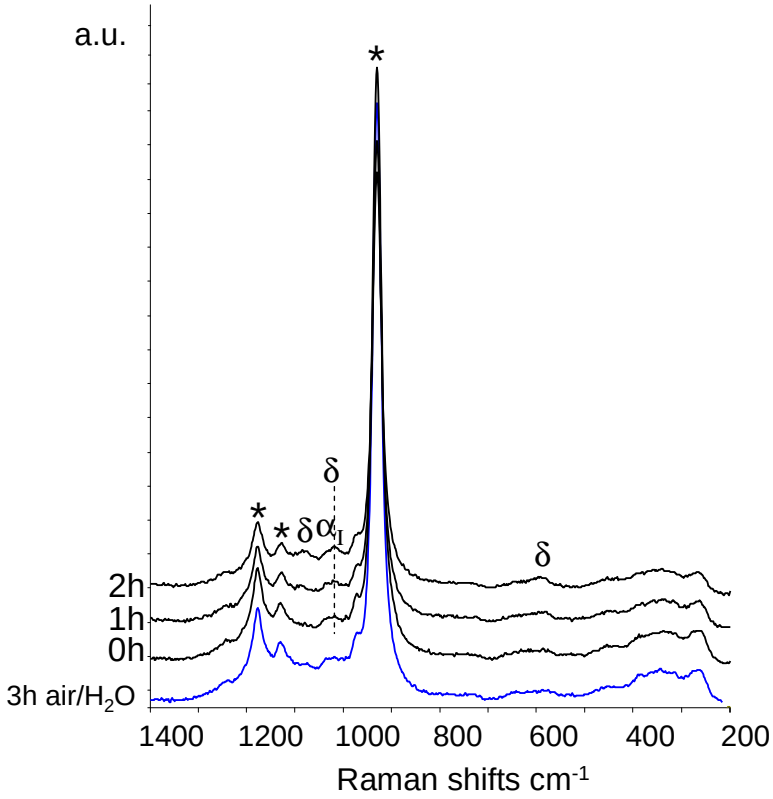

Fig. 3.38_Raman in-situ test (air, 440°C) with the equilibrated undoped VPP catalyst: spectra showed at room temperature (bottom), then during isotherm period at 440°C (every 30 min, from bottom to top). Symbols: * = VPP; δ = δ-$VOPO_4$.

Spectra of the equilibrated Nb-doped VPP catalyst, during the in-situ treatment in humid air flow (440°C), are reported in figure 3.39: after about one hour, although very weakly, broad bands attributable to δ-$VOPO_4$ formed (1085, 1013 cm^{-1}); however also α_I-$VOPO_4$ (1030 cm^{-1}) was observed.

Even after waiting for a few hours under isothermal conditions at 440°C, the spectra did not show any noticeable change.

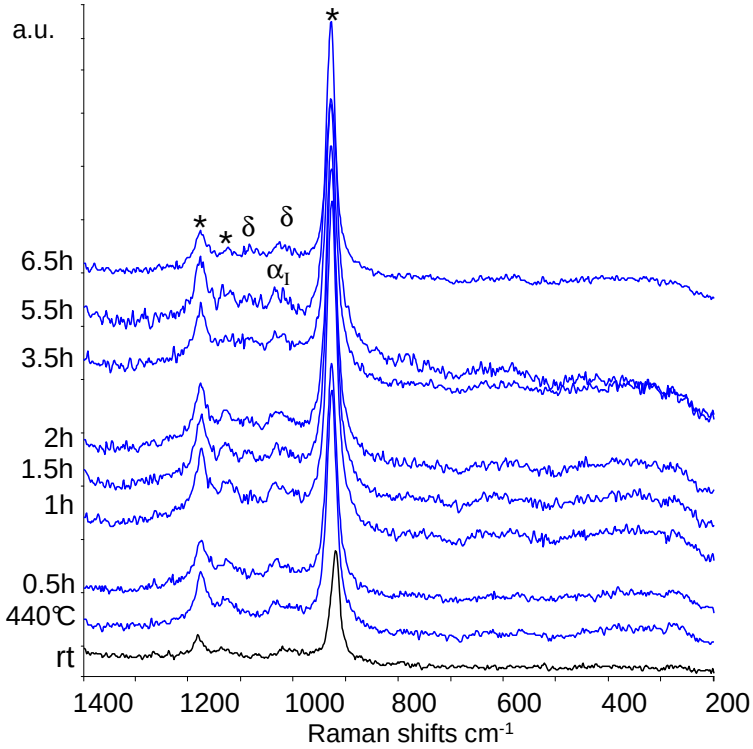

Fig. 3.39_Raman in-situ test (humid air, 440°C) with the equilibrated Nb-doped VPP catalyst: spectra shown at room temperature (bottom), and then during the isothermal period at 440°C (from bottom to top). Symbols: * = VPP; δ = δ-$VOPO_4$; α_I = α_I-$VOPO_4$.

However the formation of δ-$VOPO_4$ was better observed (fig.3.40) when the sample was left in dry air flow for some hours; during this period, the intensity of bands at 1080, 1014, and 590 cm^{-1} increased, showing the unequivocal presence of δ-$VOPO_4$ phase.

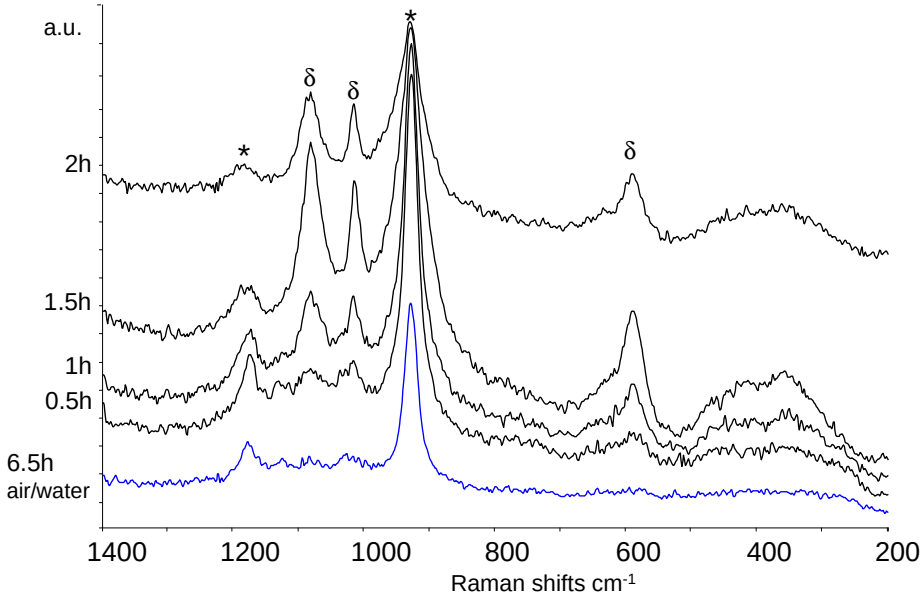

Fig. 3.40_Raman in-situ test (humid air, 440°C) with the equilibrated Nb-doped VPP catalyst: spectra shown at 440°C in humid flow (bottom), then during the isothermal period at 440°C in dry air (from bottom to top). Symbols: * = VPP; δ = δ-$VOPO_4$.

These experiments confirmed that water vapour influenced the VPP surface reactivity and accelerated δ-$VOPO_4$ formation; in the sample containing a small amount of Nb, the formation of the δ-$VOPO_4$ was slightly more favoured than in the undoped sample. Final experiments were

carried out at even stronger conditions, in order to better highlight differences between the two samples. The spectra registered during the in-situ treatment in dry air at 500°C, are reported in figures 3.41-3.42. In the case of the undoped sample, once the the isothermal temperature was reached (500°C), the bands attributable to δ-$VOPO_4$ formed only after several hours (> 5h). Conversely, in the case of the Nb-doped sample, the characteristic bands of the oxidized phase appeared sooner, after about 1 hour only (fig.3.32). Furthermore, with the undoped sample the predominant phase formed was α_I-$VOPO_4$ (strong band centred at 1030 cm^{-1}) while with the Nb-doped catalyst, α_I-$VOPO_4$ phase was present in a minor amount (shoulder at ca 1027 cm^{-1} to the band at 1013 cm^{-1}).

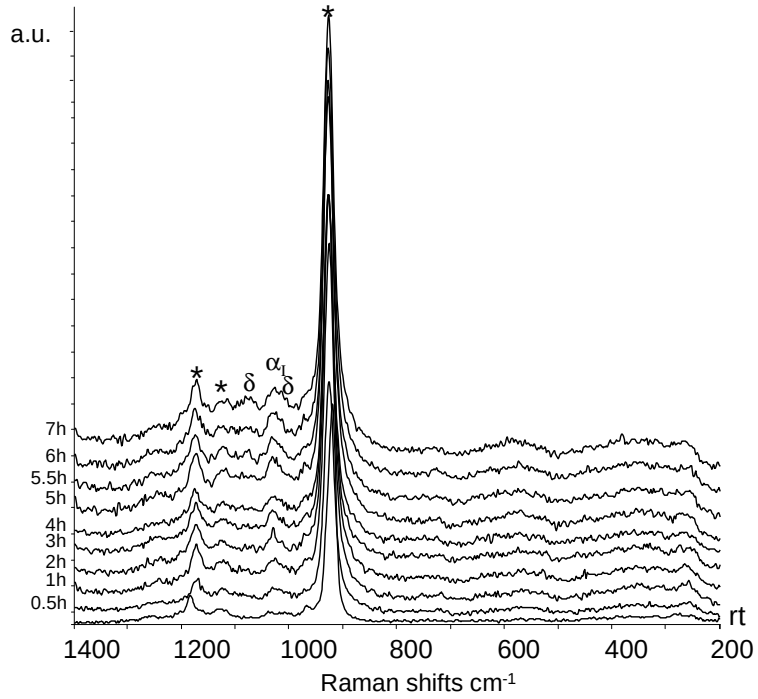

Fig. 3.41_Raman in-situ test (air, 500°C) with the equilibrated undoped VPP catalyst: spectra shown from room temperature (bottom), and then during the isothermal period at 500°C in dry air (from bottom to top). Symbols: * = VPP; δ = δ-$VOPO_4$; α_I = α_I-$VOPO_4$.

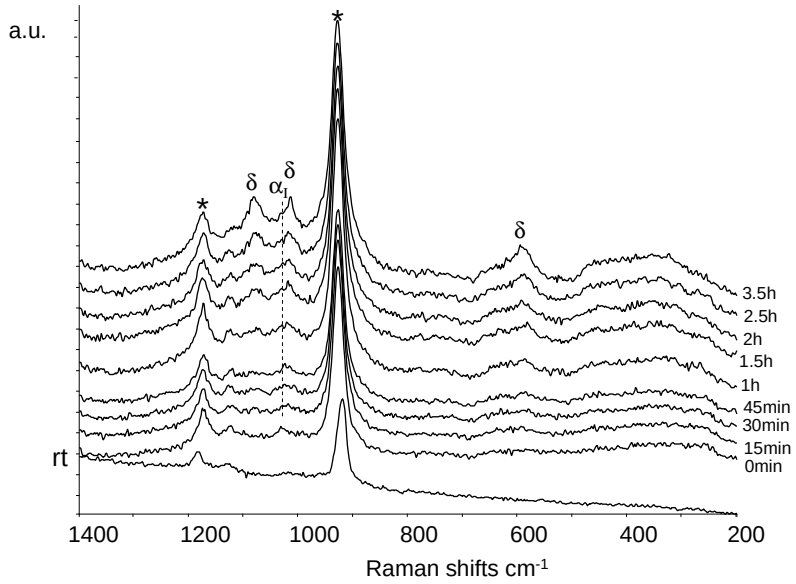

Fig. 3.42_Raman in-situ test (air, 500°C) with the equilibrated Nb-doped VPP catalyst: spectra shown from room temperature (bottom), and then during the isothermal period at 500°C in dry air (from bottom to top). Symbols: * = VPP; δ = δ-$VOPO_4$; α_I = α_I-$VOPO_4$.

For both catalysts, spectra registered after cooling down to room temperature showed the presence of δ-$VOPO_4$.

These experiments demonstrated that the presence of Nb affects the rate of formation of δ-$VOPO_4$. The different thermal treatments were repeated at least twice for each catalyst, and results were exactly reproduced.

We finally carried out some experiments with the used O80 catalyst. In this case, the in-situ treatment in flowing dry air, at 380°C, was carried out using small operando reactor (Chapter 7). The sample was heated up to the isothermal temperature (380°C), and simultaneously spectra were collected (fig.3.43): δ-$VOPO_4$ already appeared at 300°C and remained present during the isotherm period at 380°C (1086, 1013, 586 cm^{-1}). This was not the only oxidized phase present; in fact, also the α_I-$VOPO_4$ strongest band (at 1033 cm^{-1}) was visible. Even after waiting for 4 hours, the spectrum did not show any change; the band attributable to α_I-$VOPO_4$ still remained the stronger one (fig.3.44).

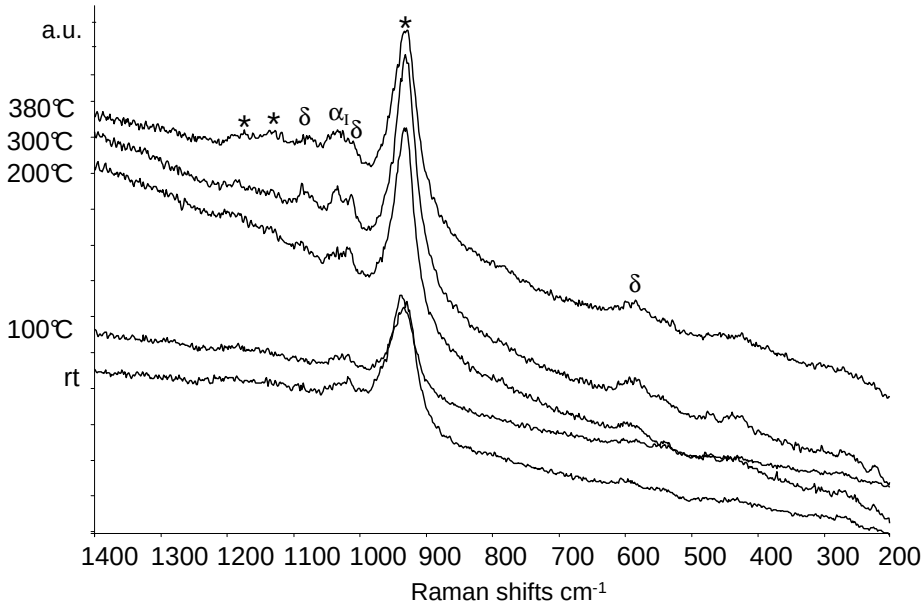

Fig. 3.43_Raman in-situ test (air, 380°C) with the used catalyst O80 (V/Nb=80): spectra shown from room temperature (bottom) up to 380°C (top). Symbols: * = VPP; $\delta = \delta$-$VOPO_4$; $\alpha_I = \alpha_I$-$VOPO_4$.

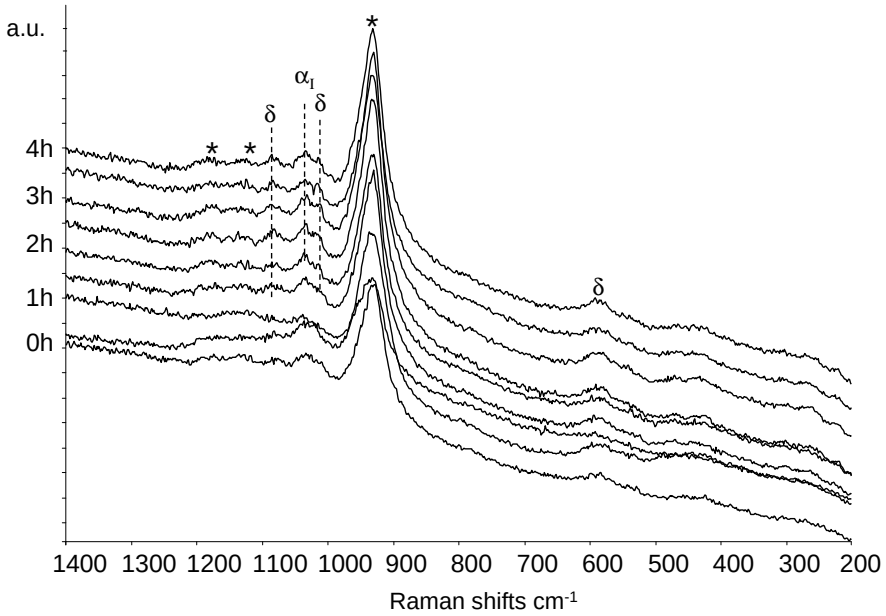

Fig. 3.44_Raman in-situ test (air, 380°C) with used catalyst O80 (V/Nb=80): spectra shown during the isothermal step at 380°C, from 0h (bottom) to 4h (top). Symbols: * = VPP; $\delta = \delta$-$VOPO_4$; $\alpha_I = \alpha_I$-$VOPO_4$.

The spectrum collected after cooling down at room temperature (fig.3.45), showed bands attributable to VPP, δ-$VOPO_4$ (1086, 1015, 590 cm^{-1}) and α_I-$VOPO_4$ (1041 cm^{-1}).

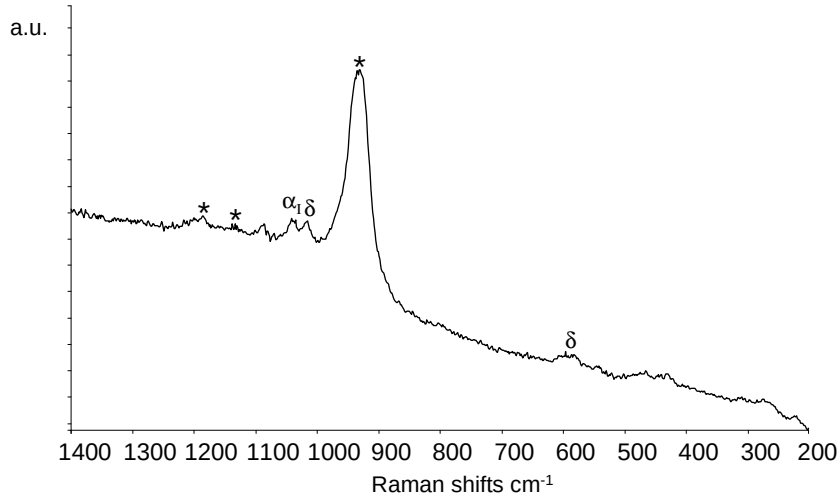

Fig. 3.45_Raman in-situ test (air, 380°C) with catalyst O80 (V/Nb=80): spectra shown at the end of thermal treatment. Symbols: * = VPP; $\delta = \delta$-$VOPO_4$; $\alpha_I = \alpha_I$-$VOPO_4$.

This catalyst demonstrated an intermediate behaviour, between that of sample O46 and that of the equilibrated Nb-doped VPP sample: δ-$VOPO_4$ formed at very low temperature, but in small amount and together with α_I-$VOPO_4$.

Finally, we carried out the thermal treatment in flowing air, up to 500°C, on sample O80. The spectra are shown in figure 3.46: during the first isothermal step, at 380°C, spectra registered clearly showed the presence of α_I-$VOPO_4$ (bands at 1039, 576, 542 cm^{-1}), while δ-$VOPO_4$ formed in minor amount only (bands at 1081, 1014, 589 cm^{-1}). This result contrasted with the previous treatment, and suggests that a certain surface heterogeneity may affect the result of the experiment.Before reaching the temperature of 500°C, the catalyst was heated up to 440°C and during this second isothermal step, water vapour (~10%) was added to the inlet flow: spectra still showed the strong α_I-$VOPO_4$ band, while bands relative to δ-$VOPO_4$ were not affected (fig. 3.47).

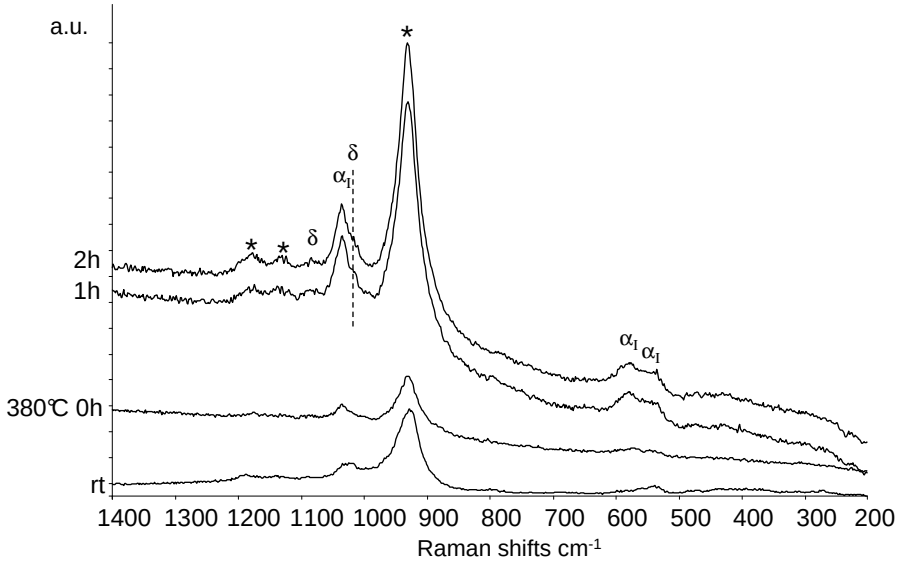

Fig. 3.46_Raman in-situ test (air, 380°C) with catalyst O80 (V/Nb=80): spectra shown from room temperature (bottom) and at 380°C, from 0h to 2h (top). Symbols: * = VPP; $\delta = \delta$-$VOPO_4$; $\alpha_I = \alpha_I$-$VOPO_4$.

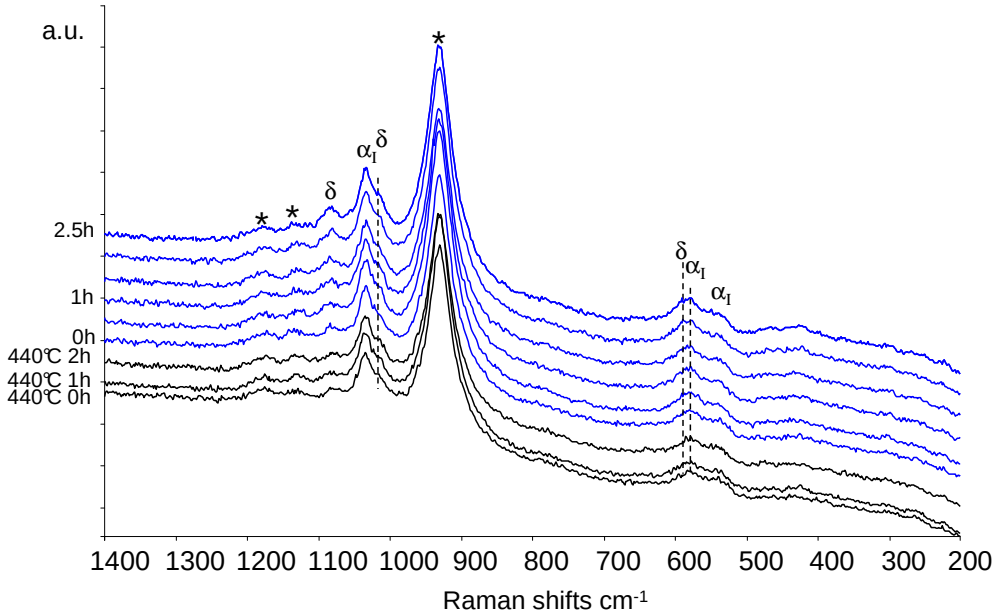

Fig. 3.47_Raman in-situ test (air, 380°C) with catalyst O80 (V/Nb=80): spectra shown during the isothermal step at 440°C, first in dry air (bottom), and then in humid air, from 0h to 2.5h (top). Symbols: * = VPP; δ = δ-$VOPO_4$; α_I = α_I-$VOPO_4$.

Once reached 500°C, while keeping the humid air flow, the spectra showed an increase of the intensity for the bands attributable to δ-$VOPO_4$ and perhaps to α_I-$VOPO_4$ also, which still was present (fig. 3.48).

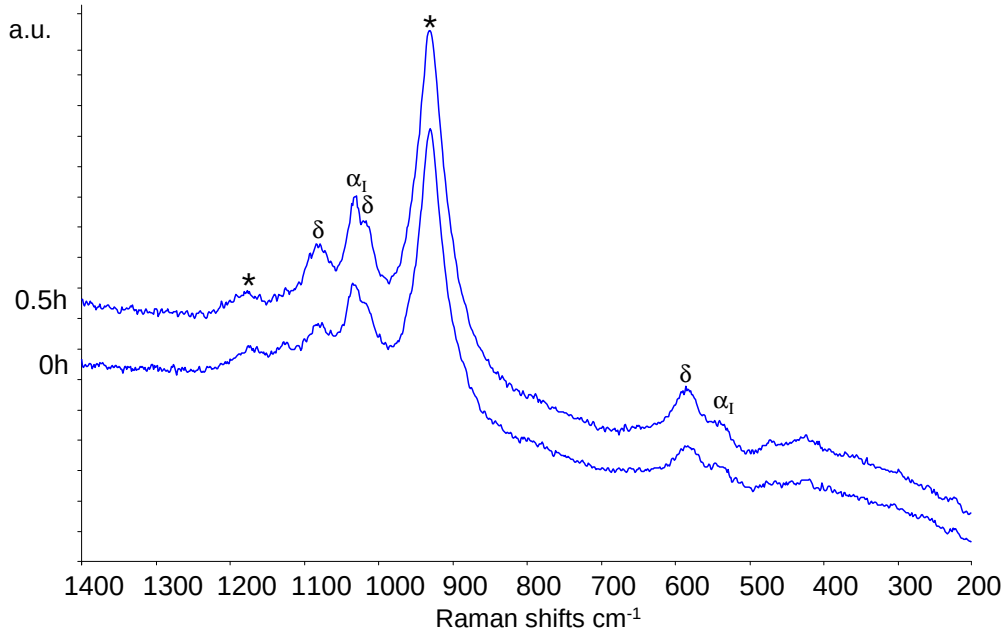

Fig. 3.48_Raman in-situ test (air, 380°C) with catalyst O80 (V/Nb=80): spectra shown during the isothermal step in humid air flow at 500°C. Symbols: * = VPP; δ = δ-$VOPO_4$; α_I = α_I-$VOPO_4$.

The spectrum collected at room temperature (fig.3.49) showed only the presence of α_I-$VOPO_4$ and VPP; moreover the presence of V_2O_5 was witnessed by bands at 995 and 700 cm^{-1}, which were the strongest ones. The formation of this compound was likely due to prolonged treatment in humid air flow.

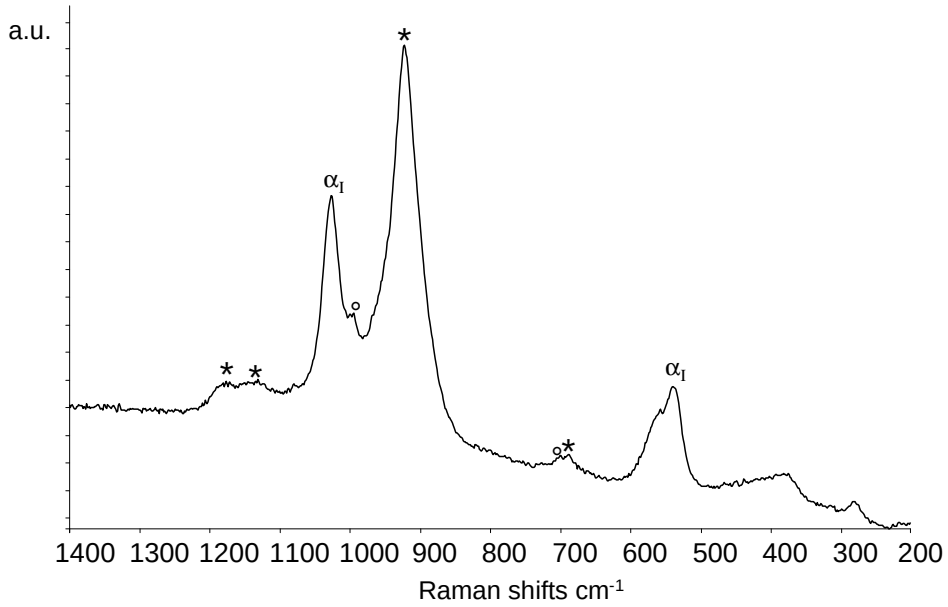

Fig..3.49_Raman in-situ test (air, 380°C) with catalyst O80 (V/Nb=80): spectra shown at the end of thermal treatment. Symbols: * = VPP; $\delta = \delta$-$VOPO_4$; $\alpha_I = \alpha_I$-$VOPO_4$.

This last experiment demonstrated that the surface of the O80 catalyst was not homogeneous, and that depending on the spot area focussed by the beam, different compounds were formed in function of the temperature of treatment and of gas-phase composition. Nevertheless, even when the preferred compound formed by VPP oxidation was the α_I-$VOPO_4$, the generation of δ-$VOPO_4$ was anyway observed, especially in an humid air flow at high temperature.

Conclucions

In conclusion, we found that with increasing the Nb content in VPP catalysts (V/Nb=∞-80), at low reaction temperature (<400°C) a better selectivity to MA (with respect to the undoped sample) was obtained while, in contrast, at high temperature (440°C) only for very low Nb concentration (V/Nb=150) the MA selectivity resulted improved. However, from the in situ experiments, it was evident that Nb favours the formation, and also the stability, of oxidized $VOPO_4$ phases, in particular of δ-$VOPO_4$. This effect resulted positive at low T while with stronger oxidizing reaction conditions it resulted detrimental, as an excessive amount of oxidized compounds caused over-oxidation of reactants and product, lowering MA yield. The optimal amount of Nb was a function of reaction conditions (temperature, inlet composition). The catalyst having V/Nb=46 gave the worst performances, because at all conditions used it was excessively oxidized. Differently, the catalyst prepared using a different synthesis method (80% v/v of isobutanol, 20% v/v of 1,4-butanediol and using $NbCl_5$) gave outstanding performance, due to peculiar characteristics coming from the preparation; moreover, this was the unique doped catalyst which reported the absence of δ-$VOPO_4$.

3.3 REFERENCES

[1] F. Cavani, F. Pierelli, F. Ghelfi, G. Mazzoni, and C. Fumagalli, EP 1514598 (2003).
[2] G. J. Hutchings App. Cat. 72 (1991)1.
[3] N. F. Dummer, J. K. Bartley, G. J. Hutchings, Adv. Catal., Vol. 54 (2011) 189.
[4] I. Mastuura, T. Ishimura, S. Hayakawa, N. Kimura, Cat Tod 28 (1996) 133.
[5] P.G. Pries de Oliveira, J.G. Eon, M. Chavant, A.S. Richè, V. Martin, S. Caldarelli, J.C. Volta, Cat Tod 57 (2000) 177.
[6] H. Oppermann, F. von Woedtke, T. Reich, M. A. Denecke, H. Nitsche, M. Doerr Fresenius, J Anal Chem 363 (1999) 202.
[7] W. Rudorff, J. Marklin, Z. Anorg. Allgem. Chemie 334 (1964) 142.
[8] A.M. Duarte de Farias, W. De A. Gonzalez, P.G. Pries de Oliveira, J. G. Eon, J.M. Herrmann, M. Aouine, S. Loridant, J.C. Volta, J Cat 208 (2002) 238.
[9] V.V. Guliants, J.B. Benziger, S. Sundaresan, I.E. Wachs, A.M. Hirt, Catal. Lett. 62 (1999) 87.
[10] I. Mastuura, T. Ishimura, S. Hayakawa, N. Kimura, Cat Tod 28 (1996) 133.
[11] F. Pierelli “Catalizzatori per ossidazione di n-butano e n-pentano ad anidride maleica e ftalica”, PhD Thesis in Industrial Chemistry, Bologna University, A.A. 2000-2002.
[12] I. Nowak, M. Ziolek, Chem. Rev. 99 (1999) 3603.
[13] F. Cavani, S. Luciani, E. Degli Esposti, C. Cortelli, R. Leanza, Chem. Eur. J. 16 (2010) 1646.
[14] J. Jehng, I.E. Wachs, Chem. Mater., Vol. 3, No. 1 (1991) 100.
[15] F. Cavani, S. Ligi, T. Monti, F. Pierelli, F. Trifirò, S. Albonetti, G. Mazzoni Catal. Today 61 (2000) 203.
[16] V.V. Guliants, J.B. Benziger, S. Sundaresan, I.E. Wachs, J.-M. Jehng, J.E. Roberts, Cat Tod 28 (1996) 275.
[17] F. Cavani, D. De Santi, S. Luciani, A. Löfberg, E. Bordes-Richard, C. Cortelli, R. Leanza App. Cat. A: General 376 (2010) 66.
[18] N. Ballarini, F. Cavani, C. Cortelli, F. Gasparini, A. Mignani, F. Pierelli, F. Trifirò, C. Fumagalli, G. Mazzoni, Catal. Today 99 (2005) 115.
[19] A. Datta, M. Agarwal, S. Dasgupta, J. Mater. Chem. 12 (2002) 1892.
[20] A. L. Garcia-Ponce, L. Moreno-Real, A. Jimenez-Lopez, Inor. Chem. vol. 27 (1988) 3372.
[21] E.Bordes, P. Courtine, J. Solid State Chem. 55 (1984) 270.
[22] S. Albonetti, F.Cavani, S. Ligi, F. Pierelli, F. Trifirò, F. Ghelfi, G. Mazzoni, Stud. Surf. Sci. Catal. 143 (2002) 963.

4

SYNTHESIS OF BULK DIHYDRATED VANADYL ORTHOPHOSPHATE AND MIXED V/Nb HYDRATED PHOSPHATES

4.1 INTRODUCTION

The first dihydrated vanadyl orthophosphate ($VOPO_4 \cdot 2H_2O$) synthesis was reported in the literature by Ladwig et al. [1].

This hydrated vanadium-phosphorus oxide is a common and well known V/P/O compound [2,3]: it has the same tetragonal crystal group of the α_I and α_{II} $-VOPO_4$ phase, and it is constituted of layers, where the two crystallization water molecules are located.

More in detail, the structure, as for the other $VOPO_4$ phases, is formed by two repeated principal units, octahedral [VO_6] and tetrahedral $[PO_4]^{3-}$: in the equatorial plane each octahedra is bonded with four tetrahedra by means of a V-O-P bond; in the axial plane, each octahedra is connected with the first water molecule by forming in one corner a long V-O bond while, in the opposite corner, there is the shorter vanadyl bond (V=O). The second water molecule is weakly bonded by H-bonds to the oxygen of the $[PO_4]^{3-}$ units and to the first water molecule [4,5].

All of the $VOPO_4$ phases, after either an hydration treatment or simply standing at room temperature, convert more or less easily to $VOPO_4 \cdot 2H_2O$ [6], in particular the α_I–$VOPO_4$ is the $VOPO_4$ phase which is more quickly hydrated to $VOPO_4 \cdot 2H_2O$, and in the same way $VOPO_4 \cdot 2H_2O$ dehydrates firstly to α_I–$VOPO_4$, and not to other $VOPO_4$ polymorphs.

Due to its layered structure, the vanadyl ortophosphate dihydrate is also an intercalation compound; in the literature, there are several papers dealing with the intercalation with organic molecules [4,7-9] or with alkali metals [10,11] to get a compound with interesting chemical-physical features.

This compound is also utilized to prepare $VOHPO_4 \cdot 0{,}5H_2O$, the precursor of $(VO)_2P_2O_7$ (VPP): this is also called the “two-step” route, because during the first step the formation of the phase $VOPO_4 \cdot 2H_2O$ (VPD) occurs, while during the second step the reduction of the intermediate VPD compound is carried out, by adding an alcohol or mixture of alcohols [2-3,12-16].

Moreover, it is worth noting that the $VOPO_4 \cdot 2H_2O$ phase is sometimes observed during the ex-situ characterization of the used VPP (the catalyst used for the selective oxidation of n-butane to maleic anhydride): the compound may form as a result of the hydration of $VOPO_4$ phases, occurred either during reaction or during the used catalyst download procedure.

Furthermore, as reported by Cavani et al. [17], this phase was observed during the in-situ oxidative and hydrolytic treatment over a VPP equilibrated catalyst (P/V=1.2). This treatment was carried out inside a Raman cell, to boost the VPP surface transformations, by simulating the reaction conditions at high temperature; the surface change was monitored by in-situ Raman spectroscopic. It was shown that the $(VO)_2P_2O_7$ surface, depending on its P/V atomic ratio, is affected by the treatment: with a catalyst having P/V ratio of 1.2, the $VOPO_4 \cdot 2H_2O$ phase formed at 380°C by feeding an air flow saturated with steam (about 10%); then, after water withdrawal, the $VOPO_4 \cdot 2H_2O$ converted into δ-$VOPO_4$. Furthermore a correlation was found between the Raman in-situ results and the non-steady catalytic performance: the δ-$VOPO_4$ (in the form of small amorphous aggregates or "patches" dispersed over the VPP surface) is the phase giving the best catalytic performance; it formed at high temperature, regardless of the catalyst P/V atomic ratio.

Taking into account these results, and the reversible reciprocal transformation of VPP and δ–$VOPO_4$, we extrapolated that an alternative approach for the development of a selective V/P/O catalyst might be developed by starting from the δ-$VOPO_4$ phase, which during reaction might generate the VPP at its surface, in the same way as the latter generates the former. In other words, we considered that the relative amount of the V^{4+}- and V^{5+}-containing compounds were only a function of the gas-phase composition, and that therefore starting from either of the two compounds might finally lead to a similar catalytic behaviour. Moreover, we also speculated that the incorporation of Nb^{5+} dopant in the V/P/O compound, an important requisite for achieving a promotion effect by this element on catalytic behaviour, should be much easier starting from the V^{5+} phosphate than from the VPP. Indeed, our hypothesis contrasts with some experimental results, published in the past, that bulk $VOPO_4$ is not a good catalyst for n-butane oxidation. However, it should be considered that most of reactivity experiments were carried out with V^{5+} phosphates other than the δ-compound.

This opportunity is attractive since in the literature the dehydration of $VOPO_4 \cdot 2H_2O$ into δ-$VOPO_4$ yet has not been investigated; in fact, it is reported that the $VOPO_4$ phases obtained by $VOPO_4 \cdot 2H_2O$ dehydration are the α_I (200°C-600°C) and α_{II} (750°C) structures [18]. Furthermore, the possibility of obtaining δ-$VOPO_4$ by means of this procedure would be interesting because it might be an easier synthesis route for the active catalyst than that one typically used: the latter starts from the $VOHPO_4 \cdot 0{,}5H_2O$ precursor [18-22], while an alternative method uses $VOHPO_4 \cdot 4H_2O$ as the precursor. Both methods are long and troublesome [23].

Nb is a well-known important dopant for the VPP catalyst but a clear explanation of its role has not yet been reported in the literature. Our hypothesis, which was discussed in Chapter 3, is that Nb favours the δ-$VOPO_4$ phase development over the VPP surface during reaction. For this reason, we also investigated how the presence of Nb affects the $VOPO_4 \cdot 2H_2O$ structure and transformations. In

other words, we hypothesized that the presence of Nb might favour the dehydration into the desired δ-$VOPO_4$ and not into other V^{5+} phosphates. This was done by synthesizing a series of mixed V/Nb hydrated phosphates, prepared adding to the VPD synthesis (par. 4.2.1) increasing amounts of Nb (in the form of hydrated Nb_2O_5), and characterizing the samples by means of different techniques.

4.2 EXPERIMENTAL

4.2.1 Synthesis of $VOPO_4 \cdot 2H_2O$

Dihydrated vanadyl orthophosphate (VPD) was prepared using V_2O_5, H_3PO_4 and water as solvent, according to the procedure reported in the literature [3]. The synthesis details are reported in chapter 2. The orthophosphoric acid was used in large excess (P/V= 4) in accordance with most literature: the reason of using such a high amount of H_3PO_4 is not clear; probably using a stoichiometric amount of H_3PO_4 does not permit a complete dissolution of V_2O_5. On the other hand, some authors [24] reported that VPD can be obtained with the required stoichiometric amount of H_3PO_4. However, when we tried the synthesis using an atomic ratio of P/V=1, we obtained an incomplete V_2O_5 conversion, and only small amounts of VPD formed; therefore, we decided to use an excess of P.

The solid obtained after filtration, washing and drying is called VPD sample 1. A more crystalline VPD sample was obtained by first filtering the mother-liquor which had been left for one day at room conditions, and then leaving the solid obtained one day in air, at room temperature: this permitted a slow crystallization of the VPD phase (sample 2).

The two VPD samples were analyzed by X-Ray fluorescence analysis (XRF) to determine the P/V ratio: values of 1.18 and 1.09 were found for sample 1 and sample 2, respectively. This means that although a large amount of H_3PO_4 was used, much greater than the stoichiometric value required for $VOPO_4 \cdot 2H_2O$, most of P remained in the liquid (in fact the pH of the mother liquor was quite low) and did not influence the final result: pure VPD phase was obtained, as shown by the characterization (par. 4.3.1).

4.2.2 Synthesis of mixed V/Nb hydrated phosphates and pure $NbOPO_4 \cdot yH_2O$

The synthesis of the mixed hydrated V/Nb phosphate was similar to the VPD synthesis: the Nb source was hydrated Nb_2O_5 (chapter 2). The synthesis mixture with high concentration of Nb, also after filtering appears to be like a very dense paste which “adsorbs” almost all the solvent, and for this reason it was quite difficult to manipulate it; the dried solid (after some hours at 100°C) was always yellowish-greenish, except in the case of pure Nb phosphate. The series of the hydrated V/Nb phosphates prepared is compiled in table 4.1.

The pure hydrated Nb phosphate (NP2) was synthesized as a reference compound, and it is referred as $NbOPO_4 \cdot yH_2O$, because it was not possible to measure exactly the content of water; however,

after calcination at 450°C in static air, the percentage of weight loss was 18%, which corresponds to about y=2,5.

The sample VPDNb was synthesized in the same way but using the Nb source described at Chapter 2 (par.2.1.1).

All samples were dried at 100°C. Thermal treatment was then carried out by in-situ Raman experiments.

	VPD	**VPDNb**	**NP5**	**NP3**	**NP4**	**NP6**	**NP2**
%V	100	99-99,5	90	75	25	10	0
%Nb	0	0,5-0,9	10	25	75	90	100
V/Nb	-	100-200	9,5	3	0,3	0,1	-
Nb/(V+Nb)%	-	0,50-0,99	10	25	75	90	-

Table 4.1_ Mixed hydrated V/Nb phosphates and two reference samples (VPD, NP2) prepared, with their main characteristics: molar % of V content, molar % of Nb content, V/Nb molar ratio and molar % of Nb.

4.3 RESULTS AND DISCUSSION

4.3.1 Characterization of $VOPO_4 \cdot 2H_2O$

The solid was characterized by means of various techniques. Figure 4.1 shows the Raman ex-situ spectra of different spots of "sample 1" VPD: $VOPO_4 \cdot 2H_2O$ phase was the main phase (1038, 985, 954, 543, 280 cm^{-1}), with traces of α_I–$VOPO_4$ (935, 580 cm^{-1}). The sample was homogeneous.

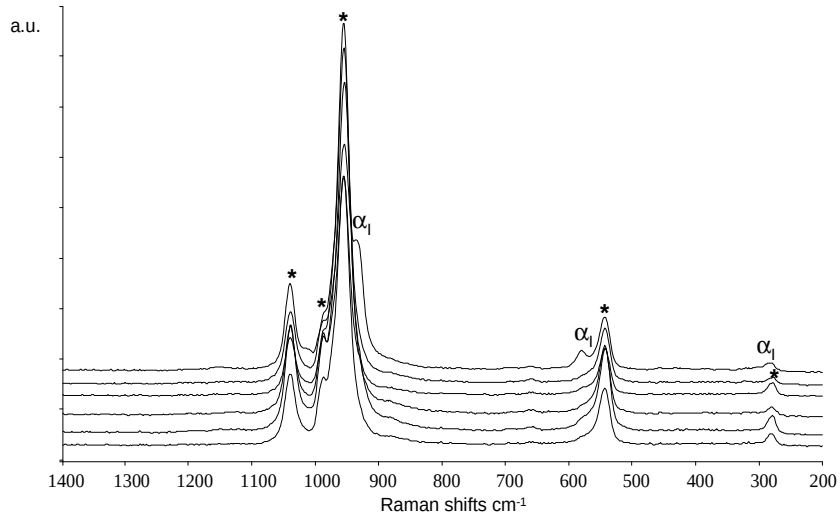

Fig. 4.1_ Ex-situ Raman spectra registered at different spots of dried VPD "sample 1". Symbols: * = $VOPO_4 \cdot 2H_2O$; $\alpha_I = \alpha_I$–$VOPO_4$.

The X-ray diffraction powder analysis (XRD) was carried out for both VPD samples: there were evident differences between them (fig.4.2). Sample 1 was definitely less crystalline and contained both $VOPO_4 \cdot 2H_2O$ and microcrystalline α_I–$VOPO_4$, while "sample 2" pattern showed the reflections of the dihydrate phase only (JCPDS 00-036-1472).

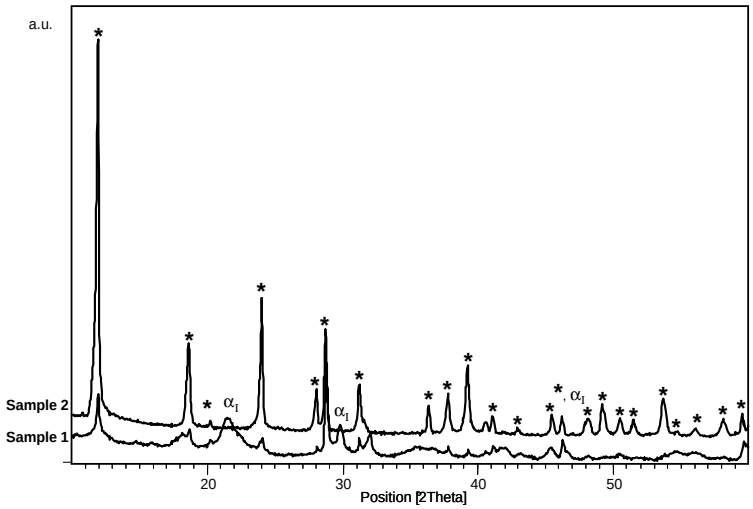

Fig. 4.2_X-ray powder diffraction analysis of dried sample 1 and sample 2 VPD. Symbols: * = $VOPO_4 \cdot 2H_2O$; $\alpha_I = \alpha_I$–$VOPO_4$.

The IR and UV-vis characterizations of the solid are in accordance with the analysis reported in the literature (respectively ref. 5,10,25 and ref. 26-27), dealing with the $VOPO_4 \cdot 2H_2O$ phase.

In figure 4.3, the IR spectra show the bands attributable to the vibrations of two different water molecules (3560, 1607 cm^{-1} and 3368 cm^{-1}), of the vanadyl group (993 cm^{-1}), of the [PO_4] groups (1171, 1084, 946 cm^{-1}) and of V-O-P (678 cm^{-1}) and O-P-O (571 cm^{-1}) lattice bonds.

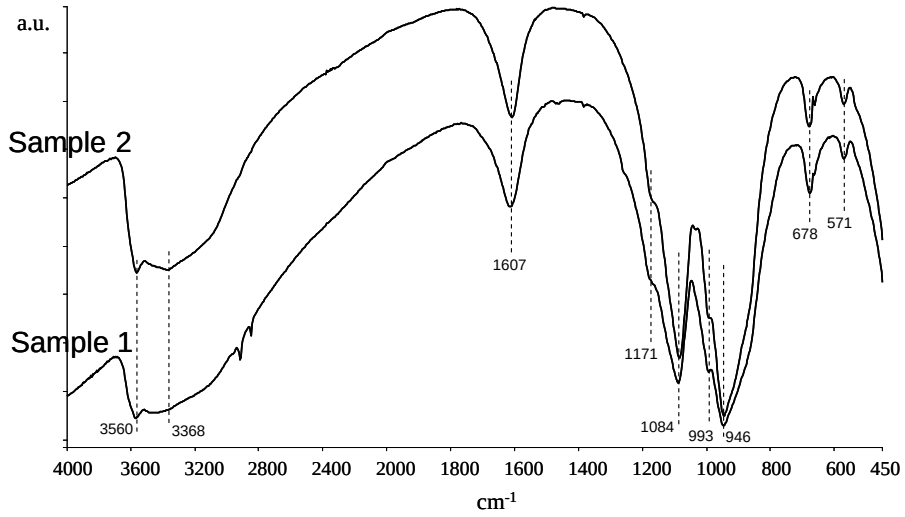

Fig. 4.3_IR spectra of dried sample 1 and sample 2 VPD.

Figure 4.4 shows the UV-vis spectra: two strong bands centred at 290 nm and 410 nm are observed, which are relative to charge transfer transitions from lattice oxide to V^{5+} species.

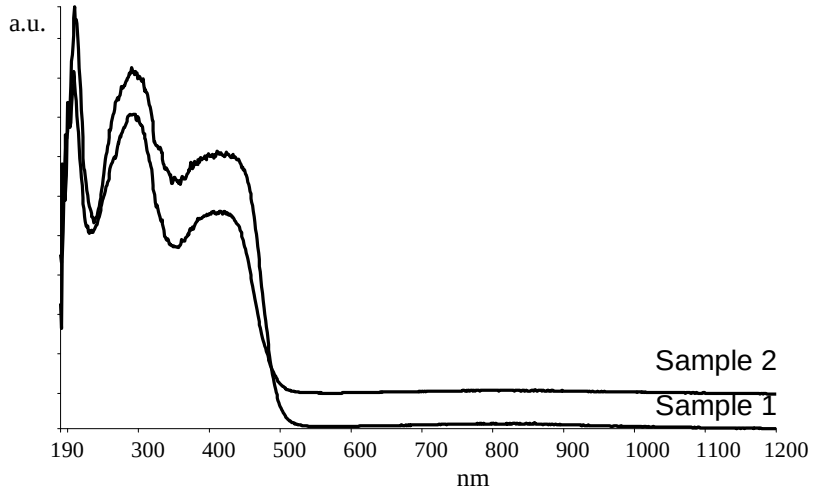

Fig. 4.4_UV-vis spectra of dried sample 1 and sample 2 VPD.

The presence of two different water molecules of crystallization was also observed by means of thermogravimetric analysis (TGA), performed in flowing air up to 550°C (fig. 4.5): the first water molecule, that was the more weakly bonded in the lattice, was completely lost at about 84°C, whereas the release of the second molecule occurred at 122°C, as plotted by the curve of first derivative of weight loss percent (dW/dT). The total experimental weight loss was about 15%, a value close to the theoretical one, 18%: this confirms that the VPD sample lost both of the two crystallization water molecules and was completely dehydrated at 130°C. The result is in agreement with what reported by Benes et al. [28] about DTA and DTG analysis, considering the same heating rate (15°C/min). It must be noted that these temperatures were shifted to lower values when the dehydration of VPD was carried out by using an in-situ XRD technique [1,29]: the first dehydration step occurred at 44°C and the second one at 80°C.

However, as shown in paragraph 4.3.2, during the in-situ Raman treatment of the sample at 80°C in flowing air, bands were registered at wavenumbers in between those of VPD and α_I–$VOPO_4$ phases, which means that an intermediate dehydrated compound formed at this temperature, in agreement with the literature [1,29]. We cannot exclude that the spectrum collected at 80°C is the result of the overlapping of the two spectra for VPD and α_I–$VOPO_4$.

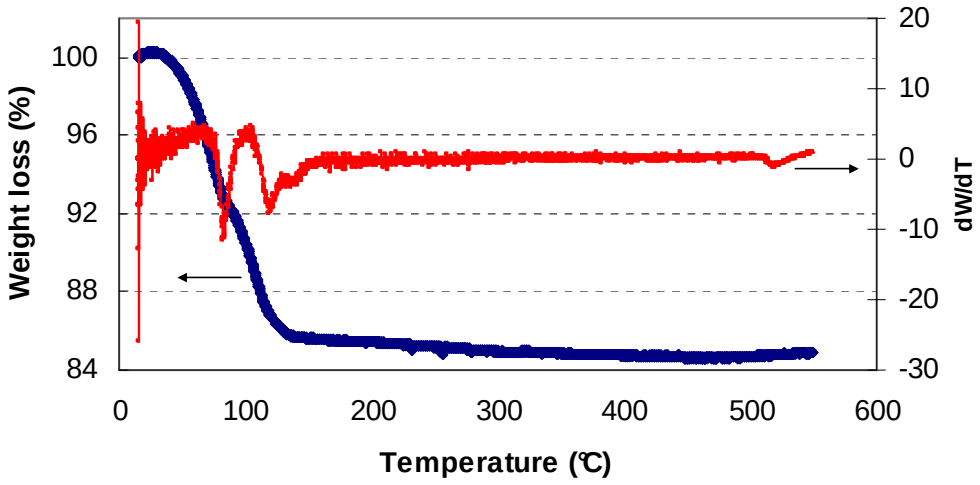

Fig.4.5_Thermogravimetric analysis of sample 1 VPD: weight loss % (blue curve) and first derivative of the weight loss % (red curve).

4.3.2 In-situ Raman analysis of $VOPO_4 \cdot 2H_2O$

The in-situ Raman analysis was carried out on the VPD samples loading a very small amount of the solid inside the Raman cell. For the first test, the temperature was increased up to 550°C (heating rate 100°C/min) and kept at this latter temperature for 5 hours, while a flow of dry air (~10 ml/min) was flown over the sample. Raman spectra were collected during all the experiment. The pure VPD phase (1032, 982, 950, 538, 274 cm^{-1}) started to dehydrate at 80°C: it is noticeable that there was a shift of the bands (1030, 988, 941, 535, 279 cm^{-1}) but no new band formed, neither any trace of $VOPO_4 \cdot H_2O$ - which is claimed by some authors to show a band at 1009-1010 cm^{-1} [2,30] - was observed. The spectrum at 80°C was due to a change of the VPD structure because of the first water molecule release; in fact, because this water molecule is bonded to PO_4 units, when it is released the most affected VPD band is that one of the P-O stretching (950 cm^{-1}), which is shifted towards lower energy. On the other hand, if the shift were due to the loss of the second water molecule, it would affect only the vanadyl band (995 cm^{-1}), which was not visible due to the strong VPD band (950 cm^{-1}). We can conclude, as reported in the literature, that the dehydration is a two-step process, because the two water molecules were not released at the same time.

Because of these reasons, it is likely that the spectrum collected at 80°C is attributable to the VPD after the first dehydration, considering also that, as reported by Trchová et al. [1,29], for the dihydrate and the monohydrate compound the Raman spectrum is nearly the same.

At 100°C, the characteristic spectrum of α_I–$VOPO_4$ appeared (1033, 926, 574, 539, 291 cm^{-1}) (fig. 4.6).

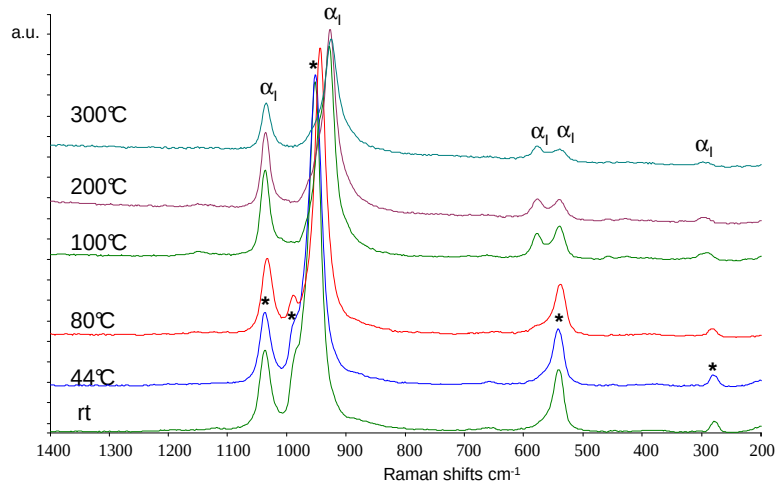

Fig.4.6_In-situ Raman treatment in dry air of dried sample 1 VPD: spectra were recorded while heating the sample from room temperature (bottom) to 300°C (top). Symbols: * = $VOPO_4 \cdot 2H_2O$; $\alpha_I = \alpha_I$–$VOPO_4$.

Up to 550°C (fig. 4.7) and during the isothermal step (fig. 4.8) at this temperature, the dehydrated phase was still present: the spectra recorded were less clear due to higher temperature, but the spectrum of α_I–$VOPO_4$ was always unambiguous; at the end of the treatment, after cooling down to room temperature, the collected spectrum was that one characteristic of the α_I–$VOPO_4$ phase (1142, 1037, 964, 929, 665, 579, 541, 459, 432, 298 cm^{-1}) (fig.4.9).

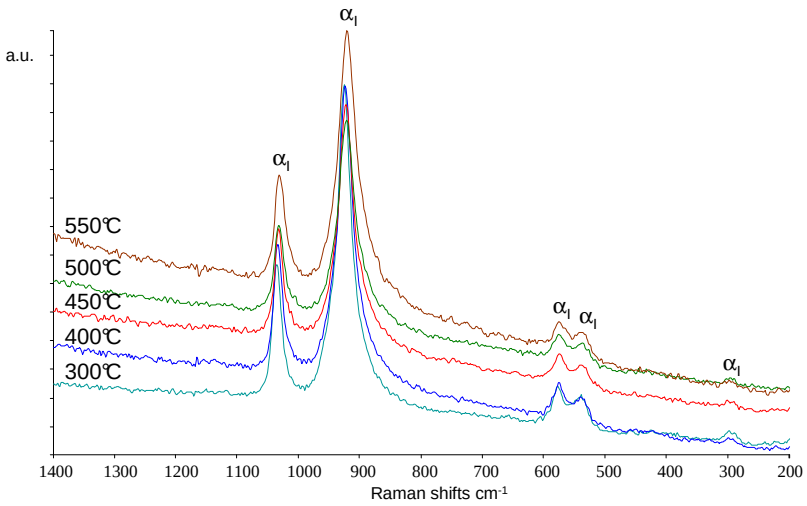

Fig.4.7_In-situ Raman treatment in dry air of dried sample 1 VPD: spectra were recorded while heating the sample from 300°C (bottom) to 550°C (top). Symbols: $\alpha_I = \alpha_I$–$VOPO_4$.

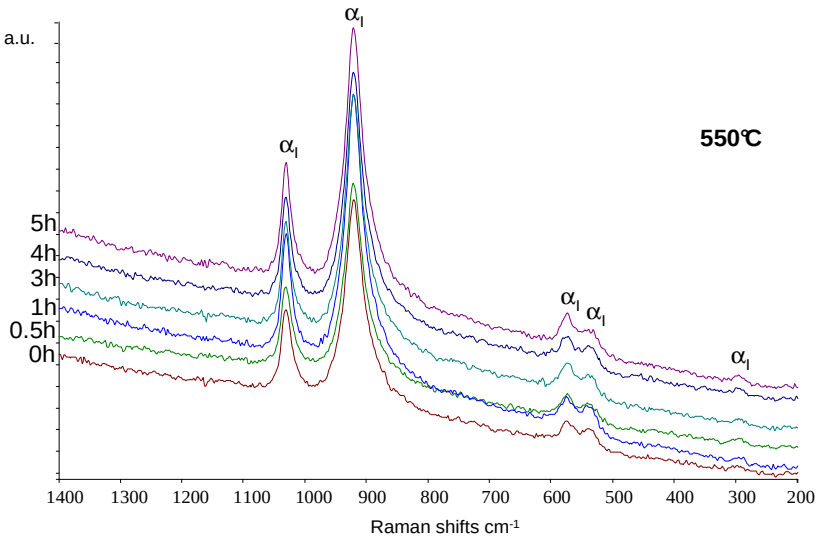

Fig. 4.8_In-situ Raman treatment in dry air of dried sample 1 VPD: spectra were recorded during the isothermal step at 550°C, at increasing time (from the bottom to the top). Symbols: $\alpha_I = \alpha_I$–$VOPO_4$.

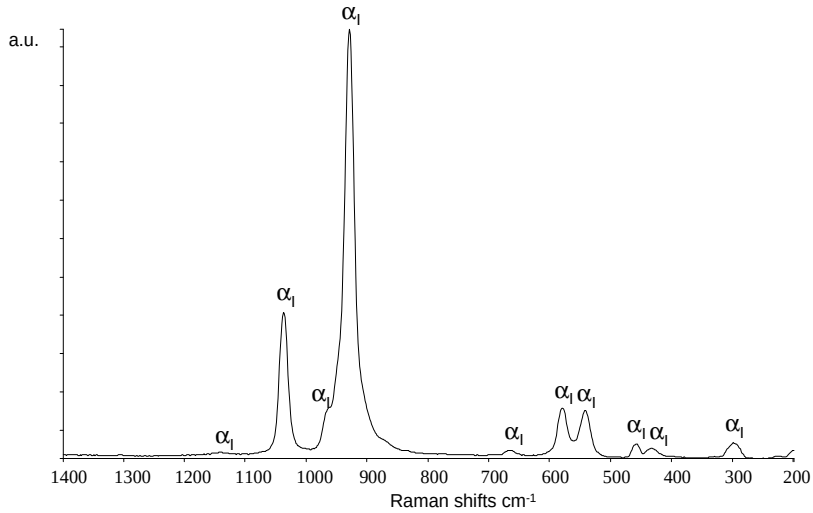

Fig. 4.9_In-situ Raman treatment in dry air of dried sample 1 VPD: final spectrum recorded at room T, after the treatment at 550°C. Symbols: $\alpha_I = \alpha_I$–$VOPO_4$.

This test was repeated with sample 2 VPD, which was more crystalline than sample 1: the transformation of VPD into α_I–$VOPO_4$, formerly observed with sample 1, was reproduced, at the same conditions. This means that the crystallinity did not cause any difference between these two compounds with regard to this transformation.

We also tried another treatment, in flowing air saturated with water vapour (~10%), with the aim of keeping the hydrated form (VPD) during increasing temperature; this treatment simulated the conditions at which δ-$VOPO_4$ formed during the in-situ experiment carried out with VPP. Despite the presence of steam, the VPD phase dehydrated at 100°C, forming α_I–$VOPO_4$ which remained stable during all the isothermal period (5h at 450°C); during cooling in a dry air flow, the α_I–$VOPO_4$ was still present, but at 200°C this phase rehydrated to yield back the VPD.

These tests demonstrate that it is not possible to form δ-$VOPO_4$ from bulk $VOPO_4 \cdot 2H_2O$, in air or humid air, at relatively high temperature (450°C-550°C). In fact, we confirmed the strong relationship between $VOPO_4 \cdot 2H_2O$ and α_I–$VOPO_4$. Moreover, this result highlights the important

role of the $(VO)_2P_2O_7$, which during reaction probably acts as a "template" for the generation of δ-$VOPO_4$ over its surface.

4.3.3 Characterization of the mixed hydrated V/Nb phosphates and of pure $NbOPO_4 \cdot yH_2O$

For the clarity of the discussion, the series of hydrated V/Nb phosphates is divided in two groups: the first one is inherent to the samples with high V content (VPDNb, NP5, NP3), while the second one deals with the high-Nb-content samples (NP4, NP6), and with the reference compound $NbOPO_4 \cdot yH_2O$ (NP2).

Mixed hydrated V/Nb phosphates with high V content and reference $VOPO_4 \cdot 2H_2O$

Figure 4.10 shows the ex-situ Raman spectra of the samples with high V content (VPDNb, NP3, NP5), compared with the pure reference compound (VPD): the samples were homogeneous and all of them contained $VOPO_4 \cdot 2H_2O$. In particular it must be noted that, especially for VPDNb, the strongest band of the VPD phase (948 cm^{-1}) was larger and less intense than in the reference compound, whereas the band at 538 cm^{-1} showed a shoulder. This means that the Nb-doped samples were dehydrated in part (α_I–$VOPO_4$).

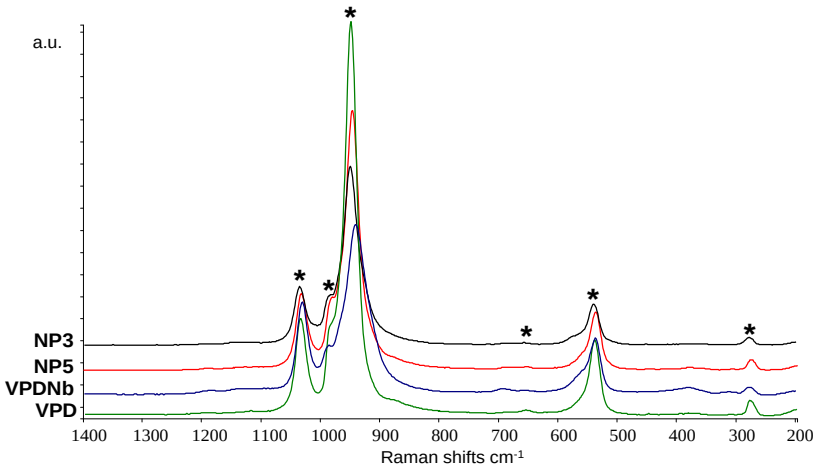

Fig.4.10_Ex-situ Raman analysis of dried samples VPD, VPDNb, NP5, NP3. Symbols: * = $VOPO_4 \cdot 2H_2O$.

The X-Ray diffraction analysis revealed additional informations about samples characteristics (fig.4.11): the main phase observed was $VOPO_4 \cdot 2H_2O$ (JCPDS 00-036-1472), but for samples NP5 and NP3 also the presence of hydrated $NbOPO_4$ (JCPDS 01-070-2653, JCPDS 00-037-0376) was shown, with its typical reflections at 2θ = 9° - 19,5° - 27,3°.

The diffraction pattern of VPDNb was not clear: the pattern showed the presence of VPD, but apparently there was also a small amount of α_{II}–$VOPO_4$ (2θ= 24,9° - 29,7°).

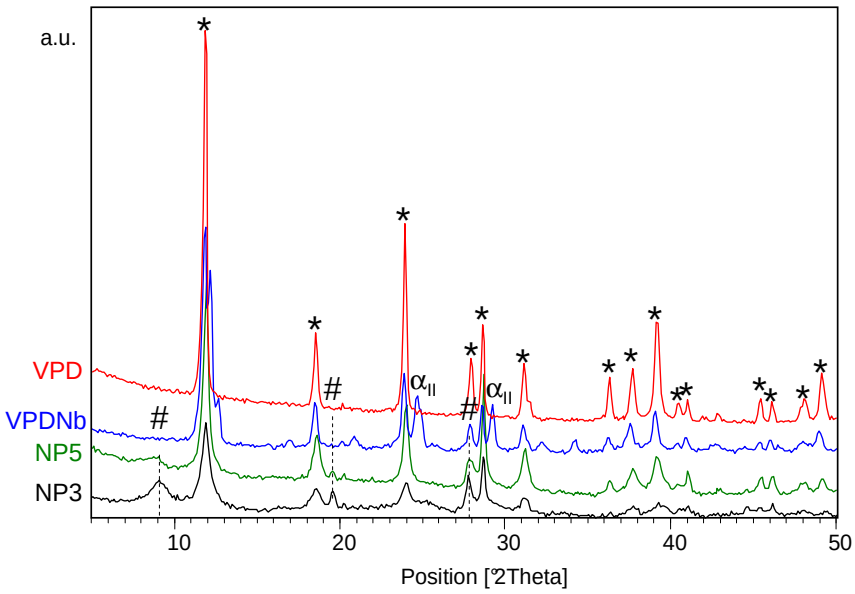

Fig. 4.11_X-Ray powder diffraction patterns of dried samples VPD, VPDNb, NP5, NP3. Symbols: * = $VOPO_4 \cdot 2H_2O$; # = hydr. $NbOPO_4$; α_{II} = α_{II} -$VOPO_4$.

To confirm that samples NP3 and NP5 were not V/Nb/P/O solid solutions, two samples were prepared by mixing the adequate quantities of the pure reference phases (VPD and NP2) to get the same molar V/Nb ratio of the former samples. The comparison of these "mixtures" with the corresponding samples, by means of XRD, was not an easy task, because the intensity of reflections in NP3 and NP5 patterns was very weak: the samples, being either a truly mixed compound (e.g., a solid solution), or a mixture of two phosphates, were microcrystalline or amorphous. In other words, we could neither confirm nor exclude that V might in part have been incorporated in the hydrated $NbOPO_4$ lattice.

Matsura et al. [31] showed that it is possible to synthesize $V_{1-x}Nb_xOPO_4 \cdot yH_2O$ solid solutions with x=0-0.2. Although the synthesis is not sufficiently described, it is likely that they used a method very similar to that one employed here. They reported that with high Nb content (x=0.3), similarly to sample NP3, it was not possible to form a solid solution; however, when x=0.1 (a composition similar to that of sample NP5), the solid solution formed.

The IR spectra reported in figure 4.12, showed little differences between samples: all the bands were already observed in spectra of VPD samples (fig. 4.3), but it is shown that when the Nb content was increased, the band relative to the vanadyl group (992 cm^{-1}) became more intense in comparison to the neighbouring band at 950 cm^{-1}.

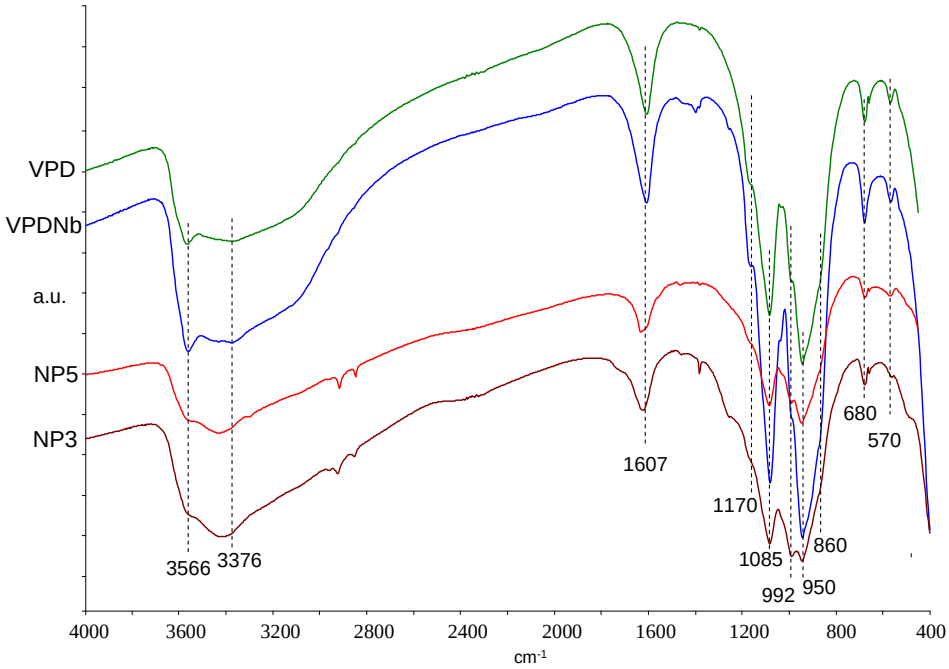

Fig. 4.12_IR spectra of dried samples VPD, VPDNb, NP5, NP3.

The UV-vis DR spectra (fig. 4.13) showed the characteristic bands of V^{5+}, at 290 and 410 nm. The shoulder at 263 nm observed in the spectrum of sample NP3 (Nb% = 25) is attributable to Nb^{5+}, as it will be described later. The very large and weak band centred at 770 nm is difficult to attribute; interestingly, it was present only for sample VPDNb, which was synthesized using a different Nb source.

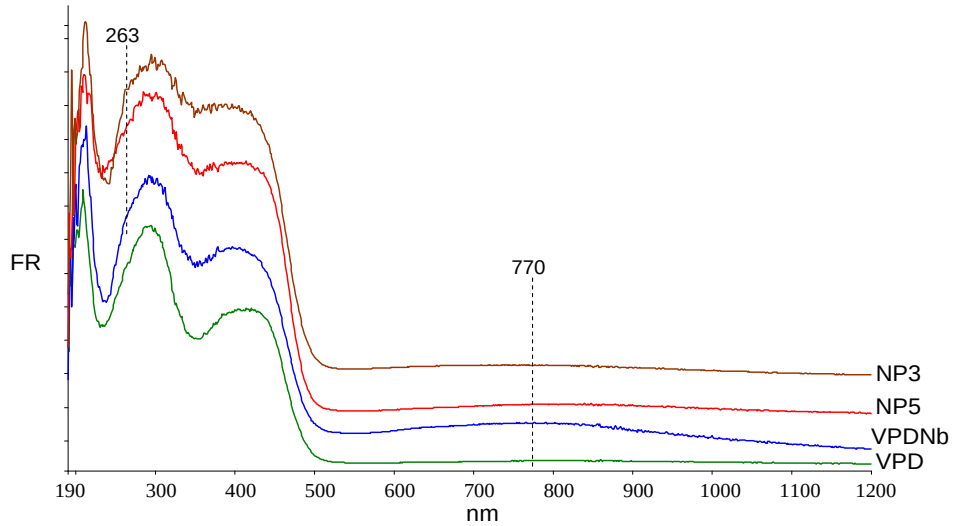

Fig.4.13_UV-vis analysis of dried samples VPD, VPDNb, NP5, NP3.

Mixed hydrated V/Nb phosphates with high Nb content and pure reference $NbOPO_4{\cdot}yH_2O$

Figures 4.14-4.15 show the ex-situ Raman spectra of samples with high Nb content (NP6, NP4), compared to the reference compound $NbOPO_4{\cdot}yH_2O$ (NP2). The spectrum of the latter sample (NP2) showed the following bands: at 1117, 985, 924, 510, 429, 235 cm^{-1}; these are in agreement with bands reported in the literature about the hydrated $NbOPO_4$ phase [5]. However, the absence of

some bands, reported in the literature, may be attributed to an higher degree of dehydration of the NP2 sample, a possible consequence of the different synthetic route used.

The bands at 985, 924 cm^{-1} may be related to P-O bond stretching [32], although Moreno-Real et al. [33] attribute the band at 950 cm^{-1}, which could also be present -but not well defined- in our samples, to the niobyl group. Moreover these latter authors report that [PO_4] units show bands at 1017, 995 cm^{-1}, while bands below 525 cm^{-1} are relative to O-P-O and O-Nb-O bending vibrations with a high degree of coupling; in particular they attribute a band around 250 cm^{-1} to the O-Nb-O bending mode. This analysis is consistent with NP2 Raman spectra.

The Raman spectrum of sample NP6, registered at different surface spots, was similar to that of NP2: in fact, the strongest bands of NP2 were present (985, 930 cm^{-1}). However, NP6 was not homogeneous, as shown in figure 4.14 (reporting the spectra recorded at different spots of the sample). Moreover, there was a band at 852 cm^{-1}, which is difficult to attribute, but is anyway close to the range of vibration of the niobyl bond (813-800 cm^{-1}) for α-$NbOPO_4$. However, in the literature this band was observed only after calcination at very high temperature [32].

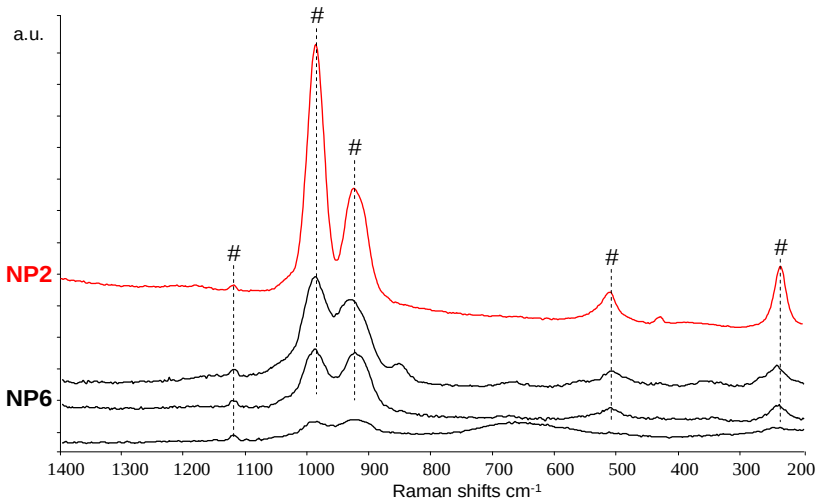

Fig. 4.14_Ex-situ Raman analysis: comparison of NP2 and NP6 dried samples. Symbols: # = $NbOPO_4 \cdot yH_2O$.

Figure 4.15 compares Raman spectra of samples NP2 and NP4; spectra were very different, because the mixed V/Nb phosphate showed principally bands attributable to $VOPO_4 \cdot 2H_2O$ (1033, 946, 536 cm^{-1}), although there were also weak bands relative to $NbOPO_4 \cdot yH_2O$ (1121, 985, 927, 502 cm^{-1}) and α_I–$VOPO_4$ (925sh, 572, 541 cm^{-1}). Sample NP4 was not homogeneous, and the strongest band (946 cm^{-1}) was broader, highlighting a possible contribution of different phases.

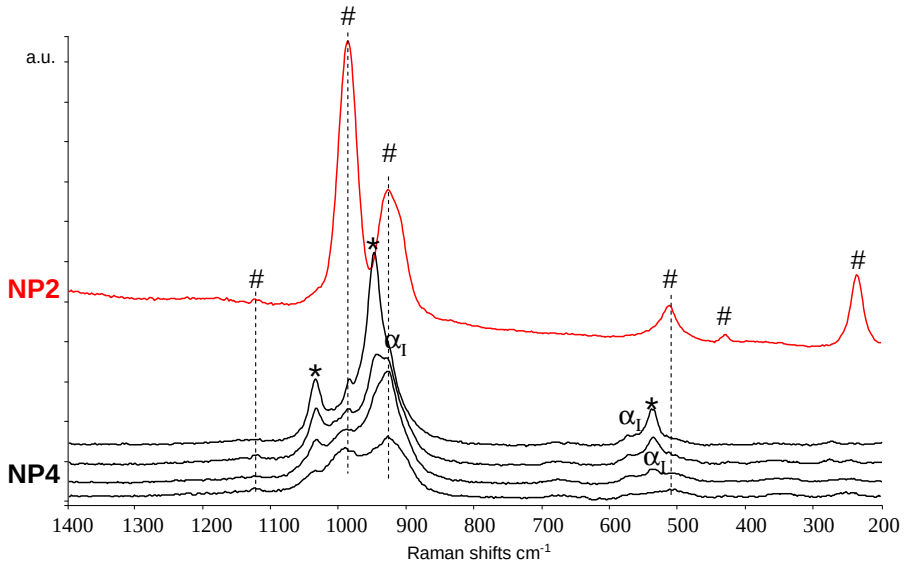

Fig. 4.15_Ex-situ Raman analysis: comparison of NP2 and NP4 dried samples.
Symbols: * = $VOPO_4 \cdot 2H_2O$; $\alpha_I = \alpha_I$–$VOPO_4$; # = $NbOPO_4 \cdot yH_2O$.

Figures 4.16 and 4.17 compare the XRD patterns of NP6 and NP4, respectively, with that of the reference compound NP2. The interpretation of diffraction patterns was not easy, because patterns were affected by the water content, which was probably different for each sample. It is shown that reflections are attributable to the $NbOPO_4$ phase only; apparently, there was no trace of any V/P/O phase.

The diffraction peak at about 2θ = 9,2°-9,5° (fig. 4.16), also reported in the literature [27,34], is characteristic of the hydrated $NbOPO_4$ phase. The water content may shift or enlarge (or even split), this diffraction peak [27], because of the layered nature of the compound: the pattern of NP2 showed two peaks at around 2θ = 8° (fig.4.16), differently from other patterns previously registered (fig.4.17).

The attribution of these several diffraction peaks is difficult also because samples were microcrystalline. At least, it is possible to identify other important reflections: the most intense one at 2θ = 27,6°-27,9° is attributable either to $NbOPO_4$ (JCPDS 01-070-2653) or to $NbOPO(OH)_2$ (niobium hydrogen phosphate hydroxide hydrate, JCPDS 00-037-0376) [35]; there were other intense peaks at 2θ = 19,5° - 25,2° - 29,2° - 39,5° - 44,6° – 57,1° – 60,8° – 64,6° (in the pattern of NP2), which are also reported in the JCPDS files already cited.

In conclusion, it can be assumed that NP2, NP6 and NP4 samples are made of hydrated $NbOPO_4$.

However it must be noted that there was a difference between NP2 and NP6 or NP4: all the reflections of the latter samples were shifted to higher value of 2θ with respect to NP2; furthermore, this effect was more marked for reflections falling at the higher diffraction angle. This means that NP6 and NP4 were probably solid solutions, with general formula $Nb_{1-x}V_xOPO_4 \cdot yH_2O$.

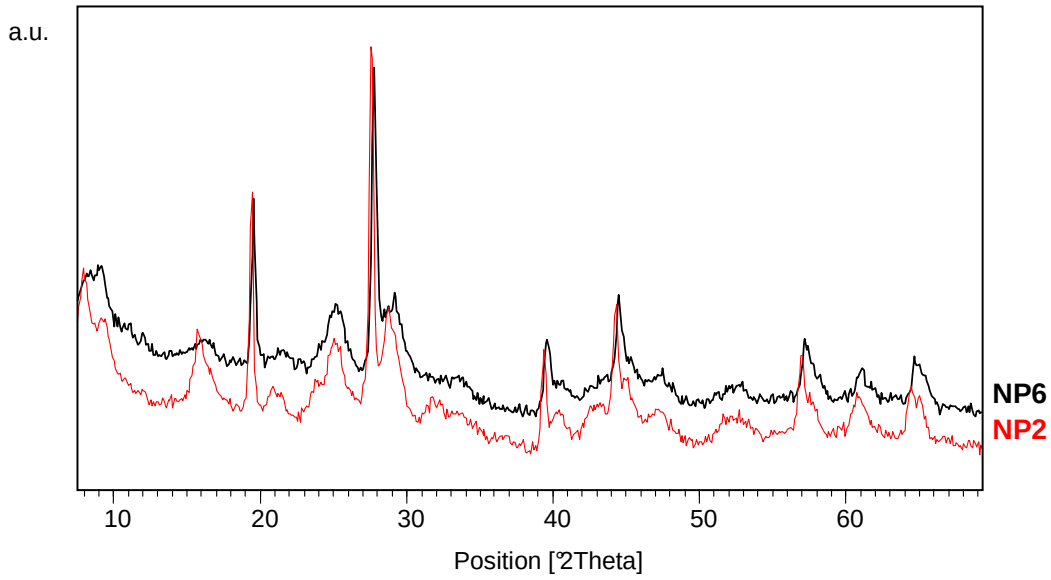

Fig.4.16_XRD analysis: comparison of NP2 and NP6 dried samples. Reflection peaks can be attributed only to hydrated $NbOPO_4$ phase (JCPDS 01-070-2653, JCPDS 00-037-0376).

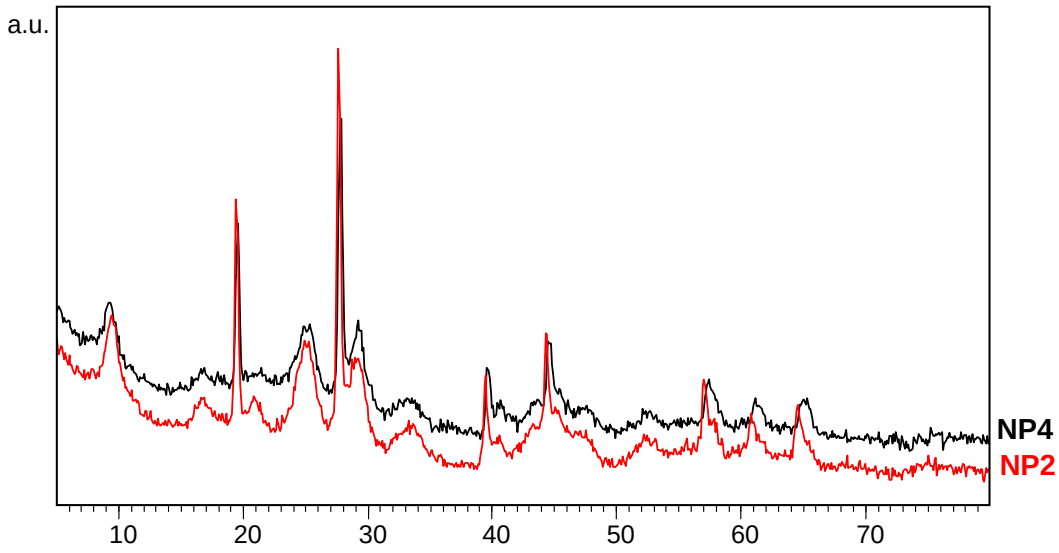

Fig.4.17_XRD analysis: comparison of NP2 and NP4 dried samples. Reflection peaks can be attributed only to hydrated $NbOPO_4$ phase (JCPDS 01-070-2653, JCPDS 00-037-0376).

It is not surprising that with samples NP4 and NP6 we could form solid solutions, theoretically represented by the formulas $(Nb_{0,75}V_{0,25})OPO_4 \cdot xH_2O$ and $(Nb_{0,9}V_{0,1})OPO_4 \cdot xH_2O$, respectively (under the hypothesis of a complete incorporation of V in the $NbOPO_4$). In fact, as reported by Jiménez-López et al. [27], the synthesis of mixed niobyl-vanadyl phosphate hydrates (with high Nb content) can be considered as a process of isomorphic substitution of the Nb (in the niobyl phosphate structure) by V. This process is favoured because the V^{5+} atomic radius is only slightly different from that of Nb^{5+} (e.g. for the six coordinated ion, respectively 0,54 Å and 0,64 Å [39]), and the replacement does not cause important distortions in the original phosphate crystal lattice, but only a contraction of the volume cell. In fact, the authors were able to synthesize a series of mixed vanadium-niobium hydrated phosphates with V/(Nb+V)% (molar percentages) between 4 and 20,6%.

Furthermore, Jiménez-López et al. [27] found that with a V loading higher than 30, the final product always contained 20% of V (experimental V/(Nb+V)%), which means that there was a limit in V incorporation. In other words, the mixed phosphate with the highest V content that can be synthesized, at least using the synthesis procedure reported [27], is $(Nb_{0,79}V_{0,21})OPO_4 \cdot 2{,}7H_2O$.

Figure 4.18 shows the IR spectra for samples NP2, NP6 and NP4: the spectra were quite similar. The bands at 683 and 490 cm^{-1} are attributable to vibrations of the lattice (Nb-O bonds); the shoulder at 940 cm^{-1} may be associated to the niobyl group (Nb=O) [36]; the bands at 1014 cm^{-1} (with a shoulder at about 1120 cm^{-1}) and 1260 cm^{-1} are due to the stretching vibrations of $[PO_4]$ groups, in particular of the P=O bond [37]; finally the vibration bands at 1630 and 3430 cm^{-1} are attributable to hydroxyl groups [27,35,37].

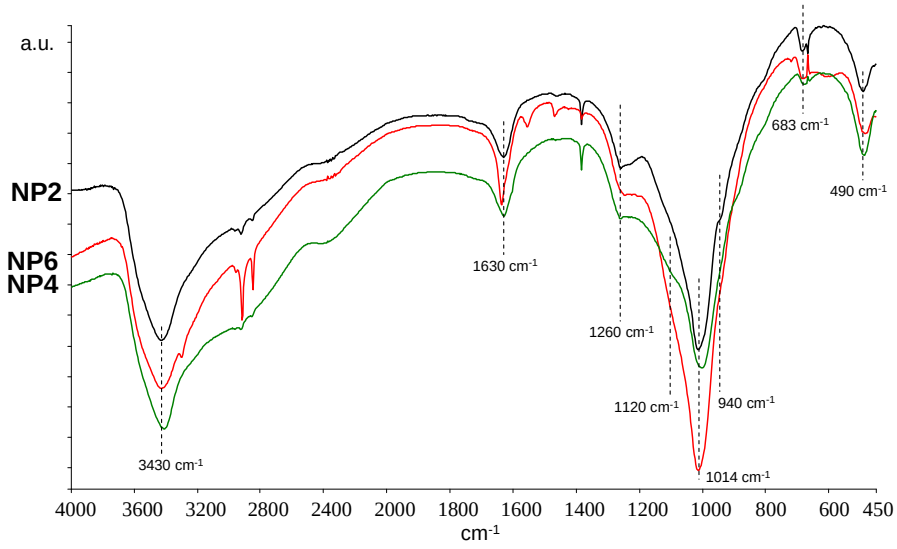

Fig. 4.18_IR spectra: comparison of NP2, NP6 and NP4 dried samples.

Figure 4.19 reports the comparison of the UV-vis DR spectra for samples NP2, NP6 and NP4. The spectrum of pure $NbOPO_4 \cdot yH_2O$ phase (NP2) showed only one band (257 nm), in accordance with the literature [33], relative to a charge-transfer transition.

The spectrum of NP6 showed the same band, but in addition there was a stronger band (330 nm) with a shoulder (410 nm). The spectrum of NP4 was more similar to that one of VPD (fig. 4.4), because it showed two strong bands (310-410 nm), but the shoulder to the first one (260 nm) suggests the presence of $NbOPO_4 \cdot yH_2O$.

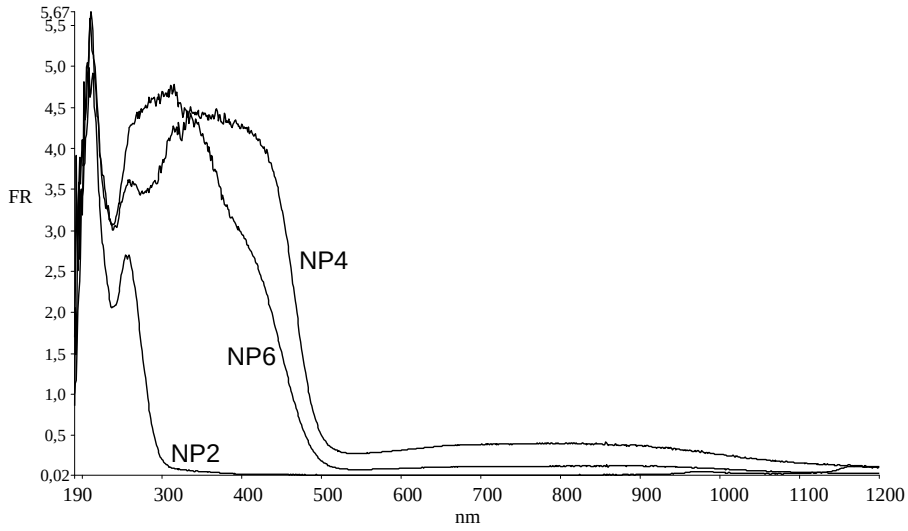

Fig. 4.19_UV vis DR spectra: comparison of NP2, NP6 and NP4 samples.

4.3.4 In-situ Raman analysis of mixed hydrated V/Nb phosphates and of pure $NbOPO_4 \cdot yH_2O$

In-situ Raman thermal treatment: sample NP5

The first in-situ Raman test was carried out with sample NP5; the conditions were the same also used for tests on VPD samples (par. 4.3.2). The spectrum recorded at room temperature (rt) corresponds to that one of $VOPO_4 \cdot 2H_2O$ (1031, 979, 945, 535, 272 cm^{-1}); at 80°C, the dehydration of the VPD phase began, as demonstrated by the shift of the characteristic bands (1027, 983, 937, 532, 276 cm^{-1}); at 200°C, the VPD phase was completely converted into α_I–$VOPO_4$ (1134, 1030, 921, 571, 533, 290 cm^{-1}) (fig. 4.20).

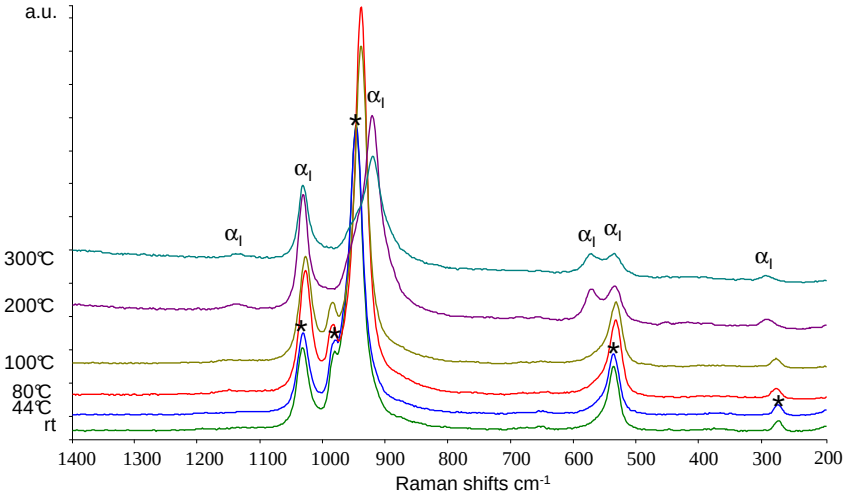

Fig. 4.20_ In-situ Raman treatment in dry air of dried NP5: spectra were recorded while increasing the temperature from room T (bottom) up to 300°C (top). Symbols: * = $VOPO_4 \cdot 2H_2O$; $\alpha_I = \alpha_I$–$VOPO_4$.

This latter phase was stable during all the isothermal period at 450°C, and even at higher temperature, 550°C (fig. 4.21); after cooling down to room temperature, the spectrum recorded confirmed the presence of α_I–$VOPO_4$ only (1034, 926, 577, 539, 458, 294 cm^{-1}) (fig. 4.22).

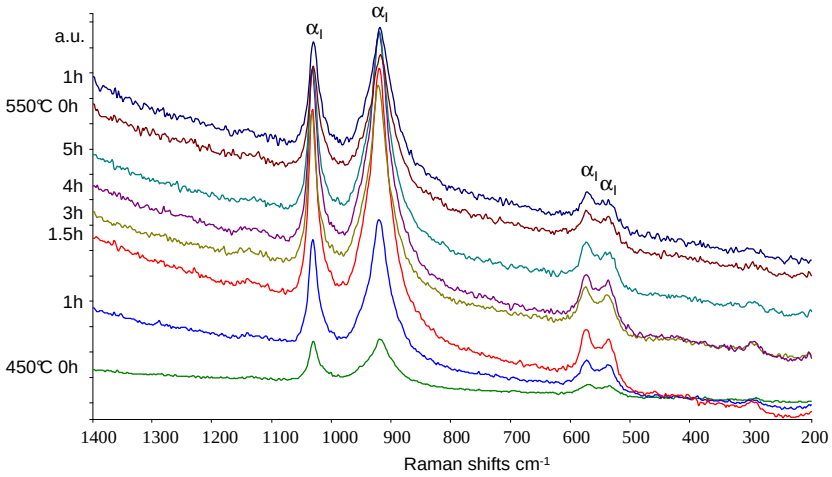

Fig. 4.21_ In-situ Raman treatment in dry air of dried NP5: spectra were recorded during the isothermal step at 450, and at 550°C, at increasing time (from the bottom to the top). Symbols: $\alpha_I = \alpha_I$–$VOPO_4$.

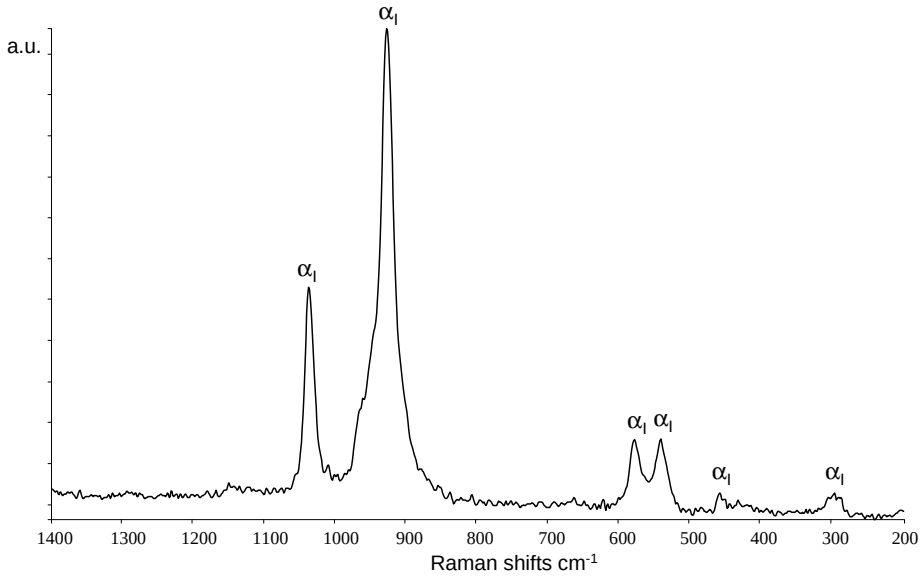

Fig. 4.22_ In-situ Raman treatment in dry air of dried NP5: the spectrum was recorded at room T, after the treatment at 550°C. Symbols: $\alpha_I = \alpha_I$–$VOPO_4$.

The same results, were also obtained with samples VPDNb and NP3, after similar in-situ Raman experiments.

It can be concluded that the presence of Nb did not affect the high-temperature transformation of $VOPO_4 \cdot 2H_2O$; in fact, still the compound was transformed into α_I–$VOPO_4$.

In-situ Raman thermal treatment: sample NP4

The in-situ Raman treatment, described above, was finally carried out on mixed phosphates having high Nb concentration (NP6, NP4), and also with the pure hydrated niobium phosphate (NP2).

It must be noted that NP4 sample was not homogeneous, since it did not contain the VPD phase only (fig. 4.15); however, the in-situ Raman experiment was carried out by focussing the beam over a particle showing the presence of the VPD phase as the main one.

Figure 4.23 reports the spectrum of NP4 registered at room temperature, showing the characteristic bands of the VPD phase (1031, 985, 943, 536 cm^{-1}), even though the strongest band was quite large, suggesting a possible contribution of other V/Nb/P/O phases; moreover, a band attributable to α_I–$VOPO_4$ (929 cm^{-1}) was also present.

The band at 985 cm^{-1} was observed in the VPD spectrum but, as discussed above (fig. 4.15), is also typical of NP2 (hydrated $NbOPO_4$); moreover, in this latter case it was the strongest band. We can infer that either hydrated $NbOPO_4$ was present, (being however most of its bands covered by VPD bands), or, more likely, a solid solution of composition $Nb_{1-x}V_xOPO_4$ formed.

Again, the dehydration began at 80°C, but only at 200°C the α_I–$VOPO_4$ spectrum was well developed (fig.4.23). Interestingly, at 250°C a new band formed (1288 cm^{-1}), and at higher temperature (400°C) all the bands attributed to α_I–$VOPO_4$ disappeared.

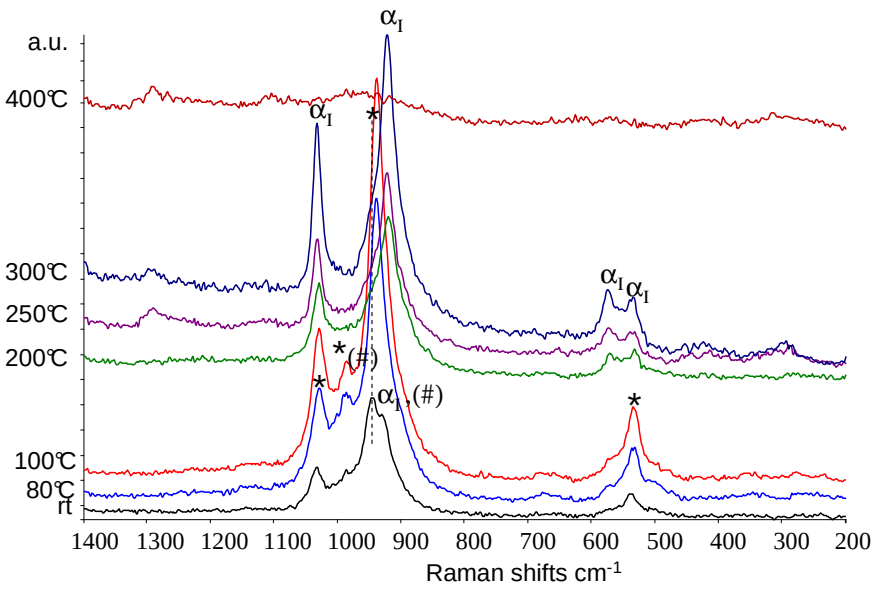

Fig.4.23_ In-situ Raman treatment in dry air of dried NP4: spectra were recorded while increasing the temperature from room T (bottom) up to to 400°C (top). Symbols: * = $VOPO_4{\cdot}2H_2O$; α_I = α_I–$VOPO_4$; # = $NbOPO_4{\cdot}yH_2O$.

Therefore, we can hypothesize that at 400°C the NP4 sample was transformed either into an amorphous compound, or into a compound with a very low Raman cross-section.

Figure 4.24 shows the spectra registered during the isothermal step at 450°C, and then at 550°C: large and less intense bands are visible (1288, 1105, 970, 900, 591, 419, 294 cm^{-1}), but spectra appeared to be very noisy.

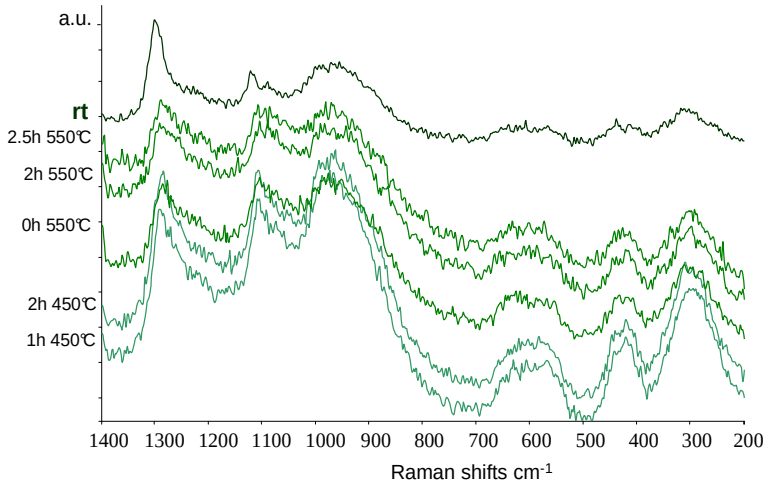

Fig.4.24_ In-situ Raman treatment in dry air of dried NP4: spectra were registered during the isothermal steps at 450°C (bottom) and 550°C, and then at room T (top spectrum), after cooling down the sample.

The spectrum at room temperature (after the in-situ thermal treatment) still showed the same bands registered at high temperature.

In regard to the attribution of the bands, the comparison with the spectra registered under the same conditions for NP6 and NP2 will allow us draw a more precise picture. Nevertheless, it is possible to conclude that, in contrast with what found with the V-rich samples (NP5), the final structure stable at high temperature was not the α_I–$VOPO_4$.

In-situ Raman thermal treatment: sample NP6

The in-situ Raman treatment of NP6 sample was then carried out, under the same conditions used previously for NP4 and NP5. The spectra in fig. 4.25-4.26 were taken while heating the sample from room temperature (bands at 1117, 985, 924, 850, 672, 555, 505, 430, 352, 239 cm^{-1}) up to 400°C; some of the changes observed may be attributed to dehydration. An interesting change occurred at 400°C: bands at 1033, 920, 570 cm^{-1} are attributable to α_I-$VOPO_4$, but the strongest band centred at 962 cm^{-1} is attributable to a phosphate stretching mode in $NbOPO_4$. After 30 minutes at this temperature, bands of α_I $VOPO_4$ disappeared, while the strong band at 962 cm^{-1} was left, and other bands with low intensity also formed (1260, 1104, 907, 604, 422, 265 cm^{-1}).

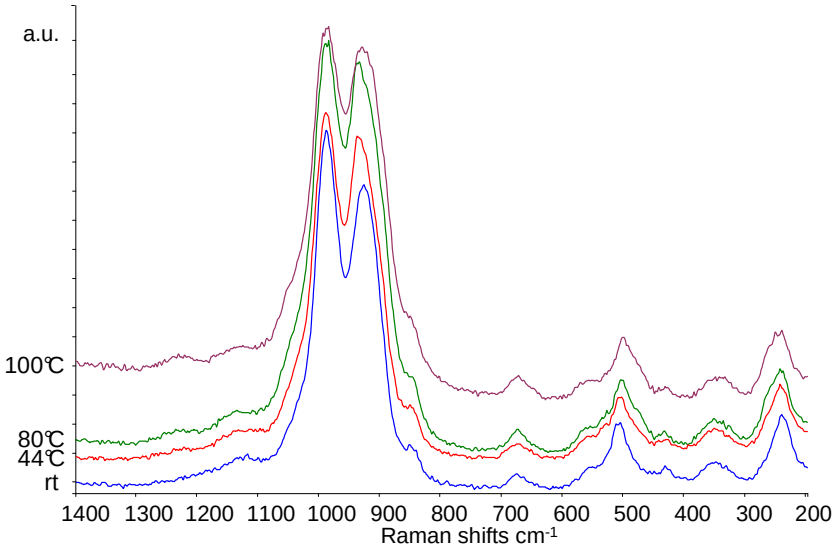

Fig. 4.25_ In-situ Raman treatment in dry air of dried NP6: spectra were recorded while increasing the temperature from room T (bottom) up to 100°C (top).

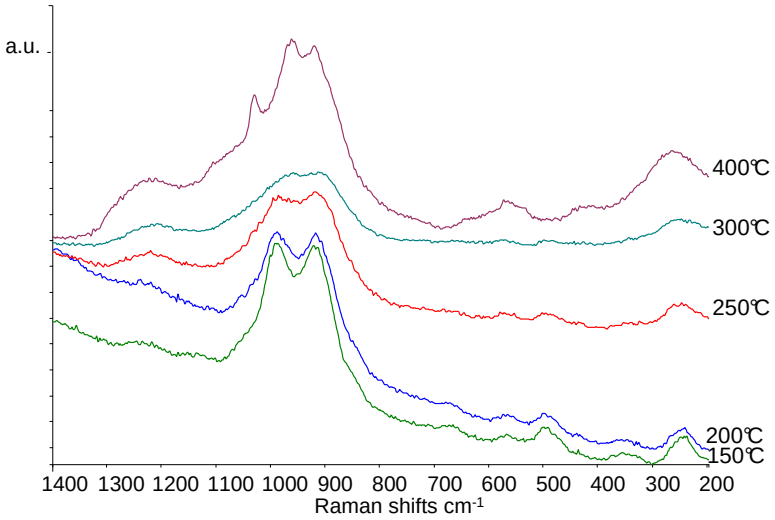

Fig. 4.26_ In-situ Raman treatment in dry air of dried NP6: spectra were recorded while increasing the temperature from 150°C (bottom) up to 400°C (top).

These bands were stable during all the isothermal step at 450°C (fig.4.27).

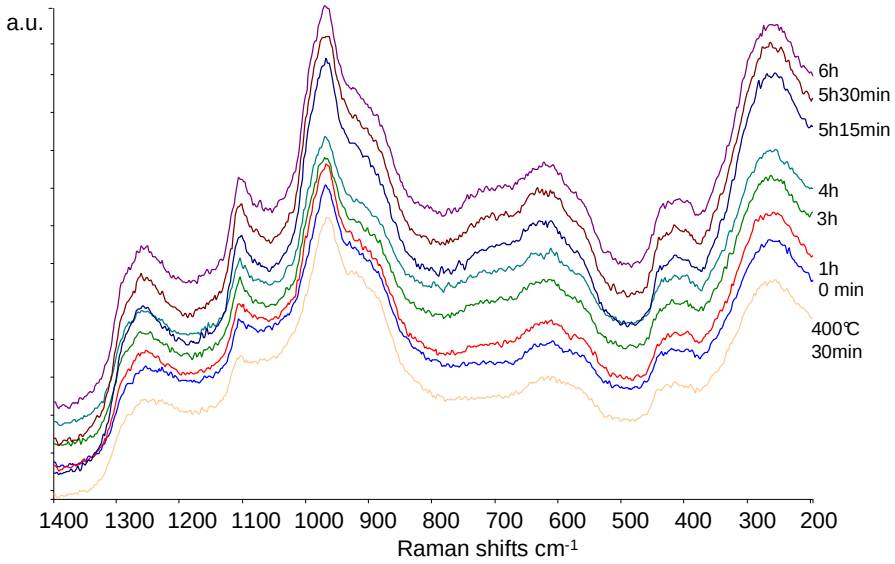

Fig. 4.27_ In-situ Raman treatment in dry air on dried NP6: spectra were recorded at 400°C – 30 min (bottom), and then during the isothermal at 450°C.

Finally, after returning down to room temperature, the spectrum showed bands at 1297, 1250, 1114, 1034, 966, 924, 574, 536, 422, 274 cm^{-1} (green spectrum, fig. 4.28); however, it must be noted that the sample was quite heterogeneous, because slightly different spectra were recorded by focussing the beam over other spots (blue spectra, fig. 4.28). This result shows that α_I-$VOPO_4$ formed (bands at 1034, 924, 574, 536 cm^{-1}), together with amorphous $NbOPO_4$.

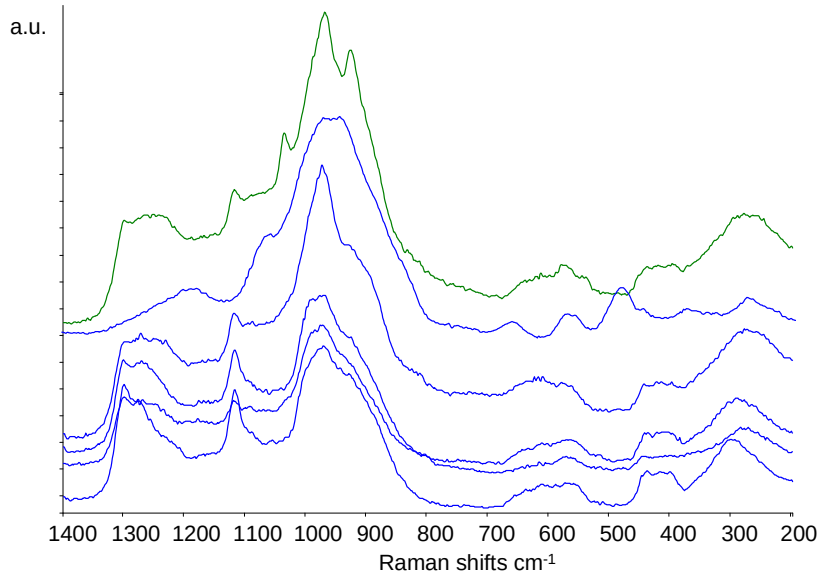

Fig. 4.28_ In-situ Raman treatment in dry air on dried NP6: spectra were recorded after cooling at room temperature, focussing the beam at different spots.

In-situ Raman thermal treatment: sample NP2

In order to interpret the spectroscopic results, we carried out the in-situ treatment also with the NP2 sample. As shown in fig. 4.29, the bands typical of the hydrated phosphate (986, 911, 233 cm^{-1}) changed at 400°C and a new spectrum was recorded at this latter temperature (fig. 4.30): the strongest band was observed at 962 cm^{-1}, with a shoulder at 890 cm^{-1} and other bands at 1225,

1080, 600, 418, and 260 cm^{-1}. The spectrum recorded at 400°C was quite similar to that one of NP6, registered after 30 min at 400°C (fig.4.27); however, after some hours at 400°C the strongest band was progressively shifted to higher energy (966-968 cm^{-1}) and also broadened, and the intensity of the shoulder at 890 cm^{-1} decreased. Interestingly at 450°C, after 30 minutes, a shoulder to the band at 968 cm^{-1} appeared (while the other shoulder at 890 cm^{-1} kept on losing intensity), the intensity of which increased during the isothermal step (fig. 4.31).

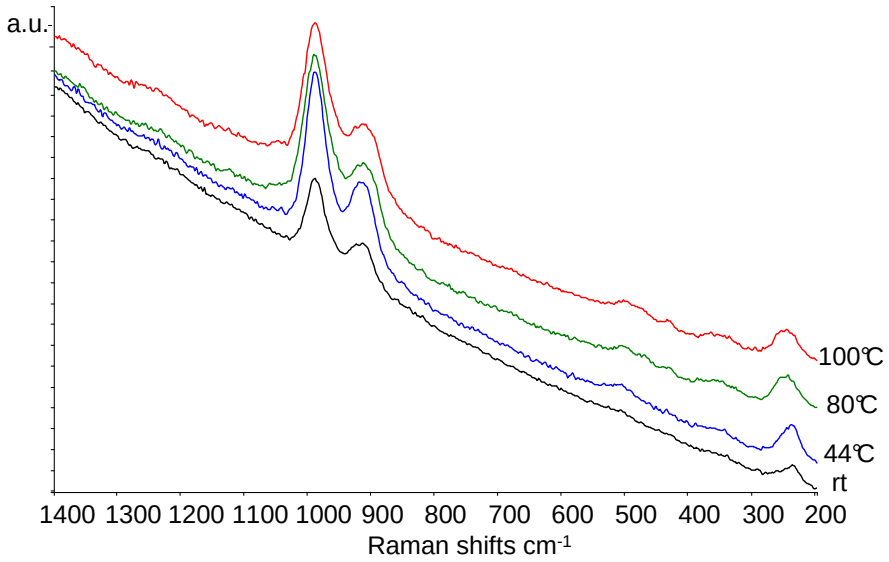

Fig.4.29_ In-situ Raman treatment in dry air of dried NP2: spectra were recorded while heating from room T (bottom) up to 100°C.

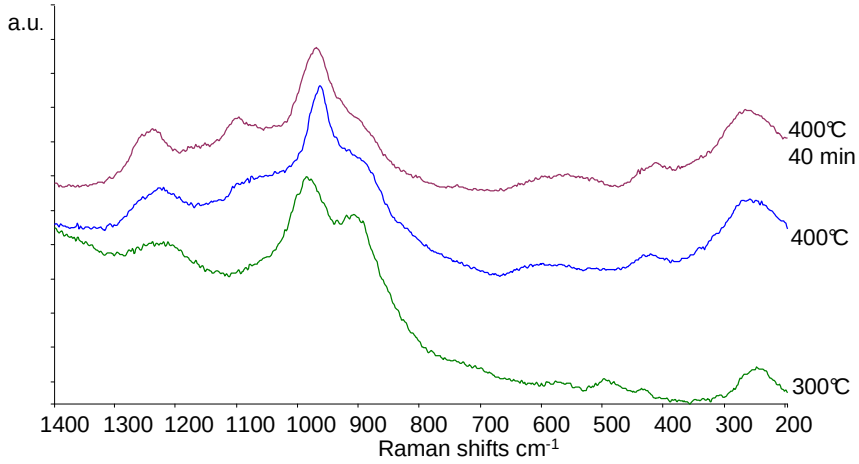

Fig.4.30_ In-situ Raman treatment in dry air of dried NP2: spectra were recorded while heating from 300°C (bottom) up to 400°C (intermediate and top).

During the isothermal step, also other bands were visible (1241, 1164, 1102, 988, 971, 413, 263 cm^{-1}), which progressively became more intense and sharper, which is in favour of an increase of the crystallinity degree.

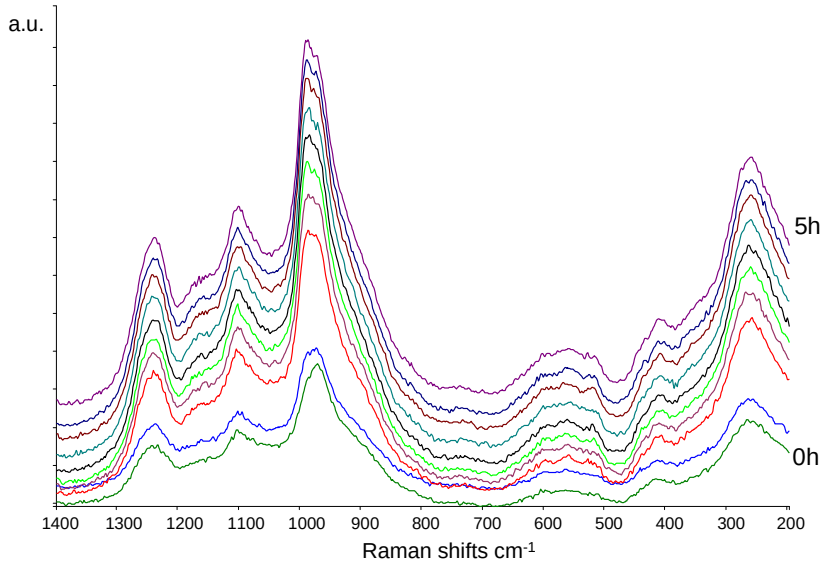

Fig.4.31_ In-situ Raman treatment in dry air of dried NP2: spectra were recorded during the isothermal step at 450°C, every 30 min, from 0h (bottom) to 5h (top).

Finally, after cooling down to room temperature, the spectrum recorded was more clearly defined, showing bands at 1245, 1170, 1115, 990, 972, 913, (803, 738), 600, 561, 520, 445, 410, and 267 cm^{-1} (fig. 4.32).

Bands at high Raman shifts (> 1000 cm^{-1}) are correlated to metaphosphate units, in particular the peak at ca. 1100 cm^{-1} is attributable to the symmetric stretching of the non-bridging oxygen in phosphate bond, while its asymmetric vibration shows a peak at 1280 cm^{-1} [39]; however it has also been reported that this peak could be due to P=O symmetric stretching [40].

Changes occurring were due to the dehydration process; however, spectra of the phase finally formed were different, although not completely, from that reported for $NbOPO_4$, obtained by calcination at 450°C of pure $NbOPO_4 \cdot 3H_2O$ [32]: in fact, the the strong band at 813 cm^{-1} (relative to Nb=O bond in calcined $NbOPO_4$) was absent. In the literature, other Raman spectra of Nb/P/O phases were not reported, which could be useful to interpret our experimental spectra. On the other hand, we can hypothesize that these strong bands associated to phosphate groups could be due to an excess P in the compound, which could also delay the dehydration process of the hydrated niobium phosphate.

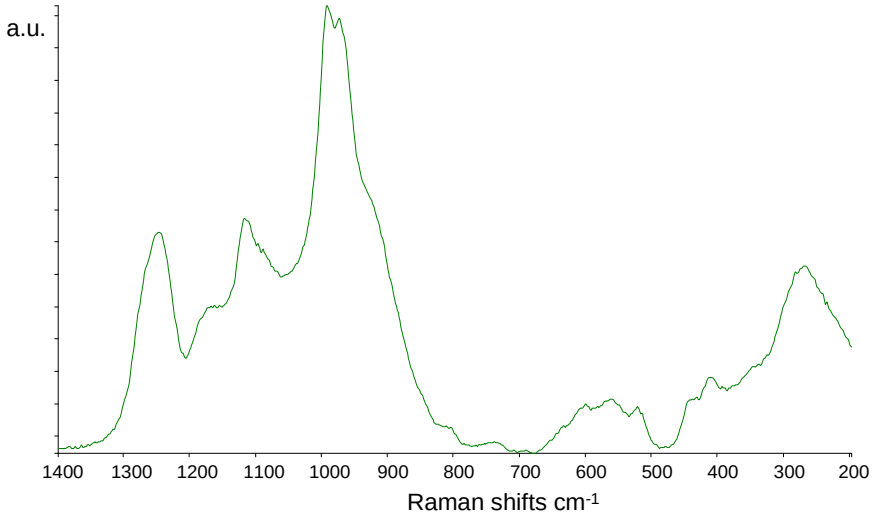

Fig.4.32_ In-situ Raman treatment in dry air of dried NP2: spectrum was recorded after cooling down to room T.

To sum up, it is useful to compare the spectra of NP2, NP6 and NP4 (having increasing amounts of V), during the isothermal step at 450°C (fig. 4.33): for example, differences in spectra for NP6 and NP4, compared with that of reference NP2, were the following: (a) the different relative intensity of the two bands at ca 990 and 960 cm^{-1}, and (b) the band at 890 cm^{-1}, which was very weak in NP2, but became more intense when the V content was increased. We can tentatively attribute it to a vibration of the mixed V/Nb phosphate.

Moreover, many other bands were shifted. Another important difference concerned bands in the 1200-1300 cm^{-1} spectral range; the spectrum of NP2 showed a band at ca. 1240 cm^{-1} (corresponding to the very intense band at 1247 cm^{-1} in the spectrum of fig. 4.32), the intensity of which decreased when the V content increased; this band is attributable to the P=O stretching in phosphate units. On the other hand, in NP6 and NP4 a band at ca 1290 cm^{-1} appeared, with an intensity which grew up with the V content. This band is not attributable to any V/P/O compound, and it can be tentatively attributed to a P=O group perturbed by the presence of V, for instance in a V-O-P=O type moiety; this band was also observed in the in-situ Raman spectrum of NP4 (fig. 4.24). The intensity of the two bands at ca 1290 and 1260 cm^{-1} increased progressively in spectra recorded while heating sample NP6 (fig. 4.26), and was present also in the spectrum of NP6 recorded at room T after in-situ experiments (fig. 4.28). In the case of NP2, instead, the heating of the sample led to intensity growth only for the band at ca 1240-1260 cm^{-1} (figs. 4.30, 4.31 and 4.32).

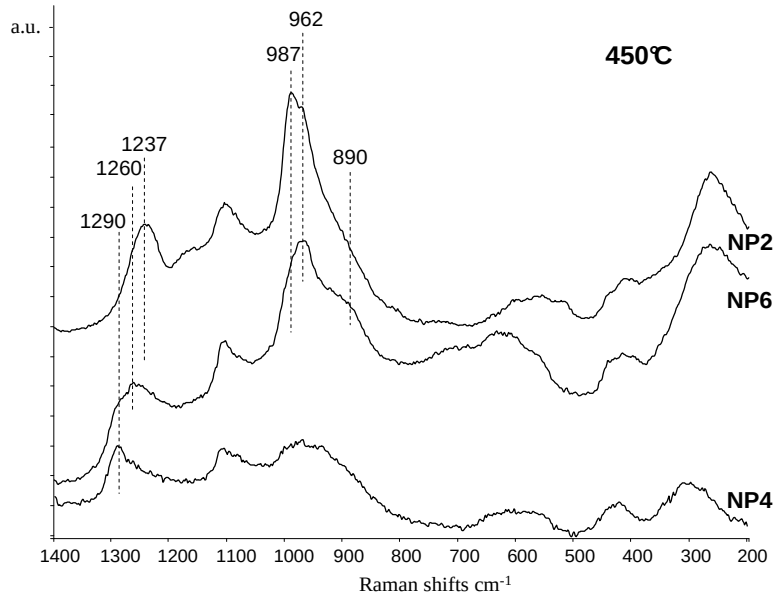

Fig.4.33_Comparison of spectra recorded during the in-situ Raman treatment in dry air (450°C): samples NP2 (top), NP6 and NP4 (bottom).

It must be noted however, that even in the spectrum of the NP6 sample, containing a relatively low amount of V (10%), still there were bands which can be attributed to α_I-$VOPO_4$. This means that the incorporation of V in the Nb phosphate anyway occurred at a limited extent.

In order to confirm the results obtained, samples NP2, NP4 and NP6 were also calcined in muffle, in static air at 450°C for 6 hours (heating rate 1°C/min), and then characterized by means of XRD (fig. 4.34) and ex-situ Raman spectroscopy (fig.4.35).

The XRD patterns showed the presence of orthorhombic $NbOPO_4$ phase (JCPDS 00-040-0124) in both NP6 and NP4; the reflections sharpness and the intensity were a clear indication of the presence of a crystalline phase. However, there was also a background in the pattern, pointing out for the possible presence of some amorphous phase, which might be the mixed Nb/V phosphate. No traces of crystalline V/P/O compounds were observed; on the contrary, the XRD pattern of calcined NP5 sample (not reported) showed the presence of both VPD and α_I-$VOPO_4$.

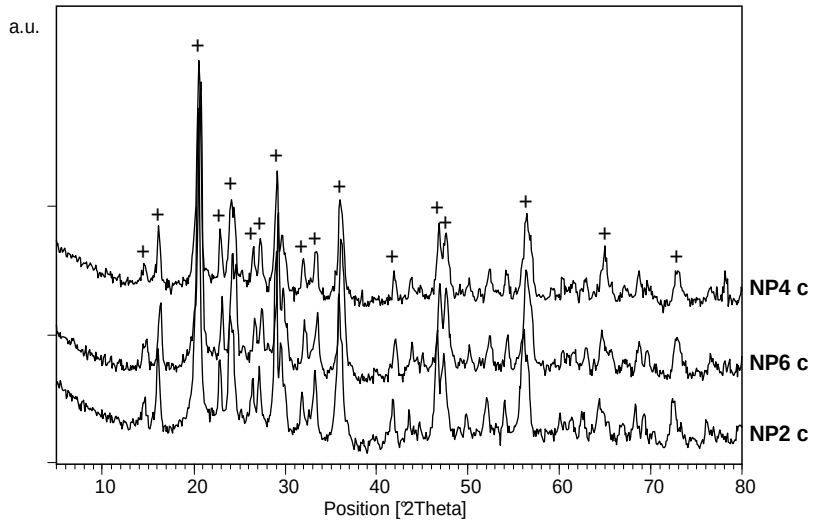

Fig.4.34_XRD analysis: comparison of NP2, NP6 and NP4 calcined samples (static air, 450°C for 6h). Symbols: + = $NbOPO_4$ (JCPDS 00-040-0124).

Raman spectroscopy analysis (not reported) showed that samples were homogeneous. A comparison between a representative Raman spectrum for each sample is reported in figure 4.35: NP4 spectrum was different from the other spectra because of the strongest band at 924 cm^{-1} (attributed to α_I-$VOPO_4$) and the less intense band at 512 cm^{-1} (near to 541 cm^{-1} of α_I-$VOPO_4$). Both NP4 and NP6 showed a band at 1297 cm^{-1}(also discussed in regard to spectra reported in fig. 4.33). All spectra showed the strong band at 1115 cm^{-1}, and were similar in the spectral range at low Raman shifts (< 700 cm^{-1}), which suggests that these bands were not affected by V doping.

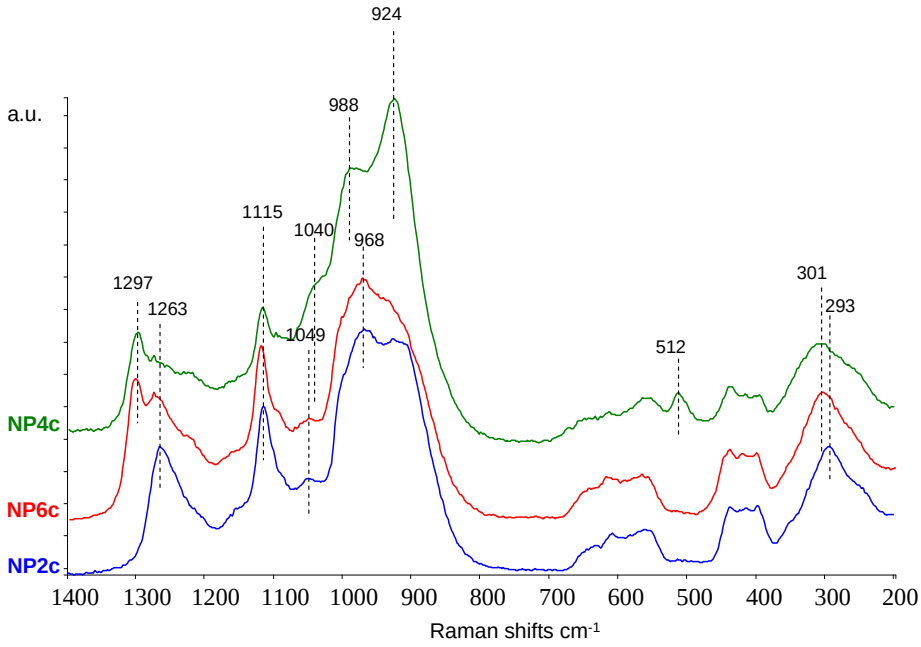

Fig.4.35_Ex-situ Raman spectra: comparison of NP2, NP6 and NP4 calcined samples (static air, 450°C for 6h).

The Raman analysis of calcined samples (static air) is in accordance with the results of in-situ thermal treatment. Raman spectra of NP6 recorded in-situ highlighted that this sample was non homogeneous (fig. 4.28); indeed, some of the spectra were similar to that of NP4, calcined in static

air. In fact, bands at 537, 570, 924, 1033 cm^{-1} are all attributable to α_I-$VOPO_4$, which indicates that a fraction of V did not form a mixed phosphate with Nb.
For sample NP4, this result was expected, since V/P/O phases were already visible in the Raman spectrum of the hydrated sample (fig. 4.15).
Since reflections attributable to α_I-$VOPO_4$ were not observed in the XRD pattern of NP6, we may hypothesize a preferential surface segregation of the α_I-$VOPO_4$; on the other hand, we cannot exclude that Raman bands attributed to the α_I-$VOPO_4$ compound may indeed be attributed also to a mixed V/Nb phosphate, isostructural with both the $NbOPO_4$ and the α_I-$VOPO_4$ compounds.

Conclusions

Our results demonstrate that it is possible to incorporate V^{5+} in the structure of $NbOPO_4$, even though in limited amount. A solid solution with general composition $Nb_{1-x}V_xOPO_4$ can be obtained by thermal treatment at 450°C (both in static air and in air flow in the Raman cell). This mixed compound shows some peculiar Raman bands, which are present neither in α_I-$VOPO_4$ nor in $NbOPO_4$. It seems that in order to obtain the incorporation of V it is necessary, at least with the procedure adopted by us, to start from Nb-rich hydrated phosphates. In fact, when V-rich compounds were prepared, we could not obtain any evidence for the incorporation of Nb^{5+} in the structure of α_I-$VOPO_4$. This result contrasts with the literature, reporting about the formation of mixed V/Nb phosphates in the same range of V/Nb atomic ratios used by us [27, 31]; discrepancies may be attributed to the method used for the preparation of samples, which was different from that described in those literature reports.
Another important output of our investigation is that the presence of Nb does not boost the development of δ-$VOPO_4$. This means that the preferred generation of the δ-$VOPO_4$ at the surface of the vanadyl pyrophosphate, especially favoured in Nb-doped catalysts (that is, in more selective catalysts), probably is not due to the formation of Nb^{5+}-containing δ-$VOPO_4$.

4.4 REFERENCES

[1] G. Ladwig, Z. Anorg. Allg. Chem. 338 (1965) 266.
[2] F. J. Cabello Sanchez, J. A. Lopez-Sanchez, R. P. K. Wells, C. Rhodes, A. Isfahani, G. J. Hutchings, Catal. Lett. vol. 77 No. 4 (2001) 189.
[3] L. Griesel, J. K. Bartley, R. P. K. Wells, G. J. Hutchings, J. Mol. Cat. A: Chem. 220 (2004) 113.
[4] S. De, A. Dey, S.K. De, J. Phys. Chem. Solids 68 (2007) 66.
[5] M. Trchová, P. Čapková, P. Matějka, K. Melánová, L. Beneš, E. Uhlířová, J. Solid State Chem.148 (1999) 197.
[6] C. J. Kiely, A. Burrows, S. Sajip, G. J. Hutchings, M. T. Sananes, A. Tuel, J. C. Volta, J. Catal. 162 (1996) 31.
[7] N. Yamamoto, T. Okuhara, T. Nakato, J. Mater. Chem. 11 (2001) 1858.

[8] A. Datta, S. Sakthivel, M. Kaur, A. M. Venezia, G. Pantaleo, A. Longo, Micropor. Mesopor. Mat. 128 (2010) 213.
[9] J. W. Johnson, A. J. Jacobson, J. F. Brody, S. M. Rich, Inorg. Chem. 21 (1982) 3820.
[10] A. Chauvel, M.E. de Roy, J.P. Besse, A. Benarbia, A. Legrouri, A. Barroug, Mater. Chem. Phys. 40 (1995) 207.
[11] A. J. Jacobson, Jack W. Johnson, J. F. Brody, J. C. Scanlon, J. T. Lewandowski, Inorg. Chem. 24 (1985) 1782.
[12] Y. H. Taufiq-Yap, C. K. Goh, G. J. Hutchings, N. Dummer, J. Bartley, Catal. Lett. 130 (2009) 327.
[13] Y. H. Taufiq-Yap, A. A. Rownaghi, M. Z. Hussein, R. Irmawati, Catal. Lett. 119 (2007) 64.
[14] N. Yamamoto, N. Hiyoshi, T. Okuhara, Chem. Mater. vol 14 no.9 (2002) 3882.
[15] J. K. Bartley, J. A. Lopez-Sanchez, G. J. Hutchings, Catal. Today 81 (2003) 197.
[16] G. J. Hutchings, M. T. Sananes, S. Sajip, C. J. Kiely, A. Burrows, I. J. Ellison, J. C. Volta, Catal. Today 33 (1997) 161.
[17] F. Cavani, S. Luciani, E. Degli Esposti, C. Cortelli, R. Leanza, Chem. Eur. J. 16 (2010) 1646.
[18] F. Benabdelouahab, J. C. Volta, R. Oliver, J. Catal. 148 (1994) 334.
[19] E. Bordes, Catal. Today 1 (1987) 499.
[20] E. Bordes, Catal. Today 3 (1988) 163.
[21] Z.G. Li, R.L. Harlow, N. Herron, H.S. Horowitz, E.M. McCarron, J. Catal. 171 (1997) 506.
[22] F. Ben Abdelouahab, R. Olier, N. Guilhaume, F. Lefebvre, J.C. Volta, J. Catal. 134 (1992) 151.
[23] F. Girgsdies, M. Schneider, A. Brückner, T. Ressler, R. Schlögl, Solid State Sci. 11 (2009) 1258.
[24] J. A. Lopez-Sanchez, J. K. Bartley, R. P. K. Wells, C. Rhodes, G. J. Hutchings, New J. Chem. 26 (2002) 1613.
[25] S.Bruque, M. Martinez-Lara, L. Moreno-Real, A. Jimenez-Lopez, B. Casal, E. Ruiz-Hitzky, J. Sanz, Inorg. Chem. Vol. 26, No. 8 (1987) 847.
[26] A. Datta, M. Agarwal, S. Dasgupta, J. Mater. Chem. 12 (2002) 1892.
[27] A. L. Garcia-Ponce, L. Moreno-Real, A. Jimenez-Lopez, Inor. Chem. vol. 27 No.19 (1988) 3372.
[28] L. Beneš, E. Černošková, J. Málek, K. Melánová, P. Patrono, V. Zima, J. Incl. Phenom. Macro. Chemistry 36 (2000) 163.
[29] V. Zima, L. Beneš, J. Málek, M. Vlček, Mater. Res. Bull. vol. 29 No.6 (1994) 687.
[30] Kari E. Birkeland, Scott M. Babitz, Gregory K. Bethke, H. H. Kung, George W. Coulston, Simon R. Bare, J. Phys. Chem. B Vol. 101 No. 35 (1997) 6895.
[31] I. Mastuura, T. Ishimura, S. Hayakawa, N. Kimura, Catal. Today 28 (1996) 133.
[32] G.T. Stranford, R.A. Condrate Sr., J. Solid State Chem. 76 (1988) 407.
[33]L. Moreno-Real, E. R. Losilla, M. A.G. Aranda, M. Martinez-Lara, S. Bruque, M. Gabás, J. Solid State Chem. 137 (1998) 289.

[34] J. C. G. Silva, M. D. Vieira, W. De Oliveira Andrade, A. C. B. Dos Santos, J. Mater. Sci. 40 (2005) 4455.
[35] M. K. de Pietre, L. C. P. Almeida, R. Landers, R. C. G. Vinhas, F. J. Luna, Reac Kinet Mech Cat 99 (2010) 269.
[36] T. Armaroli, G. Busca, C. Carlini, M. Giuttari, A. M. Raspolli Galletti, G. Sbrana, J. Mol. Cat. A: Chem. 151 (2000) 233.
[37] M. H. C. de La Cruz, Â. S. Rocha, E. R. Lachter, A. M.S. Forrester, M. Castro Reis, R. A. S. San Gil, S. Caldarelli, A. D. Farias, W. A. Gonzalez, Appl. Cat. A: General 386 (2010) 60.
[38] R.D. Shannon, Acta Cryst. A32 (1976) 751.
[39] M.G. Donato, M. Gagliardini, L. Sirleto, G. Messina, A.A. Lipovskii, D.K. Tagantsev, G.C. Righini, Appl. Phys. Lett. 97 (2010) 231111.
[40] J.J. Hudgens, R.K. Brow, D.R. Tallant, S.W. Martin, J. Non-Cryst. Solids 223 (1998) 21.

5

VANADYL PYROPHOSPHATE CATALYSTS PREPARED BY A NEW METHOD: THE MICROWAVE SYNTHESIS OF $VOHPO_4 \cdot 0.5H_2O$

5.1 INTRODUCTION

5.1.1 General aspects of microwave-assisted synthesis

Microwave (MW) assisted synthesis is an alternative method for carrying out organic and inorganic reactions, considering the evidence that every reaction which needs heating can be accelerated by using microwaves. Microwave permits in fact to reach the reaction temperature faster compared to conventional synthesis (by thermal conduction). In the literature, several examples of preparations involving microwave irradiation are reported, regarding zeolites, mesoporous molecular sieves and other different nanoporous solids [1]. The mechanism of microwave heating process is quite complicated, considering the different parameters involved in this physical phenomenon.

First, we have to consider that the energy of microwaves (λ=1mm–1m; f=0.3-300 GHz) is relatively low, in comparison with other electromagnetic waves, because it is not sufficient to break chemical bonds and the electric field generated (E) cannot shift a chemical equilibrium [1]. However the microwave energy is able to heat materials, essentially by two mechanisms: i) inducing rotational movements of molecules, having a permanent or induced dipolar moment, and ii) causing ionic conduction. The rotational movements, typically present for liquid samples, are generated by the oscillating electric field (E): molecules constantly try to realign but, being the electric field continuously oscillating, they cannot indeed totally realign and create a continuous movement, which causes finally heat generation by collisions and attrition. The ionic conduction (or conductivity, σ) occurs when a ionic material is irradiated by microwaves: a ionic current is generated due to the mobility of ions, as consequence of the applied electric field [2].

In both cases, the penetration of the microwave energy into the sample (in the present work, the synthesis mixtures) is a consequence of the material permittivity and of the MW frequency involved.

For liquid samples, the permittivity (ε , dielectric constant) is affected by the pH of the solution and by the temperature. The dielectric constant consists of two contributions (ε^{I},ε^{II}), and their combination represents the "tangent-loss" ($\tan(\delta) = \varepsilon^{II}/\varepsilon^{I}$): the greater is this factor, the less is the penetration of the microwave energy into the material, at a specific frequency, because the MW energy is more well dissipated (great interaction) [1]. For example, most part of ionic materials possess high δ, and therefore they are good dissipators due to the electronic transport [2]. Regarding liquid samples, an high dissipation solvent (e.g. ethylene glycol in comparison to water) leads to a faster heating, or MW dissipation. For these reasons, the choice of the mixture solvent is very important: the heating process is (in first analysis) favoured when using a polar or a ionic solvent, however, this is not always obvious (different parameters affect MW energy distribution). Finally, we have also to note that other parameter influence the MW assisted synthesis: the reactor configuration (geometry) and the microwave system characteristics (oven, waveguide, etc.) [1].

The main advantage of microwave irradiation, compared to conventional heating, is the high efficiency in heat-transfer: it is fast, localized and not limited by inertia phenomena because microwave irradiation affects reactants and solvent, while excluding the reactor walls. Microwave irradiation permits to transfer higher quantity of energy, involving the same bulk temperature (of the reaction vessel). For these reason, MW heating brings about an improvement of reaction kinetics and, at the same time, degradation and other undesired reactions are avoided. These aspects render microwave-involving processes environmentally friendly, as they require lower energy than conventional processes [1].

Because of this, microwave assisted synthesis appears attractive for industrial preparations, as lower energy waste and higher yield in the desired product can be obtained. Nowadays, microwave heating is used in industry for a lot of different applications, generally involving a drying treatment.

5.1.2 Literature analysis about microwave heating applied to V/P/O systems

In the literature some examples of microwave heating, used for the synthesis of V/P/O materials, are reported. Benes et al. [3] used microwave heating to treat the pre-formed $VOPO_4 \cdot 2H_2O$ compound: microwave irradiation for few minutes led to an intercalated compound, with molecules of alcohols and glycols retained between the layers. The authors found that the nature of the starting material strongly influenced the result: microwave irradiation permitted the intercalation process because the compound possessed water molecules which, being dipoles, were easily removed and substituted by organic molecules. In fact the intercalated compound did not form when the correspondent dehydrated compound, $VOPO_4$, was used as the starting material.

The previous study was motivated by the discover of Chatakondu et al. [4], who reported about the possibility of intercalation of organic molecules (pyridine, 4-methylpyridine, 4-phenylpyridine) in $VOPO_4 \cdot 2H_2O$ compound, by treating it with microwave irradiation.

Capkova et al. [5], reported the preparation and the characterization of $VOPO_4 \cdot 2CH_3CH_2OH$: they treated $VOPO_4 \cdot 2H_2O$ with ethanol, using microwave (2450 MHz) for very short time (0.5-1 minutes). Melanova et al. [6] investigated the intercalation process of $VOPO_4 \cdot 2H_2O$, with microwave heating, using different mixtures of alcohols (atom carbon content, from 2 to 6). Benes et al. [7] utilized unsaturated alcohols (2-propenol, 2-propyn-1-ol and 2-butene-1-ol): the alcohols were made react with $VOPO_4 \cdot 2H_2O$ employing microwave irradiation, for very short time (0.5-2 minutes).

Frequently, the aim of these investigations was the understanding of the structure of dihydrate vanadyl phosphate, rather than studying the effect of microwave irradiation on the V/P/O compound.

Microwave irradiation was effectively applied for the synthesis of vanadyl hydrogen phosphate ($VOHPO_4 \cdot 0.5H_2O$) by Pillai et al. [8]. In this wok, the authors prepared three samples of $VOHPO_4 \cdot 0.5H_2O$, using V_2O_5, a mixture of alcohols (2-butanol and benzyl alcohol) and H_3PO_4: i) sample 1 from one-step synthesis (100°C, 1h); ii) sample 2 from a two-step synthesis, obtained first by irradiating the mixture of alcohols and V_2O_5 (100°C, 0.5h) and then, after H_3PO_4 addition, by irradiating the final mixture (100°C, 0.5h); iii) sample 3 from a two-step synthesis, obtained first by irradiating the mixture of alcohols and V_2O_5 (100°C, 1h) and then, after H_3PO_4 addition, irradiating the final mixture (100°C, 1h). The power utilized for microwave irradiation was 300 W.

The XRD pattern of sample 1 revealed the formation of an amorphous compound while the XRD patterns of sample 2 and sample 3, calcined, showed the crystallographic reflections of $(VO)_2P_2O_7$. The surface areas measured for these samples were higher compared to those of precursors prepared by either conventional or by ultrasound methods. Final catalysts were tested in the liquid phase oxidation of cycloalkanes.

Zeng et al. [9] utilized microwave irradiation to treat the pre-formed $VOHPO_4 \cdot 0.5H_2O$ compound, synthesized by a two-step method, and doped with different elements (Ce, La, Bi, Mo). The irradiation process was carried out using a power of 160W, for 2 minutes. The precursors obtained showed high surface areas: this result was attributed to a peculiar capacity of microwave irradiation, which permits an homogeneous heating of the inner and the outer part of the solid.

In a following investigation, Taufiq-Yap et al. [10] prepared $VOHPO_4 \cdot 0.5H_2O$ by a two-step method, using microwave irradiation for treating the final product of each step (first $VOPO_4 \cdot 2H_2O$, then $VOHPO_4 \cdot 0.5H_2O$). The authors obtained very crystalline compounds, with high surface area; they tested the catalysts in the oxidation of n-butane to maleic anhydride (MA). The “MW”-derived catalysts demonstrated the higher catalytic activity but also the best selectivity to MA, due their peculiar morphologic characteristics.

Sydorchuk et al. [11] prepared supported vanadyl pyrophosphate (VPP) catalysts: the one-step synthesis was carried out in a microwave oven (0.5-1h, 175°-240°C), mixing V_2O_5, citric acid, H_3PO_4 and the support (carbosil).

Rownaghi et al. [12-17] prepared $VOHPO_4 \cdot 0.5H_2O$ by means of both the one-step and the two-step method, and testing different alcohols (e.g. glycol, 1-butanol) and different metallic salts, used as dopants in the aim of improving the catalytic performance. In the first case (one-step synthesis) the compound $VOHPO_4 \cdot 0.5H_2O$ was prepared using an autoclave, at high temperature and pressure (solvothermal method). In the second case, the microwave irradiation (few minutes, power 160W) was limited to a treatment of the product, obtained from each step: first $VOPO_4 \cdot 2H_2O$, and then $VOHPO_4 \cdot 0.5H_2O$. In general, catalysts obtained by means of the MW-heating showed improved performances, although sometimes masked by the effect of the dopant, which clearly affected the precursor physical and chemical characteristics. The authors found that some preparations involving MW led to precursors with high surface area, and to VPP showing the prevailing exposure of the (020) planes. However, both the temperature of synthesis and the choice of the alcohol strongly affected the final product characteristics.

Finally, Sydorchuk et al. [18] prepared $VOHPO_4 \cdot 0.5H_2O$ by means of the one-step synthesis, using an autoclave and strongly reducing agents (e.g. citric acid, maleic anhydride, glycerol, salicylic acid). Some experiments were carried out by heating the autoclave with microwave irradiation (170°C, 2h). Their results were in accordance with what already described by other authors; in particular they highlighted the important role played by pressure and by the solvent used in the synthesis.

In conclusion, it is possible to say that MW heating, when applied to the synthesis of V/P/O compounds, especially as a post-treatment of the pre-formed $VOHPO_4 \cdot 0.5H_2O$, led to an increase of surface area and to a preferential exposure of (020) planes. Nevertheless, in the literature the synthesis of $VOHPO_4 \cdot 0.5H_2O$ with the aid of microwave irradiation has not yet been investigated deeply, probably as a consequence of unexciting results [8], but also because hard irradiation conditions were necessary to obtain a crystalline compound [18].

In the present work, we investigated the one-step synthesis of $VOHPO_4 \cdot 0.5H_2O$, using microwave heating; in particular, different solvents were used (isobutanol and ethanol), and the presence of Nb as a dopant element was also taken into consideration.

5.2 RESULTS AND DISCUSSION

5.2.1 Synthesis of $VOHPO_4 \cdot 0.5H_2O$ by microwave method

The new method used for the synthesis of $VOHPO_4 \cdot 0.5H_2O$ employs microwave irradiation by means of a CEM Discover S-class system [19]. The apparatus consists of a single-mode self-tuning cavity: the energy of microwave irradiation is focused on the internal cavity, where the sample is located, generating an uniform electric field (E); moreover, the microwave power is automatically regulated, by monitoring temperature and pressure, which is set up before the experiment beginning. Figure 5.1 reports an image of the instrument and a schematic representation of its internal part, where the microwaves are generated continuously and focused with the maximum

efficiency on the sample vial. The syntheses were carried out at the Dept. of Chemistry and Industrial Chemistry, Pisa University (Prof. Anna Maria Raspolli Galletti and co-workers).

Fig.5.1_CEM Discover instrument for MW-assisted synthesis of V/P/O samples (left); internal part of the instrument, showing microwaves generation and distribution, surrounding the reactor chamber, at the centre of the internal cavity (right) [1].

A vial having 80 ml capacity was used as a vessel for the synthesis mixture. At the beginning, about 2,5 g of vanadium pentoxide (99%) were dispersed in 15 ml of alcohol (100%), then phosphoric acid (99%) and finally, the remaining part of the solvent (15 ml) were also added. Since pure 99% phosphoric acid is a solid, this reagent was previously fused and then added to the mixture: the suspension was left under stirring for some minutes.

Subsequently, the vial was introduced in the CEM instrument chamber, after which the heating process was started. The reaction mixture was kept under stirring during all the experiment. Generally the “Dynamic” method was used, and the power employed was 250 W.

The synthesis was carried out setting a fixed temperature (125°C), and the instrument was able to change automatically the power, in order to maintain this temperature constant. The sample was initially heated by microwave irradiation, at the maximum power (250W), to permit reaching the solvent boiling temperature; then the power was lowered (10 W) to avoid over-heating phenomena and to keep the reaction chamber temperature at a constant value.

It must be noted that, as a consequence of either the different solvents used or the presence of the Nb compound, some operative conditions were different from one experiment to the other: for the synthesis of MW4, MW5 and MW10 samples, the pressure registered in the chamber reaction was about 35 Psi; for sample MW17, the fixed temperature (125°C) was reached with 170 W of power instead of 250 W, which was instead necessary in the other cases.

At the end of the synthesis, the mixture was left at ambient conditions for cooling, then it was filtered and washed with fresh solvent. The solid was finally dried at 120°C for 8 hours: samples referred as MW precursors were obtained. Table 5.1 compiles the MW samples synthesized.

A VPP precursor sample was also prepared using the standard organic procedure, referred as VHP sample. In this case, the reagents used for the synthesis were the same also used for MW precursors, and the main characteristics are summarized in table 5.1. It must be noted that the quantities

involved for the standard preparation (described in Chapter 2) were greater compared to those utilized for microwave synthesis; however the same molar ratio between V_2O_5 (the limiting reagent) and solvent, and also between V_2O_5 and H_3PO_4, were used. The advantage of using a microwave-based synthetic method instead of the traditional one (VHP), is clearly shown by the time necessary to complete the synthesis: for MW samples a very shorter synthesis time permitted to obtain the same V_2O_5 conversion.

	P/V	V/Nb	Solvent	Temperature (°C)	Synthesis time (h)
VHP	**1.1**	**-**	**isobutanol**	**reflux**	**6**
MW4	**1.1**	**-**	**isobutanol**	**125**	**0.5 + 0.5**
MW5	**1.1**	**-**	**isobutanol**	**125**	**1**
MW10	**1.1**	**-**	**ethanol**	**125**	**1**
MW17	**1.1**	**155**	**ethanol**	**125**	**1**
MW18	**1.1**	**155**	**isobutanol**	**125**	**1**

Tab.5.1_Table of VPP catalysts precursor, synthesized by microwave method (MW) and by traditional method (VHP): theoretical molar P/V ratio, theoretical molar V/Nb ratio, solvent use for the synthesis, synthesis temperature and synthesis time (h).

The preparation of MW4 differed from that of MW5, because the synthesis was carried out in two steps: the mixture was heated for half an hour, then stopped for few minutes, and finally heated again for 30 minutes more.

The use of ethanol instead of isobutanol could be advantageous for the precursor preparation, especially for an hypothetical industrial process: work-up procedures would be easier, and the organic products coming from the oxidation of ethanol would be more easily removed and treated, as compared to the preparation carried out using isobutanol.

Furthermore, the use of ethanol would lead to milder conditions (lower boiling temperature and lower endogen pressure). However, in order to permit a comparison with samples prepared using isobutanol, the synthesis with ethanol were carried out while keeping the temperature at 125°C. It is worth noting that in the traditional thermal synthesis of the precursor, the use of ethanol does not allow V_2O_5 reduction.

Samples listed in Table 5.1 represent only a small part of a larger series of samples, prepared in the aim of investigating the microwave-based synthesis of $VOHPO_4 \cdot 0.5H_2O$. The choice of these samples derives from their peculiar characteristics (par. 5.2.2): sample MW4 possessed chemical-physical characteristics very similar to those of the VHP sample, the reference one. On the other hand, MW5 and MW10 showed a particular morphology, never shown before for $VOHPO_4 \cdot 0.5H_2O$. Finally, MW17 and MW18 are interesting because both contained Nb, an important VPP dopant (Chapter 3), but they were prepared with different organic solvents.

All samples were calcined by means of the usual thermal treatment (Chapter 2): the first step was carried out in flowing air (300°C, 6h) and the second step in flowing nitrogen (550°C, 6h). Samples obtained after the thermal treatment are referred as calcined samples, since they were made of VPP (fresh catalysts), ready for reactivity tests.

The characterization of precursors, calcined and used catalysts, together with reactivity data, are described below (par. 5.2.2).

5.2.2 Characterization of VPP precursor: microwave samples (MW) vs thermal sample (VHP)

The dried precursors reported in table 5.1 were characterized by means of Raman and UV-vis DR spectroscopy, and of XRD and SEM.

Raman spectra of MW4, MW5, MW18 dried samples were similar to those recorded for the reference sample (VHP): all spectra were clearly affected by fluorescence and only the strongest band relative to vanadyl hydrogen phosphate hemihydrate ($VOHPO_4 \cdot 0.5H_2O$) at 986 cm^{-1} was observed (fig. 5.2). Conversely, for the ethanol-based preparations (MW10 and MW17), well defined spectra relative to $VOHPO_4 \cdot 0.5H_2O$ were obtained (fig. 5.3), with bands at 1209, 1150, 1103, 980, 904, 510, 453, 335, and 280 cm^{-1}.

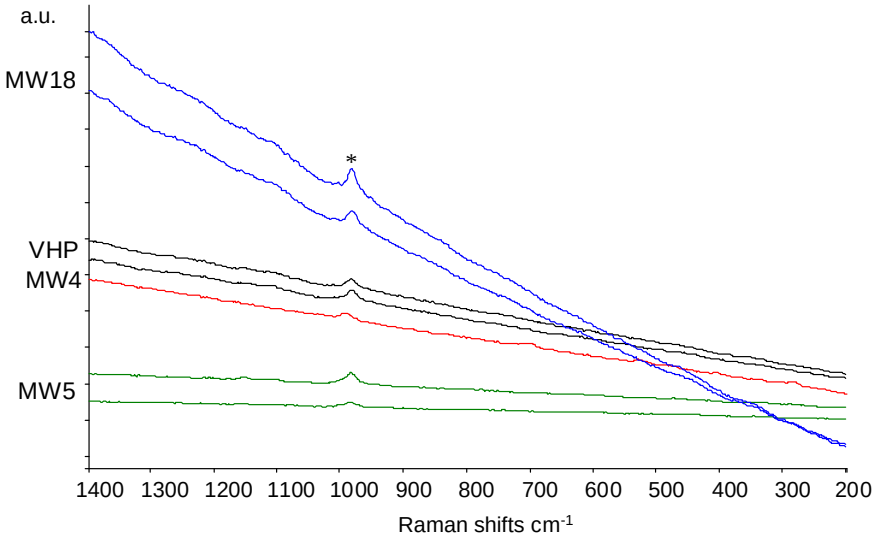

Fig. 5.2_Raman spectra taken at different spots for dried samples: VHP, MW4, MW5 and MW18 (isobutanol preparation). Symbols: *=$VOHPO_4 \cdot 0.5H_2O$.

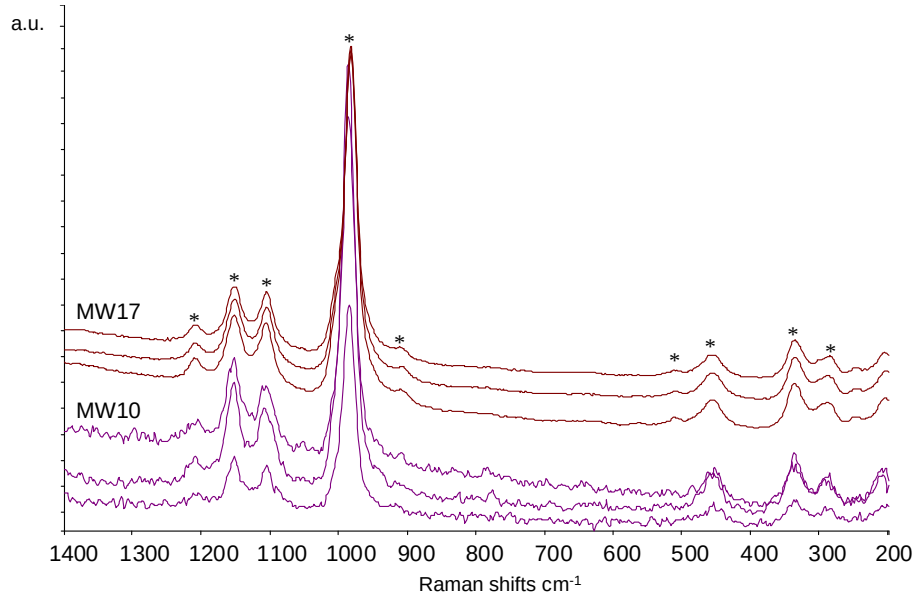

Fig. 5.3_Raman spectra taken at different spots for dried samples: MW10 and MW17 (ethanol preparation). Symbols: *=$VOHPO_4 \cdot 0.5H_2O$.

However, in the case of MW4 and MW5 also bands attributable to V_2O_5 were found at some surface spots (at 990, 696, 523, 478, 401, 300, 280 cm^{-1}) (fig.5.4). The presence of this phase, which however was present in minor amount only, was sometimes observed also with standard preparations, due to an incomplete V_2O_5 conversion during synthesis.

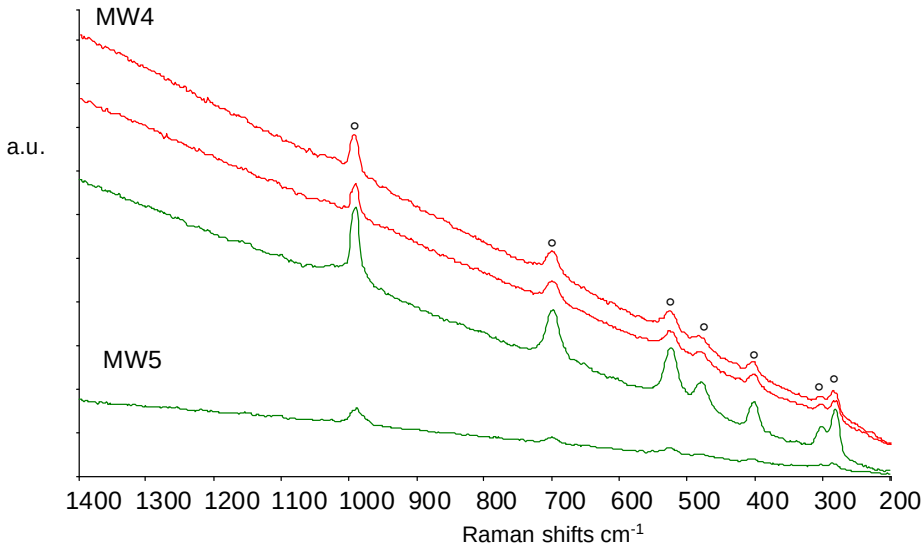

Fig. 5.4_Raman spectra taken at different spots for dried samples: MW4 and MW5. Symbols: °=V_2O_5.

In regard to the XRD patterns, some peculiar aspects were observed: samples VHP and MW4 showed quite similar patterns, with all reflections attributable to $VOHPO_4 \cdot 0.5H_2O$ (JCPDS 00-037-0269) (fig. 5.5); in contrast, samples MW5 and MW10, although displaying the strongest reflections for the same compound (at 2θ=15,6-30,5°-37,5°), appeared to be less crystalline (fig.5.5).

In particular, these latter samples all showed an interesting feature: the presence of a broad reflection at low diffraction angle (centered at 2θ= 11,8°), relative to a higher inter-layer distance (along the c axis). This reflection was quite unusual, since it was observed only when a mixture of

various organic solvents was used for the synthesis [20]. The attribution was confirmed by UV-vis DR analysis: in fact, it could not be associated to any $VOPO_4 \cdot 2H_2O$ phase ($2\theta = 12°$), because the UV-vis spectra of MW5 and MW10 precursors (fig.5.7) did not show any band attributable to a V^{5+} species. Moreover, it has to be noted that patterns like that shown by the MW10 sample, with only a few intense reflections, all the other reflections being much weaker and broader (moreover, for most of them not even corresponding to the expected ones for the precursor), have to be attributed to lamellar-like (anisotropic) crystallite morphologies, in which the crystalline order is maintained only along some specific directions.

In regard to the differences observed between MW4 and MW5 (the preparation of which only differed in the fact that the heating of MW4 was carried out during two separate steps), characterization data reported below will demonstrate that MW5 likely contained a much greater fraction of retained organic compounds than MW4. Indeed, the amount of organic compound can affect the crystallinity of the precursor [20].

Finally, regarding doped MW samples (MW17 and MW18), two different XRD patterns were registered (fig. 5.6): for the sample synthesized in pure isobutanol (MW18), the characteristic pattern of $VOHPO_4 \cdot 0.5H_2O$ was observed, with very intense reflections conducive to a highly crystalline compound. In contrast, the sample prepared with pure ethanol (MW17), and with the same Nb source as for MW18, showed a pattern similar to that of the MW10 samples, indicating the formation of a compound with anisotropic crystallinity.

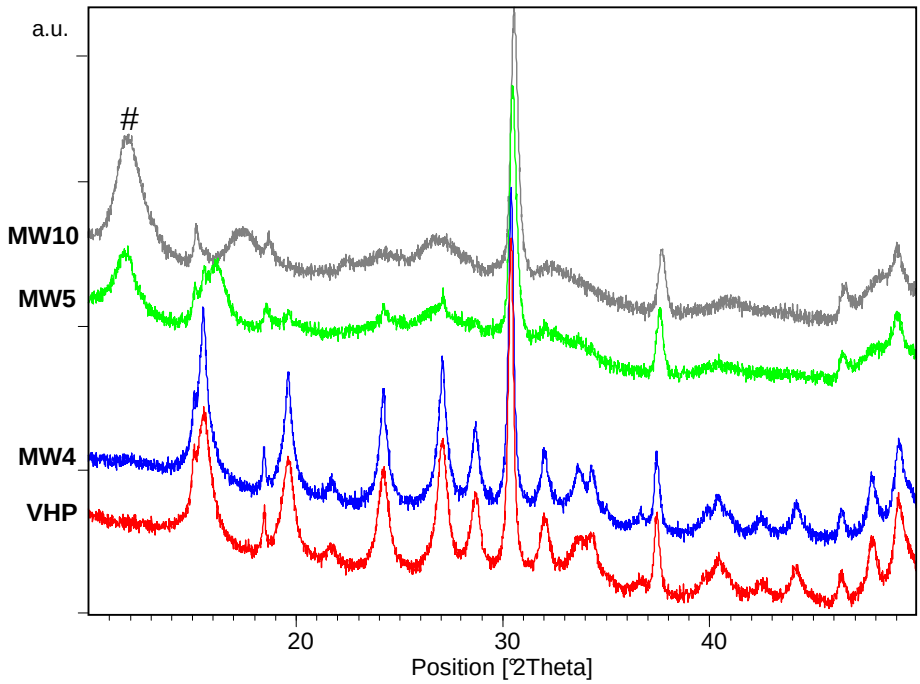

Fig. 5.5_XRD patterns of VHP, MW4, MW5 and MW10 dried samples. Symbols: # = reflection sometimes observed for samples having intercalation of glycols [20].

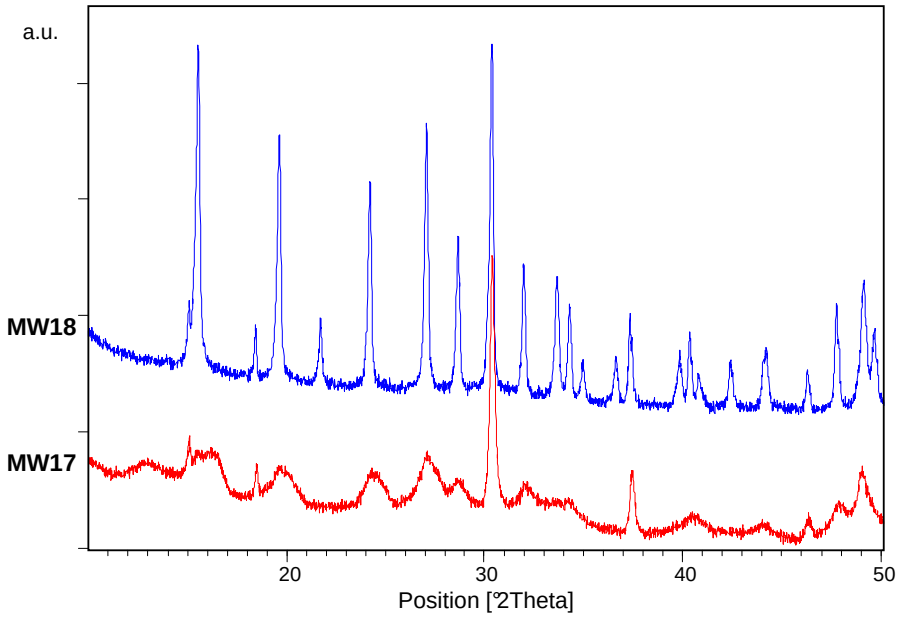

Fig. 5.6_XRD patterns of MW17 and MW18 dried samples.

The UV-vis DR spectra are shown in fig. 5.7: characteristic bands relative to V^{4+} species (at 265, 640, 830 nm) were observed [21]; the presence of any V^{5+} species can be excluded, because the corresponding bands (at 320, 420 nm for $VOPO_4$) were not visible (Chapter 4).

In particular, for samples MW17-MW18 a contribution at high energy (<300 nm) was present: in the literature bands at 240-290 nm are related to V^{5+} species in Td coordination [22-24], but these species were probably not present in our samples; on the other hand, the unknown band could be attributed to V^{5+} in octahedral coordination, as in V_2O_5 [22], but since the other bands attributable to this compound were absent, we could disregard also this possibility. Another possibility can be considered, that the band at about 250 nm can be attributed to a Nb/P/O species; in fact, hydrated $NbOPO_4$ possesses a characteristic single CT band at 257 nm [25].

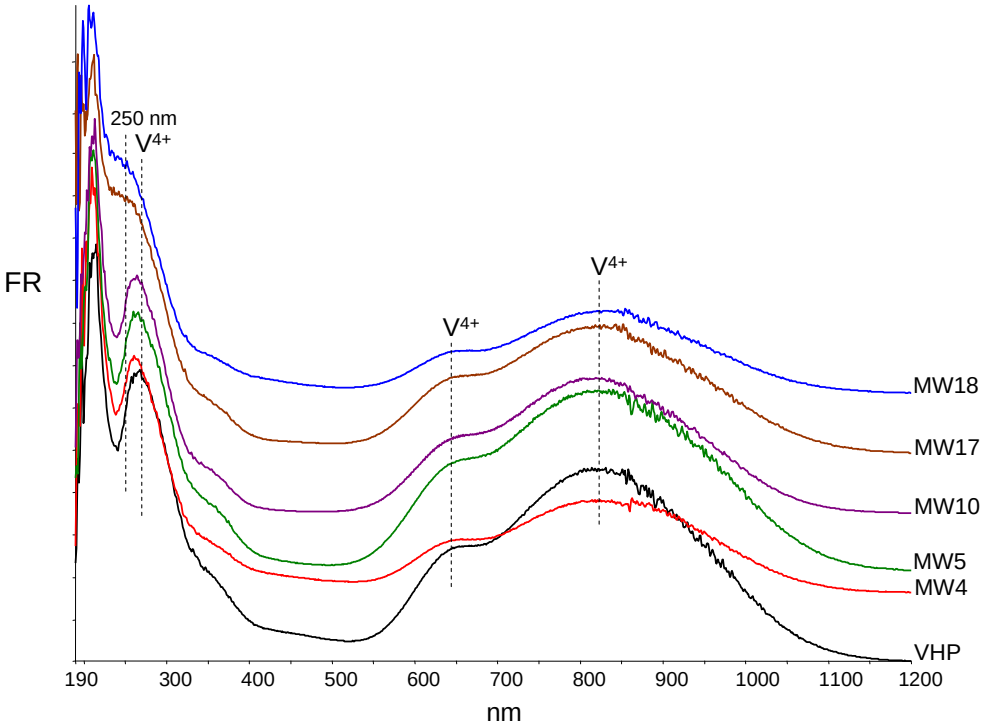

Fig. 5.7_UV-vis DR spectra for VHP, MW4, MW5, MW10, MW17 and MW18 dried samples.

SEM images were taken for each dried sample (figs. 5.8-5.13). We again confirmed the similar features of MW4 and VHP samples; in fact, both showed the typical rosette-like morphology, that is the common aspect of $VOHPO_4 \cdot 0.5H_2O$ prepared by means of the standard procedure (fig.5.8-5.9).

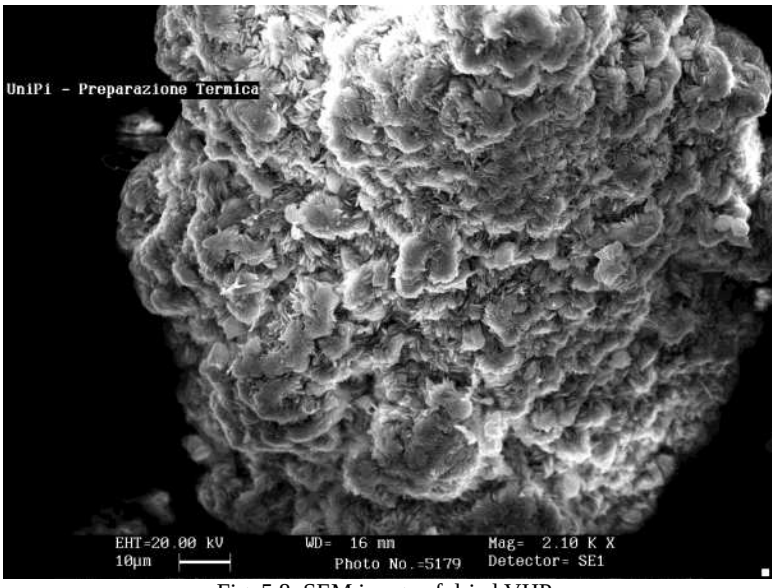

Fig. 5.8_SEM image of dried VHP.

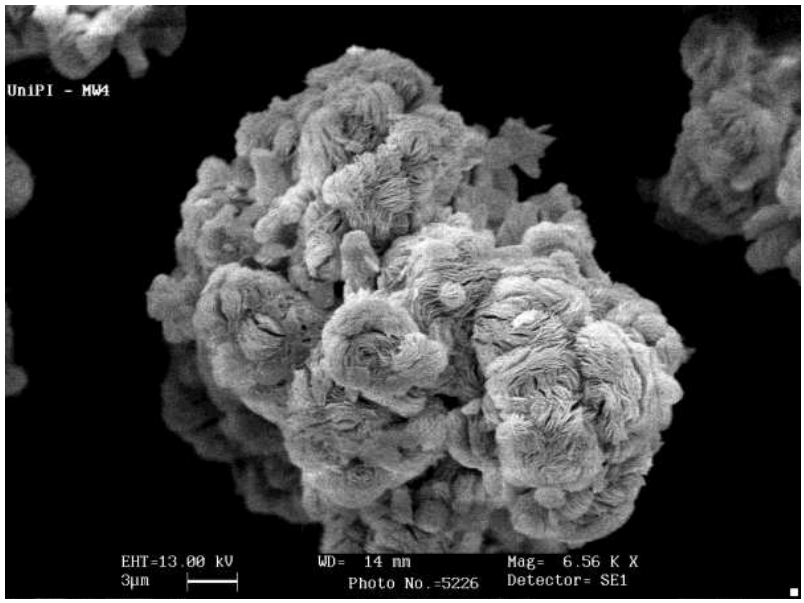

Fig. 5.9_SEM image of dried MW4.

Conversely, samples MW5 and MW10 showed a similar more “open” and unusual sponge-like morphology, with an high degree of emptiness (figs. 5.10-5.11).

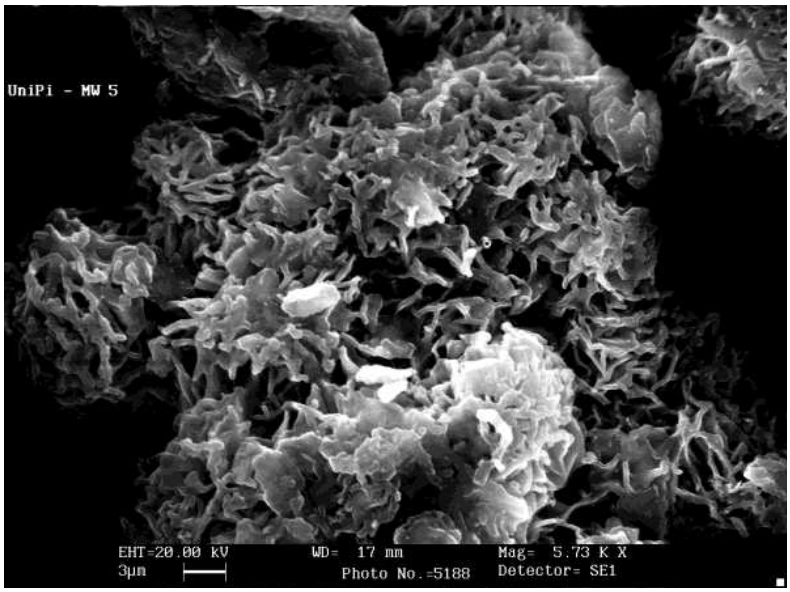

Fig. 5.10_SEM image of dried MW5.

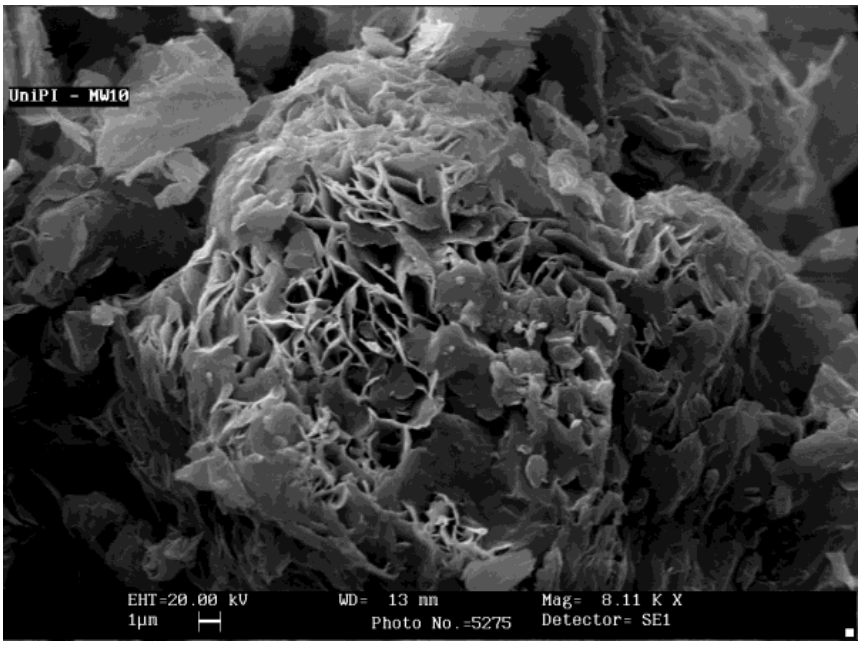

Fig. 5.11_SEM image of dried MW10.

MW17 showed a rosette-like morphology similar to that of MW4 and VHP samples (fig. 5.12); also sample MW18 showed a rosette-like morphology (fig. 5.13_left), although some particles had a different aspect, similar to a coral-like structure (fig. 5.13_right). It was concluded that sample MW18 possessed an heterogeneous morphology, which may be related to an inaccurate dispersion of Nb.

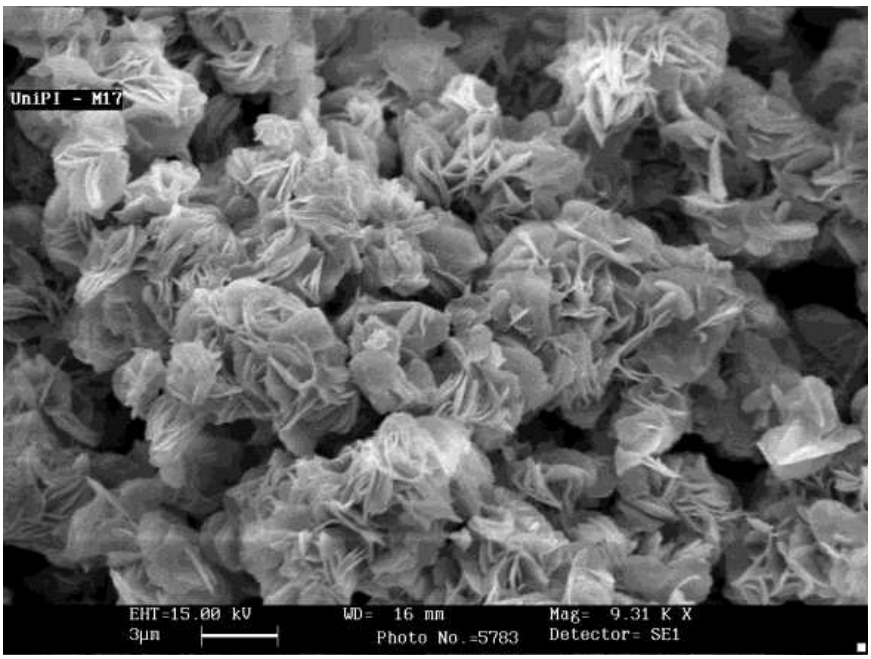

Fig. 5.12_SEM image of dried MW17.

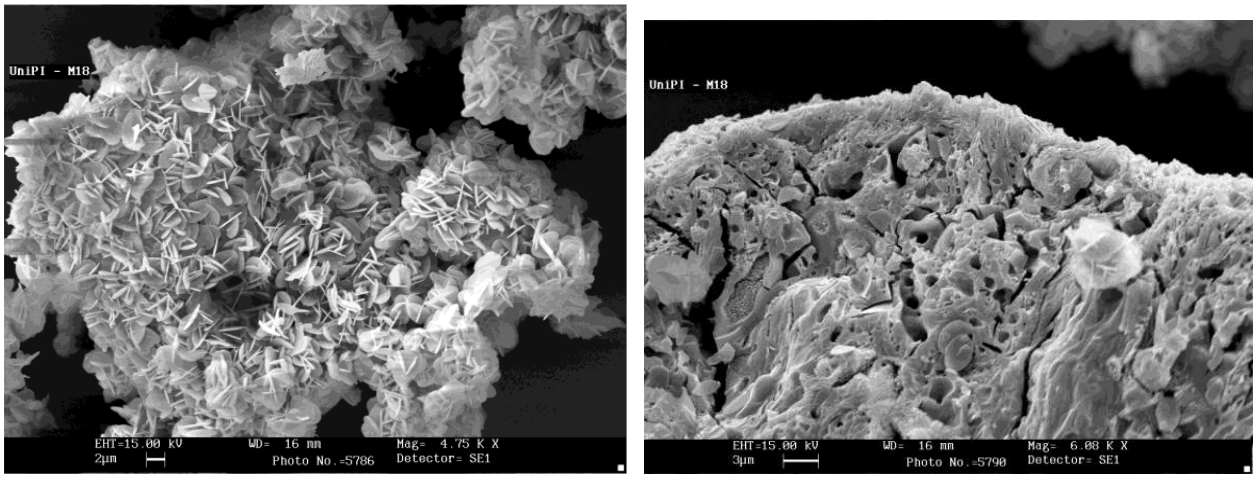

Fig. 5.13_SEM images of dried MW18: left) rosette morphology; right) "coral" morphology.

These experiments clearly indicate that it is possible to obtain the catalyst precursor, $VOHPO_4 \cdot 0.5H_2O$, by means of microwave heating; interestingly, by changing the solvent it was possible to obtain samples with distinctly different characteristics.

5.2.3 Characterization of calcined microwave samples (MW) and thermal sample (VHP)

The calcined samples, also referred to as "fresh" catalysts, were characterized by Raman, XRD and UV-vis DR analyses.

For clarity of discussion, because many spectra were recorded at different spots of the particles, the Raman spectra are shown in separate figures for each catalyst (figs. 5.14-5.18).

The VPP was always present, as shown by the typical bands (1184, 1133, 920 cm^{-1}). Some oxidized compounds were also present: $VOPO_4 \cdot 2H_2O$ (1033, 986 cm^{-1}), α_I-$VOPO_4$ (1028, 580, 535 cm^{-1}), α_{II}-$VOPO_4$ (1090, 990 cm^{-1}) and δ-$VOPO_4$ (1084, 1015, 592 cm^{-1}). Interestingly, this latter compound was observed solely in doped samples (MW17, MW18), which indicates an important role of Nb in boosting the generation of this specific oxidized phase. Furthermore, it must be noted that sample MW18 was the most homogeneous, showing only bands of δ-$VOPO_4$ and VPP compounds (fig. 5.19).

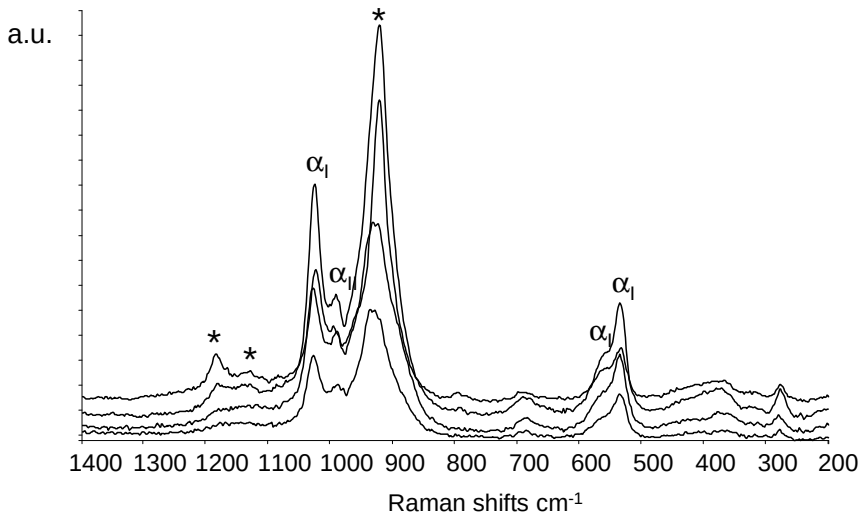

Fig. 5.14_Raman spectra taken at different spots for calcined VHP. Symbols: *=$(VO)_2P_2O_7$; α_I= α_I–$VOPO_4$; α_{II}= α_{II}–$VOPO_4$.

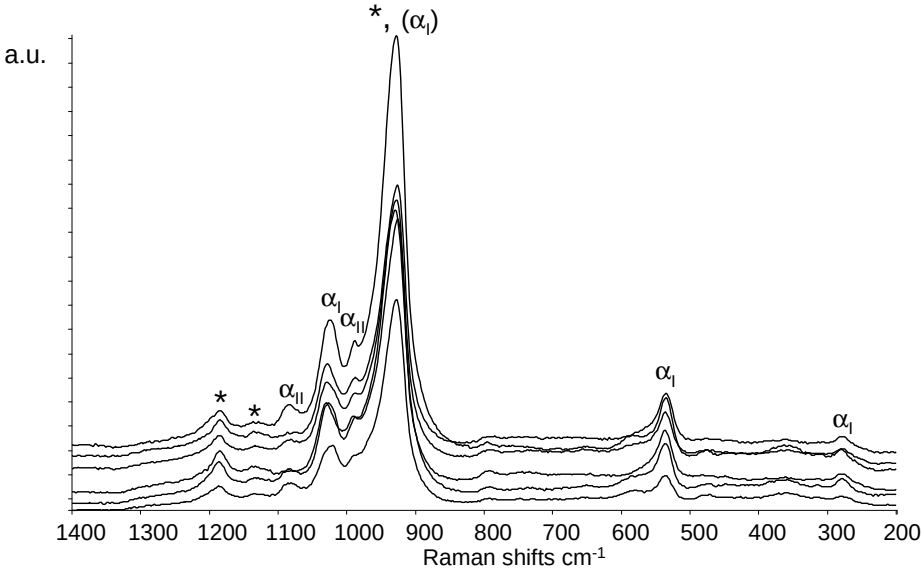

Fig. 5.15_Raman spectra taken at different spots for calcined MW4. Symbols: *=$(VO)_2P_2O_7$; α_I= α_I–$VOPO_4$; α_{II}= α_{II}–$VOPO_4$.

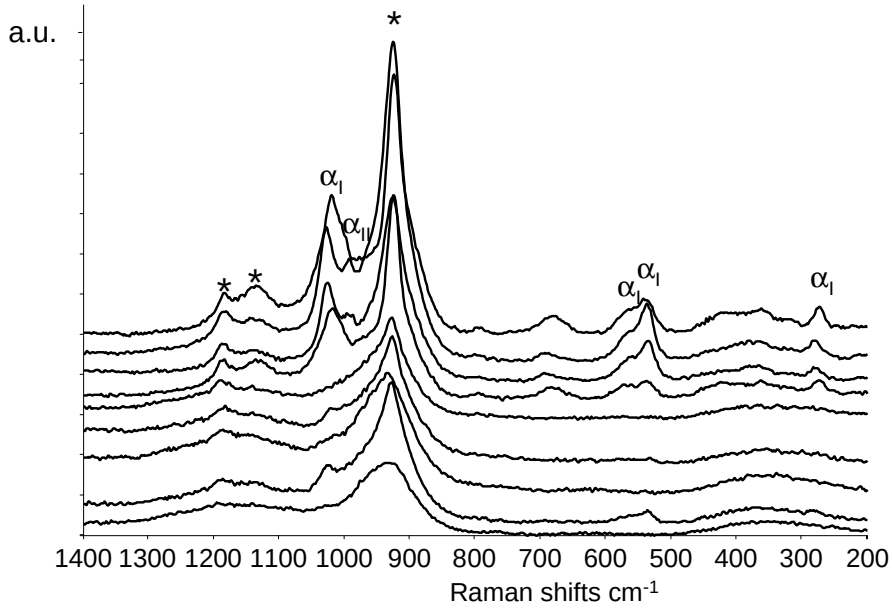

Fig. 5.16_Raman spectra taken at different spots for calcined MW5. Symbols: *=$(VO)_2P_2O_7$; α_I= α_I–$VOPO_4$; α_{II}= α_{II}–$VOPO_4$.

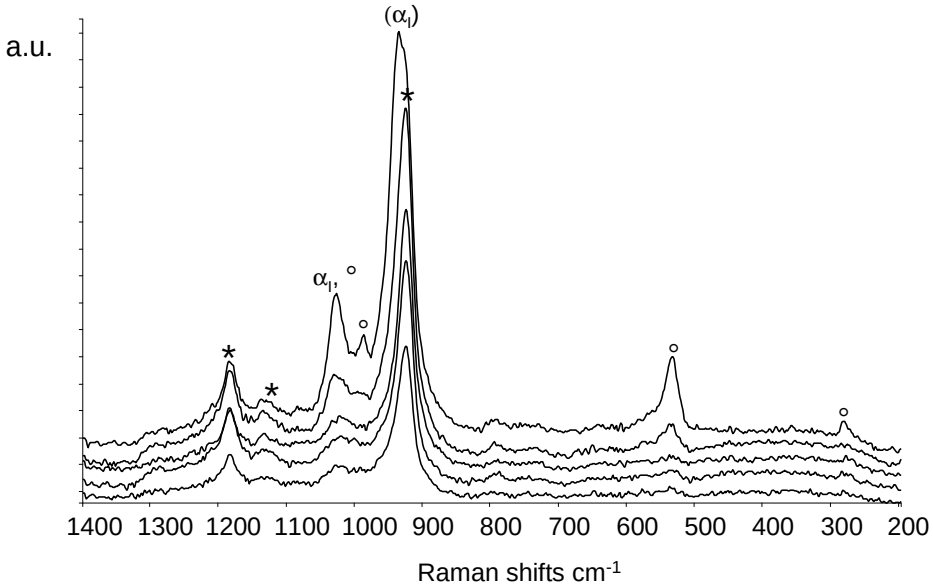

Fig. 5.17_Raman spectra taken at different spots for calcined MW10. Symbols: *=$(VO)_2P_2O_7$; α_I= α_I–$VOPO_4$; °= $VOPO_4{\cdot}2H_2O$.

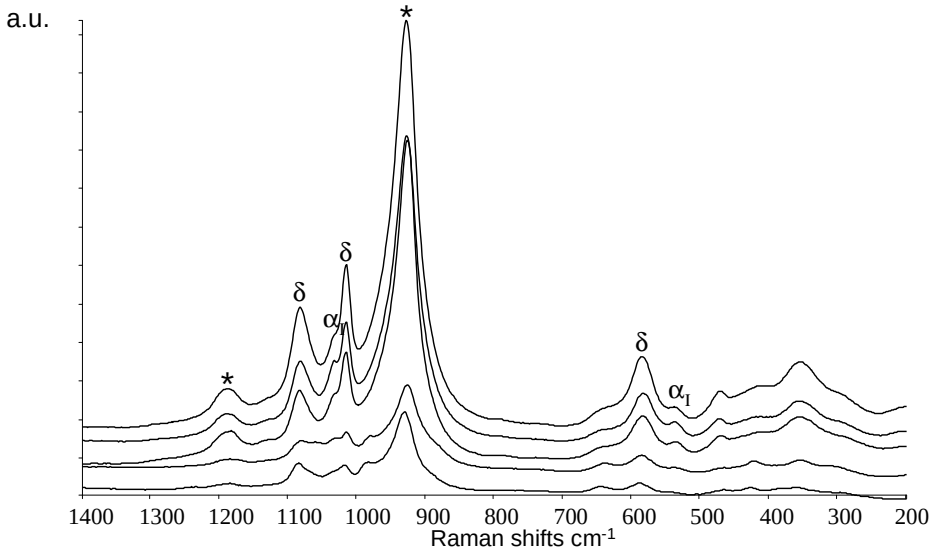

Fig. 5.18_Raman spectra taken at different spots for calcined MW17. Symbols: *=$(VO)_2P_2O_7$; α_I= α_I–$VOPO_4$; δ= δ –$VOPO_4$.

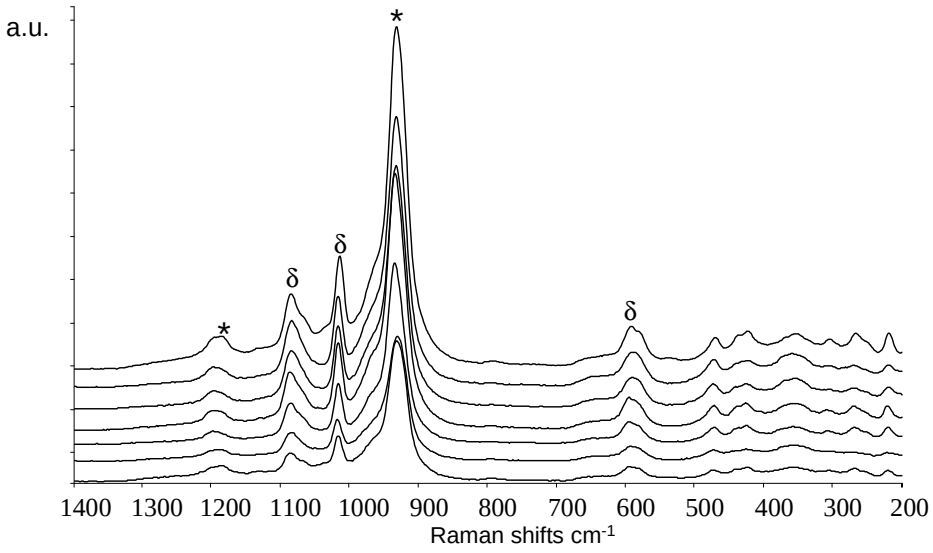

Fig. 5.19_Raman spectra taken at different spots for calcined MW18. Symbols: *=$(VO)_2P_2O_7$; δ= δ –$VOPO_4$.

Figure 5.20 reports the XRD patterns for VHP, MW4, MW5 and MW10 calcined samples. Sample VHP, apparently containing a more crystalline VPP as compared to the other samples, possessed strong reflections at 2θ=18,7° and 2θ=21,4°, relative to ω-$VOPO_4$ (JCPDS 00-037-0809). The other samples appeared to be less oxidized, and to consist of a less crystalline VPP.

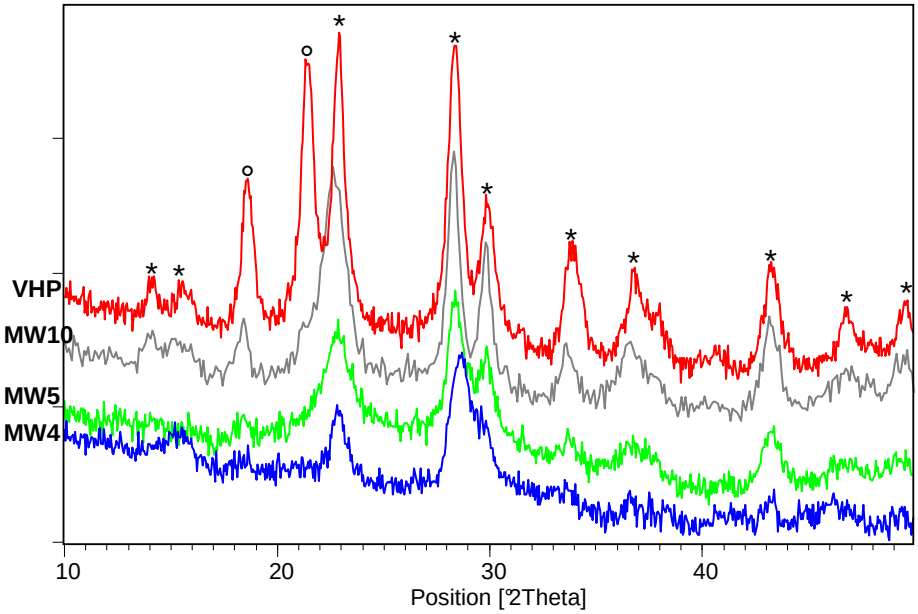

Fig. 5.20_XRD pattern of VHP, MW4, MW5 and MW10 calcined samples. Symbols: *=$(VO)_2P_2O_7$; ° =ω-$VOPO_4$.

Catalysts MW17 and MW18 (fig. 5.21) resulted to be mainly constituted of VPP. In particular, MW17 also showed the characteristic reflections attributable to ω-$VOPO_4$ and $VOPO_4 \cdot 2H_2O$ (strongest peak at 2θ=12°, JCPDS 00-036-1472), while MW18 showed the presence of ω-$VOPO_4$ and δ-$VOPO_4$ (2θ=19,6° - 22° - 24,2°, JCPDS 00-047-0951).

These results confirmed Raman analyses, and also indicated that, probably, Nb-doped samples were more oxidized than the other catalysts.

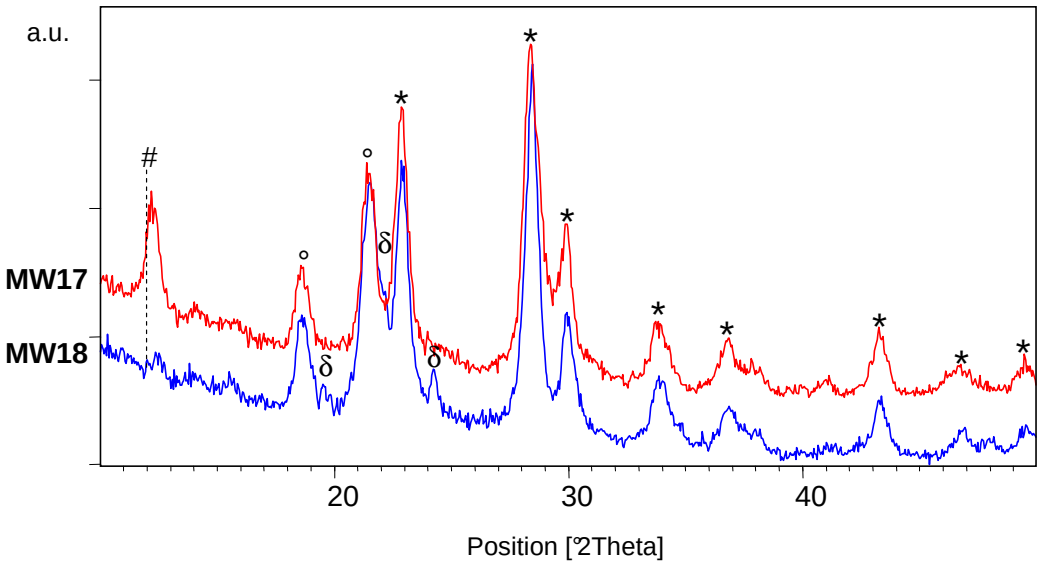

Fig. 5.21_XRD pattern of MW17 and MW18 calcined samples. Symbols: *=$(VO)_2P_2O_7$; °= ω-$VOPO_4$; δ= δ–$VOPO_4$; #= $VOPO_4 \cdot 2H_2O$.

A more clear picture regarding the degree of oxidation of fresh catalysts was drawn by means of UV-vis DR analyses (fig. 5.22): bands relative to V^{4+} species in VPP compound (at 300, 650, 850 nm) were present for all samples. Furthermore, with the exception of sample MW5, bands belonging to V^{5+} species in $VOPO_4$ compounds (at 310 and 410 nm) were also visible, in accordance with XRD and Raman analyses. It must be noted that sample MW5 resulted to be quite reduced; for example, the band at about 550 nm can be attributed to a V^{3+} species [21].

The high degree of reduction of MW5 is probably due to an high amount of organic molecules retained between layers of the precursor structure. These species are removed by combustion, during the first step of the thermal treatment; however, when these molecule are strongly retained, the removal may also occur during the subsequent step, carried out in flowing nitrogen and at higher temperature (550°C): this involves a redox reaction between the organic compounds and the $VOPO_4$ species, the latter having been generated during the first step of thermal treatment in air, at 300°C. For this reason, we can hypothesize an high organic content for the MW5 sample, and this is probably also a reason for its surprising morphology.

Besides MW5, the least oxidized samples were MW10, MW18 and MW17; moreover, MW18 also possessed a unique feature: a band centered at about 250 nm, which was observed neither with the other Nb-doped sample (MW17), nor with the other undoped samples. This signal was already observed in spectra of dried MW17-MW18 samples (par. 5.2.2), and was tentatively attributed to a Nb^{5+} species. We can conclude that in the case of calcined sample MW18, the Nb species still was present at the surface of the VPP (either as a Nb/P/O compound or as a dispersed Nb^{5+} species), whereas in the case of MW17 the thermal treatment probably led to a more preferred migration of Nb into the bulk.

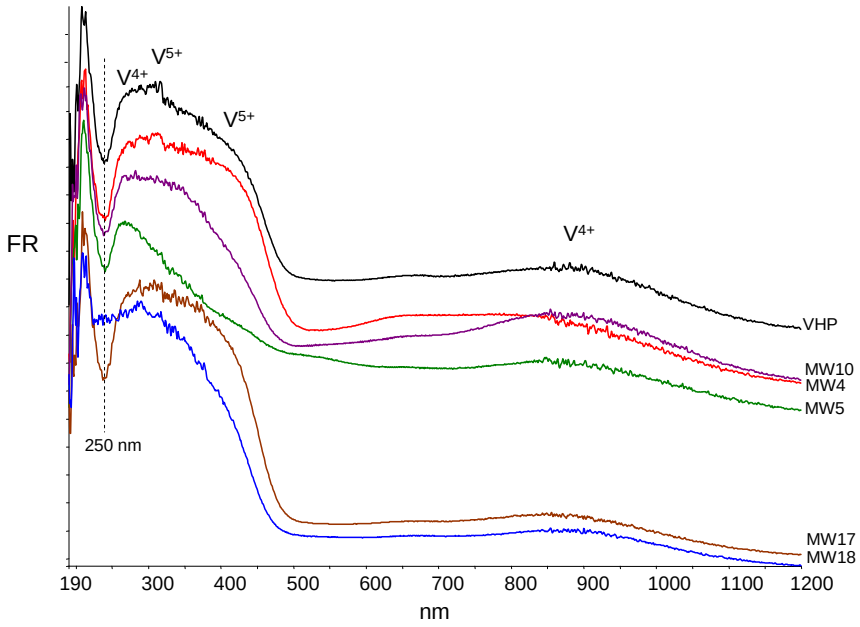

Fig. 5.22_UV-vis spectra for VHP, MW4, MW5, MW10, MW17 and MW18 calcined samples.

5.2.4 Reactivity of VPP catalysts obtained from MW precursors

The reactivity tests were carried out with calcined samples (VHP, MW4, MW5, MW10, MW17, MW18), which were previously equilibrated by letting the catalysts at 440°C in the reactive mixture for a period of about 100 hours. The reaction conditions were the following: 1,7% mol. of n-butane, 17% mol. of O_2; W/F=1.33 g·s·ml^{-1}.

For samples VHP, MW4, MW5 and MW10, the n-butane conversion is plotted in fig. 5.23, while figs. 5.24-5.25 report the MA and CO + CO_2 (CO_x) selectivities, respectively, all plotted in function of the reaction temperature (340°C-440°C).

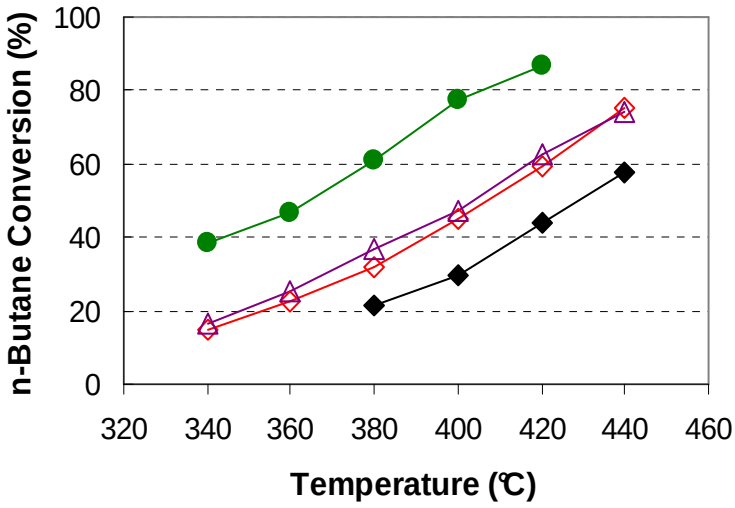

Fig. 5.23_ Conversion of n-butane for VHP (♦), MW4 (◊), MW5 (●) and MW10 (△) samples. Conditions: 1,7% n-butane, 17% O_2; W/F=1.33 g·s·ml^{-1}.

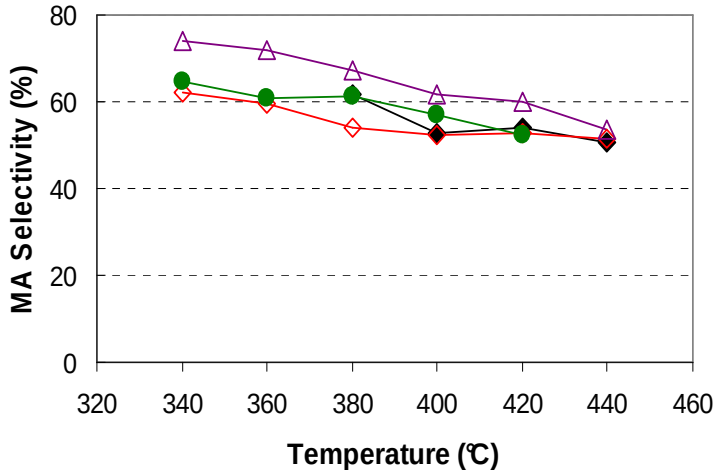

Fig. 5.24_ Maleic anhydride (MA) selectivity for VHP (♦), MW4 (◊), MW5 (●) and MW10 (△) samples. Conditions: 1,7% n-butane, 17% O_2; W/F=1.33 g·s·ml^{-1}.

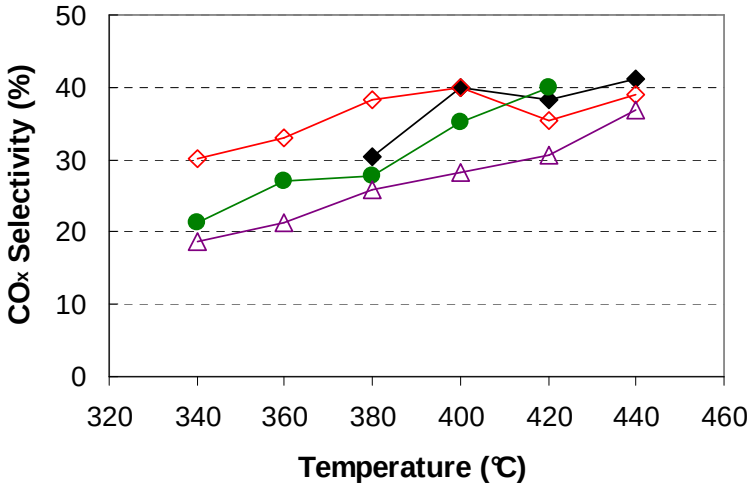

Fig. 5.25_ CO and CO_2 (CO_x) selectivities for VHP (♦), MW4 (◊), MW5 (●) and MW10 (△) samples. Conditions: 1,7% n-butane, 17% O_2; W/F=1.33 g·s·ml^{-1}.

The rank of catalytic activities were in agreement with the surface areas of samples, measured on used catalysts at the end of catalytic experiments (Table 5.2). Catalyst MW5, which showed the highest n-butane conversion in the entire range of temperatures, was the sample also showing the greater value of surface area. Since the final surface area of VPP samples was a function of the morphology of the catalyst (the latter being affected by the morphology of the corresponding precursor), these results demonstrate that catalysts with the sponge-like morphology for corresponding precursors (MW5 and MW10) were those finally displaying the greater surface area. On the other hand, the very high activity of MW5 cannot be attributed to the higher surface area only; in literature, it is reported that strongly reduced samples, containing small amounts of V^{3+} because of the V overeduction occurred during the thermal treatment, were those showing an unexpected high activity [21 and refs therein]. This was attributed to the generation of vacancies in the VPP, which acted as strong Lewis sites for hydrocarbon activation.

Catalyst MW10, synthesized with ethanol, displayed a peculiar and unexpected behavior: MA selectivity was clearly higher than that of the other samples, in the entire range of temperatures tested. This peculiar behavior may result from the combination of various factors; as a matter of fact, this sample was that one combining a good crystallinity (as inferred from XRD pattern) with a relatively low amount of oxidized V^{5+} phase, as evident from both Raman and UV-Vis DR spectrum. Also sample MW5 showed a good selectivity to MA, if plotted against the n-butane conversion (see fig. 5.29). Instead, samples MW4 and VHP were more oxidized than MW5 and MW10.

Moreover, MA selectivity was improved over the entire temperature range investigated; indeed, it was a peculiarity of all the MW catalysts to maintain relatively high and similar MA selectivity at both low and high temperature.

For samples VHP, MW17 and MW18, the n-butane conversion is plotted in fig. 5.26, while figs 5.27-5.28 report the MA and CO_x selectivity, all plotted in function of the reaction temperature (340°C-440°C).

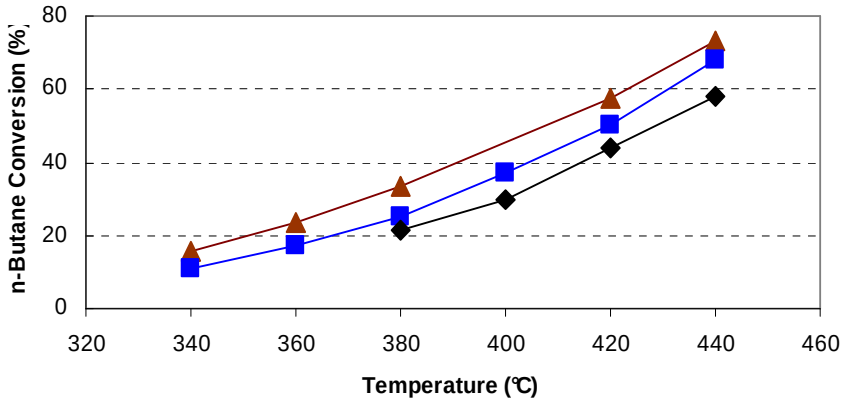

Fig. 5.26_ Conversion of n-butane for VHP (♦), MW17 (▲) and MW18 (■) samples. Conditions: 1,7% n-butane, 17% O_2; W/F=1.33 g·s·ml^{-1}.

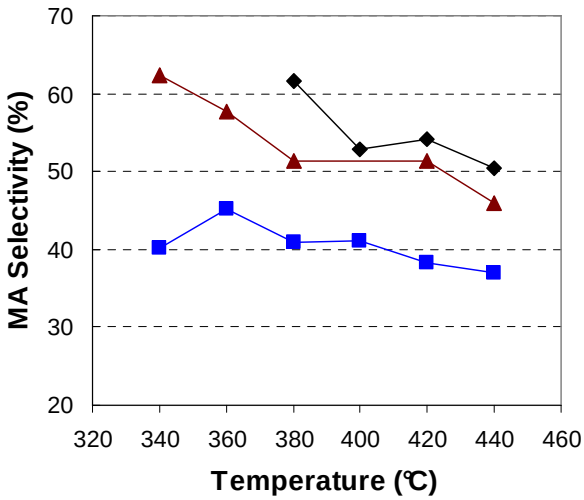

Fig. 5.27_ Maleic anhydride (MA) selectivity for VHP (♦), MW17 (▲) and MW18 (■) samples. Conditions: 1,7% n-butane, 17% O_2; W/F=1.33 g·s·ml^{-1}.

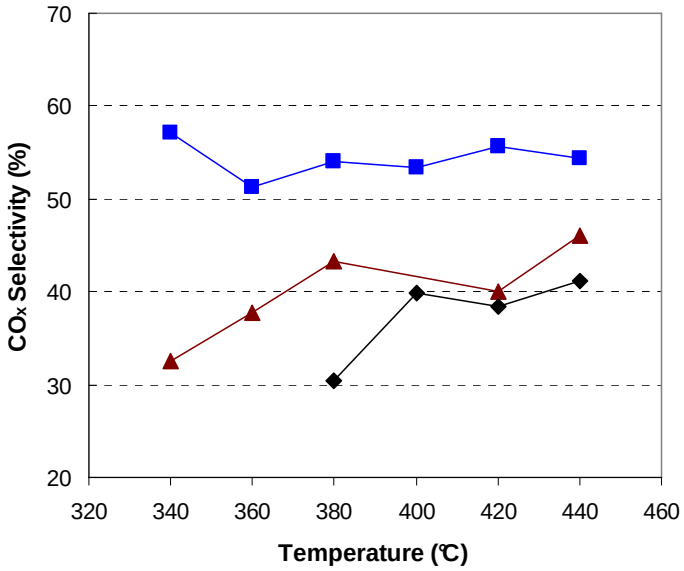

Fig. 5.28_ CO and CO_2 (CO_x) selectivities for VHP (♦), MW17 (▲) and MW18 (■) samples. Conditions: 1,7% n-butane, 17% O_2; W/F=1.33 g·s·ml^{-1}.

The presence of Nb positively affected n-butane conversion: it is worth noting that this was not simply due to the specific surface area (Table 5.2), because very similar values were obtained for MW17, MW18 and VHP used catalysts. On the other hand, the activity of MW17 (the most active Nb-doped sample) was not as much high as that of MW5 (fig. 5.26). Catalyst MW18 showed a lower MA selectivity than both MW17 and VHP, whereas MW17 showed a small selectivity improvement (probably more important at low temperatures), with respect to the reference catalyst (VHP).

We conclude that the promoter effect of Nb on catalytic behaviour may be greatly affected by its final degree of dispersion and incorporation in the structure; indeed, Nb may even have a negative effect on selectivity. In overall, other parameters, such as the amount of organic compound which is retained in the precursor - a parameter which greatly affects the morphology of the precursor and which is enormously affected by the method of preparation used for catalyst precursor – may have much more remarkable effect on catalytic behaviour than the presence of Nb. In this regard, the method of preparation involving the use of microwaves is a powerful tool for the control of the main chemical-physical properties of the precursor.

Figure 5.29, plotting the selectivity to MA in function of n-butane conversion, permits a better overview of the catalytic results.

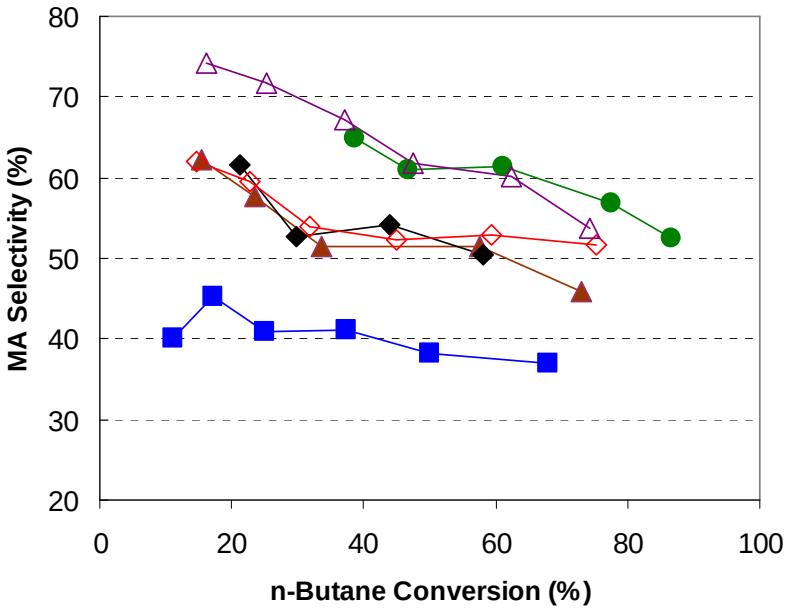

Fig. 5.29_ MA selectivity plotted as a function of n-butane conversion, for catalysts VHP (♦), MW4 (◊), MW5 (●), MW10 (△) MW17 (▲) and MW18 (■) samples. Conditions: 1,7% n-butane, 17% O_2; W/F=1.33 g·s·ml^{-1}.

Figure 5.29 allows dividing catalysts into 3 categories: a) catalysts showing improved selectivity as compared to the standard catalyst VHP (MW5, MW10); b) catalysts with performance similar to that of the standard preparation (MW4, MW17); c) catalysts with worse performance (MW18). The main peculiarity of catalysts belonging to class 1 is the presence of an "open" (sponge-like) morphology for the precursor, and moreover these catalysts were less oxidized than the other samples (see figs. 5.20 and 5.22). MW17 (which was prepared using ethanol, like sample MW10), had morphological features which were close to those observed for the best catalysts (MW5 and MW10), but was more oxidized than the latter, as evident from both XRD pattern and UV-Vis DR spectrum.

Used catalyst	Surface area (m^2/g)
VHP	14
MW4	22
MW5	29
MW10	24
MW17	15
MW18	12

Table.5.2_ Values of surface area (BET analyses) for used catalyst: VHP, MW4, MW5, MW10, MW17 and MW18.

5.2.5 Characterization of used VPP catalysts

XRD patterns of used catalysts are shown in figs. 5.30-5.31; after reactivity tests, all samples showed the presence of the crystalline VPP phase as the main component. In particular, the reference catalyst (VHP) still possessed, but in minor amount, traces of oxidized phases: α_I-$VOPO_4$

(reflection at 2θ=25,2°), α_{II}-$VOPO_4$ (reflection at 2θ= 28,8°) and $VOPO_4 \cdot 2H_2O$ (reflection at 2θ=12,4°).

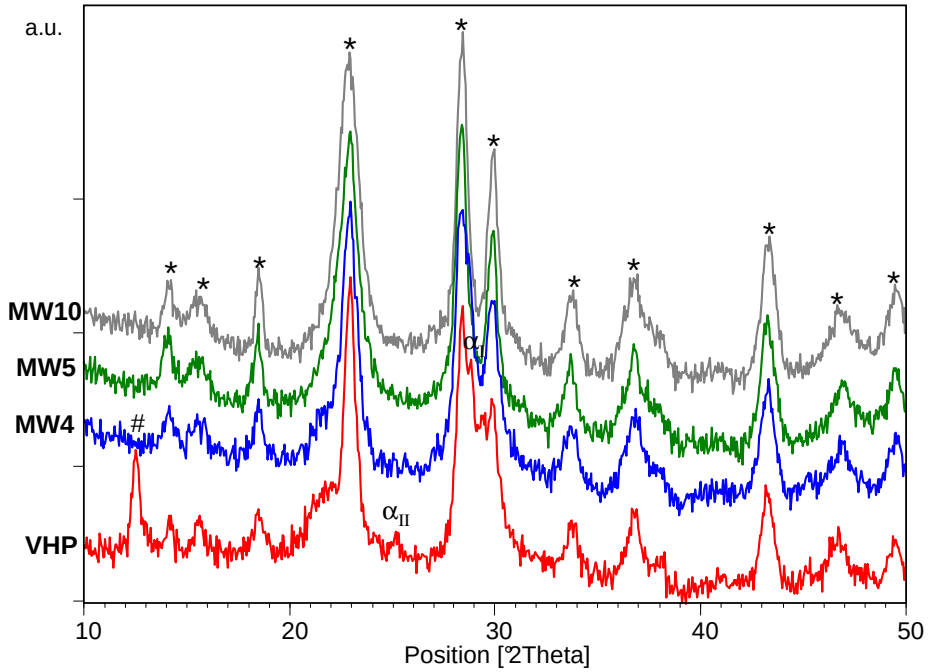

Fig. 5.30_XRD patterns of VHP, MW4, MW5 and MW10 used samples. Symbols: *=$(VO)_2P_2O_7$; α_I=α_I-$VOPO_4$; α_{II}=α_{II}-$VOPO_4$; #= $VOPO_4 \cdot 2H_2O$.

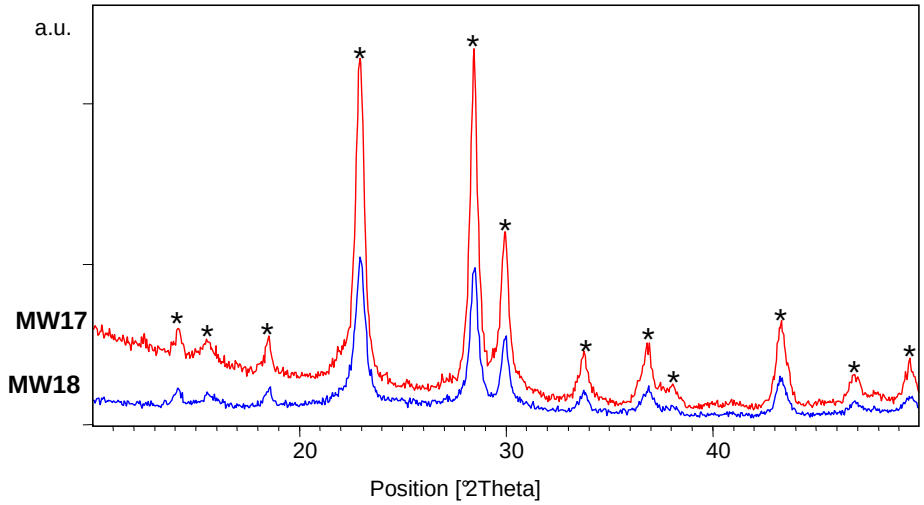

Fig. 5.31_XRD patterns of MW17 and MW18 used samples. Symbols: *=$(VO)_2P_2O_7$.

Raman analyses of used catalysts are shown in figs 5.32-5.37. Catalysts VHP and MW4 showed the presence of VPP and α_I-$VOPO_4$ (fig.5.32-5.33); samples MW5 and MW10 showed the only presence of VPP (fig.5.34-5.35); finally, samples MW17 and MW18 showed the presence of VPP as the major compound, but a peculiar spectrum was also registered by focussing the laser beam on specific spots: this spectrum can be attributed to an amorphous Nb/P/O compound (figs. 5.36-5.38). The presence of an amorphous niobium phosphate is possible since it is known, as reported in the literature, that hydrated Nb/P/O remains amorphous until temperatures as high as 900-1000°C. Furthermore, for catalyst MW17 also Raman bands characteristic of α_{II}-$VOPO_4$ were recorded.

In conclusion, the analysis of spent catalysts confirms the hypothesis put forward in regard to the catalytic behaviour; samples showing the best catalytic behaviour were those containing the lower fraction of V^{5+}, ie, those that after calcination contained the lower amount of the undesired crystalline $VOPO_4$ compounds. In regard to this last consideration, it is worth noting that we confirmed the results obtained with the Nb-doped $VOPO_4$ and VPP catalysts (see previous chapters): the main peculiarity of the VPP showing the best performance is that one of being able to generate in-situ domains of the δ-$VOPO_4$ dispersed at the VPP surface. When, instead, the fresh catalysts already contain relatively large amounts of $VOPO_4$, including the δ phase, the catalytic behaviour is finally not good.

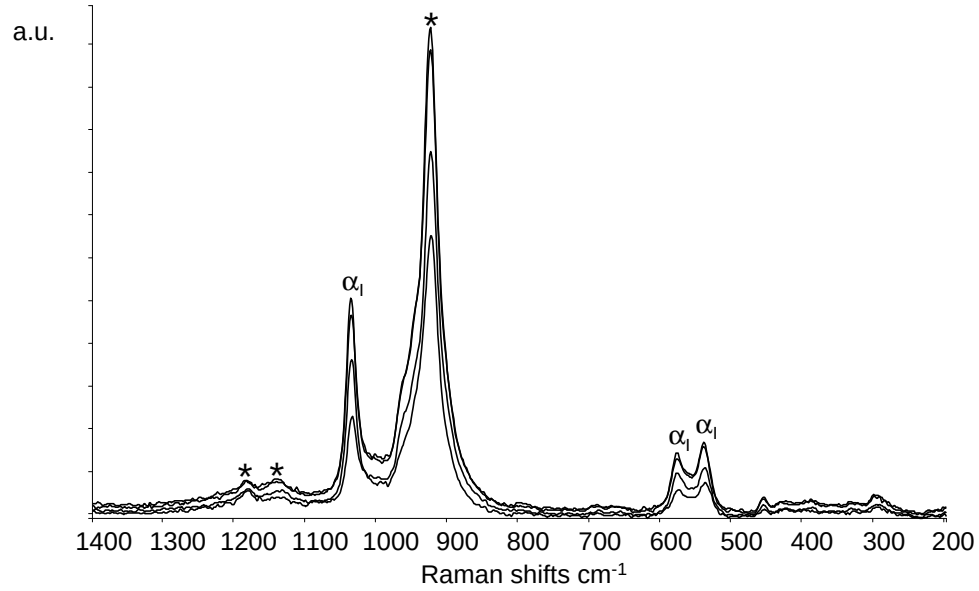

Fig. 5.32_Raman spectra taken at different spots for used VHP. Symbols: *=$(VO)_2P_2O_7$; α_I= α_I–$VOPO_4$.

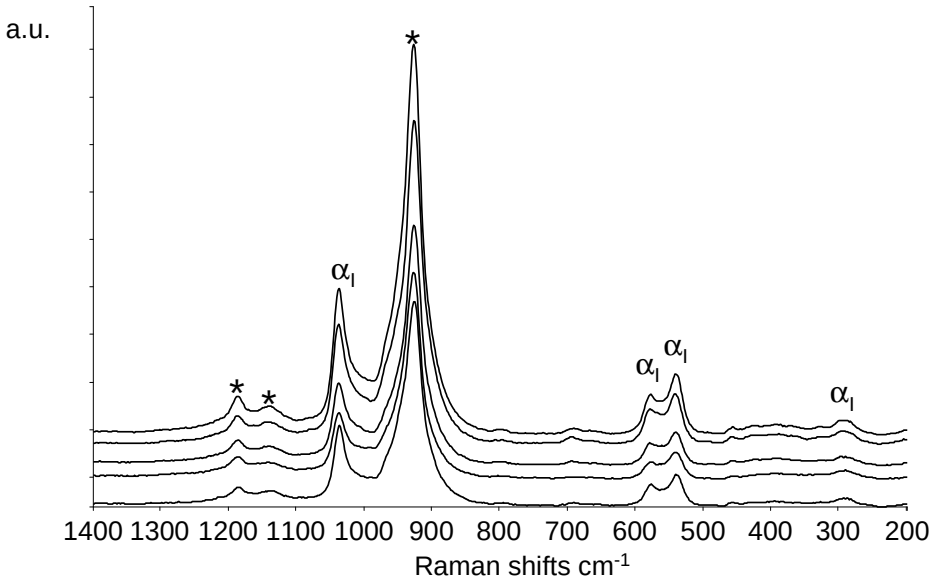

Fig. 5.33_Raman spectra taken at different spots for used MW4. Symbols: *=$(VO)_2P_2O_7$; α_I= α_I–$VOPO_4$.

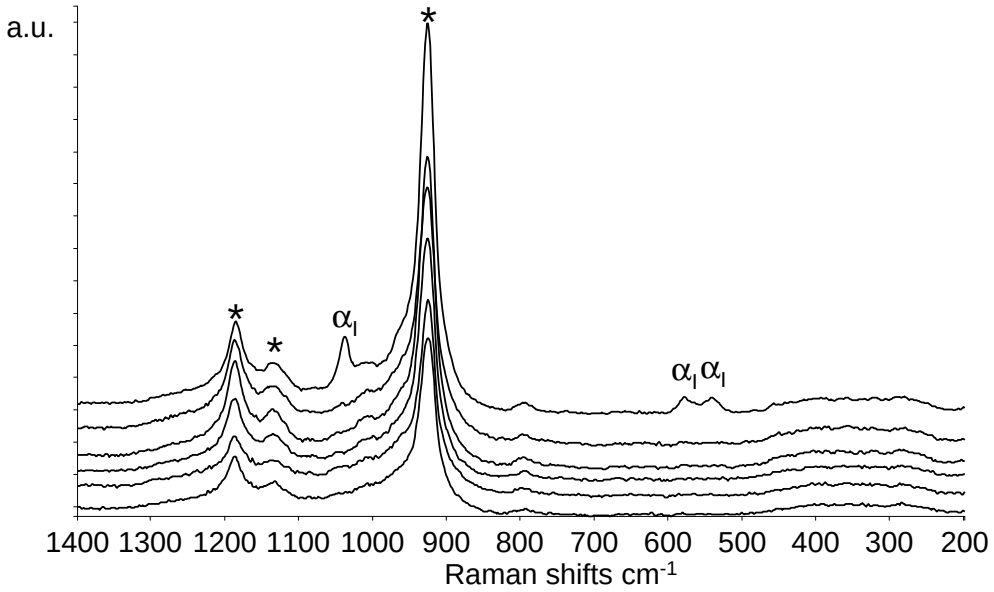

Fig. 5.34_Raman spectra taken at different spots for used MW5. Symbols: *=$(VO)_2P_2O_7$; α_I= α_I–$VOPO_4$.

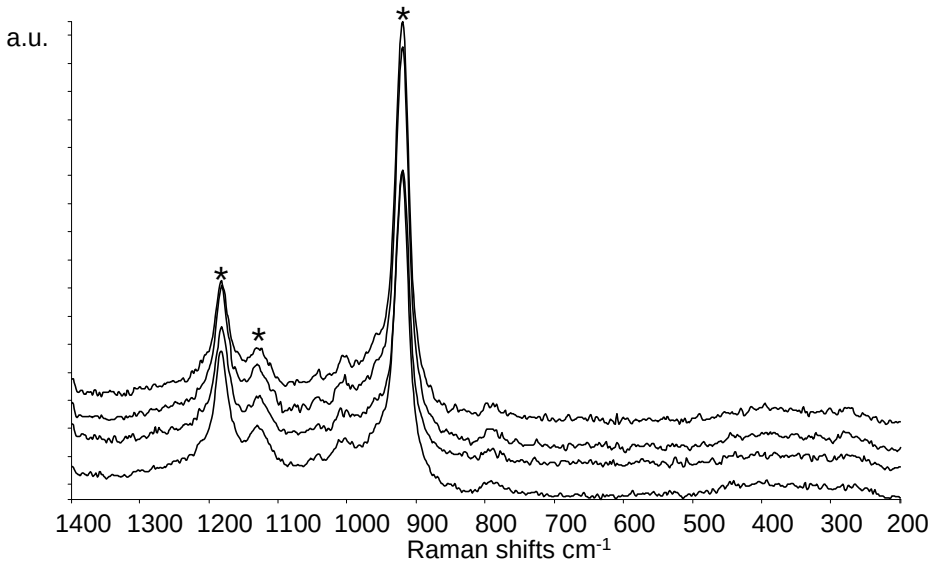

Fig. 5.35_Raman spectra taken at different spots for used MW10. Symbols: *=$(VO)_2P_2O_7$.

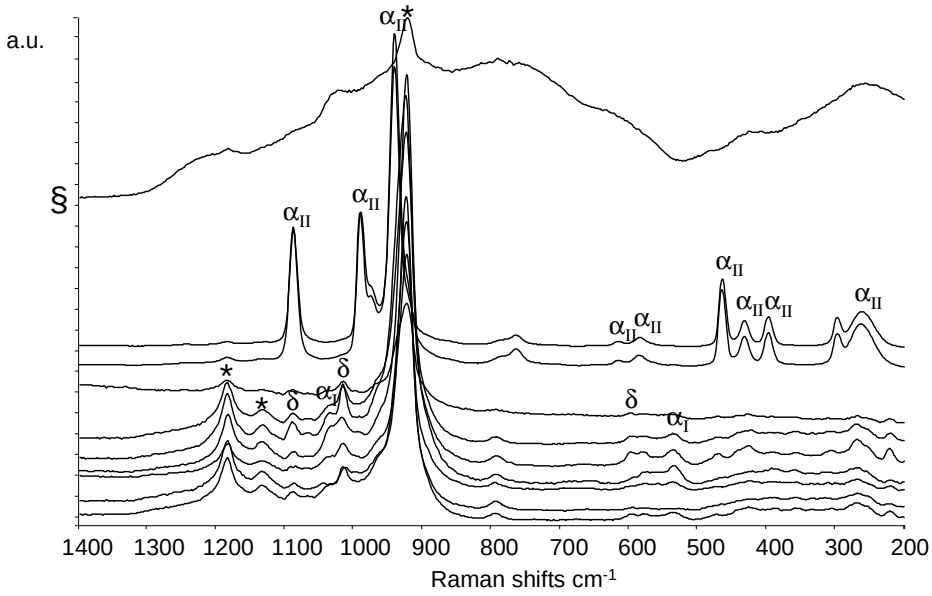

Fig. 5.36_Raman spectra taken at different spots for used MW17. Symbols: *=$(VO)_2P_2O_7$; α_I= α_I–$VOPO_4$; α_{II}= α_{II}–$VOPO_4$; δ= δ–$VOPO_4$; §= amorphous Nb/P/O compound.

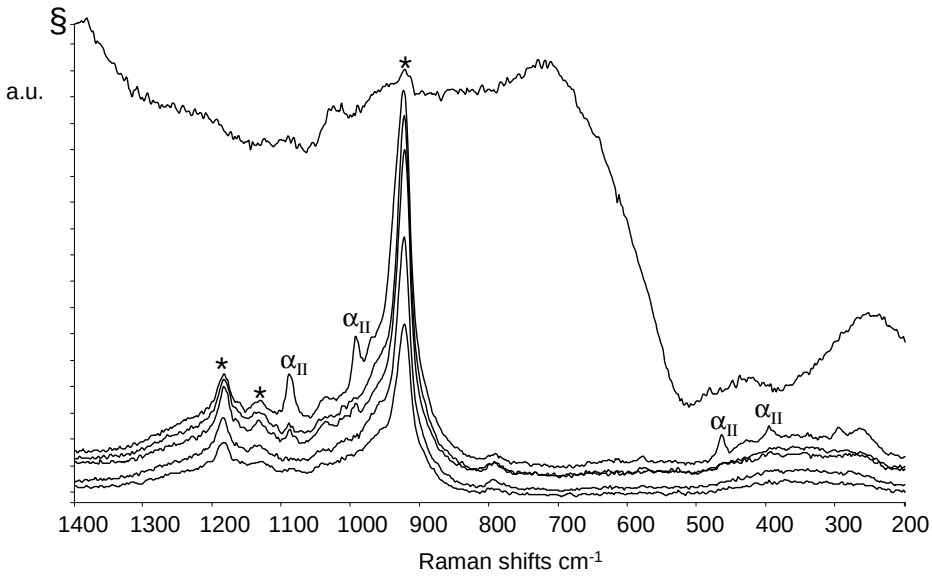

Fig. 5.37_Raman spectra taken at different spots for used MW18. Symbols: *=$(VO)_2P_2O_7$; α_{II}= α_{II}–$VOPO_4$; §= amorphous Nb/P/O compound.

5.3 CONCLUSIONS

Microwave synthesis was a valid method alternative to the standard preparation of vanadyl pyrophosphate catalyst precursor ($VOHPO_4 \cdot 0.5H_2O$), considering the easy methodology and the possibilities offered by microwave instrumentation. The main advantage is that the required synthesis time is much shorter compared to that of the standard preparation; for example, practically total conversion of V_2O_5 was always obtained (which instead is not always the case with the standard procedure). Also with the microwave-based method, as it is for the standard one, one important parameter to control the characteristics of the precursor is the type of alcohol used. One remarkable advantage of the microwave synthesis is that this control is possible even using ethanol (which instead cannot be used with the standard method, because it does not permit the reduction of

V_2O_5); the use of ethanol allows a much easier handling of the synthesis slurry and an easier management of the calcination procedure.

5.4 ACKNOWLEDGMENTS

I would like to gratefully acknowledge Polynt and Pisa University (especially Prof. Anna Raspolli Galletti), for the characterization of samples and for the synthesis of precursors.

5.5 REFERENCES

[1] G. A. Tompsett, W. Curtis Conner, K. Sigfrid Yngvesson, Chem. Phys. Chem. 7 (2006) 296.
[2] K. J. Rao, B. Vaidhyanathan, M. Ganguli, P. A. Ramakrishnan, Chem. Mater., Vol. 11, No. 4 (1999) 882.
[3] L. Benes, K. Melanova, V. Zima, J. Kalousova, J. Votinsky, Inorg. Chem. 36 (1997) 2850.
[4] L. Chatakondu, M. L. H. Green, D. M. P. Mingos, S. M. Reynolds, J. Chem. Soc., Chem. Commun. (1989) 1515.
[5] P. Capkova, D. Janeba, L. Benes, K. Melanova, H. Schenk, J. Mol. Model. 4 (1998) 150.
[6] K. Melanova, L. Benes, V. Zima, J. Kalousova, J. Votinsky, J. Incl. Phenom. Macro. 33 (1999) 391.
[7] L. Benes, K. Melanova, V. Zima, M. Trchova, E. Uhlirova, P. Matejka, Eur. J. Inorg. Chem. (2001) 713.
[8] U. R. Pillai, E. Sahle-Demessie, R. S. Varma, Appl. Catal. A: Gen. 252 (2003) 1.
[9] L. Zeng, H. Jiang, J. Niu, J. Mol. Catal. A: Chem. 232 (2005) 119.
[10] Y. H. Taufiq-Yap, A. A. Rownaghi, M. Z. Hussein, R. Irmawati, Catal. Lett. 119 (2007) 64.
[11] V. V. Sidorchuk, J. Skubiszewska-Zieba, S. V. Khalameida, V. A. Zazhigalov, R. Leboda, Russ. J. Appl. Chem. 81 (8) (2008) 1325.
[12] A. A. Rownaghi, Y. H. Taufiq-Yap, T. W. Jiunn, Catal. Lett. 130 (2009) 593.
[13] A. A. Rownaghi, Y. H. Taufiq-Yap, Catal. Lett. 130 (2009) 504.
[14] A. A. Rownaghi, Y. H. Taufiq-Yap, F. Rezaei, Ind. Eng. Chem. Res. 48 (2009) 7517.
[15] A. A. Rownaghi, Y. H. Taufiq-Yap, F. Rezaei, Chem. Eng. J. 155 (2009) 514.
[16] A. A. Rownaghi, Y. H. Taufiq-Yap, F. Rezaei, Chem. Eng. J. 165 (2010) 328.
[17] A. A. Rownaghi, Y. H. Taufiq-Yap, Ind. Eng. Chem. Res. 49 (2010) 2135.
[18] V. Sydorchuk, V. Zazhigalov, S. Khalameida, E. Diyuk, J. Skubiszewska-Zieba, R. Leboda, L. Kuznetsova, Mater. Res. Bull. 45 (2010) 1096.
[19] www.cem.com.
[20] S. Albonetti, F. Cavani, S. Ligi, F. Pierelli, F. Trifirò, F. Ghelfi, G. Mazzoni, Stud. Surf. Sci. Catal. 143 (2002) 963.
[21] F. Cavani, S. Ligi, T. Monti, F. Pierelli, F. Trifirò, S. Albonetti, G. Mazzoni, Catal. Today 61 (2000) 203.

[22] G. Catana, R. Ramachandra Rao, B.M. Weckhuysen, P. Van Der Voort, E.Vansant, R.A. Schoonheydt, J. Phys. Chem. B vol 102, 41, (1998) 8005.
[23] P. Van Der Voort, M. White, M. Mitchell, A. Verberckmoes, E.F. Vansant, Spectrochim. Acta 53 A (1997) 2181.
[24] P. Van Der Voort,, M. Morey, G. D. Stucky, M. Mathieu, E. F. Vansant, J. Phys. Chem. B 102 (1998) 585.
[25] L. Moreno-Real, E. R. Losilla, M. A.G. Aranda, M. Martinez-Lara, S. Bruque, M. Gabás, J. Solid State Chem. 137 (1998) 289.

6

1-BUTANOL AS AN ALTERNATIVE REAGENT FOR THE PRODUCTION OF MALEIC ANHYDRIDE

6.1 INTRODUCTION

Given the increase in greenhouse gas emissions due to the use of fossil fuels, there is a need to develop renewable resources such as biomass as the feedstock for the chemical industry and as an energy source. The switch to the use of biomass as a feedstock is an important global initiative in the aim of developing a more sustainable growth [1-18]. In this context, biobutanol has the potential to play a significant role in a sustainable, non-petroleum-based, chemical and energy industry, e.g., as a transportation fuel [19], potentially substituting bioethanol.

Biobutanol possesses in fact interesting advantages compared to other biofuels [20]: i) it has an energy content that is 30% more than ethanol and it is closer to the gasoline energy content; ii) it can be transported and used in existing pipelines, having lower vapour pressure, being less corrosive and less prone to water contamination than ethanol; iii) it is less flammable, consequently less hazardous than other fuels, and it can be mixed with gasoline in any proportion. Biobutanol is produced by the well known process ABE (Acetone, Butanol, Ethanol).

This process is one of the oldest fermentation processes: the biomass mainly involved are molasses and cornstarch and the bacteria utilized are *Clostridium acetobutylicum* or *C. beijerinckii*, able to convert carbohydrates to short-length solvents. Commercial solvent minimum concentration is at about 20 g/L, considering 55-60 g/L of substrate, and it results in solvent yields of about 0.35 g/g sugar; butanol-to-solvent molar ratio is typically 0.6, with an A:B:E ratio of 3:6:1 [21].

This process is very old, since commercial plants were operational during the first half of the last century; successively, with the increasing availability of fossil fuels, which could be used for butanol production, the bio-based butanol plants loosed importance; however, recently, this process regained importance as several improvements have been developed (both for process technology, and regarding bacteria, e.g. increasing their life’s length), also induced by the increasing price of petroleum and being today recognized the added value for chemicals derived from renewable

feedstock. Moreover, it must be said that the advantage of using these solventogenic microbes, especially those genetically modified, is that they are able to metabolize long-length sugars (hexoses and pentoses) in contrast with traditional ethanol-producing yeasts; furthermore the production of the biobutanol occurs with higher yields and similar process efficiency, in comparison with first generation yeasts for bioethanol process. Biobutanol is thought to potentially substitute, in the future, both ethanol and biodiesel in the biofuel market [21].

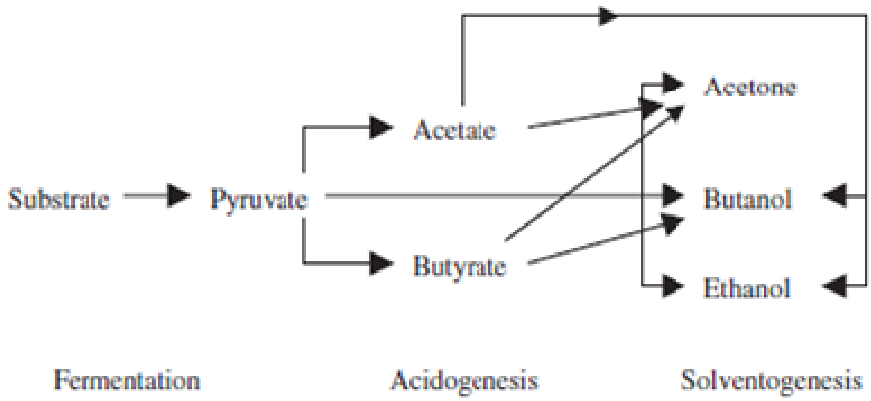

Fig. 6.1_Phases of the fermentation process named ABE (Acetone, Butanol, Ethanol), for the production of biobutanol, using Clostridia Bacteria: first, acetic and butyric acids are produced, then these acids are re-assimilated by the bacteria into ABE solvents [20].

1-Butanol can be produced also chemically, by means of various technologies [22]:

a) the most important industrial process is propylene hydroformylation (oxo synthesis) with subsequent hydrogenation of the aldehyde formed, i.e., 1-butyraldehyde (and minor amount of 2-methylpropanal as the by-product);
b) the Reppe process, consisting in the direct hydroxycarbonylation of propylene into 1-butanol (with 2-methylpropanol as the by-product);
c) the aldol condensation of acetaldehyde into acetaldol in basic conditions, the dehydration of acetaldol into crotonaldehyde in the presence of an acid, and finally the hydrogenation of the aldehyde into 1-butanol. The source for the process can be bioethanol, which can be (oxi)dehydrogenated into acetaldehyde. However, the multi-step process can occur in a single step starting directly from ethanol (which also serves as internal H-transfer reagent, so acting as a MPV-type reduction), using a single bifunctional catalyst, and proper reaction conditions (Guerbet synthesis of alcohols [23-30]).
d) Catalytic hydrogenation of CO into higher alcohols; nowadays, however, this process has no commercial importance.

The large availability and low cost of 1-butanol renders this compound an interesting bioplatform molecule for the synthesis of chemicals. Alcohols generally decompose by either dehydrogenation to produce a carbonyl or dehydration to produce an alkene; dehydration and dehydrogenation routes are competitive in the gas phase in the absence of O_2 up to 500°C, while dehydrogenation predominates at higher temperatures [31]. On dehydrogenating catalysts, 1-butanol transforms into two main products, butyraldehyde and 4-heptanone (a symmetric ketone: ketonization reaction)

[32,33], and smaller amounts of hydrocarbons, such as butene, heptene, and 3-methylheptane, and of other oxygenated compounds, such as 4-heptanol, dibutyl ether and butyl butyrate. Butyraldehyde (like all aldehydes) may undergo reactions such as Tishchenko dimerisation (to form butyl butyrate), aldolisation and ketonisation [34-40]; however, also deep dehydrogenation, aromatization and finally carbonisation may occur. In function of the catalyst and of conditions used, other reactions which may occur are decarbonylation to yield CO, H_2 and C_3H_6, or demethylation to yield propanal and a CH_x radical [41]; the butenes formed by 1-butanol dehydration may decompose to produce propylene and a CH_x radical [42]. In the presence of oxygen, 1-butanol yields butyraldehyde by means of oxidehydrogenation [41,43].

Acid catalysts for 1-butanol dehydration into butenes include heteropolycompounds [44-46], $AlPO_4$ [47,48], sulfated alumina [49], hydroxyapatite [50], Ta-montmorillonite and Ta/Si mixed oxides [51,52], silica-alumina [53], Al/P and Al/Ga/P oxynitrides [54,55].

In this chapter, we report about a study aimed at investigating the possibility of transforming 1-butanol into maleic anhydride (MA), by means of gas-phase oxidation. MA is currently produced by oxidation of either *n*-butane or benzene [56-59], but it may also be produced starting from butenes and butadiene [60-77]; indeed, in the past butenes were also used industrially as starting material for MA synthesis. Therefore, a bifunctional catalyst able to carry out both the dehydration of 1-butanol and the oxidation of the intermediately formed butenes into MA might render the direct transformation of the alcohol into MA feasible.

The hypothetic reaction mechanism, for the oxidehydration of 1-butanol to maleic anhydride, is similar to that one for the selective oxidation of n-butane to maleic anhydride (Figure 6.2): 1-butene (which also isomerizes) represents the common reaction intermediate (formed by dehydration of the alcohol or by oxidehydrogenation of the alkane). This is progressively and selectively converted into MA by means of a series of consecutive oxidation steps.

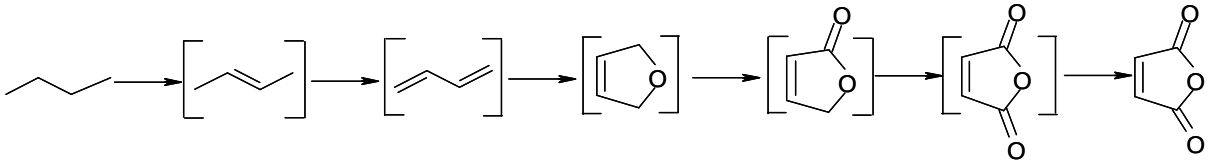

Fig. 6.2_ Mechanism for the selective oxidation of n-butane to maleic anhydride.

6.2 RESULTS AND DISCUSSION

6.2.1 Catalysts tested and reaction conditions

The catalysts used in the present investigation are listed in Table 6.1.

Catalyst	Composition or Structure (XRD or Raman)	Surface area (m^2/g)
VPP	$(VO)_2P_2O_7$	33 [from ref 86]
VPO	α_I-$VOPO_4$	2±1
M1	$Mo_1V_{0.28}Sb_{0.13}Nb_{0.15}O_x$	13±2
VTiO	7 wt% V_2O_5/TiO_2 (anatase)	22
MoWV	$(MoVW)_5O_{14}$-type oxide	4
K1	$H_4PMo_{11}VO_{40}$	Nm
K2	$K(NH_4)_2PVMo_{11}O_{46}$	Nm

Table 6.1_ Catalysts used for the gas-phase selective oxidation of 1-butanol to maleic anhydride: name, composition (analyzed by Raman and/or XRD measurement) and surface area of the fresh catalyst, before reaction.

The VPP catalyst was an industrial sample, delivered by DuPont, and formerly used in the DuPont plant operating in Spain for the production of tetrahydrofuran. The catalyst is also known as "Calcined VPO" and its features are reported in the literature [86,87]: it consists of a VPP core (ca. 150 μm) and of a silica shell (ca. 2 μm), which surrounds it, giving higher attrition resistance. The XRD pattern is that typical of the $(VO)_2P_2O_7$, with apparently no additional crystalline compounds, and the surface P/V ratio, as determined by XPS, is about 1.5-1.6 [86,87]; even though the bulk P/V ratio is not reported, we can assume that it is higher than 1.0.

The VPO catalyst (Table 1) was prepared by refluxing (100°C, for 17 h) an aqueous slurry containing V_2O_5, (99% wt) and phosphoric acid (85% wt), with an atomic P/V ratio of 4. A precipitate was obtained, which was then filtered, washed with water and acetone; the precipitate was crystalline $VOPO_4.2H_2O$ (as determined by XRD) and the analytical P/V ratio was 1.18 (as determined by XRF): this sample corresponds to sample 2 VPD (Chapter 4). The precipitate was then thermally treated in air, at 450°C ; this led to the development of the α_I-$VOPO_4$ crystalline structure. The α_I-$VOPO_4$ was unselective in n-butane oxidation to MA, since it promoted the combustion of n-butane, because of both the high surface density of V^{5+} sites, and the lack of the structural/geometric features of the VPP structure, which are considered essential in the aim of the activation and selective transformation of the alkane.

The Mo oxide-based catalysts investigated were the following: (1) a so-called M1 phase, which is a crystalline molybdate of V, Sb and Nb; (2) a Mo/W/V mixed oxide, a system which is used commercially for the oxidation of acrolein into acrylic acid, and (3) Keggin-type phosphomolybdates.

The VTiO catalyst consisted of 7% wt V_2O_5 supported over titania (anatase); it was prepared by means of the wet impregnation technique, by immersion of TiO_2 in an aqueous solution of

ammonium metavanadate (NH_4VO_3, 99%); then the dried precursor was calcined in static air (3h at 150°C, then 5h at 450°C). A similar system is used for the oxidative scission of butenes [88-90].
The reactivity tests were carried out by feeding 1% mol. of pure 1-butanol in air (or in He); the alcohol was vaporized in the inlet heated line, before the reactor (Chapter 2). The W/F parameter (WHSV) corresponded to 1.33 $g \cdot s \cdot ml^{-1}$. In experiments carried out by changing this latter parameter, we modified the catalyst weight inside the reactor while keeping constant the inlet flow.
Before catalytic tests, we investigated the gas-phase reactivity of 1-butanol, in the absence of any catalyst, with or without oxygen (blank experiments). In particular, an inert material, steatite ($Mg_3Si_4O_{10}(OH)_2$), was used to fill the reactor volume.

6.2.2 Reactivity experiments

Blank experiments

First, we carried out experiments aimed at studying the reactivity of 1-butanol in the gas-phase, without any catalyst, both with and without oxygen. Figure 6.3 plots the results obtained in the presence of oxygen; the reactor was filled with inert material (steatite). During catalytic experiments, this inert material is used to fill the empty space of the reactor. The range of temperature chosen for experiments was that typically used for C_4 olefins oxidation to MA, that is, higher than 300°C.
Under aerobic conditions 1-butanol already converted completely at 350°C; reported in Figure 6.3 are the main products obtained, i.e., C_4 olefins, butyraldehyde and CO_x (mainly CO_2); the latter prevailed at 400°C, while olefins were the predominant products at the intermediate temperature of 350°C. However, the overall selectivity to these compounds was largely lower than 100% at 300°C, whereas it was close to 80% at 350 and 400°C. In fact, many other by-products formed, especially at low temperature (these compounds were not individually quantified): formaldehyde, formic acid, acetic acid, acrylic acid, tetrahydrofuran, dihydrofuran, 1-propanol, propionaldehyde, dibutylether, and the butyl esters of formic acid, acetic acid, propionic acid, and butanoic acid; besides butenes, other olefins formed were propylene, isobutene and butadiene.

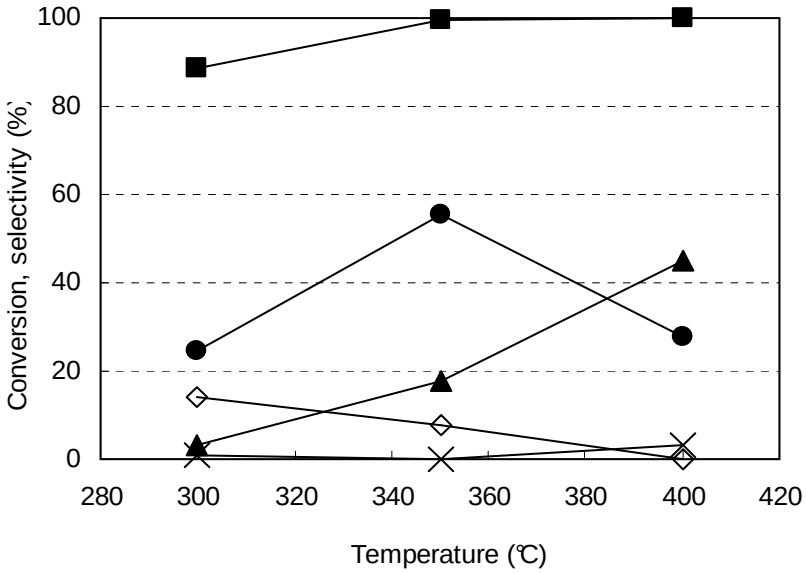

Fig. 6.3_ 1-Butanol conversion and selectivity to the main products as functions of temperature, with no catalyst, and with steatite filling the reactor. Feed composition: 1% 1-butanol in air; W/F (WHSV) 1.33 g s mL^{-1}; 1-butanol conversion (■); selectivity to C4 olefins (●), to butyraldehyde (◇), to CO_x (▲), and to light acids (acrylic + acetic acids, mainly acetic) (×).

Compounds formed in the greater amount were butylformiate and propionaldehyde. The overall amount of these by-products was considerably less at 350°C than at 300°C, but in the former case compounds formed in the greater amount were propionaldehyde, tetrahydrofuran and butylformiate; moreover, also 2-butenal, benzene and 2-ethylacrolein (compounds which did not form at 300°C) were observed. At 400°C, the only by-products formed were: propenal, furan, acetic acid, methylvinylketone, tetrahydrofuran and benzene.

We repeated the same experiment, but with the reactor completely empty (that is, without the inert material) (fig. 6.4). We found that 1-butanol conversion was slightly less than that recorded with the inert filling the reactor. The nature of products formed was similar in the two cases, but with a different relative amount of the various compounds; in fact, the formation of CO_x was greatly suppressed, and the yield to butyraldehyde was greater over the entire range of temperature, whereas that to C4 olefins was 44% (instead of 28%, fig. 6.3) at 400°C. These results indicate that 1-butanol is extremely reactive, and transforms into a wide range of oxidized compounds, typically observed in gas-phase radicalic oxidations; the presence of a solid in the reactor may facilitate the occurrence of these reactions, especially those involving oxidative transformations of both reactant and products intermediately formed.

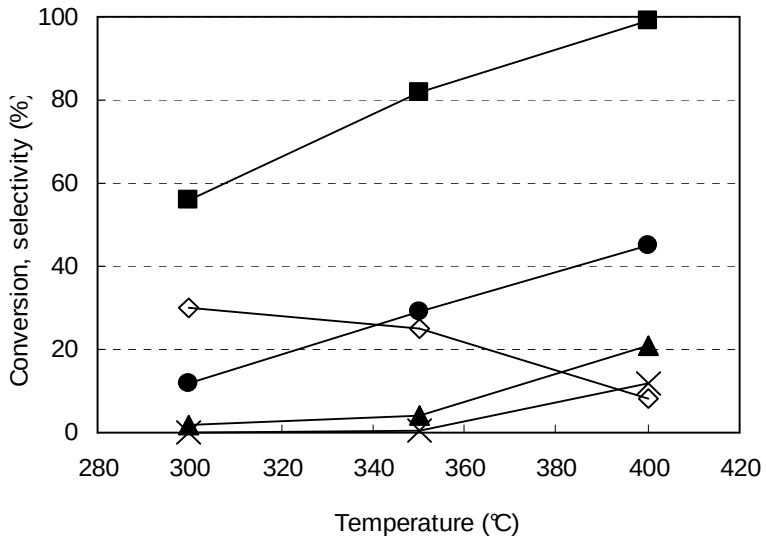

Fig. 6.4_ 1-Butanol conversion and selectivity to the main products as functions of temperature, with no catalyst, and the empty reactor. Feed composition: 1% 1-butanol in air; 1-butanol conversion (■); selectivity to C4 olefins (●), to butyraldehyde (◇), to CO_x (▲) and to light acids (acrylic + acetic acids, mainly acrylic) (×).

When the same experiments were carried out without oxygen in feed (fig. 6.5), but still with the inert material filling the reactor, 1-butanol conversion was 39% at 300°C, 88% at 350°C and 98% at 400°C; the prevailing products were the C4 olefins (overall selectivity 56%, 68% and 77% at 300, 350 and 400°C, respectively), whereas the selectivity to butyraldehyde was always less than 3% over the entire range of temperature examined, and there was no formation of CO_2 and of light acids. In fig. 6.5, we have also reported the selectivity to Others, because of the presence of remarkable amounts of a light unidentified compound (present in small amount in the case of tests shown in figs. 6.3 and 6.4), which we tentatively attribute to formaldehyde. The low C balance at low T is a clear indication about the formation of a great number of other by-products at these conditions.

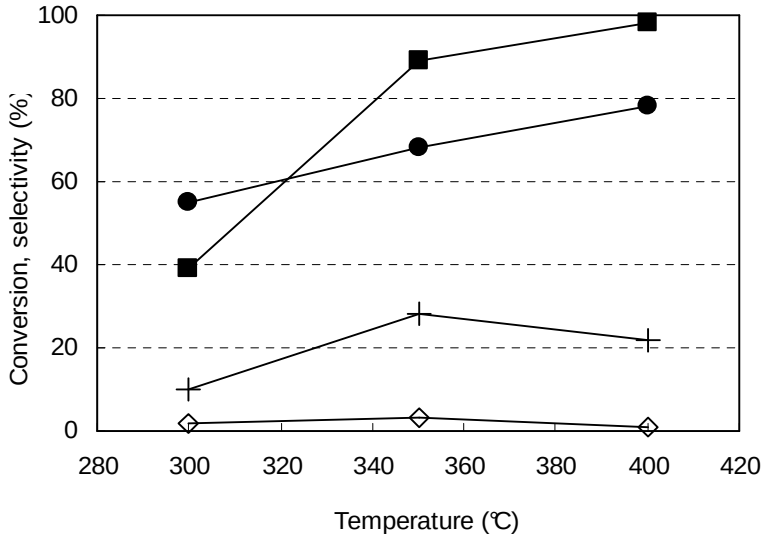

Fig. 6.5_ 1-Butanol conversion and selectivity to the main products as functions of temperature, with no catalyst, and with steatite filling the reactor. Feed composition: 1% 1-butanol in He (no oxygen); 1-butanol conversion (■); selectivity to C4 olefins (●), to butyraldehyde (◇), and to Others (+).

It can be concluded that in the interval of temperature examined, the thermal dehydrogenation of 1-butanol occurs only at a minor extent; in the presence of oxygen, however, the formation of butyraldehyde becomes more important. The thermal dehydration of 1-butanol, is greatly favored at all the conditions examined.

The most important output of these experiments is that in order to be selective to MA, a catalyst for 1-butanol oxidative dehydration -operating in an oxidizing atmosphere- has to be very efficient in 1-butanol dehydration, in order to further enhance the rate of catalytic 1-butene formation as compared to the thermal dehydration, in the aim of rendering less relevant the parallel formation of butyraldehyde (which is the precursor of several by-products identified, but cannot be transformed into MA). Furthermore, it also has to be very efficient in 1-butene oxidation into MA, in order to limit the side reactions of allylic oxidation, which may lead to the formation of 3-butenal, the latter also being one possible precursor for other oxygenated by-products. This indicates vanadyl pyrophosphate (VPP) - the catalyst industrially used for n-butane oxidation to MA- as the possible optimal candidate catalyst for this reaction, since VPP not only is a selective catalyst in butenes oxidation to MA [60-63], but also possesses remarkable acid properties [78,79]. Indeed, 1-butanol has been already tested as a possible reactant for MA synthesis in some papers [80,81], in the aim of demonstrating the polyfunctional characteristics of VPP. In those papers, the authors proposed that the relatively high yield to MA obtained from 1-butanol could be attributed to a shorter reaction pathway than from n-butane, because of the intramolecular dehydrocyclization of 1-butanol into tetrahydrofuran, a possible precursor for MA formation. In another paper [82], it was reported that with VPP, 1-butanol dehydrates into 1-butene, which is then oxidehydrogenated into butadiene and finally oxidized to MA; the authors also reported about the formation of phthalic anhydride by-product, especially at 300°C.

Given these results, and indications reported in the literature, we decided to compare the catalytic behavior of VPP with that of various catalysts which are also active in butenes oxidation into MA, e.g., metal molybdates [74-76], as well catalysts which not only possess acidic characteristics, but also are active in n-butane and n-pentane oxidation into MA, such as polyoxometalates [83-85].

Our further aim was to understand whether the production of MA goes through the formation of either butenes or tetrahydrofuran as the key intermediate product. This not only in the aim of unraveling the reaction mechanism, but also in order to propose alternative production processes for MA from biomass-derived compounds. For instance, furanic rings (such as furan, dihydrofuran, tetrahydrofuran, and 2-substituted or 2,5-disubstituted furanics, such as furfural or HMF) can be obtained from hexoses and pentoses decomposition [4-6, 8, 14]; furanics may be possible reactants for MA production.

Catalytic experiments

Figure 6.6 reports the results achieved using the VPP catalyst. Under the conditions chosen, the conversion of 1-butanol was complete over the entire range of temperature investigated; products obtained were MA, light acids (acrylic and acetic acids, formed in comparable amounts), and

carbon oxides; butenes formed at 340°C only. At the latter temperature, also minor amounts of several by-products were detected, with overall selectivity less than 5%.

The highest selectivity to MA was observed at 370°C (28-29%); at high temperature, the selectivity to MA declined, with a concomitant increase of selectivity to CO_x. In the range 340-370°C, the slight increase of selectivity to MA occurred with a concomitant decrease of selectivity to C4 olefins; however, it is possible to note that the selectivity to C4 olefins was already very low at 340°C. In other words, from these experiments it is not possible to infer about the chemical relationship between C4 olefins and MA, inside a kinetically consecutive reaction scheme (experiment carried out by changing the contact time will allow us to draw a more clear picture about this aspect).

Over the entire temperature range examined, selectivity to light acids declined, with a corresponding higher selectivity to CO_x. These results indicate that at low temperature the preferred reactions were the transformation of 1-butanol into butenes and the oxidative cleavage of either the alcohol or the olefins into acetic acid and acrylic acid. When the temperature was raised, the butenes were transformed into MA and CO_x, whereas the light acids were oxidized into CO_x. It is also worth noting that there was no formation of butyraldehyde; this means that the aldehyde, if formed, was quickly transformed into other by-products (including CO_x). It is also evident, from the trend of selectivity shown in fig. 6.6, that temperatures lower than 340°C might enhance the selectivity to C4 olefins and to light acids, but not to MA.

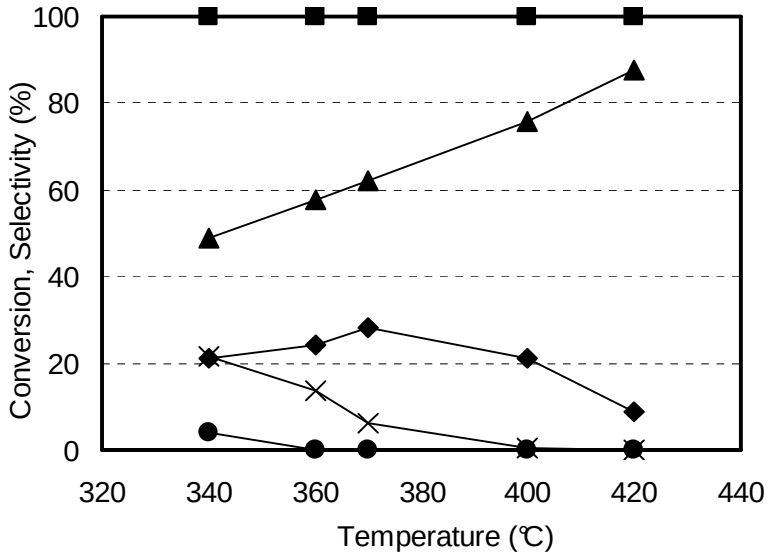

Fig. 6.6_1-Butanol conversion and selectivity to the main products as functions of temperature, with VPP catalyst (Table 6.1). Feed composition: 1% 1-butanol in air; W/F (WHSV) 1.33 g s mL^{-1}; 1-butanol conversion (■); selectivity to C4 olefins (●), to MA (◆), to CO_x (▲) and to light acids (acetic and acrylic acids) (×).

The selectivity to MA achieved with our VPP catalyst was lower than that reported in the literature with 1-butanol and catalysts made of VPP [80-82]; the lower selectivity to MA was mainly due to the greater selectivity to CO_x, which in our case were by far the prevailing products. This discrepancy is apparently mainly due to the fact that, at low temperature, our catalyst was not much selective to CO_x, but also it was not able to oxidize butenes into maleic anhydride; on the opposite, it gave oxidative scission of either 1-butanol or butenes into light acids. At medium-high

temperature, instead, the formation of CO_x became largely predominant. Therefore, one key reaction probably limiting the selectivity to MA was the formation of light acids, which also were precursors for CO_x formation. This can be due to an excessive catalyst acidity (the acidity of VPP is one peculiarity of this catalyst, and is essential in the aim of transforming n-butane into MA), which may eventually derive from the slight excess of P which is added during catalyst preparation (a P/V ratio of about 1.1 is typically used for the VPP in n-butane oxidation, the stoichiometric ratio for VPP being 1.0 [57,58,79]).

In literature, the oxidative scission of butenes into acetic acid has been investigated by Brückner et al [88-90]; it was reported that butenes interact with acid sites in V_2O_5-TiO_2 catalysts, generating the butoxide intermediate species, which then evolves into methylethylketone and then into acetic acid and acetaldehyde by the oxihydrative scission of the C-C bond. On the other hand, too strong adsorption of 1-butene, in the presence of strong acidity, could lead to further oxidation giving rise to cyclic anhydride intermediate (i.e., to the lactone, possibly formed from butadiene) and carbon oxides, finally. Therefore, one key property of the catalyst, which however has to be modulated in order to properly address the transformation of 1-butene, is the surface acidity.

We can extend this concept to our VPP catalyst: the transformation of the intermediately formed butenes into either MA or light acids is probably controlled by the surface acidity of the catalyst; this property is essential in order to control the relative rates of butenes transformation into either MA, or light acids, or CO_x. In this sense, it is likely that the acidity of the VPP-based catalyst used in this work is excessive, and should be properly tuned. We would like to point out that our initial scope was to use an acid catalyst in order to facilitate the dehydration of 1-butanol into 1-butene, as compared to the parallel oxidehydrogenation of the alcohol into butyraldehyde. On one hand, our preliminary results confirmed the importance of an efficient dehydration of 1-butanol as a key-step of the process; on the other hand, the results obtained with the VPP-based catalyst indicate that an excessive acidity may be detrimental for the selectivity to MA. This hypothesis is also confirmed by the experiments reported in refs [60-63]: in order to be selective in the oxidation of 1-butene into MA, a P/V ratio not higher than 1.0 had to be used (instead this ratio is not the optimal one for the oxidation of n-butane into MA). A selectivity of 55% to MA in 1-butene oxidation could be obtained by using a P/V ratio for VPP close to 1.0, but selectivity became lower than 40% when P/V ratio of ca 1.1 and 1.2 were used. Excess P in VPP-based catalysts may enhance the number of surface acid sites, which derive from the P-OH groups, present both in “free” (poly)-phosphoric acid and in the phosphate groups incorporated in the VPP, which at the termination of crystals give rise to the formation of dangling hydroxyl groups.

In order to confirm the possible role of the P/V ratio on catalytic behavior, we compared the performance of two home-made samples, still VPP, but prepared with P/V bulk ratio of 1.0 (sample B1) and 1.1 (the latter corresponds to sample B2, Chapter 3), respectively. The two samples were prepared with the conventional “isobutanol” procedure, calcined with the method that is described in the literature [56,57] and first pseudo-equilibrated in the reaction environment at 400°C. Then we carried out the experiments at 340°C, the other reaction conditions being the same as for the experiments shown in fig. 6.6. We found that sample B2 (VPP with P/V 1.1) gave 13% selectivity

to MA and 59% to CO_x, whereas sample B1 (VPP with P/V 1.0) gave 22% selectivity to MA and 40% to CO_x (with also 32% selectivity to light acids), in both cases with total conversion of 1-butanol. Even though these experiments are not fully consistent with those obtained with the calcined DuPont VPP, they provide a clear indication that for VPP-based catalysts prepared by means of the same method, but holding different P/V ratio, this latter parameter greatly affects the catalytic behavior, especially in regard to the selectivity to the products.

The hypothesis made on the reaction network were confirmed by experiments made at 400°C with variation of the contact time (fig. 6.7).

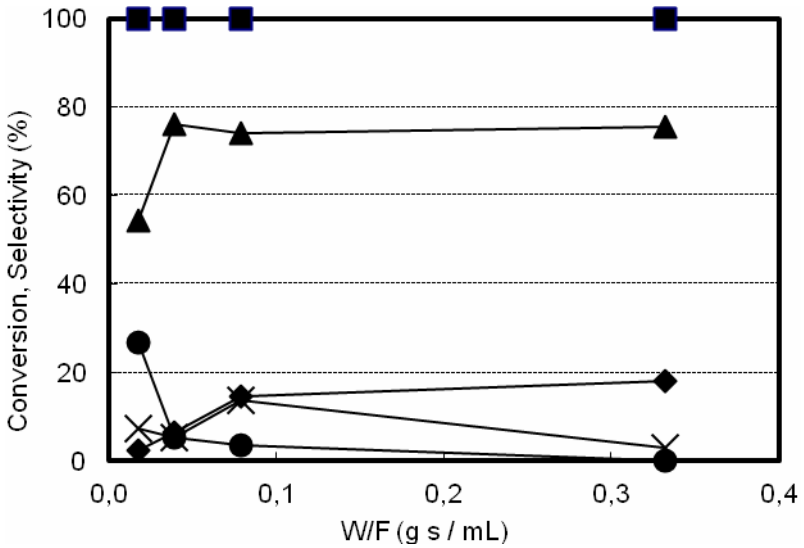

Fig. 6.7_ 1-Butanol conversion and selectivity to the main products as functions of contact time, at 400°C, with VPP catalyst. Feed composition: 1% 1-butanol in air. 1-butanol conversion (■); selectivity to C4 olefins (●), to MA (◆),to CO_x (▲) and to light acids (acetic and acrylic acids) (✕).

The experiments highlighted the following:

a) at the high temperature used for experiments, the conversion of 1-butanol was total even for extremely low contact time;
b) the only "primary" products (that is, formed by direct 1-butanol transformation) were C4 olefins (the selectivity of which, when extrapolated to nil conversion, was clearly higher than zero). Interestingly, there was no butyraldehyde, which indicates that at the reaction conditions used, the aldehyde, once formed, was very quickly oxidized;
c) in regard to CO_x formation, it is not clear whether also a primary contribution exists (it is difficult to state whether the selectivity went down to zero or still was higher than zero for nil 1-butanol conversion); nevertheless, there was clearly a secondary contribution to CO_x formation, which derived mainly from the consecutive oxidation of C4 olefins;
d) MA also was a secondary product, as expected, and its selectivity increased when the contact time was increased, because of the consecutive oxidation of C4 olefins;
e) the selectivity to the light acids showed a maximum value for W/F value close to 0.1 $g \cdot s \cdot ml^{-1}$, and then decreased, because of the consecutive reaction of combustion.

The key role of the VPP structure in the transformation of the intermediately formed C4 olefins into MA is also evident from the comparison of the catalytic behavior of the VPP (fig. 6.6) with that of the VPO catalyst, which consists of α_I-$VOPO_4$ (fig. 6.8; Table 6.1).

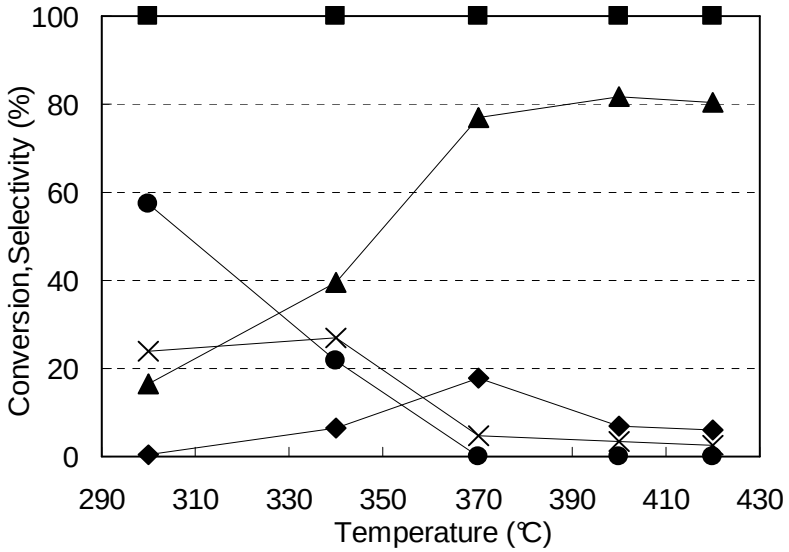

Fig. 6.8_1-Butanol conversion and selectivity to the main products as functions of temperature, with VPO catalyst (Table 6.1); W/F (WHSV) 1.33 g s mL^{-1}; feed composition: 1% 1-butanol in air. 1-butanol conversion (■); selectivity to C4 olefins (●), to MA (◆), to CO_x (▲) and to light acids (acetic and acrylic acids) (×).

Data reported in fig. 6.8 show that the VPO was not totally unselective to MA from 1-butanol; the highest selectivity to MA was 18%, at 370°C. The conversion of 1-butanol was complete over the entire range of temperature investigated, despite the very low surface area of the catalyst. If we compare the distribution of products obtained at 340°C with the VPP and the VPO catalysts (Table 6.2), we realize that the latter was much less efficient in butenes conversion, that explains both the much lower selectivity to MA (7% for the VPO, vs 22% for the VPP) and the lower selectivity to CO_x as well (39% for VPO, vs 49% for VPP); on the other hand the VPO catalyst was slightly more selective to light acids. These data highlighted that the VPO catalyst lacks the active sites required for an efficient transformation of C4 olefins into MA.

%	VPP	VPO
1-butanol conv.	100	100
Select. MA	21	7
Select. C4 olefins	3	22
Select. COx	49	39
Select. acids	21	27
Select. others	6	5

Table 6.2_ Comparison of VPO and VPP catalysts in 1-butanol oxidehydration at 340°C.

In regard to the surface acid characteristics, fig. 6.9 compares the ammonia-TPD profiles for the VPP and VPO samples; given the extremely low surface area, it is not surprising that the desorption profile of VPO indicates the presence of a very low number of acid sites. However, in terms of relative acidity, the profiles of VPP and VPO were not much different; in both cases, in fact, there is a high-T contribution, a clear indication of the existence of strong acid sites.

Concluding, the VPP may be a good catalyst for the single-step oxidehydration of 1-butanol into MA, but several aspects still have to be investigated: (a) one important issue is the optimization of the P/V ratio, which in turn affects the surface acidity; (b) a second point concerns the optimization of reaction parameters, such as the reactant feed composition; it is likely that the feed ratio between 1-butanol and oxygen may greatly affect the catalytic behavior. One important point might be the need to work under conditions of incomplete 1-butanol conversion, in order to disfavor the consecutive combustion reactions (indeed, in all of our tests the alcohol was completely converted). However, the results obtained also indicate that temperatures higher than 320-340°C are anyway necessary in order to convert the intermediate C4 olefins into the consecutive products (including MA); in fact, at low T the VPP catalyst was not so efficient in the oxidation of butenes, even under conditions leading to total 1-butanol conversion. This implies that it should be necessary to use relatively high temperatures with very short contact times, in order to achieve partial 1-butanol conversion; indeed, this is what we did in the case of experiments reported in fig. 6.7. However, the output of these experiments is that using lower contact time did not lead to a better selectivity to MA. Still it seems that the crucial point is addressing the issue of a better selectivity by means of an optimization of VPP surface features.

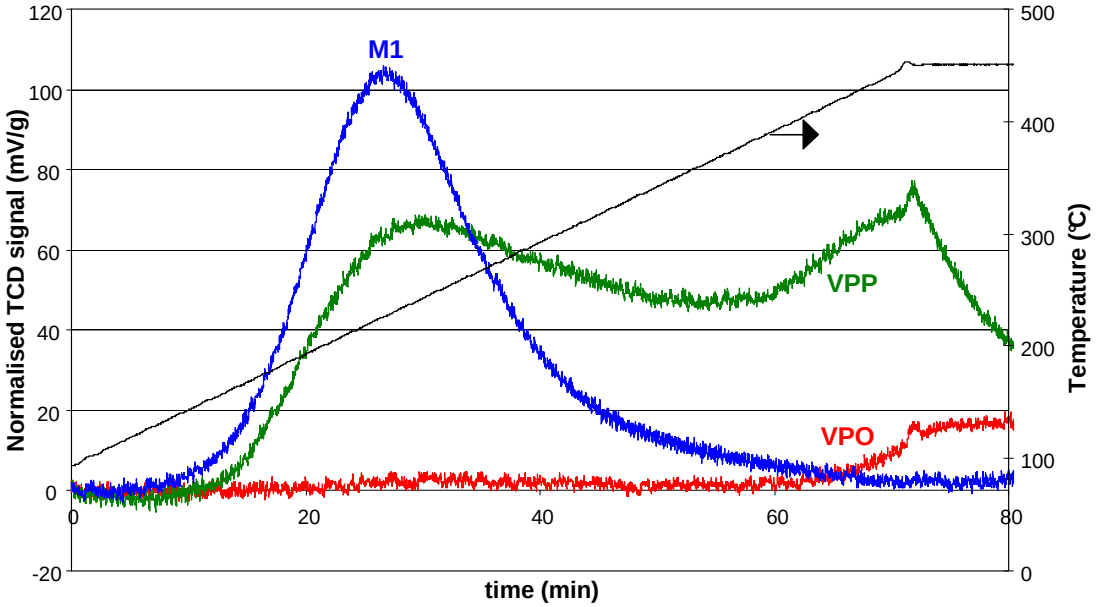

Fig. 6.9_ Ammonia-TPD profiles of selected catalysts.

Finally, we also tested the reactivity of a VTiO catalyst made of TiO_2(anatase)-supported V_2O_5 (Table 6.1), that is a system similar to that used for the oxidative scission of butenes [88-90]. These experiments were carried out in the aim of confirming the hypothesis that the undesired side reaction of oxidative scission, which occurs with the butenes on vanadium oxide-based catalysts, may also occur starting from 1-butanol. Results of this experiments are shown in fig. 6.10; it is shown that the behavior of the catalyst was quite the same as that observed in the literature starting from 1-butene: formation of acetic acid (no acrylic acid) and CO_x, with traces of C4 olefins and 1.5% yield to MA at low temperature, with total conversion of 1-butanol even at 230°C. These data

confirmed that vanadium oxide is detrimental for the selectivity of the reaction, and that most likely the oxidative scission may occur directly on 1-butanol.

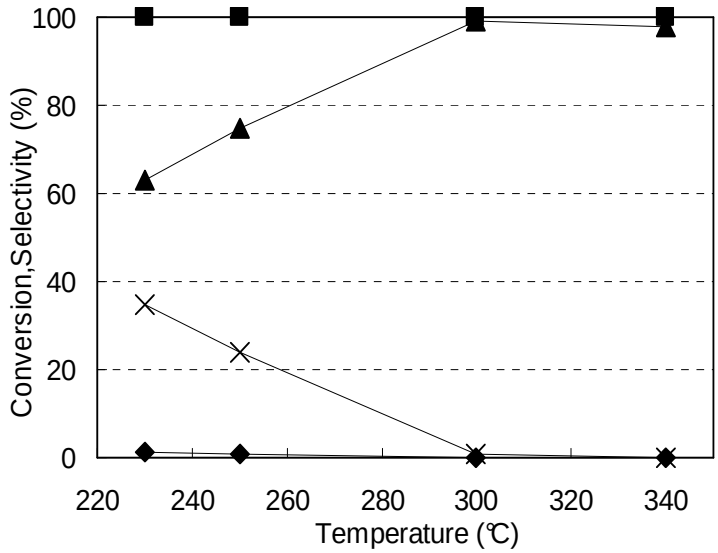

Fig. 6.10_1-Butanol conversion and selectivity to the main products as functions of temperature, with VTiO catalyst (Table 6.1); W/F (WHSV) 1.33 g s mL^{-1}; feed composition: 1% 1-butanol in air. 1-butanol conversion (■); selectivity to MA (◆), to CO_x (▲) and to acetic acid (×).

In regard to the M1 phase, there is a huge amount of literature available on this catalytic material, since it is active and selective in various oxidation reactions [91]: oxidehydrogenation of ethane into ethylene, propane oxidation to acrylic acid and propane ammoxidation to acrylonitrile. In regard to the oxidation of n-butane and n-butenes, the reactivity of various Mo/V/O-based systems has been recently studied by Lopez Nieto et al. [92]. These authors found that the catalyst of composition $Mo_1V_{0.23}Te_{0.23}Nb_{0.15}O_x$ (containing both the orthorhombic M1 phase and the orthorhombically distorted M2 phase) was active and relatively selective in n-butane oxidation to MA. At 400°C, and with 1.4% n-butane in air as feedstock, the conversion obtained was 56%, with 36% selectivity to MA; by-products were CO_x, with 1% selectivity only to acrylic acid and no acetic acid. Less selective was the M1/M2 containing Sb (in place of Te): $Mo_1V_{0.26}Sb_{0.13}Nb_{0.06}O_x$; in this case, the best selectivity to MA was 25% only at 56% conversion. When the reaction was carried out with the Te-containing M1/M2 starting from 1-butene (1.5% in air), a yield of about 40% (at total olefin conversion) was obtained at 400-420°C; the yield to acrylic acid was 10%, remainder being CO_x; in the temperature interval 340-380°C, the M1/M2 catalyst was selective into 2-butenes and butadiene. The authors attributed the good performance of the catalyst to the presence of the M1 phase as the main active component, and hypothesized that the partial oxidation of n-butane on Mo/V/Te/Nb/O catalysts can be explained by the presence of three moieties: (i) activation of n-butane on V-sites, in Mo–O–V–O–(Mo or Nb) moiety; (ii) oxidation of 1-butene to butadiene on Mo/Te sites, in Te–O–Mo–O–(Te or V); and (iii) oxidation of butadiene to MA on Mo/Nb sites, in Nb–O–Mo–O–(Nb or V). The authors did not investigate the behavior of the Sb-containing M1/M2 phase from 1-butene.
Figure 6.11 plots the results obtained from 1-butanol with our M1 catalyst; for comparison, the behavior in n-butane oxidation is also reported in figs. 6.12 and 6.13, for the M1 and the VPP catalysts, respectively. As shown in fig. 6.9, the M1 catalyst also showed a remarkable density of

acid sites of medium-strength, as also reported in the literature [93]. Figure 6.11 shows some surprising results: first, the catalyst gave a very low selectivity to MA (about 10-12%), and there was no formation of C4 olefins at all (traces at low temperature). Moreover, the catalyst was very selective to light acids: at low temperature, acrylic and acetic acid formed in similar amount, but at 370°C there was no formation of acetic acid, and acrylic acid was the only light acid formed. In overall, the catalyst still was selective to CO_x (both CO_2 and CO, but the latter was the prevailing one; in fact, selectivity to CO increased from 16% to 44% when the temperature was raised). At 300°C, several other by-products formed, such as isobutene, benzene, butanoic acid, methyl ester of acetic acid, and phthalic anhydride; these by-products were not observed in the experiment carried out at 370°C.

These data contrast with indications from the literature; given the relatively good selectivity from 1-butene reported in the literature, one would expect a selectivity to MA from 1-butanol better than that experimentally observed. This discrepancy might be attributed to either one of these two aspects: (a) the M1 phase used by us is not the preferred phase, because of the presence of Sb and not of Te; (b) using 1-butanol as the feedstock, instead of 1-butene, may be the reason for the final low selectivity to MA; given the fact that butenes were very efficiently transformed into consecutive products (the selectivity to C4 olefins was nil even at low temperature), we cannot exclude that 1-butanol was overoxidized into CO_x very quickly, eventually via the intermediate formation of butyraldehyde (the selectivity of which, however, was also nil).

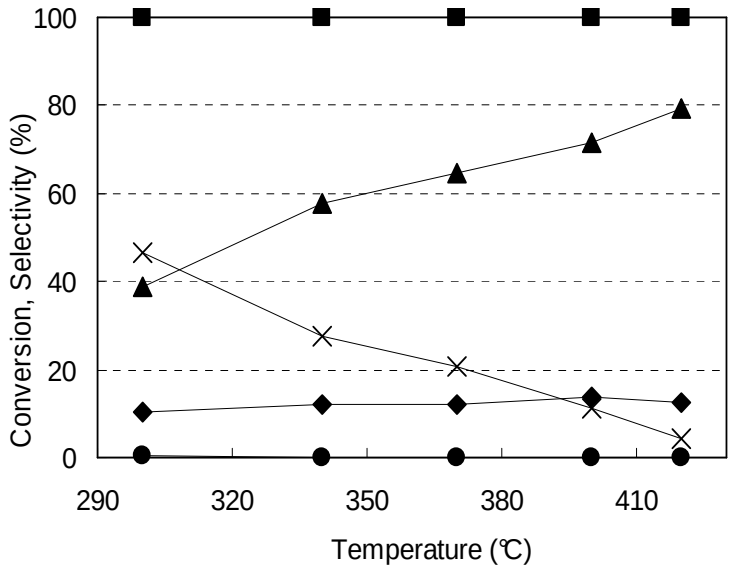

Fig. 6.11_1-Butanol conversion and selectivity to the main products as functions of temperature, with M1 catalyst (Table 6.1); W/F (WHSV) 1.33 g s mL^{-1}; feed composition: 1% 1-butanol in air. 1-butanol conversion (■); selectivity to C4 olefins (●), to MA (◆), to CO_x (▲) and to light acids (acetic and acrylic acids) (×).

In order to discriminate between these hypothesis, it should be necessary to carry out experiments either starting from n-butane or from 1-butene. We decided to feed n-butane, in order to compare the catalytic behavior of our M1 catalyst with that reported in the literature for the Sb-containing M1/M2 catalyst. Results of these experiments are plotted in fig. 6.12.

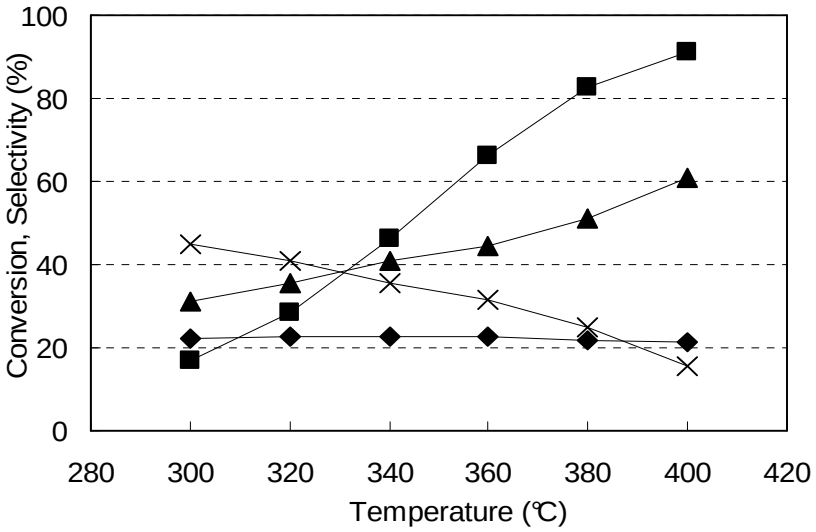

Fig. 6.12_ n-Butane conversion and selectivity to the main products as functions of temperature, with M1 catalyst (Table 6.1); W/F (WHSV) 1.33 g s mL^{-1}; feed composition: 1.7% n-butane in air. n-butane conversion (■); selectivity to MA (◆), to CO_x (▲) and to light acids (acetic and acrylic acids) (×).

Data reported in fig. 6.12 show that the selectivity to MA was quite similar to that reported in the literature for the Sb-containing M1 phase [92]; this led us to conclude that the low selectivity obtained from 1-butanol is a peculiarity of the M1catalyst. For what concerns the light acids, the latter were by far the predominant compounds below 350°C, but their selectivity declined when the temperature was raised, and finally became very low. Also this is in agreement with literature, since at 400°C an overall selectivity to acrylic and acetic acids lower than 1% is reported [92]. It is worth noting that the fall of selectivity to the light acids observed (and the concomitant increase of selectivity to CO_x, especially to CO) also in this case was mainly due to the fall of selectivity to acetic acid; in fact, selectivity to acrylic acid showed only a slight decrease. Acrylic acid also prevailed at low temperature (26% selectivity to acrylic acid and 19% to acetic acid, at 300°C).

Given that the M1, when used for propane oxidation to acrylic acid, gives the best performance at low temperature (for example, at temperature less than 380°C), these data confirm that the excellent catalytic behavior of the M1 phase in alkanes oxidation also derives from its peculiarity of being poorly active in the consecutive combustion of the products of partial oxidation, i.e., acrylic acid from propane and MA from n-butane. In fact, data reported in figs. 6.11 and 6.12 show that the selectivity to MA, albeit very low, was stable over the entire range of temperature examined. The same was not true in the case of the VPP catalyst, as shown in figs. 6.6 (from 1-butanol) and 6.13 (from n-butane). Figure 6.13 shows the characteristic behavior of an "equilibrated" VPP-based catalyst, containing a slight excess of P with respect to the stoichiometric requirement. The "equilibration" consists in making the catalyst stay under reaction conditions for several hours (typically, 100 h, at 400-440°C), in order to allow the transformation of any type of compound - either crystalline or amorphous, which had formed during the thermal treatment- into the VPP. Typically, the equilibrated catalyst contains the VPP as the largely prevailing compound, with small amount of $VOPO_4$ (oxidized) compounds; however, the exact nature of the catalyst is a function of the atomic P/V ratio used for the preparation of the catalyst [57-59]. When used in lab reactor, this

catalyst gives a selectivity to MA which is between 60 and 70% for an alkane conversion up to 70-80%; a further increase of conversion leads to a more rapid decline of the selectivity, with a concomitant increase of CO_x formation. The selectivity to light acids (both acrylic and acetic) is about 10% at low temperature, but then declines when the temperature is increased.

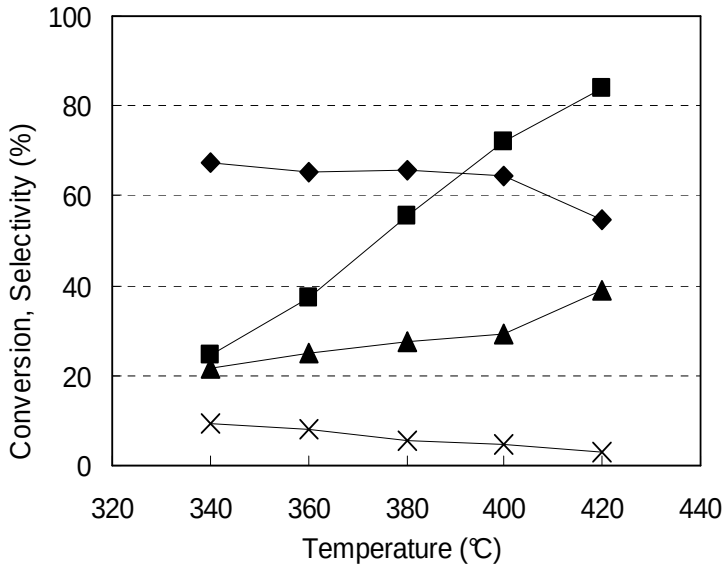

Fig. 6.13_ n-Butane conversion and selectivity to the main products as functions of temperature, typically obtained with a VPP catalyst; W/F (WHSV) 1.33 g s mL^{-1}; feed composition: 1.7% n-butane in air. n-butane conversion (■); selectivity to MA (◆), to CO_x (▲) and to light acids (acetic and acrylic acids) (×).

Figure 6.14 shows the catalytic behavior of a of a Mo/W/V mixed oxide; this system is used for the oxidation of acrolein into acrylic acid [94, and references therein]. The behavior observed has analogies with that shown by the M1 catalyst (fig. 6.11); the selectivity to MA was low (less than 10%), and prevailing products were CO_x and light acids. C4 olefins formed at 250 and 300°C; also butyraldehyde was found at 250°C. Carbon balance was good, with the exception of the experiment carried out at low T (for example, at 250°C the C balance was 75%); in this case, several by-products formed (which were not quantified), amongst which the most important were: 2-propenal, 4-methyl-1-pentene, methacrolein, 2-butanone, 2-pentanone, butanoic acid, 2,5-dihydrofuran, tetrahydrofuran, benzene, formaldehyde and phthalic anhydride.

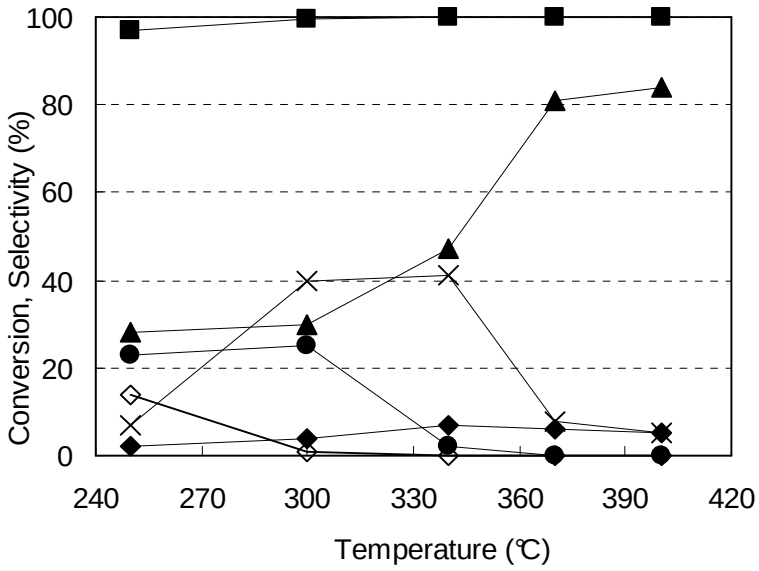

Fig. 6.14_1-Butanol conversion and selectivity to the main products as functions of temperature, with MoWV catalyst (Table 6.1); W/F (WHSV) 1.33 g s mL^{-1}; feed composition: 1% 1-butanol in air. 1-butanol conversion (■); selectivity to C4 olefins (●), to MA (◆), to CO_x (▲), to light acids (acetic and acrylic acids) (×), and to butyraldehyde (◇).

Results obtained highlight that still the main problem of these catalysts is the relatively high formation of products of oxidative scission, and of carbon oxides as well.

Further experiments were carried out using Keggin-type polyoxometalates catalysts, of composition $H_4PMo_{11}VO_{40}$ (K1) and $K(NH_4)_2PVMo_{11}O_{46}$ (K2, Table 6.1). Phosphomolybdates, especially those which also contain V as an addendum element, are catalysts for several oxidation reactions, both in the gas and in the liquid phase [refs 95-98 and references therein]. For example, Keggin polyoxometalates are active and selective in the phase oxidation of isobutane to methacrolein and methacrylic acid and of propane to acrylic acid; they have also been used as catalysts for n-butane oxidation [83]. Results obtained with K1 and K2 are reported in figs. 6.15 and 6.16, respectively.

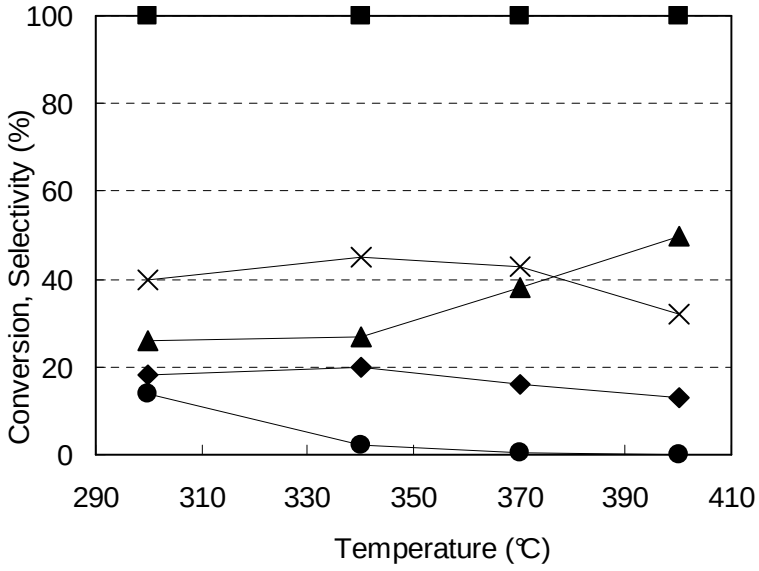

Fig. 6.15_1-Butanol conversion and selectivity to the main products as functions of temperature, with K1 catalyst (Table 6.1); W/F (WHSV) 1.33 g s mL^{-1}; feed composition: 1% 1-butanol in air. 1-butanol conversion (■); selectivity to C4 olefins (●), to MA (◆), to CO_x (▲), and to light acids (acetic and acrylic acids) (×).

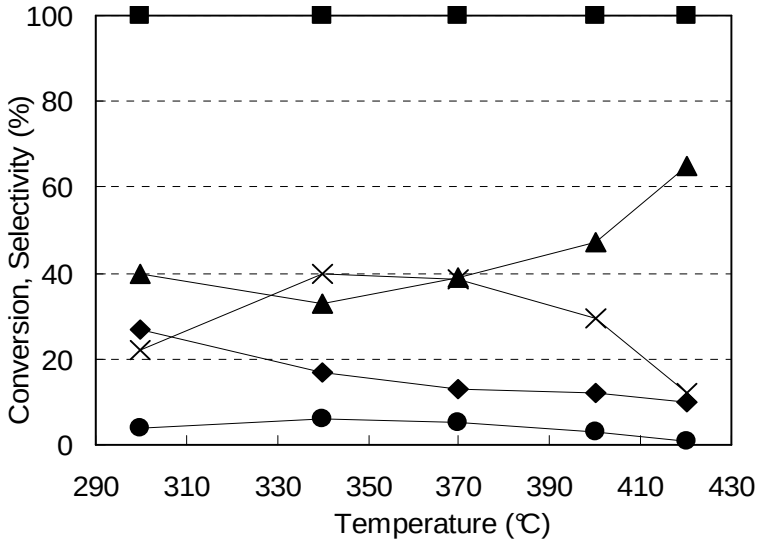

Fig. 6.16_1-Butanol conversion and selectivity to the main products as functions of temperature, with K2 catalyst (Table 6.1); W/F (WHSV) 1.33 g s mL^{-1}; feed composition: 1% 1-butanol in air. 1-butanol conversion (■); selectivity to C4 olefins (●), to MA (◆), to CO_x (▲), and to light acids (acetic and acrylic acids) (×).

The polyoxometalates-based catalysts showed a catalytic behavior which was intermediate between that of VPP and of molybdates; in fact, on one hand, the maximum selectivity to MA obtained was close to 28% with K2 (that is, higher than that obtained with M1 and MoWV, and similar to the best one obtained with VPP), at total 1-butanol conversion, but on the other hand both catalysts showed high selectivity to light acids (both acetic and acrylic), which is a peculiarity of molybdates-based catalysts. Figure 6.17 details selectivity to the C4 olefins, for the K2 catalyst; it is shown that at low temperature preferred olefins were butenes, but when the temperature was raised, butenes were converted into butadiene by means of oxidehydrogenation.

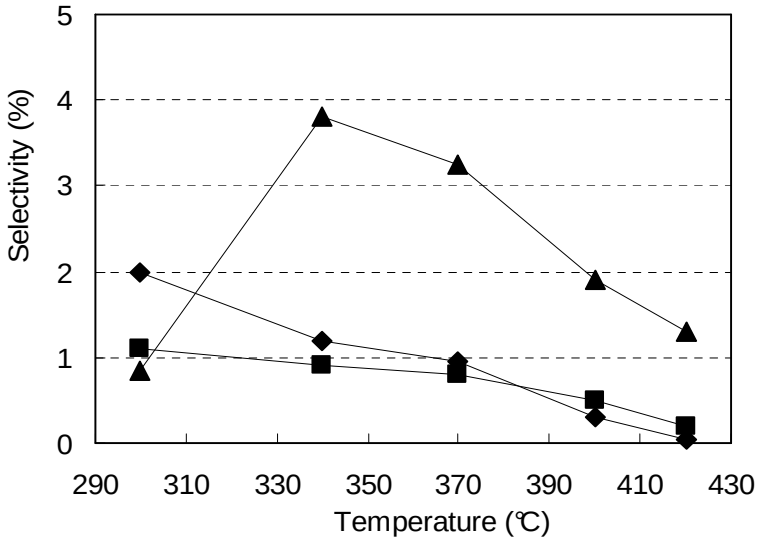

Fig. 6.17_Detail of selectivity to C4 olefins as functions of temperature, with K2 catalyst (Table 6.1); W/F (WHSV) 1.33 g s mL^{-1}; feed composition: 1% 1-butanol in air. Selectivity to 1-butene (■); 2-butenes (◆), and to butadiene (▲).

In overall, the behavior of Keggin-type polyoxometalates is promising, in terms of selectivity to MA. However, one peculiarity of these catalysts, which is always met when they are used as catalysts for gas-phase oxidations (especially when the temperatures used are higher than 350°C, an

event which may occur at the catalyst surface with exothermal reactions even when the gas-phase temperature is relatively low) was the deactivation due to thermal structural degradation. This also occurred with our polyoxometalates catalysts; for example, in the case of the K2 sample, when we repeated the experiment at 300°C (after all the experiments over the entire temperature range had been carried out), we found the following results: conversion 100%, selectivity to CO_x 17%, to light acids 12%, to MA 0.5%, to butyraldehyde 12% (which was 0.2 % with the fresh K2), to 1-butene 20%, to 2-butenes 29%, and to butadiene 9%. In other words, the deactivated K2 catalyst still was active in 1-butanol transformation, but catalyzed prevalently the dehydration to C4 olefins and the oxidehydrogenation into butyraldehyde, with almost nil selectivity to MA.

6.3 CONCLUSIONS

This preliminary catalyst screening, aimed at studying the feasibility of a process for the one-step oxidehydration of 1-butanol into MA, allowed us conclude that some catalysts are potentially good candidates for this reaction. The most selective to the desired product, and the more stable as well, is based on vanadyl pyrophosphate. The data obtained indicate that the reaction network includes several reactions, which contribute to lower the selectivity to MA. Amongst these side reactions, those giving the greater contribution were the oxidative C scission into light acids (acrylic and acetic acid), and the combustion to CO_x. In order to improve the selectivity to MA, it will be necessary to optimize reaction parameters, and also modify catalyst surface properties. For instance, the results obtained indicate that surface acidity, a necessary requisite in the aim of fostering the dehydration of 1-butanol into butenes, may also play a negative role on the reaction, since it may facilitate the oxidative scission of both the reactant and the intermediately formed C4 olefins.

6.4 ACKNOWLEDGEMENTS

The research leading to these results has received funding from the European Union Seventh Framework Programme (FP7/2007-2013), under grant agreement n° 241718 EuroBioRef.

6.5 REFERENCES

[1] B.O. Palsson, S. Fathi-Afshar, F.F. Rudd, E.N. Lightfoot, Science 213 (1981) 513.

[2] B. Kamm, Angew. Chem. 119 (2007) 5146; Angew. Chem. Int. Ed. 46 (2007) 5056.

[3] A. Corma, S. Iborra, A. Velty, Chem. Rev. 107 (2007) 2411.

[4] C.H. Christensen, J. Rass-Hansen, C.C. Marsden, E. Taarning, K. Egeblad, ChemSusChem 1 (2008) 283.

[5] P. Gallezot, Green Chem. 9 (2007) 295.

[6] J.N. Chheda, G.W. Huber, J.A. Dumesic, Angew. Chem. Int. Ed. 46 (2007) 7164.

[7] F. W. Lichtenthaler in “Biorefineries—Industrial Processes and Products” (Eds. B. Kamm, P. R. Gruber, M. Kamm), Wiley-VCH, Weinheim, 2006, pp. 3.

[8] P. Gallezot, Catal. Today 121 (2007) 76.
[9] Y. Román-Leshkov, C. J. Barret, Z. Y. Liu, J. A. Dumesic, Nature 447 (2007) 982.
[10] J.J. Bozell, Clean 36 (8) (2008) 641.
[11] J.H. Clark, J. Chem. Technol. Biotechnol. 82 (2007) 603.
[12] P.N.R. Vennestrøm, C.H. Christensen, S. Pedersen, J.-D. Grunwaldt, J.M. Woodley, ChemCatChem 2 (2010) 249.
[13] J. H. Clark, F.E. I. Deswarte, T.J. Farmer, Biofuels Bioprod. Bioref. 3 (2009) 72.
[14] N. Dimitratos, J.A. Lopez-Sanchez, G.J. Hutchings, Topics Catal. 52 (2009) 258.
[15] J. van Haveren, E.L. Scott, J. Sanders, Biofuels Bioprod. Bioref. 2 (2008) 41.
[16] G. Centi, P. Lanzafame, S. Perathoner, Catal. Today 167 (2011) 14.
[17] M. Rose, R. Palkovits, Macromol. Rapid Commun. 32 (2011) 1299.
[18] D.A. Simonetti, J.A. Dumesic, ChemSusChem 1 (2008) 725.
[19] B.G. Harvey, H.A. Meylemans, J. Chem. Technol. Biotechnol. 86 (2011) 2.
[20] N. Qureshi, T. C. Ezeji, Biofuels, Bioprod. Bioref. 2 (2008) 319.
[21] E.M.Green, Current Opinion in Biotechnology 22 (2011) 1.
[22] H.-D. Hahn, G. Dämbkes, N. Rupprich, H. Bahl, in Ullmann's Encyclopedia of Industrial Chemistry, Vol. 6 (2012) Wiley-VCH Verlag GmbH & Co. KGaA, Weinheim, p. 417.
[23] T. Tsuchida, J. Kuboa, T. Yoshioka, S. Sakuma, T. Takeguchi, W. Ueda, J. Catal. 259 (2008) 183.
[24] T. Tsuchida, S. Sakuma, T. Takeguchi, W. Ueda, Ind. Eng. Chem. Res. 45 (2006) 8634.
[25] C. Yang, Z. Meng, J. Catal. 142 (1993) 37.
[26] A.S. Ndou, N. Plint, N.J. Coville, Appl. Catal. A 251 (2003) 337.
[27] K.W. Yang, X.Z. Jiang, W.C. Zhang, Chin. Chem. Lett. 15 (2004) 1497.
[28] M. León, E. Díaz, A. Vega, S. Ordóñez, A. Auroux, Appl. Catal. B 102 (2011) 590.
[29] M. León, E. Díaz, S. Ordóñez, Catal. Today 164 (2011) 436.
[30] J.I. Di Cosimo, V.K. Dıez, M. Xu, E. Iglesia, C.R. Apesteguia, J. Catal. 178 (1998) 499.
[31] M.R. Harper, K.M.V. Geem, S.P. Pyl, S.S. Merchant, G.B. Marin, W.H. Green, Combust. Flame 158 (2011) 2075.
[32] R. Horyń, R. Klimkiewicz, Appl. Catal. A 351 (2008) 184.
[33] R. Horyń, R. Klimkiewicz, Appl. Catal. A 370 (2009) 72.
[34] C. Cobzaru, S. Oprea, E. Dumitriu, V. Hulea, Appl. Catal. A 351 (2008) 253.
[35] A. Ungureanu, S. Royer, T.V. Hoang, D. Trong On, E. Dumitriu, S. Kaliaguine, Micropor. Mesopor. Mater. 84 (2005) 283.
[36] H. Hattori, Appl. Catal. A 222 (2001) 247.
[37] Kh.M. Minachev, O.K. Atal'yan, M.A. Markov, Russ. Chem. Bull. 27 (1978) 2437.
[38] H. Idriss, C. Diagne, J.P. Hindermann, A. Kiennemann, M.A. Barteau, J. Catal. 155 (1995) 219.
[39] J. Raskó, J. Kiss, Appl. Catal. A 287 (2005) 252.
[40] J. Raskó, T. Kecskés, J. Kiss, Appl. Catal. A 287 (2005) 244.
[41] J.S. Kruger, R. Chakrabarti, R.J. Hermann, L.D. Schmidt, Appl. Catal. A 411– 412 (2012) 87.

[42] A.A. Shoaibi, A.M. Dean, J. Fuel Cell Sci. Technol. 7 (2010) 041015.
[43] A. Iriondo, M.B. Guemez, J. Requies, V.L. Barrio, J.F. Cambra, P.L. Arias, J.L.G. Fierro, Stud. Surf. Sci. Catal. 175 (2010) 453.
[44] M.A. Parent, J.B. Moffat, Catal. Lett. 48 (1997) 135.
[45] J. Macht, M.J. Janik, M. Neurock, E. Iglesia, J. Am. Chem. Soc. 130 (2008) 10369.
[46] K. Hashimoto, Y. Matsumura, M. Fukuchi, Y. Kera, Catal. Lett. 19 (1993) 375.
[47] M.R. Mostafa, A.M. Youssef, Mater. Lett. 34 (1998) 405.
[48] F.M. Bautista, B. Delmon, Appl. Catal. A 130 (1995) 47.
[49] V. Macho, M. Králik, E. Jurecekova, J. Hudec, L. Jurecek, Appl. Catal. A 214 (2001) 251.
[50] S.J. Joris, C.H. Amberg J. Phys. Chem. 76 (1971) 3167.
[51] G. Guiu, P. Grange, J. Catal. 168 (1997) 463.
[52] G. Guiu, P. Grange, J. Catal. 156 (1995) 132.
[53] A. Gil, M.A. Vicente, S.A. Korili, J. Catal. 229 (2005) 119.
[54] S. Delsarte, M. Florea, F. Maugé, P. Grange, Catal. Today 116 (2006) 216.
[55] S. Delsarte, P. Grange, Appl. Catal. A 259 (2004) 269.
[56] A. Caldarelli, F. Cavani, F. Folco, S. Luciani, C. Cortelli, R. Leanza, Catal. Today 157 (2010) 204.
[57] F. Cavani, D. De Santi, S. Luciani, A. Lofberg, E. Bordes-Richard, C. Cortelli, R. Leanza, Appl. Catal. A 376 (2010) 66.
[58] F. Cavani, S. Luciani, E. Degli Esposti, C. Cortelli, R. Leanza, Chem. Eur. J., 16 (2010) 1646.
[59] N. Ballarini, F. Cavani, C. Cortelli, S. Ligi, F. Pierelli, F. Trifirò, C. Fumagalli, G. Mazzoni, T. Monti, Topics Catal., 38 (2006) 147.
[60] F.Cavani, G.Centi, I.Manenti, A.Riva, F.Trifirò, Ind. Eng. Chem. Prod. Res. Dev. 22 (1983) 565.
[61] F.Cavani, G.Centi, F.Trifirò, Ind. Eng. Chem. Prod. Res. Dev. 22 (1983) 570.
[62] F.Cavani, G.Centi, F.Trifirò, Appl. Catal. 9 (1984) 191.
[63] F.Cavani, G.Centi, I.Manenti, F.Trifirò, Ind. Eng. Chem. Prod. Res. Dev. 24 (1985) 221.
[64] E. Bordes, Stud. Surf. Sci. Catal. 55 (1990) 585.
[65] E. Bordes, Catal. Today 16 (1993) 27.
[66] E. Bordes, P. Courtine, J. Catal. 57 (1979) 236.
[67] M. Ai, J. Catal. 85 (1984) 324.
[68] M. Ai, S. Suzuki, J. Catal. 26 (1972) 202.
[69] E. Benser, R. Glaum, T. Dross, H. Hibst, Chem. Mater. 19 (2007) 4341.
[70] W. M. Brandstädter, B. Kraushaar-Czarnetzki, Ind. Eng. Chem. Res. 44 (2005) 5550.
[71] W. M. Brandstädter, B. Kraushaar-Czarnetzki, Ind. Eng. Chem. Res. 46 (2007) 1475.
[72] N.T. Do, M. Baerns, Appl. Catal. 45 (1988) 1.
[73] R.C. Gill, U.S. Ozkan, J. Catal. 122 (1990) 452.
[74] R.A. Hernandez, U.S. Ozkan, Ind. Eng. Chem. Res. 29 (1990) 1454.
[75] U.S. Ozkan, G.L. Schrader, J. Catal. 95 (1985) 137.
[76] F. Trifirò, G. Caputo, P. Forzatti, Ind. Eng. Chem. Prod. Res. Dev. 14 (1975) 22.

[77] R.L. Varma, D.N. Saraf, J. Catal. 55 (1978) 361.
[78] M. Ai, S. Suzuki, Bull. Chem. Soc. Jpn. 47 (1974) 3074.
[79] F. Cavani, F. Trifirò, Appl. Catal. A 157 (1997) 195.
[80] V.V. Guliants, J.B. Benziger, S. Sundaresan, Stud. Surf. Sci. Catal. 101 (1996) 991.
[81] V.V. Guliants, S.A. Holmes, J. Mol. Catal. A 175 (2001) 227.
[82] V.A. Zazhigalov, E.V. Cheburakova, M. Gansior, J. Stoch, Kinet. Catal. 47 (2006) 803.
[83] G. Centi, V. Lena, F. Trifirò, D. Ghoussoub, C.F. Aissi, M. Guelton, J.P. Bonnelle, J. Chem. Soc. Faraday Trans. 86 (1990) 2775.
[84] K. Brückman, J. Haber, Stud. Surf. Sci. Catal. 75 (1993) 741.
[85] G. Centi, J.M. Lopez Nieto, C. Iapalucci, K. Brückman, E.M. Serwicka, Appl. Catal. 46 (1989) 197.
[86] N.F. Dummer, W. Weng, C. Kiely, A.F. Carley, J.K. Bartley, C.J. Kiely, G.J. Hutchings, Appl. Catal. A 376 (2010) 47.
[87] L. Pérez-Moreno, S. Irusta, J. Soler, J. Herguido, M. Menéndez, Chem. Eng. J. 147 (2009) 330.
[88] U. Bentrup, A. Brückner, C. Rüdinger, H.-J. Eberle, Appl. Catal. A 269 (2004) 237.
[89] U. Bentrup, A. Brückner, M. Fait, B. Kubias, J.B. Stelzer, Catal. Today 112 (2006) 78.
[90] A. Brückner, U. Bentrup, M. Fait, B. Kubias, Catal. Today 99 (2005) 123.
[91] F. Cavani, G. Centi, P. Marion “Catalytic ammoxidation of hydrocarbons on mixed oxides”, in “Metal Oxide Catalysts”, S.D. Jackson, J.S.J. Hargreaves (Eds), Wiley-VCH, Weinheim, 2009, Ch 20, p. 771.
[92] B. Solsona, F. Ivars, P. Concepción, J.M. López Nieto, J. Catal. 250 (2007) 128.
[93] M. Baca, A. Pigamo, J.L. Dubois, J.M.M. Millet, Catal. Comm. 6 (2005) 215.
[94] G. Mestl, Topics Catal. 38 (2006) 69.
[95] I.V. Kozhevnikov, Chem. Rev. 98 (1998) 171.
[96] C.L. Hill, C.M. Prosser-McCartha, Coord. Chem. Rev. 143 (1995) 407.
[97] C.L. Hill, J. Molec. Catal. A 262 (2007) 2.
[98] F.Cavani, Catal. Today 41 (1998) 73.

7

IN-SITU RAMAN SPECTROSCOPY FOR THE CHARACTERIZATION OF V/P/O

7.1 INTRODUCTION

This last chapter of the thesis deals with an in-situ Raman spectroscopic study of V/P/O systems, carried out at the Catalytic Spectroscopy Laboratory, at the Institute of Catalysis and Petrochemistry (ICP), in Madrid.

Since each V/P/O compound (hydrated or dehydrated, having V^{5+}, V^{4+} or V^{3+}) shows a characteristic Raman spectrum [1], Raman spectroscopy represents a very suitable tool for the study of the vanadyl pyrophosphate (VPP). Moreover, the in-situ Raman spectroscopy permits to reproduce reactive atmospheres while simultaneously analysing changes of surface composition. In the literature, different studies using in-situ Raman spectroscopy with VPP catalyst are reported, simulating both the usual reactive atmosphere (n-butane/air) and more unusual ones (in air, or humid air), to boost transformations of the catalyst surface [2-4]; however it's worth to note that an important contribution is devoted, in the literature, to the in-situ Raman study of the process inherent to the transformation of $VOHPO_4\ 0.5H_2O$ (precursor) to VPP (catalyst).

In the present work, in-situ Raman spectroscopy was carried out in order to investigate on unsteady reaction conditions; in particular, the feed composition was varied alternating an oxidant flow (air/He) and a reducing flow (n-butane/He).

The aim of the investigation was to understand the conditions at which a peculiar $VOPO_4$ phase, δ-$VOPO_4$, may form over the catalyst surface. δ-$VOPO_4$, in the form of domains ("patches") dispersed over the VPP surface, is considered to be the active and selective compound for the oxidation of n-butane to maleic anhydride. Its formation is supposed to occur during reaction even though, usually, this compound is not found in the used catalyst, because its formation may be reversible, in function of temperature and gas-phase composition.

In particular, we compared the behaviour of two different catalysts, an undoped VPP and a Nb-doped one.

Moreover we investigated the generation of $VOHPO_4 \cdot 0.5H_2O$, during the "organic" synthesis: a Raman probe (NIR laser) was directly inserted into the mixture synthesis and Raman spectra were collected during all the synthesis period (6h).

7.2 RESULTS AND DISCUSSION

7.2.1 Synthesis and characterization of vanadyl pyrophosphate catalysts

Two catalysts were studied by means of in-situ Raman spectroscopy: both samples were prepared by the organic-route (Chapter 2), using a P/V atomic ratio equal to 1.1. One of the catalyst was promoted by a source of Nb, directly in the mixture of the reactants (Chapter 3). The reference catalyst is called B2 while the Nb-doped one is referred as O80. The in-situ Raman experiments were carried out loading the pellets of the used ("equilibrated") catalyst inside an "operando" reactor. The "operando" reactor and the instrumental configuration (Raman spectrophotometer, heating lines with connections to the gas-cromatograph) are used in the aim of carrying out gas-cromatographic analyses while registering Raman spectra at the same time, in order to infer correspondences between catalytic behavior and surface modifications.

The reactor is made of quartz and the dimensions of the middle part, where the catalytic bed is located, are similar to those of a common tubular micro-reactor (ca. 1,5 cm diameter). The reactor, horizontally positioned, is heated by a heating box with a couple of cartridge heaters: three reactor faces are covered while the remaining one, at the top of the reactor, is exposed to the laser beam. The catalytic bed (0.5 g) is placed at the centre of the reactor and here also a thermocouple is inserted, for a correct temperature reading. The empty space of the reactor is filled with inert material. The entry and the outlet of the small reactor are also heated (200°C), as well as the steel-made lines which connect the reactor to the gas-cromatograph, in order to avoid eventual condensation of products.

The gases, which can be fed independently to the reactor, were n-butane (10% in He), oxygen (pure) and He (pure). By varying the flow ratio between these gases, it was possible to obtain either the usual reactive mixture (1,7% n-butane, 17% of oxygen; W/F=1.33 $g \cdot s \cdot ml^{-1}$), or other compositions (Table 7.1), while maintaining the inert flow constant.

	n-Butane (%)	O_2 (%)	He (%)	He flow (ml/min)	Total flow (ml/min)
Reactive mixture	1,7	17,5	80,8	15	22,5
Oxidizing mixture	-	21	79	15	18,7
Reducing mixture	2,1	-	97,9	15	18,6

Table 7.1_Different gas-phase compositions, for in-situ Raman experiments.

In regard to experiments made to monitor structural changes during the organic synthesis, we used V_2O_5 (99%), H_3PO_4 (99%) and pure isobutanol as reagents for catalyst synthesis. The synthesis was carried out in a three-necks flask (volume capacity 100 ml), similar to the apparatus described in

Chapter 2; the mixture was heated for 6 hours at 120°C (solvent boiling temperature) while stirring; at the same time, Raman spectra were collected by means of the Raman immersion probe.
The NIR laser, utilized as the probe, should avoid the fluorescence phenomenon, which normally affects Raman analysis of organic-containing samples. Being the laser less powerful, in comparison with the laser source utilized for other investigations in the present thesis (Ar ions, 514 nm), the spectra should be quite clear, despite the presence of organics.

7.2.2 In-situ Raman spectroscopy

The first Raman in-situ experiment was carried out by feeding the reactive mixture (Table 7.1) on the doped catalyst, O80 (V/Nb=80). The catalyst was heated up from room temperature (rt) to 300°C, while feeding the mixture; Raman spectra were taken every 20°C (from 100°C to 460°C).
The spectra acquired at 100°C (and at room temperature as well) showed the characteristic bands of vanadyl pyrophosphate (1186, 1138, 924 cm^{-1}), and bands attributable to α_I-$VOPO_4$ (1039, 577, 542 cm^{-1}) (fig.7.1). However, when temperature was increased, the Raman spectrum apparently did not change: spectra recorded at higher temperatures still showed bands of α_I-$VOPO_4$ (the intensity of which increased at 360°C), but bands attributable to any other V/P/O phase were not detected. The increase of temperature led to a broadening and also to a very weak shift of the bands.
However, the asymmetric broadening of the band at 1039 cm^{-1} could indicate a contribution from another V/P/O phase: for example, δ-$VOPO_4$ shows a band at 1020 cm^{-1} but, if the latter compound was present, other contributions should also be visible (e.g., at 1090, 1070 cm^{-1}). Finally, we were not able to detect any change of surface composition during the experiment.

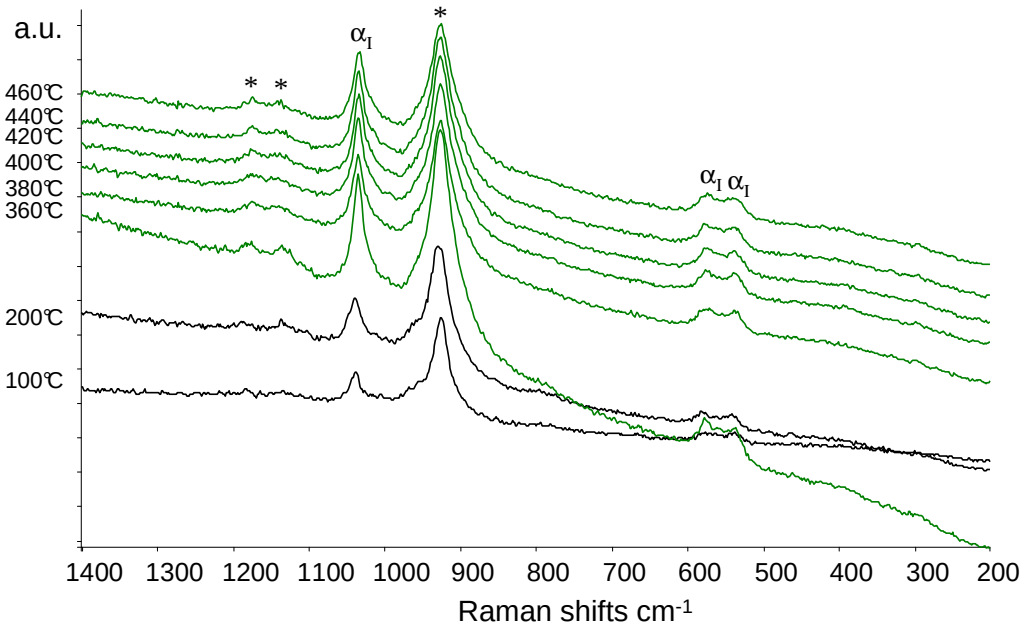

Fig.7.1_In-situ Raman experiment, while feeding the reactive mixture (1,7% n-butane and 17% O_2; W/F=1.33 $g \cdot s \cdot ml^{-1}$) with catalyst O80 (V/Nb=80): spectra from 100°C (bottom) to 460°C (top). Symbols: *= $(VO)_2P_2O_7$; α_I= α_I–$VOPO_4$.

Similar results were also found by Guliants et al. [2] when Raman spectra were recorded during in-situ experiments with a VPP catalyst, under the reactive mixture at low temperatures (25, 260, 345,

380°C). The authors, in order to explain evidences from ex-situ characterizations, proposed that a reversible oxidation of VPP into δ/γ-$VOPO_4$ could be possible, at higher temperature and under n-butane lean conditions (oxidizing conditions). In our case, even at high temperatures, in the reactive mixture (under n-butane lean conditions), it was not possible to observe any other phase except the VPP; furthermore, we also highlighted the high stability of α_I-$VOPO_4$ under reaction conditions.

Indeed, the transformation of the VPP into δ-$VOPO_4$ was an expected phenomenon, especially at high temperature. This compound was hypothesized to be involved in the selective reaction path, by menas of a redox cycle which establishes with the surface of $(VO)_2P_2O_7$ during reaction. The absence of this compound, however, could suggest that the oxidation of the VPP into δ-$VOPO_4$ is the rate-determining step of the redox cycle. This would imply that the process of reduction of δ-$VOPO_4$ to VPP is quite fast, while the oxidation of VPP into δ-$VOPO_4$ is slower.

The following tests were carried out with the aim of confirming the formation of δ-$VOPO_4$, the development of which should be favoured under an oxidizing atmosphere. The treatment was carried out by feeding an oxidizing flow (Table 7.1) on the O80 sample (a different position of the laser beam on the sample powder was chosen, with respect to experiments carried out under reactive atmosphere – fig.7.1).

The catalyst was heated up to 440°C in the reactive atmosphere, and then the n-butane flow was withdrawn (fig.7.2). Spectra recorded showed solely the presence of α_I-$VOPO_4$, both in the reactive mixture and in the oxidizing atmosphere: no changes of surface composition apparently occurred, even after waiting for a long period of time. However, it must be considered that the noise and the drift of the signal could cover weak signals of any other V/P/O compound formed in small amount on the catalyst surface.

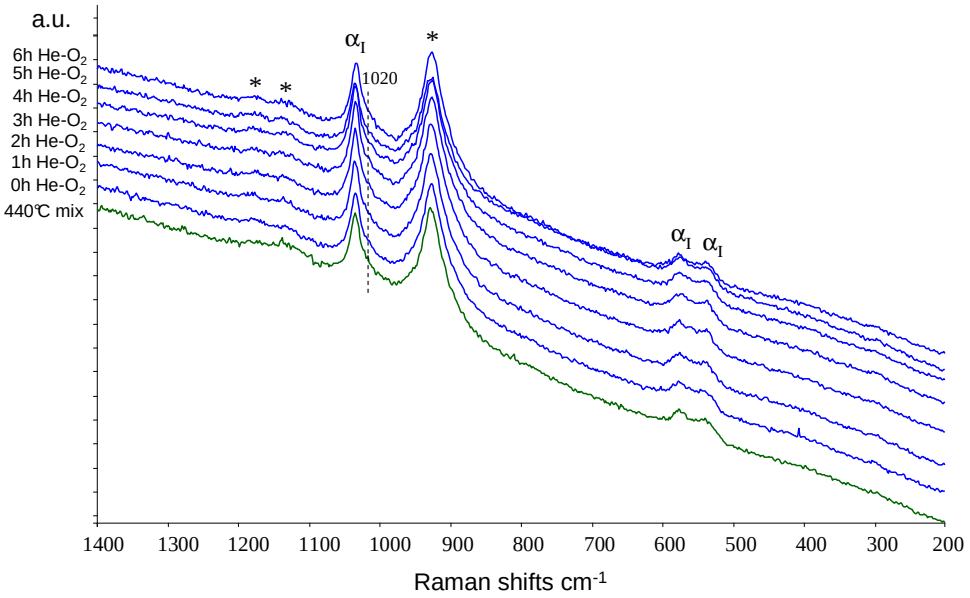

Fig.7.2_In-situ Raman experiment, with catalyst O80 (V/Nb=80), while feeding the reactive mixture (1,7% n-butane and 17% O_2) at 440°C (bottom) and then feeding an oxidizing flow (Table 7.1) at 440°C, from 0h to 6h (top). Symbols: *= $(VO)_2P_2O_7$; α_I= α_I–$VOPO_4$.

Stronger conditions were then used to boost surface changes: in order to favour the oxidation of VPP surface, the loaded catalyst was heated up to 440°C in the reactive mixture and then, after withdraw of n-butane, an humid oxidizing flow was fed (10% mol. water vapour and 21% mol. of oxygen in He, Table 7.1), at 440-500°C. Figures 7.3-7.4 show the Raman spectra registered: unexpectedly, α_I-$VOPO_4$ (band at 1036 cm^{-1}) remained during all the experiment, and no other V/P/O oxidized phase formed.

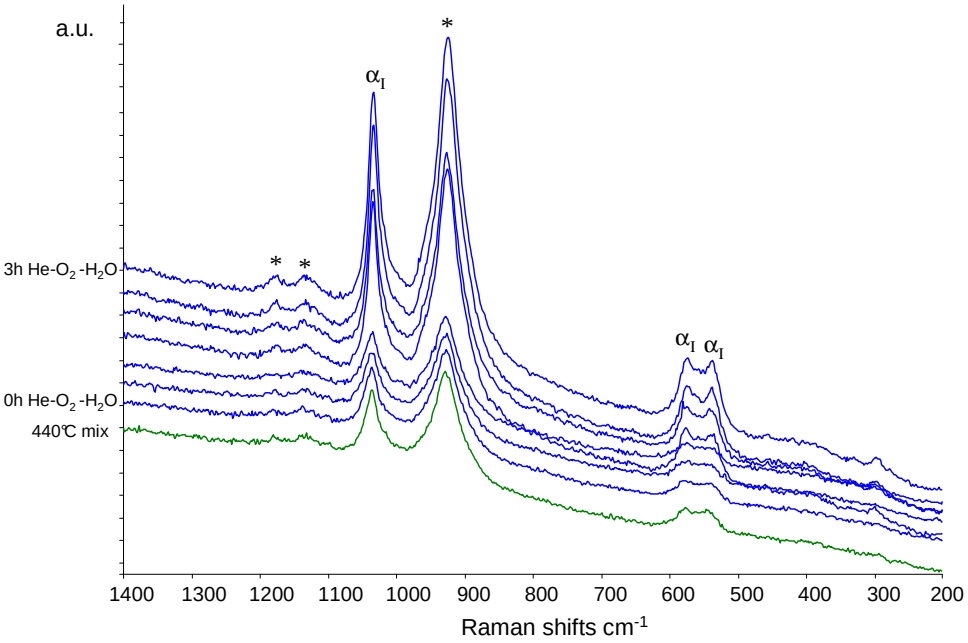

Fig.7.3_In-situ Raman experiment, with catalyst O80 (V/Nb=80), while feeding the reactive mixture (1,7% n-butane and 17% O_2) at 440°C (bottom), then feeding the oxidizing humid flow (Table 7.1) at 440°C, from 0h to 3h (top). Symbols: *= $(VO)_2P_2O_7$; α_I= α_I–$VOPO_4$.

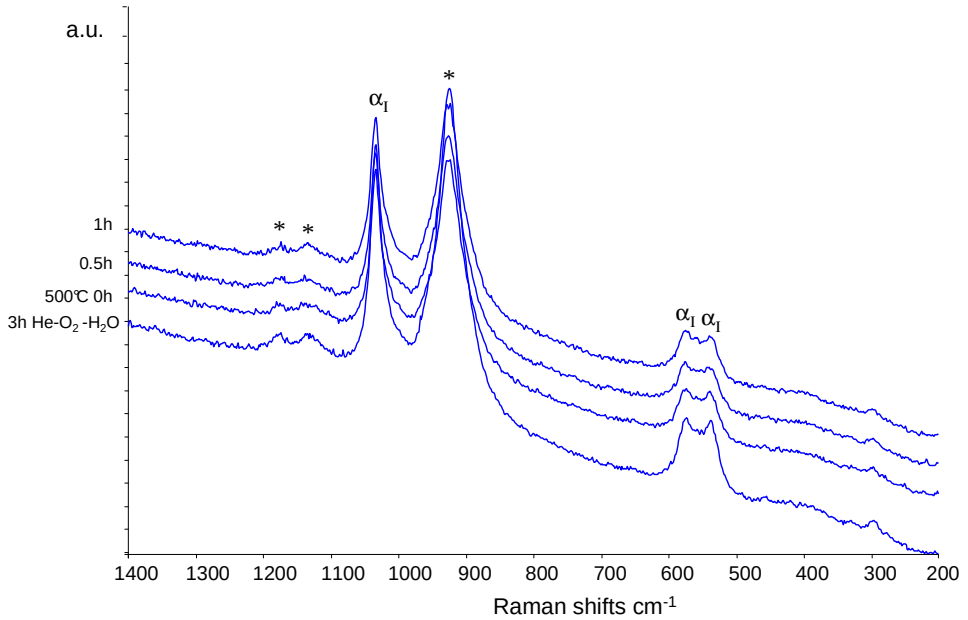

Fig.7.4_In-situ Raman experiment, with catalyst O80 (V/Nb=80), while feeding the humid oxidizing flow (Table 7.1) at 440°C (bottom) then at 500°C, from 0h to 1h (top). Symbols: *= $(VO)_2P_2O_7$; α_I= α_I–$VOPO_4$.

One additional in-situ experiment was carried out starting directly with the oxidizing flow and changing the position of the beam on the catalyst surface. It must be noted that the catalyst, during all these experiments, was never downloaded from the operando reactor.

The catalyst was heated up to 440°C in the oxidizing flow (fig.7.5); once the temperature of 440°C was reached, δ-$VOPO_4$ formed (1080, 1015, 587 cm^{-1}), but α_I-$VOPO_4$ was still present (1034 cm^{-1}). Interestingly, during the isothermal period the intensity of bands attributed to δ-$VOPO_4$ grew further, while the intensity of the band attributable to α_I-$VOPO_4$ correspondingly decreased (fig.7.5). The band at 996 cm^{-1} is attributable to α_{II}-$VOPO_4$. After 45 minutes, the reactive mixture was fed and instantaneously, as witnessed by the Raman spectrum, a relevant transformation occurred: the δ-$VOPO_4$ disappeared and a clear signal relative to α_I-$VOPO_4$ was restored (fig.7.6).

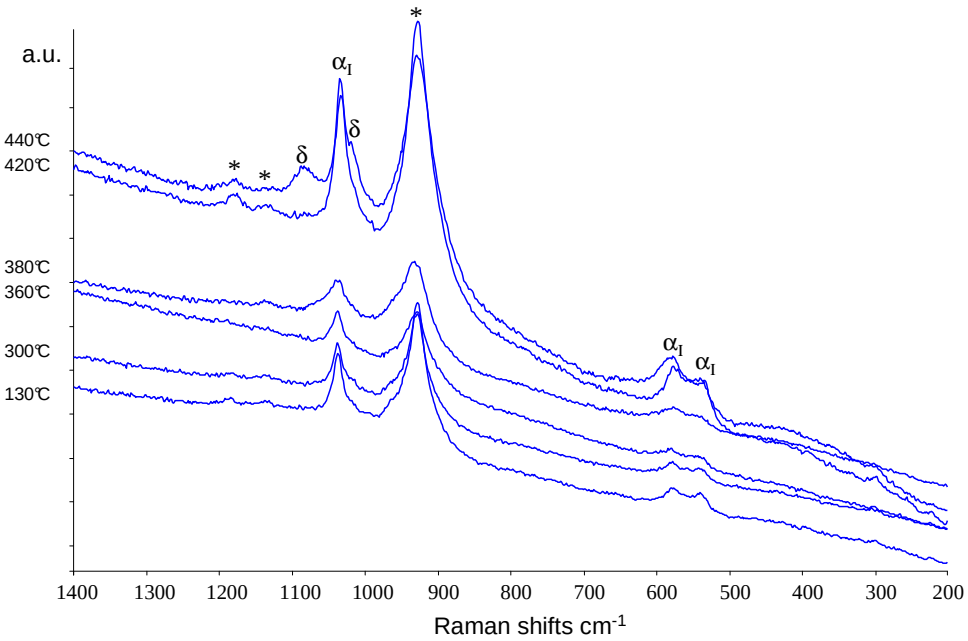

Fig.7.5_In-situ Raman experiment, with catalyst O80 (V/Nb=80), while feeding the oxidizing flow (Table 7.1) from room temperature up to 440°C (top). Symbols: *= $(VO)_2P_2O_7$; α_I= α_I–$VOPO_4$; δ= δ–$VOPO_4$.

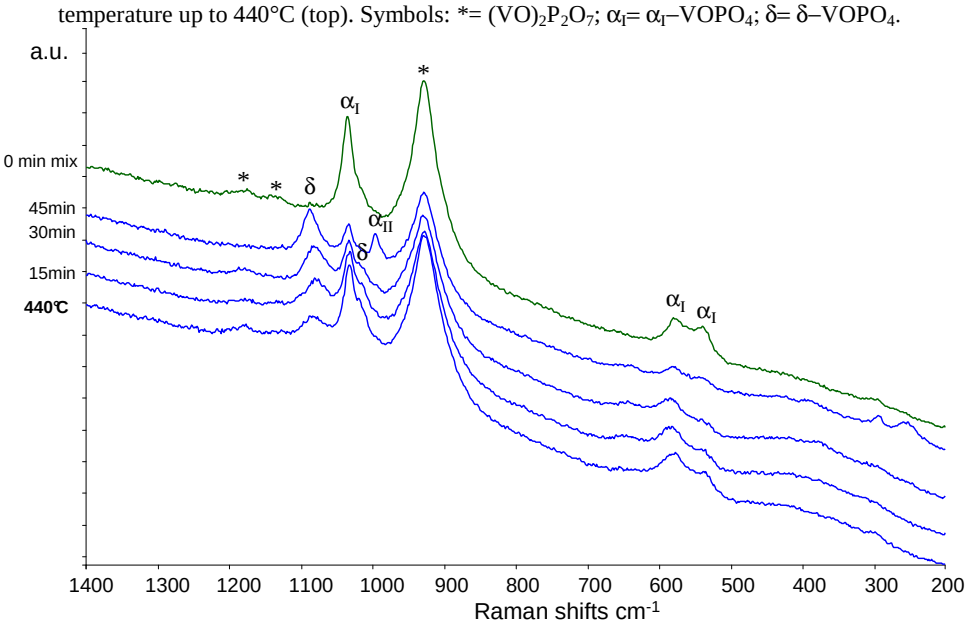

Fig.7.6_In-situ Raman experiment, with catalyst O80 (V/Nb=80), while feeding the oxidizing flow (Table 7.1) at 440°C (bottom) from 0 min to 45 min, and then feeding the reactive mixture (Table 7.1) (top). Symbols: *= $(VO)_2P_2O_7$; α_I= α_I–$VOPO_4$; α_{II}= α_{II}–$VOPO_4$; δ= δ–$VOPO_4$.

The spectra acquired showed that surface changes involved different phases: the intensity of the most intense bands attributable to VPP and α_I-$VOPO_4$ decreased during the oxidizing period; on the opposite, the intensity of the broad band centred at 1080 cm^{-1} increased. This latter band may be a result of the combination of characteristic bands of δ-$VOPO_4$ (at 1090 and 1075 cm^{-1}) and of α_{II}-$VOPO_4$ (1091 cm^{-1}); indeed, at this surface spot we observed the formation of α_{II}-$VOPO_4$. In this regard, it is interesting to note that the evidence for the transformation of δ-$VOPO_4$ into α_{II}-$VOPO_4$ under reactive flow (2,4% of n-butane in air) was also described in the literature [3]: it is likely that this transformation also occurred during our experiment, even though at a partial extent only.

In the presence of the reducing agent (n-butane), that is, of a less oxidizing atmosphere, the α_{II}-$VOPO_4$ and δ-$VOPO_4$ (traces) were reduced into VPP (whose signal returned to the original intensity), and also the α_I-$VOPO_4$ band restored its original intensity.

The experiment was continued by focussing the beam on other surface dots: when the δ-$VOPO_4$ was present, during the isothermal step under the oxidizing flow, the intensity of the corresponding bands did not increase, and the formation of α_{II}-$VOPO_4$ did not occur, but the intensities of α_I-$VOPO_4$ and VPP bands decreased. Then, when the reducing flow was fed (Table 7.1), δ-$VOPO_4$ bands still were unaffected, while α_I-$VOPO_4$ and VPP bands recovered their original intensities.

These data can be interpreted by assuming a surface heterogeneity of the sample; when the beam was focussed on a surface containing α_I-$VOPO_4$ as the predominant compound, no reaction occurred, because α_I-$VOPO_4$ is unreactive, and also covered the VPP hindering its oxidation. When instead the beam was focussed on a spot where some fraction of the VPP was exposed to the gas phase, the VPP was readily oxidized into the δ-$VOPO_4$; the latter however was then reduced when the reactive stream was flown. Some surface positions were reactive (showing weak signals due to δ-$VOPO_4$ formation), but some others resulted to be totally unaffected by the oxidizing treatment. Moreover, in some positions the δ-$VOPO_4$ phase (either already present in the used catalyst or formed during previous oxidizing treatments) turned out to be quite stable, since the intensity of the corresponding bands did not change neither during the oxidizing period, nor in the presence of the reducing flow. Even in this case, differences observed in the reactivity of δ-$VOPO_4$ can be attributed to differences of crystallinity and/or of exposure to the gas phase.

The following in-situ Raman treatments were carried out in the attempt of understanding the reactivity of surface δ-$VOPO_4$, by using more reducing conditions, that is by feeding the reactive flow without oxygen (Table 7.1). In such a way, we splitted the redox process into the two separate steps, of V^{5+} reduction by the hydrocarbon and of reoxidation of the V^{4+} by oxygen (fig. 7.7).

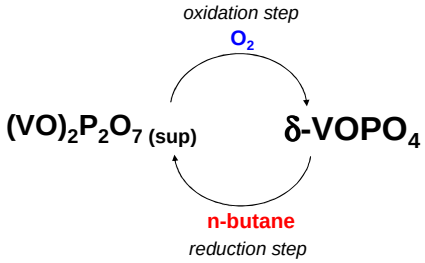

Fig.7.7_Hypothetic redox mechanism between superficial $(VO)_2P_2O_7$ and δ–$VOPO_4$ phases, during reaction: first VPP is converted by molecular oxygen to δ–$VOPO_4$ (oxidation step), then this phase is reduced to VPP by n-butane (reduction step).

The catalyst was heated up to 440°C in the oxidizing flow and then left under isothermal conditions (440°C) to monitor an eventual increase of the intensity of δ-$VOPO_4$ bands (at this surface position, δ-$VOPO_4$ was already present even in the spectrum registered at room temperature) (fig.7.8); one hour later, we fed the reducing flow (table 7.1). As shown in figure 7.9, a very quick decrease of intensity of δ-$VOPO_4$ bands and then of α_I-$VOPO_4$ band also, occurred; moreover, also the intensity of the strongest VPP band was affected.

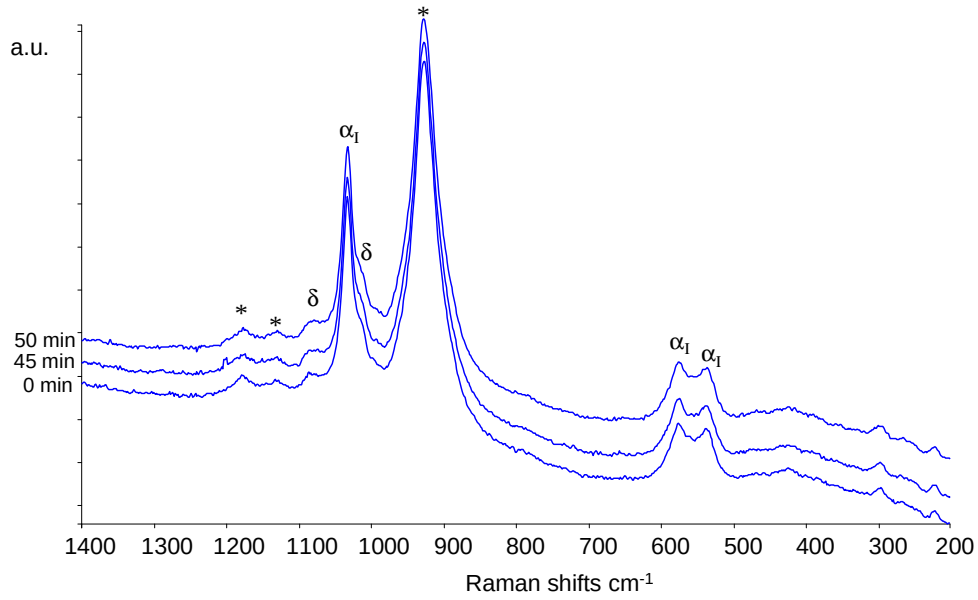

Fig.7.8_In-situ Raman experiment, with catalyst O80 (V/Nb=80), while feeding the oxidizing flow (Table 7.1) at 440°C from 0 min (bottom) to 50 min (top). Symbols: *= $(VO)_2P_2O_7$; α_I= α_I–$VOPO_4$; δ= δ–$VOPO_4$.

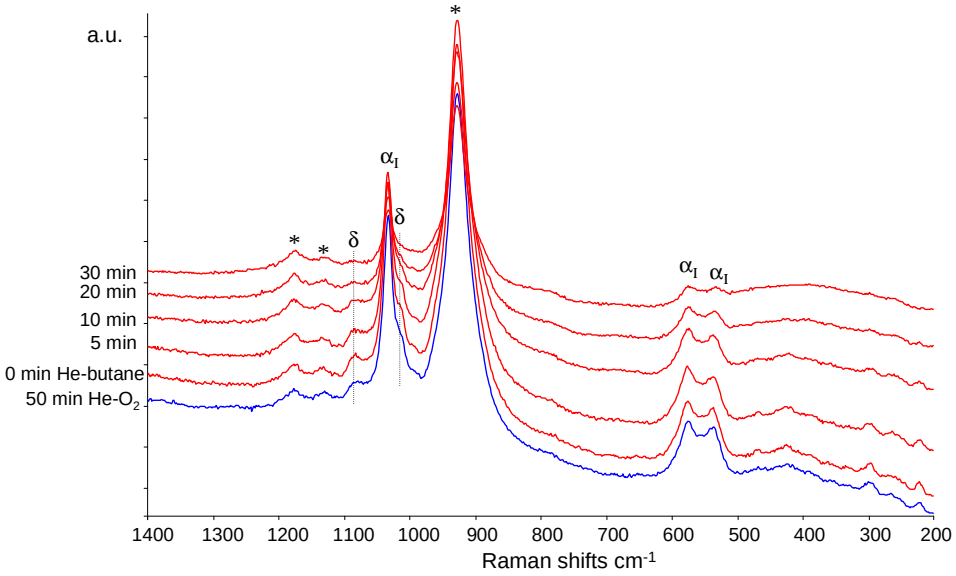

Fig.7.9_In-situ Raman experiment, with catalyst O80 (V/Nb=80), while feeding the oxidizing flow (Table 7.1), after 50 min, at 440°C (bottom), and then feeding the reducing flow (Table 7.1) from 0 min to 30 min (top). Symbols: *= $(VO)_2P_2O_7$; α_I= α_I–$VOPO_4$; δ= δ–$VOPO_4$.

The subsequent step, carried out to simulate the redox cycle (fig.7.7), was executed by feeding again the oxidizing flow, after some minutes of purging in inert flow (pure He). The spectra recorded during the second oxidizing step (fig.7.10), showed the development of δ-$VOPO_4$, α_I - $VOPO_4$ and VPP bands, already observed during the first oxidizing step (fig.7.8). However it was not possible to restore the original intensities, which indicates that the reducing treatment had remarkably affected the catalyst surface; in other words, the treatment with the reducing stream changed more profoundly the surface features than the reactive stream did.

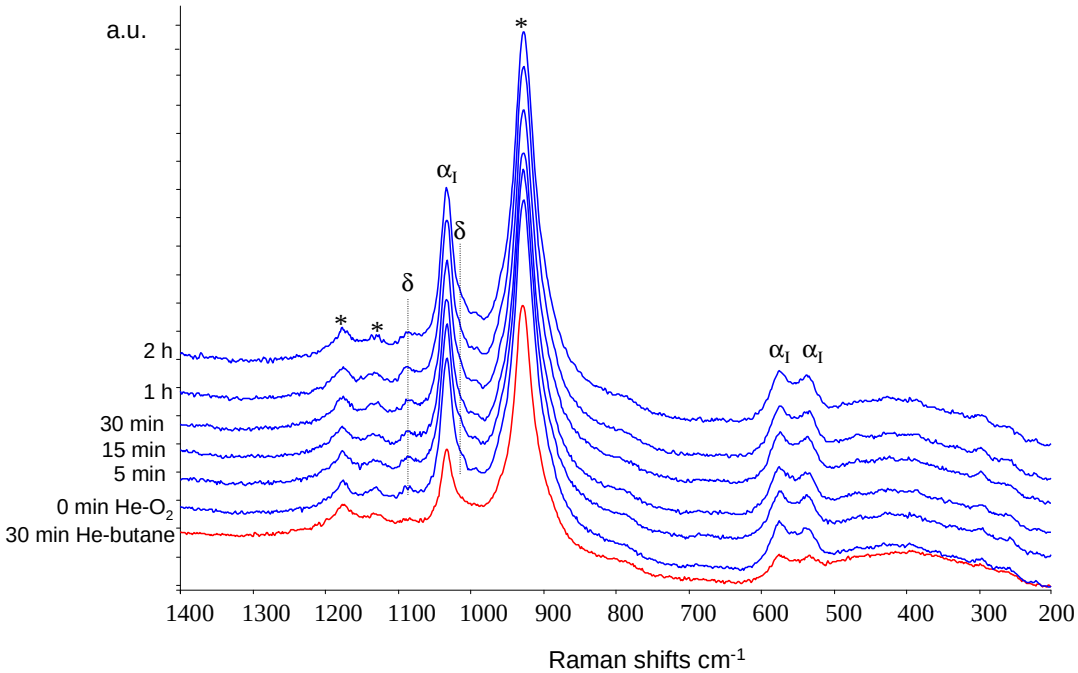

Fig.7.10_In-situ Raman experiment, with catalyst O80 (V/Nb=80), while feeding the reducing flow (Table 7.1) after 30 min at 440°C (bottom), and then feeding the oxidizing flow from 0 min to 2 h (top). Symbols: *= $(VO)_2P_2O_7$; α_I= α_I–$VOPO_4$; δ= δ–$VOPO_4$.

This experiment can be considered as a TPR-O cycle, in which oxygen is the oxidizing species and n-butane is the reducing one towards the δ-$VOPO_4$; the experiment clearly indicates that the reducing step is faster compared to the oxidizing one, which may explain the scarce reactivity observed during the oxidizing treatment, and also confirms our hypothesis that the reoxidation step (of VPP into δ-$VOPO_4$) is the rate-determining one.

The experiment was repeated once more: the catalyst was heated up to 440°C in the oxidizing flow (fig.7.11), but the bands of δ-$VOPO_4$ and of the other VPO phases maintained similar relative intensities; then the reducing flow was added (fig.7.12) and almost instantaneously all the bands showed a decrease of intensity, although some of them were more affected (apparently, those of δ-$VOPO_4$) than others. Finally, the oxidizing flow was fed again to the reactor, but bands only partially recovered their original intensity, the latter being quite lower compared to that shown in the last spectrum registered after the first step oxidizing treatment (fig.7.13). Finally, the reactive mixture was fed, in the aim of observing a different behaviour compared to that shown while feeding the reducing flow (fig.7.14): no change apparently occurred (at least after 1 hour in isotherm with the reactive mixture), but an increase of intensity of all bands, especially those characteristic of VPP, was shown.

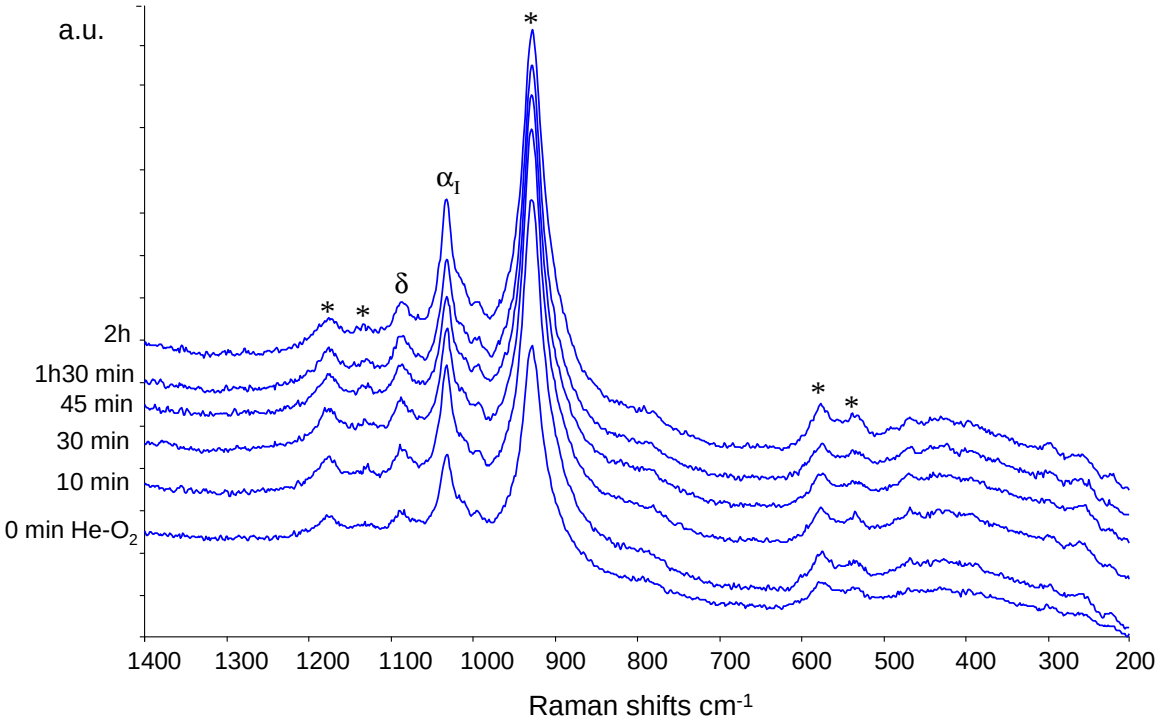

Fig.7.11_In-situ Raman experiment, with catalyst O80 (V/Nb=80), while feeding the oxidizing flow (Table 7.1) from 0 min (bottom) to 2 h (top). Symbols: *= $(VO)_2P_2O_7$; α_I= α_I–$VOPO_4$; δ= δ–$VOPO_4$.

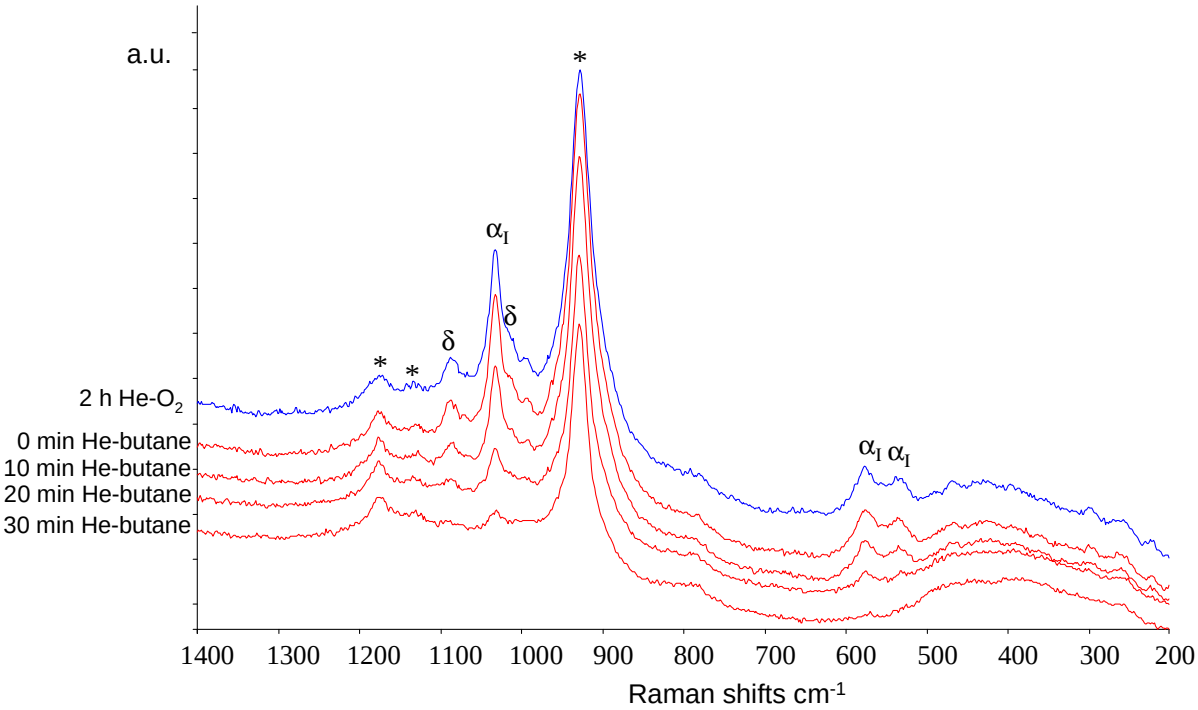

Fig.7.12_In-situ Raman experiment, with catalyst O80 (V/Nb=80), while feeding the oxidizing flow (Table 7.1) after 2 h at 440°C (top), and then feeding the reducing flow from 0 min to 30 min (bottom). Symbols: *= $(VO)_2P_2O_7$; α_I= α_I–$VOPO_4$; δ= δ–$VOPO_4$.

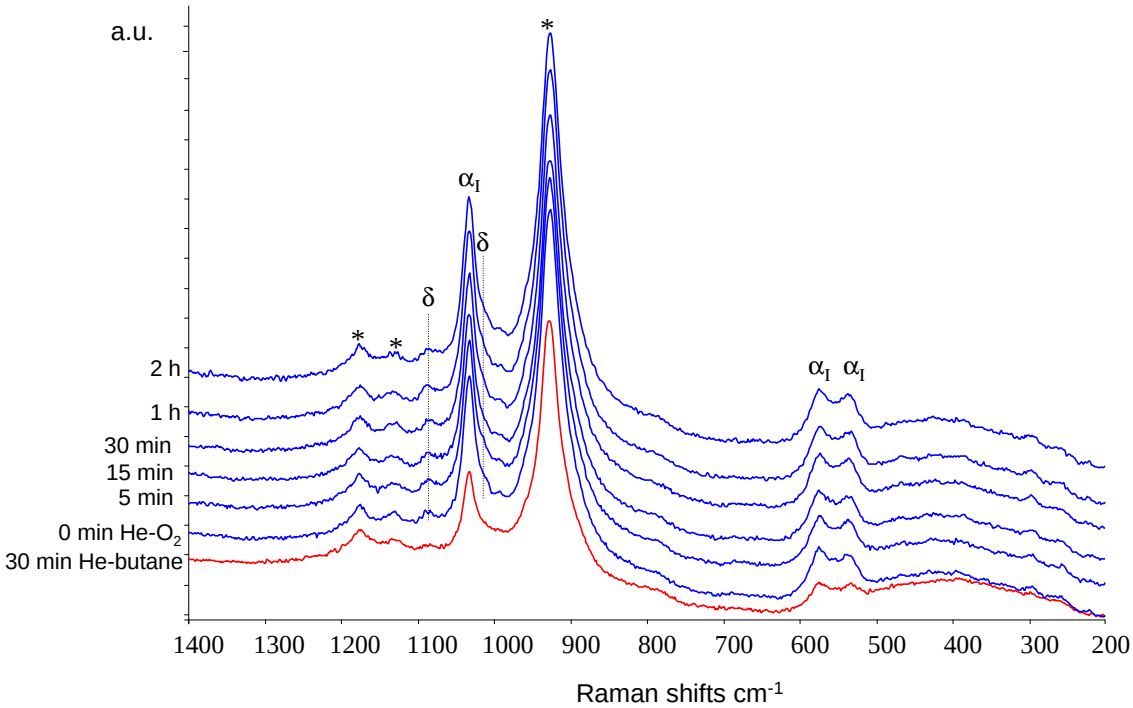

Fig.7.13_In-situ Raman experiment, with catalyst O80 (V/Nb=80), while feeding the reducing flow (Table 7.1), after 30 min at 440°C (bottom), and then feeding the oxidizing flow from 0 min to 2 h (top). Symbols: *= $(VO)_2P_2O_7$; α_I= α_I–$VOPO_4$; δ= δ–$VOPO_4$.

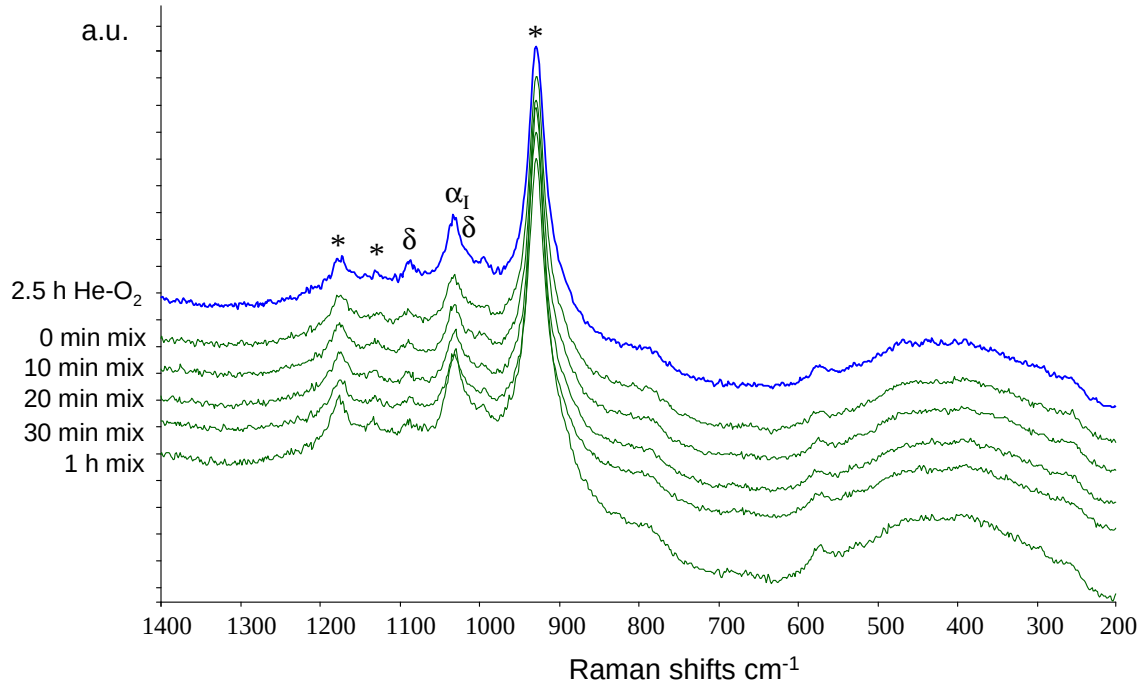

Fig.7.14_In-situ Raman experiment, with catalyst O80 (V/Nb=80), while feeding the oxidizing flow (Table 7.1) after 2.5 h at 440°C (top), and then feeding the reactive mixture from 0 min to 1 h (bottom). Symbols: *= $(VO)_2P_2O_7$; α_I= α_I–$VOPO_4$; δ= δ–$VOPO_4$.

Even though the results obtained during this last experiment, better summarized in figures 7.15-7.16, and those obtained during the previous in-situ treatment, did not permit to reproduce exactly the redox cycle between δ-$VOPO_4$ and VPP (because also other $VOPO_4$ phases turned out to be involved, and because the VPP appeared to be modified irreversibly during the reducing step with n-butane/He only), however the results clearly demonstrate that some compounds are reducible and reoxidizable under conditions simulating the redox process.

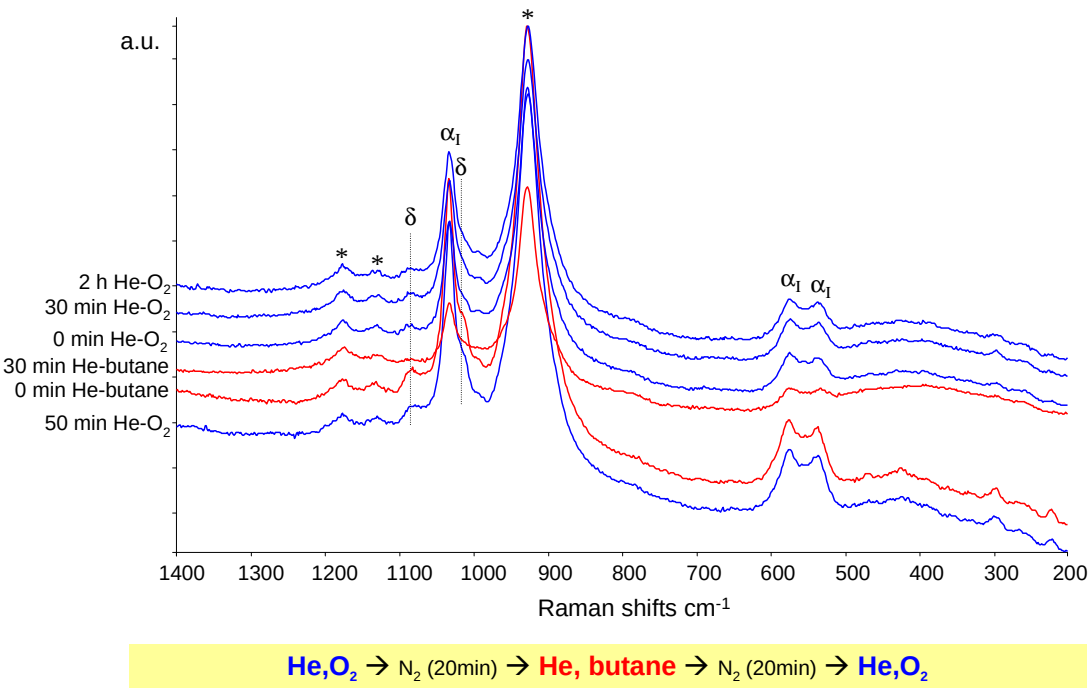

Fig.7.15_ Summary: in-situ Raman experiment, with catalyst O80 (V/Nb=80), while feeding in sequence (from bottom to top): the oxidizing flow, the reducing flow and finally the oxidizing flow (Table 7.1). Symbols: *= $(VO)_2P_2O_7$; α_I= α_I–$VOPO_4$; δ= δ–$VOPO_4$.

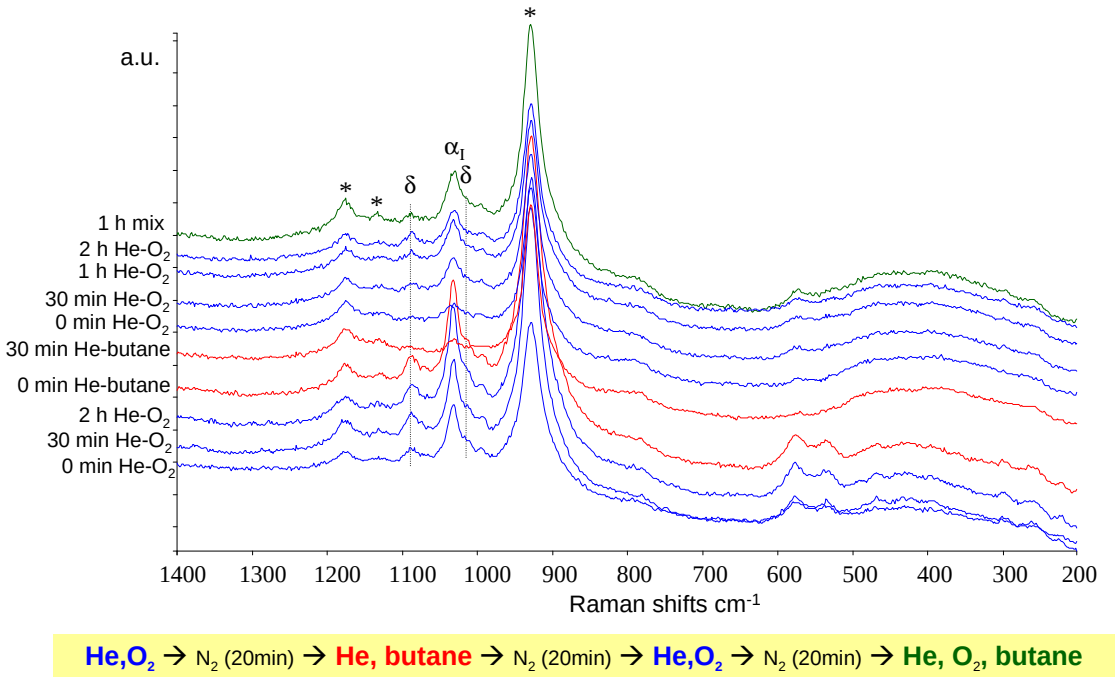

Fig.7.16_ Summary: in-situ Raman experiment, with catalyst O80 (V/Nb=80), while feeding in sequence (from bottom to top): the oxidizing flow, the reducing flow, the oxidizing flow and finally the reactive mixture (Table 7.1). Symbols: *= $(VO)_2P_2O_7$; α_I= α_I–$VOPO_4$; δ= δ–$VOPO_4$.

In-situ Raman experiments were also carried out with the used B2 sample, the reference undoped catalyst (Chapter 3, par. 3.2.3). The first experiment was carried out by feeding the reactive mixture (Table 7.1) and recording Raman spectra from room temperature up to 460°C. The results are reported in figure 7.17: the registered spectrum did not change, still showing bands characteristic of VPP and α_I–$VOPO_4$, similarly to what already observed for catalyst O80.

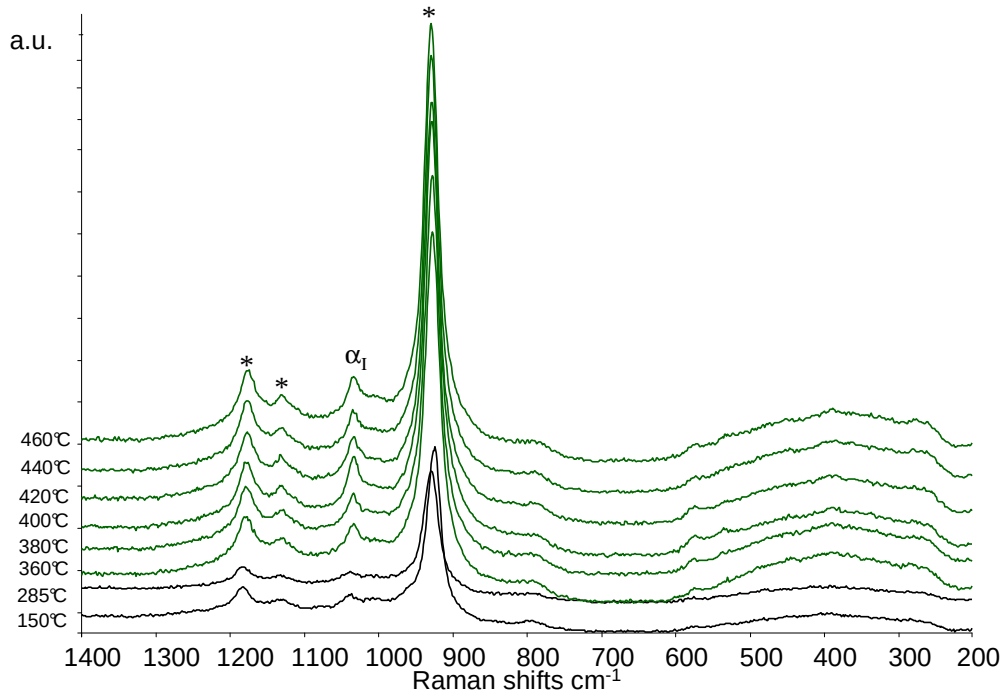

Fig.7.17_In-situ Raman experiment, while feeding the reactive mixture (1,7% n-butane and 17% O_2; W/F=1.33 g·s·ml^{-1}) with catalyst B2 (Nb=0): spectra recorded from 150°C (bottom) to 460°C (top). Symbols: *= $(VO)_2P_2O_7$; α_I= α_I–$VOPO_4$.

The successive experiment was similar to that one already carried out with sample O80: figures 7.18-7.19 report the spectra registered after a long isothermal period in an oxidizing flow, and then spectra obtained after feeding the reaction mixture, respectively. In contrast with what observed with sample O80, the intensity of bands attributable to δ-$VOPO_4$ decreased during the feeding of the reactive mixture. When the reducing flow was used (fig.7.19), the bands of α_I-$VOPO_4$ very rapidly disappeared, while bands at 1080 cm^{-1} and at 990 cm^{-1} attributable to α_{II}-$VOPO_4$ (being however the first one also attributable to δ-$VOPO_4$) remained unaffected. Another important point is that when the oxidizing flow was fed, the previously reduced $VOPO_4$ compounds did not reform.

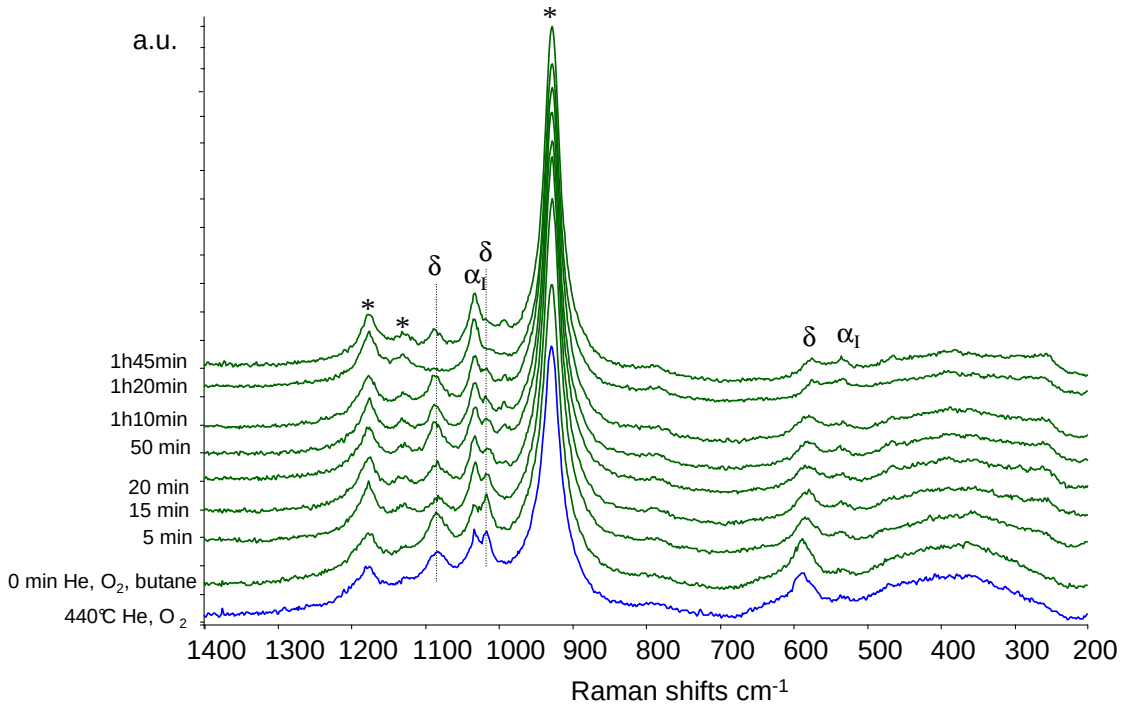

Fig.7.18_In-situ Raman experiment with catalyst B2 (Nb=0) at 440°C, while feeding the oxidizing mixture (Table 7.1) then the reactive mixture from 0 min to 1h45min (top). Symbols: *= $(VO)_2P_2O_7$; α_I= α_I–$VOPO_4$; δ= δ–$VOPO_4$.

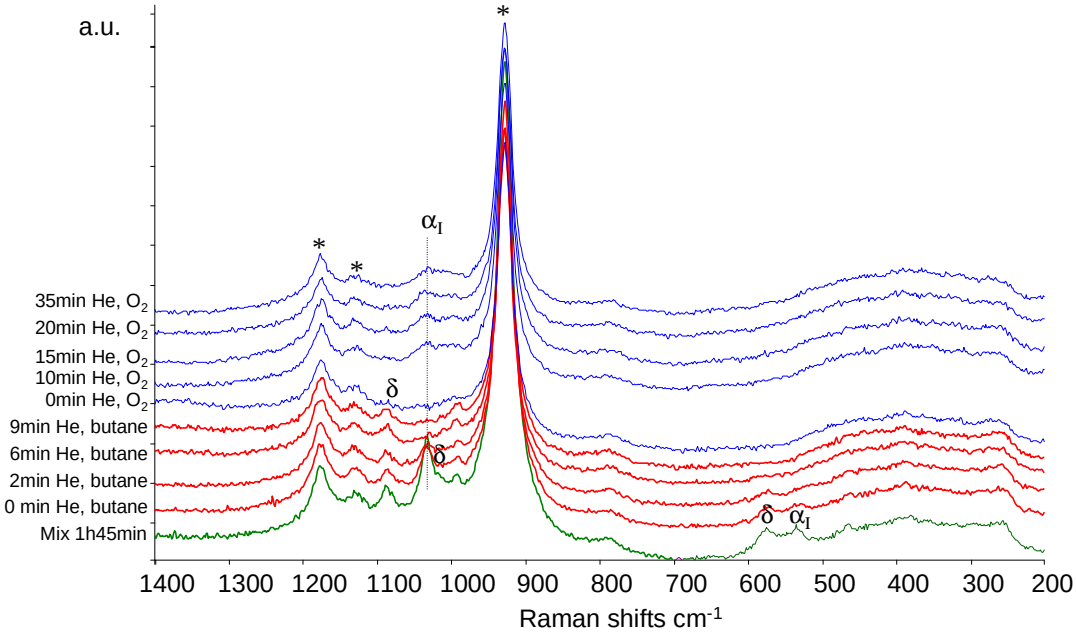

Fig.7.19_In-situ Raman experiment with catalyst B2 (Nb=0) at 440°C, while feeding the reactive mixture (bottom), then the reducing flow (intermediate spectra), and finally the oxidizing flow from 0 min to 35 min (top). Symbols: *= $(VO)_2P_2O_7$; α_I= α_I–$VOPO_4$; δ= δ–$VOPO_4$.

This latter experiment showed a difference between the doped and the undoped catalyst: the catalyst without Nb (B2) turned out to be more easily reducible; in fact, the $VOPO_4$ phase (in particular, α_I-$VOPO_4$) was strongly affected by the reducing treatment; moreover, these compounds were not reoxidized during the oxidizing treatment.

In conclusion, the in-situ Raman experiments allowed us to confirm some important hypothesis, and also add further information regarding the redox processes occurring at the heterogeneous surface of the V/P/O catalyst. With the undoped catalyst (sample B2), the reduction of V^{5+} phase is very

rapid, and the reoxidation step is very slow, and probably it occurs only at a very minor extent. The addition of Nb renders the reoxidation of the reduced V^{4+} species much easier (quicker); this implies that under steady-state reaction conditions, the catalyst surface of the Nb-doped catalyst is in average more oxidized than that of the undoped sample, which is totally in agreement with experimental evidences already obtained for the Nb-doped VPP systems. This can explain the better selectivity observed with Nb-doped samples: the redox cycle between VPP and δ-$VOPO_4$ is the selective one, allowing the transformation of n-butane into MA. The formation of CO_x may instead occur over other sites, eventually involving O species other than the O^{2-} in δ-$VOPO_4$, as also proposed in the literature. The acceleration of the rate-determining step in the selective redox cycle finally leads to a quicker rate of MA formation as compared to the rate of by-products formation, and finally to a better selectivity to MA.

The in-situ Raman characterization of the mixture during the synthesis of the vanadyl hydrogen phosphate (VHP) is described in the following part.
Raman spectra shown in figure 7.20 were registered during the evolution of the synthesis from the very first moment (first spectrum showing vanadium oxide bands) up to 40 minutes reaction time; spectra were registered every minute. Bands relative to isobutanol –IBA- (at 1463, 1449, 1368, 1341, 1297, 1249, 1175, 1126, 1050, 961, 942, 922, 900, 820, 785, 494, 420, 360 cm^{-1}) are clearly visible in the first spectrum in figure 7.20; the successive spectrum shows the presence of V_2O_5 (bands at 995, 704, 530, 480, 405, 303, 284 cm^{-1}), which was added first to the organic mixture; the third spectrum was recorded after H_3PO_4 addition; however, it was not possible to observe any new band, attributable to this latter compound. The ex-situ Raman spectrum of phosphoric acid was registered before the experiment and showed an intense band at 920 cm^{-1}: this band is apparently absent in the Raman spectrum of the mixture probably because it was covered by IBA bands between 900 and 950 cm^{-1}. Raman spectra taken at longer synthesis time have not been reported because it was not possible to distinguish the bands any more, due to the formation of a turbid solution which affected Raman spectrum resolution. However, already after less than 60 minutes, interesting changes occurred: some bands relative to IBA were still present, but some disappeared (1370, 1042, 900, 420, 350 cm^{-1}); on the other hand, new bands appeared (at 1378, 1188, 1027, 965, 930 cm^{-1}).

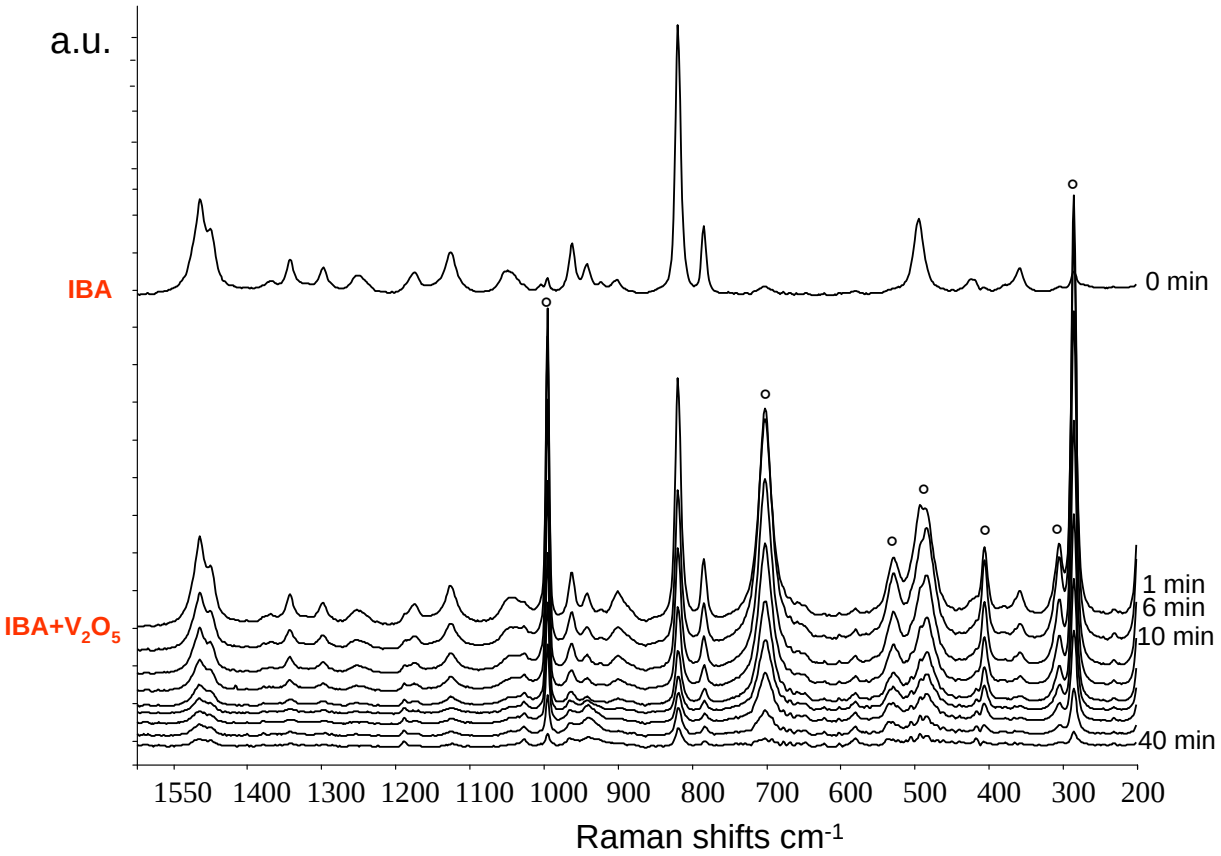

Fig.7.20_ In-situ Raman spectra during synthesis of $VOHPO_4 \cdot 0.5H_2O$. Spectra registered after addition of isobutanol (top), then of V_2O_5 (second spectrum from top) and subsequent spectra acquired every 5 min, until 40 min of synthesis. Symbols: °=V_2O_5.

The attribution of these new bands is quite difficult, also considering that during this part of the synthesis (reaction time shorter than 1h), the vanadium oxide was being reduced by the alcohol (IBA), forming vanadyl(IV) species and organic oxygenated compounds. Therefore, it can be hypothesized that no VPO compound had formed. The new bands were probably related to some compounds deriving from IBA oxidation, which was however the species present in the greater amount.

The successive spectra are not reported, because they were affected by an intense noise and could not provide any additional information. It must be noted that the bad quality of the spectra was not related to the dirtying of the probe window, which finally turned out to be clean. The synthesis was terminated after six hours of solvent refluxing, then filtered, washed and characterized by means of Raman spectroscopy. The dried precursor resulted to contain the $VOHPO_4 \cdot 0.5H_2O$ phase only.

In conclusion, in-situ Raman analysis of the VHP organic preparation is suitable only at the beginning of the synthesis procedure, to monitor changes of the composition of the liquid phase; the experiment could not provide important informations, which were instead gained with other in-situ techniques [5].

7.3 ACKNOWLEDGMENTS

I’m very grateful to prof. doc. M.A.Bañares and his team for their kindness, their participation, and for allowing me to use the Raman ”operando” and in-situ equipments.

7.4 REFERENCES

[1] V.V. Guliants, J.B. Benziger, S. Sundaresan, I.E. Wachs, J.M. Jehng, J.E. Roberts, Catal. Today 28 (1996) 275.

[2] V.V. Guliants, S.A. Holmes, J.B. Benzinger, P. Heaney, D. Yates, I.E. Wachs, J. Mol. Cat. A: Chemical 172 (2001) 265.

[3] Z.-Y. Xue, G.L. Schrader, J. Phys. Chem. B 103 (1999) 9459.

[4] F. Ben Abdelouahab, R. Olier, N. Guilhaume, F. Lefebvre, J.C. Volta, J. Catal. 134 (1992) 151.

[5] L. O'Mahony, J. Henry, D. Sutton, T. Curtin, B.K. Hodnett App. Cat. A: General 253 (2003) 409.

8

CONCLUSIONS

Several topics have been investigated and discussed in this thesis, with the focus being put especially on the study of new tools to improve the catalytic behaviour of vanadyl pyrophosphate (VPP) in n-butane oxidation into maleic anhydride (MA), and on a new process for the synthesis of MA starting from a bio-based building block, 1-butanol. All the part dealing with VPP catalyst for n-butane oxidation has been possible thanks to the financial and scientific support of Polynt S.p.A. The part dealing with the use of 1-butanol was carried out in the framework of a Large Collaborative Project supported by the FP7 program of the EC (EuroBioRef).

In regard to the tools for improving the catalytic performance of VPP, I have used various approaches:

(a) An approach aimed at the study of the effect of an element, Nb^{5+}, a promoter for the VPP; more specifically, I have studied the role of the amount of Nb, and how its presence may affect the generation of the active and selective V^{5+}/P/O compound at the surface of the VPP under reaction conditions. In fact, it is known that the true active phase involves the contribution of both VPP and δ-$VOPO_4$. In order to investigate this aspect, I have used both ex-situ and in-situ characterisation techniques. This part is described in Chapter 3. One important output of this chapter is that the presence of Nb indeed may favour, under specific conditions, the generation of the desired δ-$VOPO_4$ compound; therefore, I tried to synthesize this latter compound, in order to check whether the addition of Nb might enhance its generation via formation of some mixed V/Nb phosphate. I demonstrated that the formation of such solid solution is possible only under specific conditions, with a limited reciprocal dissolution, but I could not draw any clear conclusion on whether the formation of this mixed compound may indeed be the reason for the preferred formation of the δ-$VOPO_4$ in close redox interaction with the VPP. This part is discussed in Chapter 4.

(b) An approach aimed at finding a new procedure for the synthesis of $VOHPO_4.0.5H_2O$, the precursor of VPP. In collaboration with the University of Pisa (prof. Anna Maria Raspolli Galletti and co-workers) and with the scientific aid of Polynt S.p.A., a new method using microwave heating of the synthesis slurry was set up. This method showed several

advantages as compared to the classic thermal method, and allowed obtain VPP catalyst showing very good catalytic performance. This study is described in Chapter 5.

(c) Chapter 6 deals with a preliminary study aimed at checking the feasibility of a new process, for the oxidehydroation of 1-butanol (a bio-alcohol obtained by fermentation) into maleic anhydride. I studied various catalysts for this reaction, and finally that one giving the best performance was still based on VPP. However, the selectivity obtained was by far lower than that obtained from n-butane.

(d) Finally, chapter 7 deals with an in-situ/operando Raman study of the Nb-doped and undoped catalyst, which was carried out during my stage abroad, at the CSIC laboratory in Madrid (Dr. M.A. Bañares). This study allowed obtaining the experimental proof that the redox cycle involves the VPP and the δ-$VOPO_4$ compounds, that the reoxidation step of V^{4+} in VPP is the rate-determining one, and that the presence of Nb may accelerate the rate of this latter step. On the other hand, it was also an output of this study that the surface heterogeneity of these V/P/O samples may on one hand represent a hurdle for the clear identification of the active and selective compounds, on the other hand may explain the relatively low selectivity obtained in n-butane oxidation.

Some important aspects are now discussed more in detail.

The role of Nb as the promoter for VPP. In Chapter 3, a series of Nb-doped VPP catalysts were synthesized and characterized, in particular by means of ex-situ and in-situ Raman spectroscopy. We found that the role of Nb dopant, which is known to improve both activity and selectivity to MA, was not simply proportional to its concentration. In fact, other factors may influence its effect, for example the preparation method of catalyst precursor. The results obtained indicated that an increase of Nb content in the range between V/Nb = ∞ and 80 led to a better selectivity to MA (with respect to the undoped sample) at low reaction temperature (less than 400°C), whereas a positive effect of Nb at high temperature (440°C) was observed only for very low Nb concentration (V/Nb = 150). In fact, Nb favoured the development of oxidized $VOPO_4$ compounds (and more preferably of the desired δ-$VOPO_4$), but under more oxidizing reaction conditions the amount of the latter was eccessive, finally leading to a worse selectivity than the corresponding undoped catalyst. In other words, an important conclusion was that the optimal amount of Nb was a function of reaction conditions (temperature, inlet composition). The catalyst containing the greater amount of Nb (V/Nb = 46) gave a worse selectivity at both low and high temperature, because at all conditions used it was excessively oxidized. We also prepared, for comparison purpose, a sample using a different synthesis method: a mixture of alcohols (80% v/v of isobutanol, 20% v/v of 1,4-butanediol) instead of isobutanol only, as the reducing agent, and $NbCl_5$, instead of a Nb salt, with V/Nb=80. This catalyst gave outstanding performance, especially because of the greater conversion and finally the greater yield to MA. In this case, however, the behavior was attributed to the retention of organic molecules between precursor layers, which greatly affected the morphology of the precursor and of the final catalyst as well. Catalysts characterization showed that doped fresh

catalysts (before equilibration and reactivity tests) possessed relatively greater quantities of δ-$VOPO_4$ than the undoped sample; moreover, the corresponding used catalysts (after catalytic tests), all showed the presence of this phase, except the catalyst prepared by means of the isobutanol/glycol mixture. This demonstrated that the increasing quantity of Nb, not only favoured the formation of δ-$VOPO_4$, but also stabilized it, in an almost irreversible way, which led to a limited benefit in catalyst performances: once again, an excessive amount of the oxidized compound led to over-oxidation of reactants and product and finally to a lower MA yield. The difference shown between catalysts prepared using 100% isobutanol and the sample derived from a synthesis mixture containing isobutanol and 1,4-butandiol was probably also correlated to a more efficient dispersion of the Nb dopant for the latter system. In conclusion, there are still some aspects, related to the preparation of the doped precursor, which need to be explored.

The formation of δ-$VOPO_4$, which is supposed to be the selective and active phase in redox cooperation with the VPP (but only when the former is present in small amount, dispersed over the latter), was investigated by carrying out in-situ Raman experiments, with mixed Nb/V hydrated phosphates: in fact, the presence of Nb was hypothesized to be involved in the formation of δ-$VOPO_4$, and specifically in the transformation of $VOPO_4 \cdot 2H_2O$ (VPD) into δ-$VOPO_4$. We synthesized VPD samples doped with different Nb contents and also Nb hydrated phosphates, doped with different quantities of V. We were able to get solid solutions only in the latter case; however Raman in-situ experiments showed the formation of an amorphous compound which did not not correspond to any V/P/O phase. On the contrary, with Nb-doped VPD samples, the compound obtained after both in-situ and ex-situ calcination was α_I-$VOPO_4$. In overall, we were not able to observe the formation of δ-$VOPO_4$ from bulk VPD, and this led us to conclude that the in-situ formation of δ-$VOPO_4$ in the VPP-based catalyst does not occur because of the dehydration of $VOPO_4 \cdot 2H_2O$, but because of the localized oxidation of VPP surface; in practice, the latter acts as a template for the generation of discrete quantities of the desired δ-$VOPO_4$.

In this regard, I also carried out Raman in-situ tests, by feeding the reactive mixture and varying the percentage of the reactants (n-butane and oxygen) (Chapter 7). We found that i) the catalyst surface was unaffected while feeding the reactive mixture; ii) when air was fed, the formation of $VOPO_4$ phases, especially of δ-$VOPO_4$, occurred in a very limited amount; iii) finally, when a mixture containing only n-butane (ca. 2%) in He was fed, the δ-$VOPO_4$ was promptly reduced to VPP, but indeed all the other compounds eventually present were affected by the reducing treatment. An important remark is that heterogeneity of the catalyst surface has to be taken into account when in-situ experiments are carried out using Raman spectroscopy.

Regarding catalyst preparation, I investigated a new method of synthesis of the VPP precursor, employing the microwave heating. This method permits interesting advantages, first of all the shorter time required to complete the synthesis, due to the fact that the heat is transferred faster and more efficiently, in comparison with the traditional heating. The synthesis were performed using CEM Discover S-class system and preparations with different organic solvents (isobutanol and

ethanol), with and without Nb, were compared. The characterization of catalysts prepared showed that different morphologies were obtained after minimal changes of preparation parameters. In particular, the most interesting sample was a VPP catalyst obtained from V_2O_5, H_3PO_4 and ethanol: the catalyst showed improved catalytic performance in comparison with a reference sample prepared by means of the conventional method, as a consequence of a quite unusual morphology (spongy with an high degree of void). It is worth noting that using the MW heating it was possible to achieve the reduction of vanadium oxide by ethanol, which instead is not possible with the conventional heating. In conclusion, we found that MW-assisted synthesis is a powerful and interesting way for the preparation of the V/P/O system, worth of being further explored.

Finally, I also investigated the feasibility of the gas-phase selective oxidehydration of 1-butanol into maleic anhydride. The alcohol is recently attracting much attention, because it can be obtained from biomass and also used an alternative fuel, in place of bioethanol. However, 1-butanol may be also advantageously utilized to produce chemicals. We tested different catalysts (mixed oxides, polyoxometalates, VPO compounds) and we found that VPP permitted to obtain the highest MA yield (ca 22%) using a feed of 1% mol. of 1-butanol in air. Our tests showed that 1-butanol could be easily dehydrated into butenes at relative low temperatures (250°-300°C); however, the formed butenes were only in part oxidized into MA, and the formation of CO and CO_2 prevailed. With some catalysts, high selectivity to C3 oxidized molecules was obtained, by oxidative scission of the reactant. In conclusion, we found that the oxydehydration of 1-butanol is possible, with VPP as the best candidate catalyst for the reaction, but also that the VPP properties and the reaction conditions as well, have to be further tuned in the aim of decreasing the selectivity to by-products.